Profiling extracellular vesicles signatures and deiminated protein cargo across phylogeny and pilot assessment of in vitro application of EVs in tissue regeneration, with focus on selected taxa displaying unusual immunological properties.

D'alessio, S.

https://doi.org/10.34737/wwww0

UNIVERSITY OF WESTMINSTER

Profiling Extracellular Vesicle Signatures and Deiminated Protein Cargo Across Phylogeny and Pilot Assessment of *In Vitro* Application of EVs in Tissue Regeneration, with a Focus on Selected Taxa Displaying Unusual Immunological Properties

Stefania D'Alessio

A thesis submitted in partial fulfilment of the requirements of the University of Westminster for the degree of Doctor of Philosophy

School of Life Sciences

University of Westminster – London

June 2024

DoS: Prof. Sigrun Lange

Supervisors: Dr Pinar Uysal-Onganer, Dr Polly Hayes

"My third piece of advice is probably the hardest to take. It is to forgive yourself for wasting time…

….As you will never be sure which are the right problems to work on, most of the time that you spend in the laboratory or at your desk will be wasted. If you want to be creative, then you will have to get used to spending most of your time not being creative, to being becalmed on the ocean of scientific knowledge."

Steven Weinberg

*(*Science Convocation at McGill University, June 2003. Advice to students at the start of their scientific careers. Department of Physics, the University of Texas at Austin, Texas 78712, USA.)*

Table of Contents

Abstract

Extracellular vesicles (EVs) are small membrane-bound structures secreted by cells that have emerged as key mediators of intercellular communication, carrying a diverse cargo of proteins, lipids, and nucleic acids that regulate various physiological processes. This thesis presents a comprehensive investigation into EV-mediated processes across diverse animal species, shedding light on their significance in biological systems. EV signature profiles of purple sea urchin, sea lamprey and reindeer and their deiminated protein cargoes revealed similarity across species, highlighting the conservation of deiminated proteins involved in epigenetic regulation and innate immune responses across phylogeny. Examination of circulatory EVs under stress conditions in a hypoxia-resistant species, such as the naked mole-rat, identifies pathways linking the brain citrullinome alterations to changes in circulatory EV profiles. Moreover, the thesis explores the regenerative potential of EVs derived from Atlantic cod mucus and serum. Proteomic analysis of cod-derived EVs uncovers a distinct cargo of proteins contributing to wound healing processes. Functional assays demonstrate the efficacy of cod serum-derived EVs in enhancing wound closure and upregulating key regulators of tissue repair. Findings from the studies in this thesis aimed at advancing EV-mediated cellular communication and its implications for health and diseases. Elucidating EV signatures and functions across phylogeny offers insights into the development of EV-based biomarkers and therapeutic strategies.

List of Tables

List of Figures

Publications Resulting From the Study

1. D'Alessio, S., Thorgeirsdóttir, S., Kraev, I., Skírnisson, K. and Lange, S., 2021. Post-translational protein deimination signatures in plasma and plasma EVs of reindeer (*Rangifer tarandus*). *Biology*, *10*(3), p.222.
2. D'Alessio, S., Buckley, K.M., Kraev, I., Hayes, P. and Lange, S., 2021. Extracellular Vesicle Signatures and Post-Translational Protein Deimination in Purple Sea Urchin (*Strongylocentrotus purpuratus*) Coelomic Fluid—Novel Insights into Echinodermata Biology. *Biology*, *10*(9), p.866.
3. Rast, J.P., D'Alessio, S., Kraev, I. and Lange, S., 2021. Post-translational protein deimination signatures in the sea lamprey (*Petromyzon marinus*) plasma and plasma-extracellular vesicles. *Developmental & Comparative Immunology*, *125*, p.104225.
4. D'Alessio S, Cheng H, Eaton L, Kraev I, Pamenter ME, Lange S. Acute Hypoxia Alters Extracellular Vesicles Signatures and the Brain Citrullinome of Naked Mole-Rats (*Heterocephalus glaber*). *International Journal of Molecular Sciences* 2022:23(9):4683

Acknowledgements

I am deeply grateful to all those who have supported and guided me throughout this incredible journey of pursuing my PhD.

First and foremost, I extend my heartfelt gratitude to my supervisor, Prof. Sigrun Lange, for her invaluable mentorship, unwavering and constant support, knowledge, and expertise. Prof. Lange is an incredible inspiration for the woman I want to become. I would never be grateful enough for the time she has dedicated to supporting my research, but most of all, for my physical and mental health. Prof. Lange believed in me and my capabilities when I needed the most.

I want to extend my gratitude to my supervisory team, Dr Pinar Uysal-Onganer and Dr Polly Hayes, for their insightful comments, suggestions, and expertise, which have immensely enriched the quality of this work.

I am grateful to all doctoral researchers and academic colleagues at the University of Westminster for their encouragement, intellectual discussion, and moral support, making this journey more enjoyable and meaningful. A special recognition to the University of Westminster for funding this research.

Last but not least, I am deeply grateful to my mother and father, who have shared every moment of my PhD journey, although not physically present. Thank you for always believing in me and supporting me at every step of my life. This achievement is for you and the sacrifices you made to ensure I could have the best life possible.

Stefania

Author's declaration

I declare that all the material contained in this thesis is my own work and in accordance with the Guidelines and Regulation of the University of Westminster.

Collaborations for associated publications are declared and referenced accordingly in bibliography and throughout this thesis.

List of Abbreviations

ADI – Arginine Deiminase

BLAST – Basic Local Alignment Search Tool

C3 – Complement 3

CRP-I/CRP-II – C-reactive proteins I and II

CTRL – Control

DMEM – Dulbecco's Modified Eagle's Medium

DPBS – Dulbecco's Phosphate Buffered Saline

ECM – Extracellular Matrix

ESCRT – Endosomal Sorting Complex Required for Transport

EVs – Extracellular Vesicles

FBS – Foetal Bovine Serum

GO – Gene Ontology

HaCat – Immortalized Human Keratinocytes

HDC – High-energy C-trap Dissociation

HDFa – Human Dermal Fibroblasts, adult

HSP – Heat Shock Protein

IgG – Immunoglobulin G

IgM – Immunoglobulin M

Ii – Invariant chain

ILVs – Intraluminal Vesicles

ISEV – International Society of Extracellular Vesicles

KEGG -Kyoto Encyclopaedia of Genes and Genomes

LC/MS-MS – Liquid Chromatography with Tandem Mass Spectrometry

m/l EVs – medium/large Extracellular Vesicles

MCH – Major Histocompatibility Complex

MCS – Mesenchymal Stem Cells

MISEV – Minimal information for studies of extracellular vesicles

MVB – Multivesicular Bodies

NCBI – National Centre for Biotechnology Information

NETs – Neutrophil Extracellular Traps

NTA – Nanoparticle Tracking Analysis

Omega3 – PUFAs – Omega 3 polyunsaturated fatty acids

PADs – Peptidylarginine deiminases

PBS – Phosphate Buffered Saline

RT – Room Temperature

SDS-PAGE – Sodium dodecyl sulphate-polyacrylamide gel electrophoresis

sEVs – small Extracellular Vesicles

SLE – Systemic lupus erythematosus

STRING – Search Tool for the Retrieval of Interacting Genes/Proteins

TBS – TRIS Buffered Saline

TBS-T – TRIS Buffered Saline – Tween20

TEM – Transmission Electron Microscopy

TLR – Toll-like Receptor

VLRs – Variable Lymphocyte receptors

VPS4 – Vacuolar protein sorting-associated protein 4

WB – Western blot

Chapter 1 – Introduction

1.1. Origin and Characteristics of Extracellular Vehicles (EVs)

"*A variety of minute breakdown products of blood corpuscles*", as defined by Chargaff and West in 1946, with their studies on blood clotting, marked the discovery of a "particulate fraction" which had high clotting potential (Chargaff and West, 1946; Couch *et al*., 2021). 1966 Sun described vesicle-like structures released from alveolar cells into the alveolar space (Sun,1966; Couch *et al*., 2021). Some years later, Peter Wolf identified this 'minute product' as "platelet dust" through electron microscopy images (Wolf, 1967; Couch *et al*., 2021). In 1971, Neville Crawford showed further images of vesicles, which were described as 'microparticles' obtained from platelet-free plasma, that also contained lipids and carried cargo, including ATP and contractile proteins (Crawford, 1971; Couch *et al*., 2021). In 1974, Nunez, Wallis and Gherson described the presence of multivesicular bodies (MVBs), small extracellular vesicles within the size of 1-10nm, close to the apical plasma membrane of a bat thyroid, and how these have been released into the luminal space (Nunez, Wallis and Gherson,1974; Couch *et al.,* 2021). The field of extracellular vesicles (EVs) saw its expansion and a better understanding during the early 1980s, with the investigation on membrane trafficking and the biochemistry of the plasma membrane, using reticulocyte maturation as a model, by both Johnstone and Stahl, who showed that transferrin receptor was lost via the release of extracellular vesicles *(*Harding *et al*., 1983; Johnstone *et al.,* 1989; Couch *et al*.,2021). The field continued growing, and in later studies, between 1990 and 2000, different papers described the physical and biochemical characteristics of EVs, including their enzymatic activity (Johnston *et al.,*1991), their potential role as anti-tumoral vaccines (Zitvogel *et al.,* 1998) and their capability to present antigen when released by immune cells (Raposo *et al.,* 1996; Couch *et al*.,2021). From the year 2000 onwards, the EV field

expanded considerably with more in-depth explorations: different studies showed that EVs can be isolated from most body fluids e.g., blood, serum, plasma, urine, saliva, breast milk, amniotic, synovial fluids, and cerebrospinal fluids (Street *et al.,*2012; Yanez-Mo *et al.,*2015; Théry *et al.,*2018; Vagner *et al.,*2019;) and they can mediate cell-cell communication by direct interaction between the membrane receptors and plasma membrane, triggering downstream signalling cascade in the recipient cell, or upon fusion with plasma membrane realising their contents directly into the cytosol (Gurung *et al.,*2021). Other studies focused on the EV proteome and lipidome (Théry *et al.,* 2001; Subra *et al.,*2007), their role in the immune system (Skokos *et al.,* 2003; Van Niel, 2003), their role as potential anti-tumour therapy (Chaput *et al.,* 2003), as well as their capability to transfer nucleic acids (Valadi *et al.,* 2007), the functional effects of EVs *in vivo*, protecting animal model from disease (Colino and Snapper, 2007) and to be a mean of communication between cells in plants (An *et al.,* 2007). EVs have been shown to play central roles in normal physiological processes, such as angiogenesis, apoptosis, coagulation, cellular homeostasis, cellular differentiation, inflammation, and intracellular signalling, as well as in immune response and pathologies, e.g., carcinogenesis (Andaloussi et al., 2013; Abels and Breakefield,2016), by transferring proteins, lipids, DNA, RNA and non-coding RNA, including microRNAs, and, therefore, EVs are considered as signalosomes (Vagner et al., 2019; Turchinovich et al, 2019). Given the different and unique properties of EVs, they are deemed ideal and reliable diagnostic and prognostic biomarkers in various clinical settings (Ciferri *et al*.,2021), such as neurodegenerative (Thompson *et al.,*2016) and autoimmune diseases (Tian *et al*.,2020), different cancers (Peng *et al*.,2018; Kadota *et al*.,2017; Chang *et al*.,2019), and haematological diseases (Boyiadzis *et al*.,2017). EVs are excellent drug delivery systems due to their ability to deliver different cargoes (such as interfering RNA (siRNA)) and high stability in the blood (Aryani *et al*.,2016; Bunggulawa *et al*.,2018) and produce low immune response

(Ha *et* al., 2016) and ideal therapeutic agents for various diseases including cancer, metabolic, infectious, and neurodegenerative disorders (Chung *et al.,*2020). Different RNAs have been identified in EVs and include mRNA (messenger RNA), microRNA, rRNA (ribosomal RNA), tRNA (transfer RNA), sRNA (small RNA) and lncRNA (long non-coding RNA) (Turchinovich *et al*.,2019), and the role of EVs RNAs have been recently considered in the host-pathogen interaction and as candidate interspecies-communication molecules (Lee *et al*.,2019; Munhoz da Rocha *et al.,*2020).

1.1.1 Extracellular vesicles biogenesis and nomenclature

Throughout the years, different terms were used to describe the structures that were observed, such as "extracellular microvesicles", "microparticles", and "virus-like particles" Trams *et al.* (1981) used the term "exosome" for the first time in the context of EVs, to describe vesicles that are produced directly by outward budding at the plasma membrane, and in 1987, Rose Johnston, used the term "exosome" to describe vesicles released following the fusion of MVBs with the plasma membrane, which has then become the International Society for Extracellular Vesicles (ISEV) recommended term for this type of vesicles (Théry *et al*.,2018; Welsh *et al*.,2024). As the field grew and different biogenesis pathways were discovered, it was necessary to have precise nomenclature for each vesicle; therefore the term "extracellular vesicles" is used nowadays to describe a heterogenous family of membrane-surrounded and non-replicating structures, delimited by a lipid bilayer (Théry *et al*.,2018) released in a common and evolutionary conserved process by prokaryotic (Lee *et al.,*2009; Deatherage and Cookson, 2012) and eukaryotic (György *et al*., 2011; Van Der Pol *et al*.,2012) cells, into the extracellular space. The Minimal Information for Studies of Extracellular Vesicles (MISEV) 2018 (Théry *et al*.,2018) and updated in MISEV2023 (Welsh *et al.,*2024) proposed nomenclature recommendation based on physical characteristics, such as size, in order to refer to different EVs subtypes: "small EVs" (sEVs) are EVs that range between 30

nm and 200 nm and “medium/large EVs” (m/lEVs) are EVs, also called microparticles/microvesicles or “ectosome”, have a size range of 200-1,000 nm (Théry *et al.,* 2018); they are generated on the cell surface by budding and fission of the plasma membrane (Fig.1) (Andaloussi *et al*, 2013; Abels and Breakfield, 2016; Jadli *et al*.,2020; Clancy *et al*., 2021), a process that depends on many different factors, such as the redistribution of phosphatidylcholine and sphingomyelin, repositioning of phosphatidylserine and phosphatidylethanolamine to the outer leaflet (Jadli *et al*.,2020) the contraction of the actin-myosin machinery (Clancy *et al*., 2021), and an increase of calcium concentration in the extracellular environment, which induces membrane phospholipid reorganization and improves the formation of microvesicles by increasing the level of vesiculation (Fig.1)(Crawford, 1971; Gurunathan *et al.,* 2021; Jin *et al*., 2022;). Small EVs (sEVs), also known as “exosomes”, have been largely studied and are small EVs with a diameter of 30-100/150 nm (Théry *et al*.,2018; Doyle and Wang,2019; Jadli *et al*.,2020); they are originated from the intraluminal vesicles (ILVs) budding within multivesicular bodies (MVB) upon fusion with the plasma membrane and released in the extracellular space via the exocytotic pathway (Fig.1)(Andaloussi *et al.*,2013; Yáñez-Mó *et al.*,2015; Turchinovich *et al.*,2019; Jadli *et al*.,2020). The biogenesis of sEVs is mainly driven by the endosomal sorting complex required for transports (ESCRT)(Fig.1) (Raposo and Stoorvogel,2013; Abels and Breakfield, 2016; Hessvik and Llorente, 2017; Van Niel, D’Angelo and Raposo, 2018; Jadli *et al*.,2020). The ESCRT machinery is comprised of four subunits along with accessory protein, i.e., VPS4 (Vacuolar Protein Sorting 4), VTA1 and ALIX; ESCRT-0 complex initiates the MVB pathways by binding to PI3P (phosphatidylinositol-3-phosphate), an endosome-enriched phospholipid which regulates cell signalling and membrane trafficking. ESCRT-0 recognises clusters of ubiquitinated proteins and cargo on the outer endosomal membrane (Schmidt and Teis,2012) and recruits the ESCRT-I complex via Vps23/HR, which drives

the budding on the endosomal membrane. The ESCRT-III completes the process of sEVs formation, facilitating the membrane invagination and formation of ILVs. The accessory proteins are fundamental in disassembling and recycling the ESCRT machinery (Jadli *et al*.,2020). However, some studies have shown that sEVs release is not only ESCRT-dependent: by completely depleting the ESCRT complex, the formation of multivesicular endosomes and their release was still occurring, yet their morphology and structure appeared altered (Stuffers *et al*.,2009). One of the suggested ESCRT-independent mechanisms for the release of sEVs is the ceramide-mediated sorting of proteolipid protein into ILVs (Trajkovic *et al*.,2008), while the tetraspanins CD63 has also been considered to be involved in the formation of ILVs and the release of sEVs (van Niel *et al*.,2011). sEVs cargo includes proteins members of the tetraspanins family (CD9, CD63 and CD81), an endosomal sorting complex required for transport (ESCRT) proteins (Alix, TSG101), integrins, heat shock proteins (Hsp), actin and flotillin, but also nucleic acids such as DNA, RNA, mRNA and non-coding RNA. Moreover, the sEVs bilayer membrane consists of lipids such as sphingomyelin, cholesterol, and ceramides important for maintaining the sEVs structure, regulating secretion, cargo sorting and signalling (Gurung *et al.,*2021).

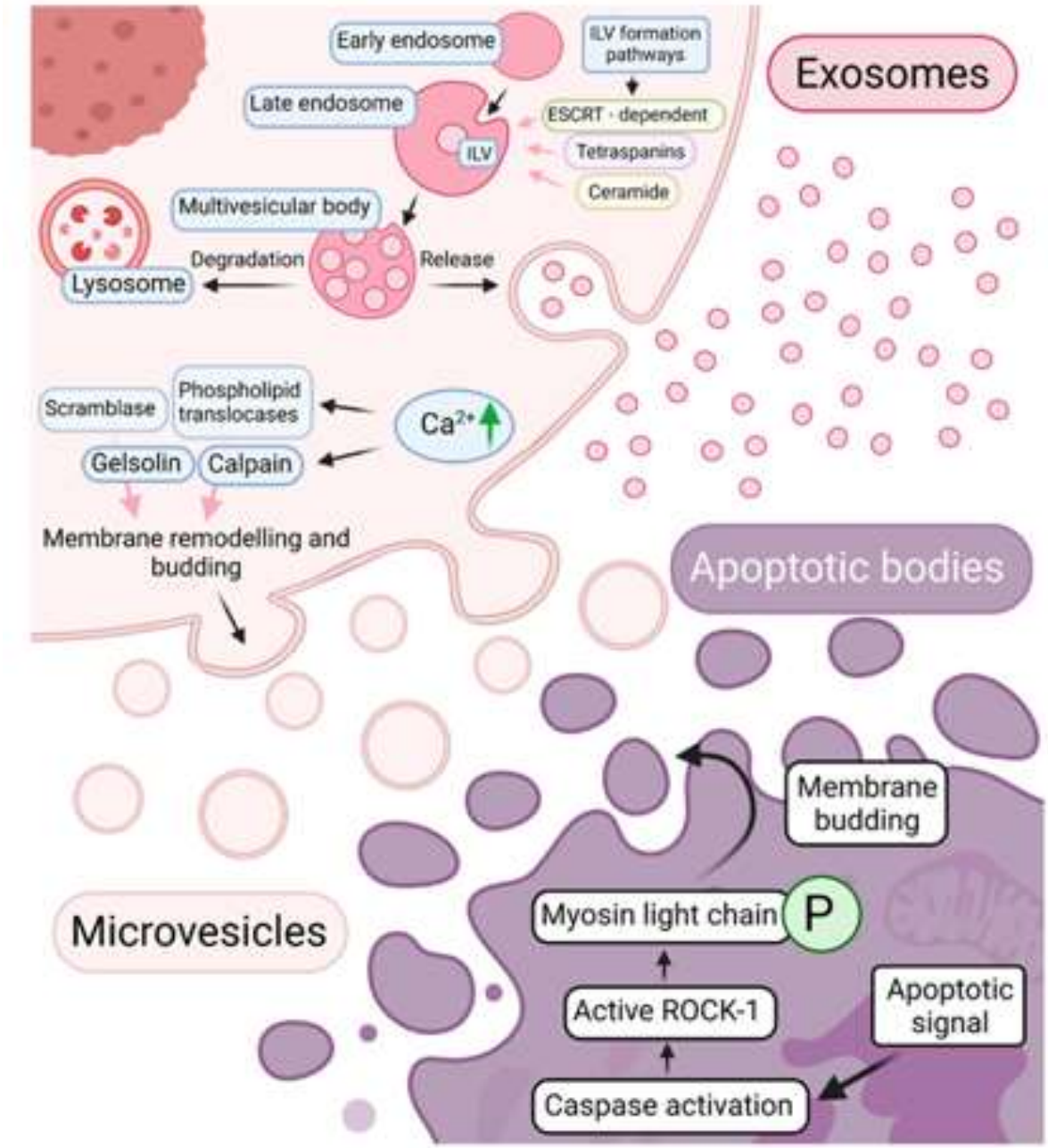

Figure 1. Biogenesis of different Extracellular Vesicles. Microvesicle biogenesis involves Ca2–dependant enzymes calpain, gelsolin, phospholipid translocases, and scramblase, which promote the distribution of phosphatidylserine (PS) on the outer cell surface, resulting in membrane remodelling and subsequent budding. Exosomes are formed during endosomal sorting. During the maturation of an early endosome, intraluminal vesicles (ILVs) are created in ESCRT – an ESCRT-dependent or independent (in the presence of tetraspanins or ceramide) manner. Late endosomes with many ILVs are called the multivesicular body (MVB), which either diffuse with lysosome for degradation or merge with the plasma membrane, releasing exosomes (Narauskaité *et al.*,2021).

1.2. Extracellular Vesicles and PADs Isozymes in Phylogeny

1.2.1. Peptidylarginine Deiminases (PADs) isozymes

Peptidylarginine deiminases (PADs) are a family of enzymes which are activated by a high calcium (Ca^{2+}) concentration and catalyse the irreversible conversion of peptidyl-arginine to peptidyl-citrulline through the basic hydrolysis of ammonia end group of the arginine side chain and the consequent ammonia release (Fig. 2) (Vossenaar *et al.*, 2003, Alghamdi *et al.,*2019). This post-translation modification, known as "citrullination" or "deimination", significantly impacts the target proteins by changing their primary, secondary, and tertiary structures, altering their function and interactions with other proteins (György *et al.*, 2006).

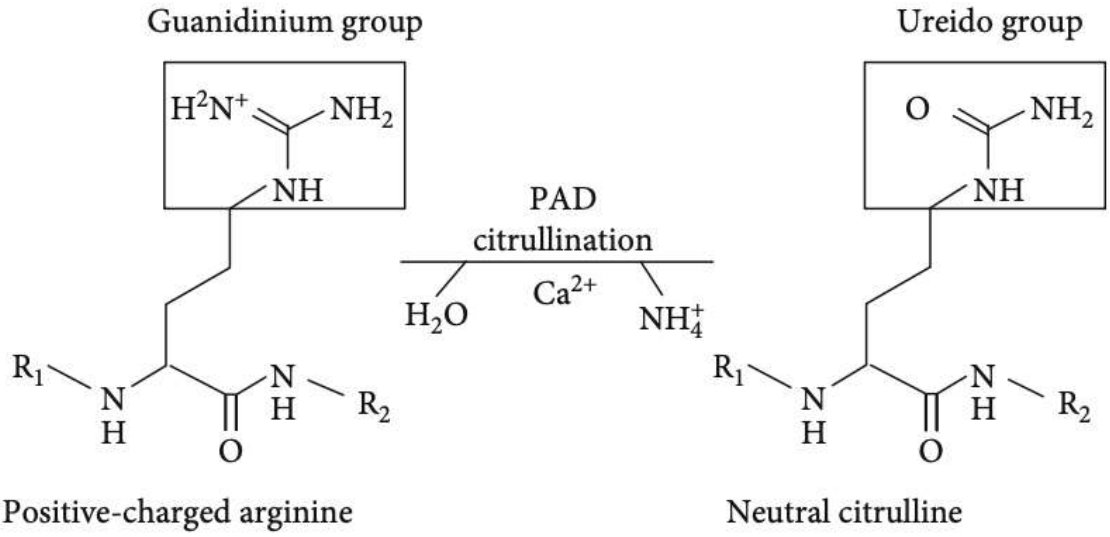

Figure 2. Citrullination or deimination chemical reaction. The citrullination or deimination is a post-translational process catalysed by peptidylarginine deiminases, which modifies the guanidinium group of the arginine amino acid and the ureido group of the citrulline amino acid. This conversion is complemented by the loss of the arginine positive charge and production of ammonium, which causes protein conformational changes that may modify the protein's binding and unfolding properties, affecting its function and half-life (Alghamdi *et al.*,2019).

PAD-mediated deimination/citrullination contributes, amongst others, to the generation of neo-epitopes, which can induce inflammatory responses and can also cause a change in or loss of protein function (Witalison *et al*.,2015; Lange *et al*., 2017). However, such post-translational modification can also allow for protein moonlighting, an evolutionary acquired phenomenon that enables proteins to exhibit different physiological, biochemical, and biophysical functions (Henderson *et al*., 2014; Jeffrey *et al*., 2018). Five highly conserved PAD isozymes have been identified in mammals: PAD1, PAD2, PAD3, PAD4 and PAD6 are found in the cytoplasm however, PAD2, PAD3 are also found in the nucleus (Vossenar *et al*., 2003; Lange *et al.,*2011), while only PAD4 has been found to contain a classic nuclear translocation site (Stadler *et al*.,2013). PADs isozymes are conserved throughout phylogeny, and different isozymes are present in other species; for instance, three PAD isozymes are found in birds and reptiles, and only one PAD form in fish, with PAD2 considered the most phylogenetically conserved isozyme (Vossenaar *et al*.,2003; Magnadóttir *et al*.,2018; Rast *et al*.,2022). In mammals, PAD isozymes have distinct tissue localisation and substrate preferences: PAD1 isozyme is found to be expressed mainly in the epidermis, facilitating the terminal differentiation of keratinocytes (Vossenaar *et al*.,2003; Nachat *et al*.,2005) and uterus, where its expression increases after oestradiol injection and female maturation (Guerrin *et al*., 2003; Uhlén *et al*.,2015); preferred substrates for PAD1 are Keratin1, Keratin10 and Profilaggrin (Nachat *et al*.,2005; Yu and Proost,2022). PAD1 has also been detected in brain tissue (Mercer *et* al.,2022) and in cancer tissue, including in various mammals (Inal *et* al.,2022). PAD3 is also expressed and localised in the hair follicle (Vossonaar *et al*., 2003; Wang and Wang, 2013), neural stem cells (U *et al*.,2014) and neutrophils (Darrah *et al*.,2012). In a comparative study by Lange *et al.* (2011), the role of PAD3 from the chick model was identified as a modulator in developing early spinal cord and its role in spinal cord injury response (Lange *et al*., 2011). PAD3 has also been found to

be involved in cancer invasion, particularly associated with aggressive cancers (Uysal-Onganer *et al*.,2020; Uysal-Onganer *et al*.,2021) and neurodegenerative diseases (Lange *et al*.,2017; Sancandi *et al*.,2020; Lange *et al.*,2021), as well as brain cancer (Kosgodage *et al*.,2019; Uysal-Onganer *et al.,*2020). PAD6 was initially found in the eggs and embryos of mice. Later its presence was confirmed in human tissue, with its function correlated to the cytoskeletal reorganisation in the egg in early embryo development (Zhang *et al*., 2004; Wang and Wang, 2013; Esposito *et al*.,2007). PAD2 and PAD4 are the most studied isoforms: PAD2 is the most ubiquitously expressed isozyme, found in most tissues and play an essential role in normal physiological processes such as apoptosis, gene regulation, immune response, also PAD2 and PAD4 are involved in many human inflammatory and autoimmune diseases (Bicker & Thompson,2013; Wang and Wang, 2013; Witalison *et al*., 2015) i.e., rheumatoid arthritis (Damgaard *et al*.,2014), neurodegenerative diseases (Lange *et* al.,2017, Sancandi *et al.,*2020) and cancers (Uysal-Onganer *et* al.,2020; Uysal-Onganer *et* al.,2021; Wang *et al*.,2020); PAD4 plays a vital role in innate immunity, as it has been established that it catalyses histone citrullination, inducing chromatin decondensation and expulsion of antimicrobial molecules via the chromosomal DNA, a fundamental process for the formation of NETs (Neutrophil Extracellular Traps) (Wang *et al*.,2009; Thiam *et al*.,2020), involved in a mechanism known as NETosis, which effectively kill different pathogens and more prominent pathogens that cannot be removed by neutrophils (Rohrbach *et al*.,2012; Liu *et al*., 2021).

1.2.2. PADs Isozymes as Modulators of EV Signatures Across Phylogeny

PAD isozymes have been identified not only in mammals but also throughout the phylogenetic tree, with the indication of horizontal gene transfer from cyanobacteria to Chordata (D'Alessio *et al*.,2021; Cummings *et al*.,2022). PAD homologues, also referred to as arginine deiminase (ADI), have been reported in parasites (Gavinho *et al.*,2020;

Krissmundsson *et al*.,2021), bacteria (Bielecka *et al*., 2014; Kosgodage *et al*.,2019 and fungi (El-Sayed *et al*.,2019). In mammals all the five PADs (PAD 1,2,3,4,6) isozymes have been identified (Vossenaar *et al*.,2003), while in birds and reptiles only PAD1, PAD2 and PAD3 isozymes are present, and only one PAD isozyme (PAD2-like isozyme) is reported in teleost and cartilaginous fish (Rebl *et al*.,2010; Magnadóttir *et al*.,2018, Magnadóttir *et al*.,2019, Criscitiello *et al*.,2019, Criscitiello *et al*.,2020c). In various disease modelling studies, PADs have been recognised as one of the modulators of EV release, which may be possibly linked to this mechanism being partly dependent on calcium level mediated pathways, and both modulation via actin and histone pathways have been suggested (Kholia *et al*.,2015). Several EV cargoes, including protein cargo, contribute to cellular communication, so deiminated/citrullinated proteins in EVs may be particularly interesting. Furthermore, citrullinated proteins in EV cargoes from different species across the phylogeny tree may provide insights into EV-mediated communication of citrullinated proteins via PAD or PAD homologue-mediated pathways. This also includes the possible roles of PADs and protein deimination in normal physiological and immunological processes and metabolic pathways, which already have been analysed in a range of comparative animal studies including vertebrates, birds, reptiles, teleost fish, cartilaginous fish (Chondrichthyes), crustaceans (Crustacea), arthropods (Arthropods), alveolates (Alveolate) and parasites (Protozoa): Magnadóttir *et al*., 2018(a); Magnadóttir *et al*.,2021 – halibut (*Hippoglossus hippoglossus L.*); Magnadóttir *et al*.,2018 (b) – Atlantic cod (*Gadus morhua L.*); Magnadóttir *et al*.,2019 – Atlantic cod mucus (*Gadus morhua L.*); Criscitiello *et al*., 2020(a) – Llama (*Lama glama*); Criscitiello *et al*.,2019 – shark (*Ginglymostoma cirratum*); Pamenter *et al.*, 2019 – naked mole-rat (*Heterocephalus glaber*); Criscitiello *et al*., 2020 (b) – Cow (*Bos taurus*); Criscitiello *et al*., 2020 (c) – Alligator (*Alligator mississippiensis*); Magnadóttir *et al*., 2020 (a)- whales/orca ; Magnadóttir *et al*., 2020 (b) – pinnipeds (Grey seal

(*Halichoerus gryptus*), Harbour seal (*Phoca vitulina*); Bowden *et al*.,2020 a – Mollusca (blue mussel (*Mytilus edilus*) soft shell clam (*Mya arenaria*) Eastern oyster (*Crassostrea virginica*)Atlantic Jacknife clam (*Ensis leei*)); Bowden *et al.,*2020 c – American Lobster (*Homarus americanus*); Bowden *et al*., 2020 b – Horseshoe crab (*Limulus polyphemus*); Phillips *et al.,*2020 – Antarctic seabirds; Kristmundsson *et al*.,2021- Alveolata); Coates *et al*.,2023 – shore crabs (*Carcinus maenas*). Moreover, extracellular vesicles have been identified in other non-mammalian vertebrates, as in the case of avian species (Luo *et al.,*2022), Chinese softshell turtle (Zhu *et al*.,2019), viper (Carregari *et al*.,2018) and cobra (Manuwar *et al*.,2020), snake venom (Ogawa *et al*.,2008), other Arthropods, as in the case of the Chinese bird spider (Xun *et al*.,2021), tick (Zhou *et al*.,2018), Drosophyla (Beer and Wehman,2017), honeybees (Peršurić and Pavelić,2021). EVs have also been explored in Nematodes, i.e., C. elegans (Ma et al.,2023), bacteria (Liu et al.,2018; Briaud and Carrol,2020) and Cnidarians, i.e., polyp Hydra (Moros *et al*.,2021) and corals (Takagi *et al*.,2020).

Due to a recent focus of interest on PADs across the phylogeny tree and EV-mediated communication, including via deiminated protein transport, this current project, therefore, focussed on identifying roles of EV-mediated communication by assessing citrullinated signatures in three representative species at three points of reference in the phylogeny tree. For this purpose, the focus was on 1) Mammals (Artiodactyla – Reindeer (*Rangifer tarandus)*); 2) Agnatha (Sea Lamprey (*Petromyzon marinus*)) and Echinodermata (Purple Sea Urchin (*Strongylocentrotus purpuratus*)). Similarly, EV signatures in these same species were compared concerning EV size profiles, surface markers, electron microscopy, and proteomic content, including citrullinated protein content. Findings will elucidate if EV profiles differ, or are conserved to some extent, across the phylogeny tree and whether the citrullinome signature of associated biological pathways indicates conservation of, or variation in, immune, metabolic, or other

physiological pathways that may be affected by citrullination. In addition to the three species above, the current study also explored two further species with unusual immune and metabolic characteristics for preliminary studies on assessing circulatory EV signatures as indicators for stress resistance and for the potential of using EVs to promote wound healing. For this purpose of determining circulating EV signatures as biomarkers of stress responses, including in the brain, the study took advantage of the naked mole-rat (*Heterocephalus glaber*), a long-living, cancer resistant and hypoxia-resistant species, which has received increasing interest in the context of various pathologies. While a previous study had assessed citrullination signatures in the naked mole rat (Pamenter *et al*., 2019), no such assessment had been carried out under pathological/stress conditions. Therefore, the current study aimed to identify whether PAD-related changes in circulating EV signatures could be placed under hypoxic conditions and reveal any PAD-related pathways linking to the unusual hypoxic resistance of this species, including the brain citrullinome. For this purpose, PAD isozymes were assessed in the brain tissue of normal and hypoxic naked mole rats, and citrullinated proteins were enriched from both circulating plasma-EVs and the brain tissue of control and hypoxia-treated animals. Protein-interaction networks were created for citrullinated proteins to identify whether brain citrullinome changes could be correlated to circulatory EV profile and citrullinome cargo changes (D'Alessio *et al.,*2022) (See Chapter 4). To assess the potential of EVs in wound healing and tissue regeneration, EVs from the teleost fish *Gadus morhua* (Atlantic cod), which shows some unusual immune characteristics, were used on mouse fibroblasts and human keratinocytes and fibroblasts *in vitro* (Chapter 5). Therefore, the species used in the different chapters of this thesis are Petromyzon marinus (Sea Lamprey), Strongylocentrotus purpuratus (Purple sea urchin), Rangifer tarandus (Reindeer), Heterocephalus glaber (naked mole-rat), and *Gadus morhua* (Atlantic cod).

1.3. Extracellular Vesicles in Regenerative Medicine

1.3.1. The Wound Healing Process

The process of wound healing is a natural self-controlled process, but at the same time, a complex physiological process which involves four time-dependent, overlapping but well-defined phases. Tissue injury, characterised by microvascular injury and extravasation of blood into the wound, triggers the immediate phase of homeostasis (Fig.3 – step 1) in which the coagulation cascade is initiated. The vessel walls start to constrict, resulting in platelet aggregation, which limits further blood loss, and fibrin clot formation, which forms a temporary seal over the injury, preventing the influx of microorganisms and supporting and guiding the aggregation of keratinocytes and fibroblasts (Strodtbeck,2001; Enoch and Leaper, 2005; Welnar *et* al.,2009; Ellis, Jin and Tartar, 2018). The inflammatory phase (Fig.3 – step 2) overlaps with the phase of homeostasis. Usually, it occurs within the first 72h after the tissue injury: a complex series of molecular signals characterise the inflammatory phase that ultimately facilitates neutrophils and macrophages infiltration in the wound bed that prevents further tissue damage and eliminates any foreign pathogen and debris (Stordtbeck,2001; Enoch and Leaper,2005; Welnar *et* al.,2009; Ellis, Jin and Tartar,2018). The key mediators that drive the host inflammatory response during normal wound healing are Interleukin-1 that promotes inflammation and helps recruit immune cells to the wound site (Eming, Krieg and Davidson,2007); Interleuikin-6 which stimulates the acute phase response and aids in the transition from inflammation to tissue repair (Gallucci *et al*.,2000), and tumour necrosis factor-alpha that induces the recruitment of neutrophils and macrophages and promotes healing processes (Barrientos *et al*.,2008). Chemokines are other key mediators of the inflammatory response. These include CCL2 (MCP-1) which attracts monocytes to the wound area, promoting the recruitment of macrophages that

are essential for clearing debris and secreting growth factors, and CXCL8 (IL-8) attracts neutrophils to the wound site to aid in the initial response to injury (Eming *et al*.,2007). Growth factors secreted by macrophages include Vascular Endothelial Growth Factor (VEGF), which promotes angiogenesis, ensuring an adequate blood supply to the healing tissue; Transforming Growth Factor-beta (TGF-beta) that has both pro- and anti-inflammatory effects and is important for transitioning to the proliferative phase (Penn *et al*.,2012). Once the immune response is in place and the injury has reached homeostasis, the proliferation phase begins (Fig.3 – step 3), which usually happens on the third day after the injury. The proliferative phase involves re-epithelialization, which occurs with the migration of keratinocytes and fibroblasts, collagen synthesis, angiogenesis and granulate tissue formation, protrusion, adhesion and traction; however, the last phase of wound healing, the remodelling phase (Fig.3 – step 4), begins with the granulate tissue formation around day eight and last for about one year (Stordtbeck,2001; Enoch and Leaper,2005; Welnar *et* al.,2009; Ellis, Jin and Tartar,2018). The primary mechanism of the remodelling phase of wound healing is the constant extracellular matrix (ECM) reshaping by cross-linking collagens, which are continuously synthesised and broken down, wound contraction, through the interactions between fibroblasts and the surrounding ECM, cell maturation and apoptosis (Stordtbeck,2001; Enoch and Leaper,2005; Welnar *et al*.,2009; Ellis, Jin and Tartar, 2018; Diller and Tabor,2022).

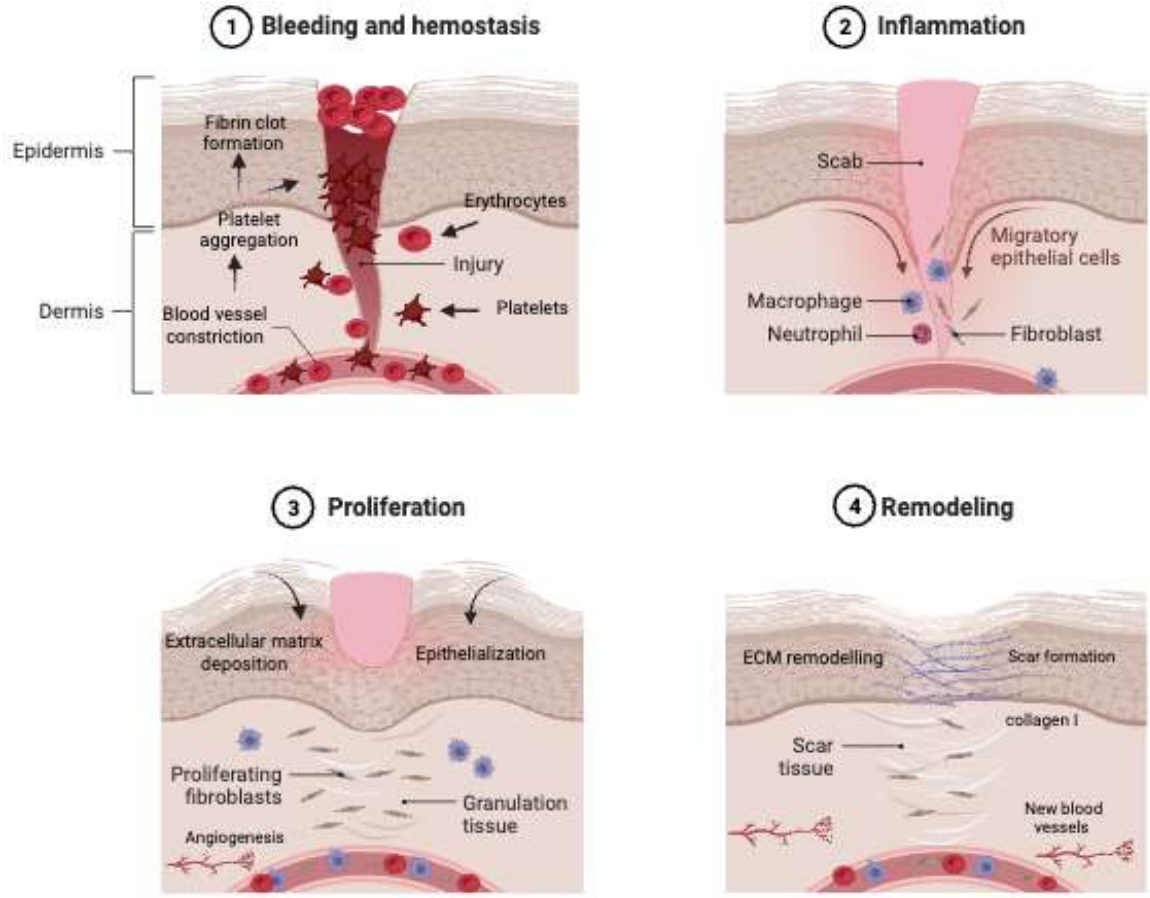

Figure 3. Natural wound healing process. (Image created using BioRender.com)

1.3.2 Extracellular Vesicles Role in the Healthy Wound Healing Process

Extracellular vesicle application is one of the most promising emerging wound healing approaches (Wei *et al*.,2020;2022;2023) and is secreted by various cells; they appear to be essential players in regeneration-promoting intracellular communication (Chung *et al*.,2020). Recent *in vivo* studies reported the presence of EVs in wounds and acknowledged their presence in routine wound healing (Clemmer *et al*.,2020). EV-based signalling plays a crucial role in all four wound healing phases (homeostasis, inflammation, proliferation, and remodelling), thus suggesting their natural capacity to be exploited to stimulate the healing process (Narauskaité *et al*.,2021). In the homeostasis phase, upon skin injury, damaged cells release danger-signalling molecules such as ADP, collagen and thrombin, causing changes in platelets cytoskeleton and inducing

plug formation to stop the bleeding temporarily (Fig.4- a); pro-coagulant EVs (PEVs) are released in the wound bed from activated platelets (Fig.4 – b): their pro-coagulant property is due to the presence of an active form of aIIbß3 integrin, a great affinity to fibrinogen, exposure of phosphatidylserine (PS) which provide a platform for coagulation factors and transfer of reactive oxygen species (ROS) producing NOX-1, which enhances platelet activation. Tissue factor (TF) dependent and independent meet in the common pathway, converting fibrinogen into fibrin, binding to aggregated platelets and forming a thrombus (Fig.4 – c). During this process, the TF-dependant coagulation pathway is either induced by PEVs by transferring P-selectin, which causes TF exposure on monocyte membrane upon PSGL-1 binding, or it can be introduced by salivary monocytes-derived EVs (Fig.4 – d) (Narauskaité *et al.*,2021).

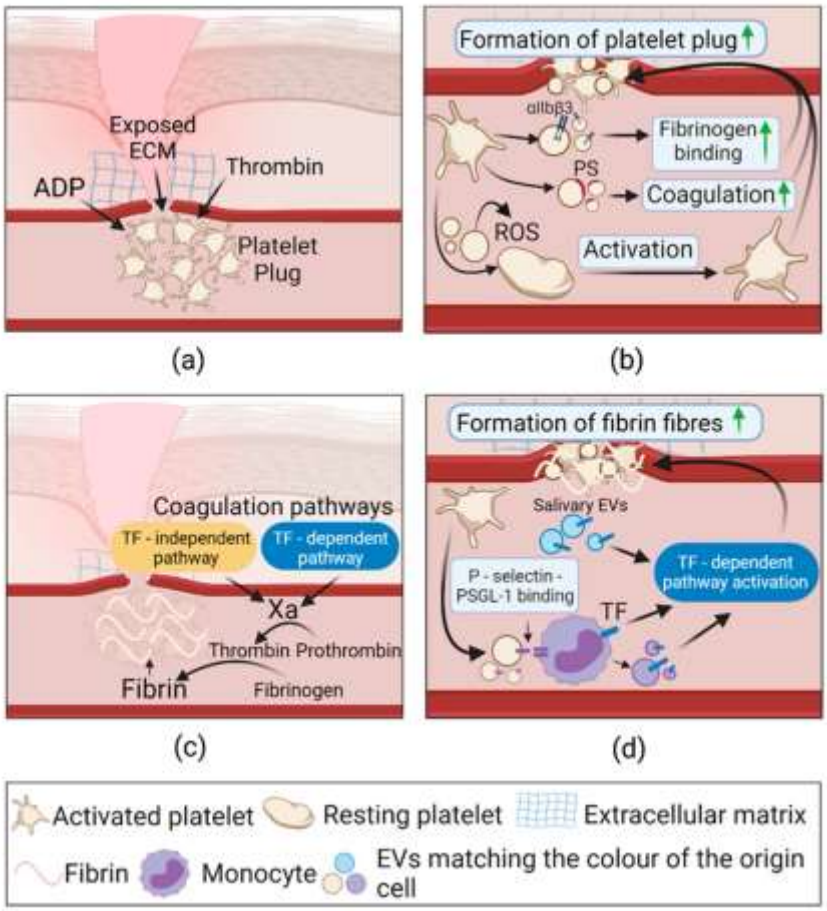

Figure 4. EVs role in the homeostasis phase of healthy wound healing (Narauskaité *et al.*,2021).

During the inflammation phase of wound healing, the first immune cells to be recruited to the wound site are neutrophils, responding to signals provided by damaged cells, microbes, and platelets. Neutrophils undergo apoptosis after clearing the wound from pathogens; the cell remains (Fig.5 - a). The neutrophil-derived EVs' (NDEVs) become activated, depending on the environmental conditions, and promote reactive oxygen species (ROS), CXCL8 (Interleukin 8) production in other neutrophils, as well as directly induce ROS and leukotriene B4 synthesis in their turn, resulting in the maintenance of a pro-inflammatory environment. In contrast, resting-state NDEVs act oppositely, and apoptotic NDEVs promote coagulation (Fig.5 - b). Macrophages infiltrate the wound site and clear the remaining pathogens and apoptotic neutrophils, shifting the macrophage phenotype from pro-inflammatory M1 to pro-resolving M2 phenotype (Fig.5 - c). This change in phenotype is regulated by the transmission of the EVs from pro-resolving macrophages or wound edge keratinocytes, active cargos, keeping in control the inducible nitric oxide synthesis (iNOS) and arginase (Arg1), M1 and M2 macrophage marker, inducing angiogenesis and re-epithelisation, accelerating the transition to the proliferative stage of wound healing (Fig.5 - d) (Narauskaité *et al.*,2021).

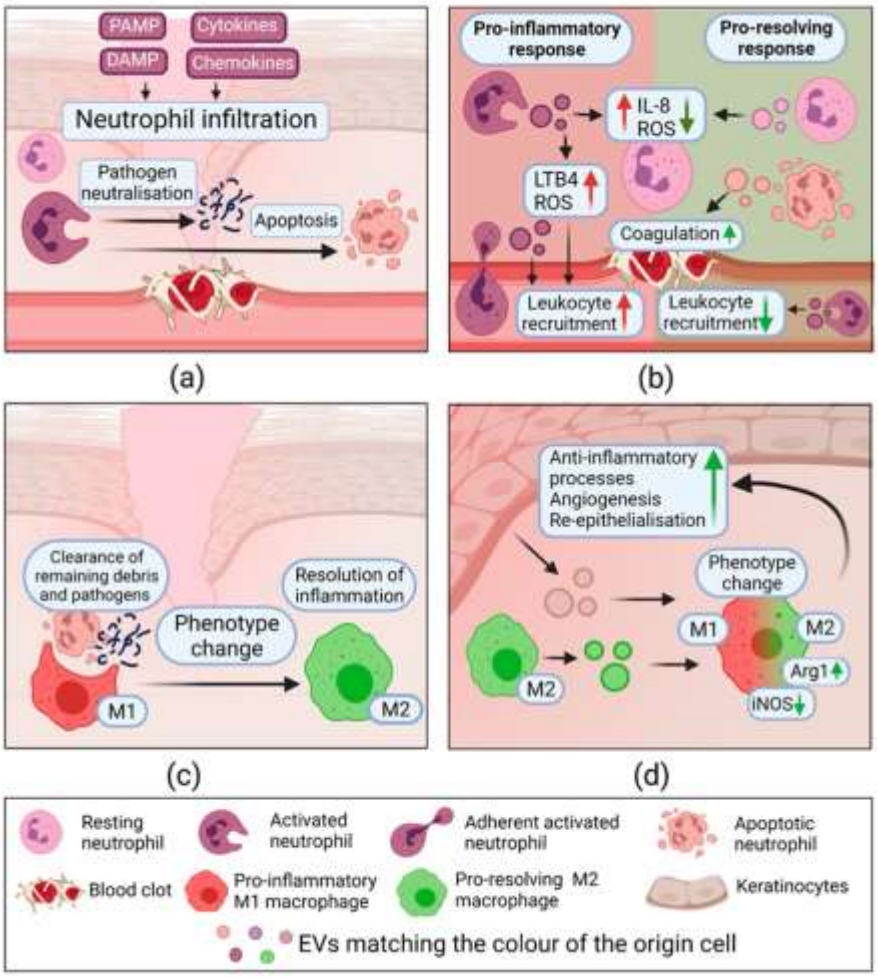

Figure 5. The role of EVs in the inflammatory phase of healthy wound healing (Narauskaité *et al.*,2021).

During the proliferative stage of wound healing, endothelial cells (ECs) that are exposed to a state of hypoxia in the injury site become activated and endothelial progenitor cells (EPCs) are recruited, promoting new vessel formation by angiogenesis and vasculogenesis, respectively (Fig.6 - a); EVs derived from saliva, macrophages, EPCs, and osteoblasts, contribute to the process of neovascularisation by promoting the critical pro-angiogenic factors. The diversity of EVs stimulates EC migration, proliferation, and vascular tube formation by transferring different cargoes (mRNA, miRNA, MMPs) (Fig.6 - b). During the proliferative stage, fibroblasts clear a path by secreting matrix metalloproteinases (MMPs) and migrate towards the wound site, where they

synthesise collagen, proteoglycans, and other granulation tissue present components (Fig.6 - c). During the phase of re-epithelialisation, EVs mediate the crosstalk between ECs, keratinocytes (KC), and fibroblasts, thus promoting the release of extracellular matrix (ECM) components, MMPs involved in the fibroblast's migration, and interleukins promoting angiogenesis, KC, and macrophage migration (Fig.6 - d) (Narauskaité *et al.*,2021).

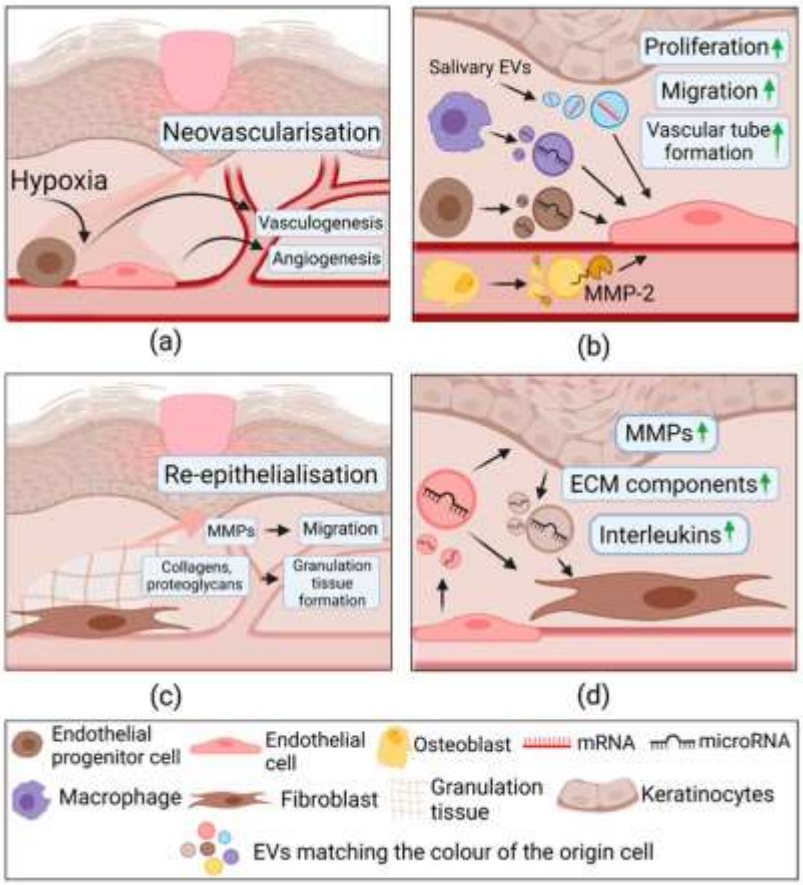

Figure 6. The role of EVs in the proliferative phase of healthy wound healing (Narauskaité *et al.*,2021).

The remodelling phase involves the reorganisation of the extracellular matrix (ECM), which is influenced by the cleavage of collagen and other ECM components of matrix metalloproteinases (MMPs), replacing type collagen III by skin collagen type I (Fig.7 –

a). The synthesis and modification of crucial ECM reorganisation components are activated by EVs derived from fibroblasts and epithelial cells (EC), which provides lysyl-oxidase-like 2 (LOXL2) enzyme, catalysing collagen crosslinking and restoring tensile strength. (Fig.7 - b) PDGF, TGF-ß, and mechanical tension initiate fibroblast differentiation to myofibroblasts, synthesising large amounts of collagen type I and promoting wound contraction. (Fig.7 – c). During fibroblast differentiation, EVs derived from keratinocytes and fibrocytes carry miRNA and induce fibroblast differentiation to myofibroblasts by increasing collagen I, alpha-SMA, and N-cadherin expression. Also, EVs released by myofibroblasts contribute to wound closure by carrying placental growth factor 1 (PGF-1) (Fig.7- d) (Narauskaité *et al*.,2021).

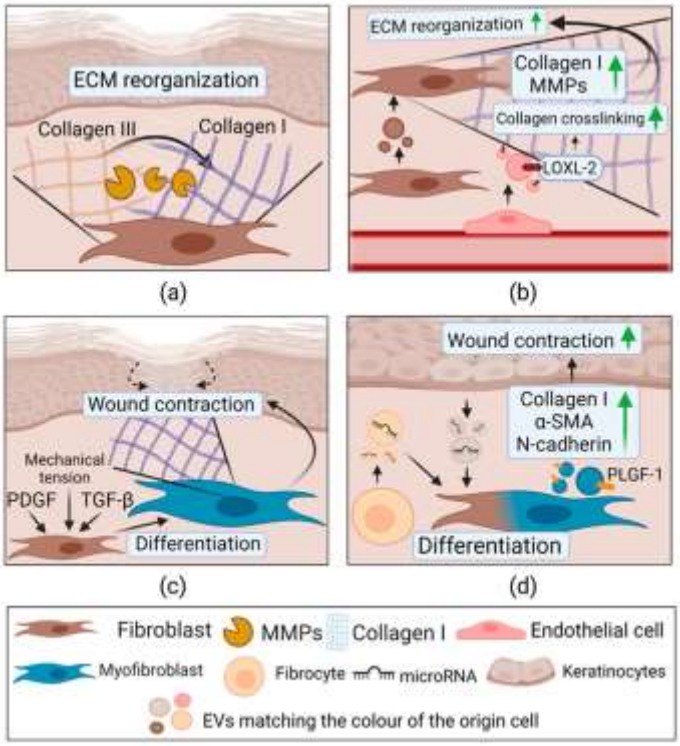

Figure 7. The role of EVs in the remodelling phase of healthy wound healing (Narauskaité *et al*.,2021).

1.3.3 Therapeutical Application of Extracellular Vesicles for Skin Wound Healing

In recent years, the use of extracellular vesicles to promote wound healing has received significant attention. Most studies on EVs in regenerative medicine have focussed their attention on the function and therapeutic properties of EVs derived from different cell sources, i.e., platelet-derived EVs (Antich-Rosselló *et al.,*2021), keratinocytes-derived EVs (Glady *et al.,*2021), oral mucosal epithelial cell-derived EVs (Sjöqvist *et al*.,2019), human trophoblasts (Young Go *et al*.,2021), but mainly, they have analysed the role of MSC-derived EVs in tissue regeneration and wound healing (Yu *et* al.,2014; Rani *et al.,*2015; Ferreira and Gomes, 2018; Yuan *et* al., 2020; Alqatawni *et al*.,2020; Barreca *et al*.,2020; Ha *et* al.,2020; Akbari *et al*.,2020; Manchon *et al*.,2021). MSC- derived EVs have therefore been identified as a potential cell-free based therapy for tissue engineering, given their advantages of being constantly produced and supplied by stem cells, they have many biological effects similar to their source stem cells, but they do not have the potential side effects such as immunological rejection or tumour formation or cell differentiation (Ma, Wang and Li,2020; Casado-Diaz *et al*.,2020); they have a more feasible storage condition than the stem cell itself, and their cargo can be easily obtained and adapted to the therapy just by changing the source cells; they can easily overcome the blood-brain barrier and also be quickly injected intravenously reaching long distances (Ma, Wang and Li,2020; Casado-Diaz *et al*., 2020). The potential for using extracellular vesicle application in wound healing and regenerative medicine, with a focus to date on mesenchymal stem cell-derived EVs, has revealed promising results. However, EVs derived from other sources, e.g., plants, fruits, and different animals, and their role in tissue regeneration and wound healing have received less attention, and their potential in regenerative medicine warrants further investigation. A recent study investigated the role of EVs-derived wound healing agents from grapefruit, showing the regenerative potential of those EVs, which increased cell viability and cell

migration while reducing intracellular ROS production in a dose dependant manner in HaCat cells and increasing tube formation capabilities of HUVEC cells (Savci *et al*.,2021). An *in-vitro* study conducted on HaCat (human keratinocytes) and HDF (human fibroblasts) assessed the potential antioxidant effect of sEVs derived from *Aloe vera* peels in the context of wound healing, showing the antioxidant activity and reduction of ROS in HaCat cells, in a dose-dependent manner, and the upregulation of mRNA expression of Nrf2, thus suggesting the A-EVs antioxidant activation and wound healing process via the Nrf2 activation (Kim *et al*.,2021). Another study explored the role of royal jelly-derived EVs (RJEVs) *in vivo* in a mouse model, demonstrating the antibacterial effects and role in the acceleration of wound healing of RJEVs (Álvarez *et al*.,2023). The role of EVs derived from biofluids of different species is still largely to be explored. Two recent studies looked at the role of extracellular vesicles derived from the plasma of olive flounder fish (*Paralichthys olivaceus*) in an *in vitro* scratch wound healing on FHM cells (epithelial cells) and *in vivo* regeneration assay in zebrafish larvae, showing the substantial cell migration and rapid closure of the open wound area (*in vitro*) and faster zebrafish larvae fin regeneration (*in vivo*) (Jayathilaka *et al*.,2022), and at the regenerative activities and wound healing of exosomes from *Streptococcus parauberis* present in olive flounder (*Paralichithys olivaceus*) (Jayathilaka *et al*.,2023). Given the promising potential of EVs derived from different animal sources, the focus of this present study is to look at the regenerative potential of Atlantic cod (*Gadus morhua L.*) serum and mucus-derived EVs, which will be explored using *in vitro* wound scratch models; moreover, cod-derived biomaterials in wound healing have mainly been explored (Kietzmann and Braun, 2006; Dort *et al.,*2012; Gudmunsdottir *et al.,* 2012; Morrow *et al.,*2016; Vieira *et al.,* 2018; Khazaeli *et al.,*2020; Kotronoulas *et al.,*2020; Kirsner *et al.,* 2020; Fiakos *et al.,*2020; Kotronoulas et al.,2021), enhancing the

interest of looking into the mechanisms and regenerative potential of Atlantic cod (*Gadus morhua)* serum and mucus derived EVs and their protein cargoes.

1.4 Aims of the Project

The present study has three key aims. The first aim is to profile EV signatures and their related deiminated protein cargoes in three species across points of the phylogeny tree, representing Mammalia, jawless fish, and Echinodermata, respectively. The second aim is to assess circulatory EVs under stress conditions and related changes in brain citrulline signatures. For this purpose, the naked mole-rat model was used to identify whether PAD-related changes in circulating EVs under hypoxic conditions could reveal any PAD-related pathways, including in the brain, linking to the unusual hypoxic resistance of this species. For this purpose, protein-interaction networks were created for citrullinated proteins to identify whether brain citrullinome changes could be correlated to circulatory EV profile and citrullinome cargo changes (See paper 4: D'Alessio *et al*., 2022). This part of the study aims to provide a platform for research on EV-based biomarkers in different animal models and increase understanding of roles for protein citrullination signatures in mediating immune and metabolic processes via EV-mediated cellular communication. The third key aim of this study is to explore the regenerative potential of EVs from cod mucus and serum in cellular wound healing models. Findings from the study will contribute to understanding how EVs and their cargoes, including via post-translational deimination, may shape immunity across phylogeny and evaluate the immune-related mechanism of EVs derived from comparative animal models with unusual immune properties in tissue regeneration.

Chapter 2 – General Materials and Methods

This chapter outlines the methodological approaches used for this thesis's different studies. Firstly, Section 2.1 - Isolation and Characterisation of EVs – will describe the general approach used following the recommendation of the Minimal Information for Studies of Extracellular Vesicles (MISEV), published by the International Society of Extracellular Vesicles (ISEV) in 2018 (Théry *et al*., 2018) and the recently 2023 updated guidelines (Welsh *et al*.,2024). Subsection 2.1.1 will explain the sample collection of the different species investigated in the study, and subsection 2.1.2 will outline the methodology used for the enrichment of EVs from sea lamprey, purple sea urchin, Atlantic cod, naked mole-rat and reindeer. Although the small-scale EV isolation protocol, adapted in our lab and based on the MISEV2018 and MISEV2023 recommendations, has been used for all the species, more details on naked mole-rat plasma-derived EVs exposed to hypoxia and normoxia, and the Atlantic cod serum and mucus EVs enrichment are outlined in more details in Chapter 4 (Section 4.2.1 – EVs isolation and characterisation) and Chapter 5 (section 5.2.1 – Cod Serum and Mucus Extracellular Vesicles Preparation, Isolation, Characterisation, and Protein Content Analysis), respectively. Moreover, this section will explain in detail other techniques used for the EVs characterisation, such as nanoparticle tracking analysis (NTA) (subsection 2.1.3), transmission electron microscopy (TEM) for assessment of EV morphology characterisation (subsection 2.1.4), while for EV surface marker characterisation by Western blotting, mentioned in subsection 2.1.5, has details of the methodology, general application of Western Blotting will be described in section 2.2. The 2.2 section also covers the assessment of PADs by Western blotting in sea lamprey, purple sea urchins, naked mole-rat and Reindeer. Section 2.3 will explain the F95 enrichment for the isolation of deiminated protein cargoes of EVs isolated from the species of interest, and section 2.4 will describe the silver staining technique for the visualisation of the whole and

deiminated EV protein cargoes in the respective biological fluid from the different species. Section 2.5, with subsections 2.5.1 and 2.5.2, explains the liquid chromatography with tandem mass spectrometry (LC-MS/MS) utilised for the analysis of deiminated protein candidates isolated by F95 enrichment and the identification of the putative deiminated protein hits. Section 2.6 explains STRING analysis and associated pathway analysis for protein-protein interaction networks related to the deiminated proteins and total proteomes. Section 2.7 describes the identification process for PADs and EVs markers sequences in the different species and the construction of neighbour-joining trees across phylogeny. Section 2.8 – Cell Culture Experiments for Wound Healing Studies – is a general explanation of the cell culture techniques adopted in this research and the different cell lines used for the pilot study on the application of cod-derived EVs in cellular models of tissue regeneration as detailed in Chapter 5, section 5.2.5. Section 2.9 of this chapter will summarise the statistical approaches for analysing the different studies in this thesis.

2.1. Isolation and Characterisation of Extracellular Vesicles

Isolation and characterisation of EVs were carried out and adapted to protocols according to the published recommendation of the Minimal Information for Studies of Extracellular Vesicles 2018-2023 (MISEV2018-2023) (Théry *et al*.,2018: Welsh *et al*.,2024), which requires a method for EV separation/enrichment that aims at either 1) high recovery/low specificity; 2) intermediate recovery/low specificity; 3) low recovery/high specificity; 4) high recovery/high specificity (still not yet achievable (Théry *et al*., 2018, Welsh *et al*.,2024)), and should report all details of the method for reproducibility; the source of EVs and the EVs preparation must be described quantitatively, and global quantification of EVs provided by either total protein amount (which can be measured by various colometric assays e.g. Bradford) or total particle

number (which can be measured by light scattering technologies such as nanoparticle tracking analysis (NTA)). For the general characterisation of EVs, at least 2-3 positive protein surface markers of EVs, including at least one transmembrane/lipid-bound protein and one cytosolic protein, must be analysed. Several methods can be used to quantify proteins to assess the presence of proteins in EV preparations. However, Western blotting is the most used (Théry *et al.,*2018).

In this study, standard approaches of sequential centrifugation and ultracentrifugation were used for EV separation/enrichment, also following and adapted to previous protocols established in our lab (Lange *et al.,*2019; Kosgodage *et al.,* 2018; Criscitiello *et al.,* 2019; Criscitiello *et* al.,2020(a,b,c); Pamenter *et al.,* 2019; Phillips *et al.,* 2020; Bowden *et al.,* 2020(a)); transmission electron microscopy (TEM) was used to assess EVs morphology (imaging of EVs by TEM was kindly carried out by Dr. Igor Kraev, Open University, Milton Keynes, UK). EVs were quantified for total particle number and assessed for size distribution profiling by nanoparticle tracking analysis (NTA). Moreover, for complete EV characterisation, two EV surface markers, Flotillin-1 and CD63, were assessed by western blotting. The whole and deiminated protein content of EVs (EV cargo) was isolated and evaluated by LC-MS/MS analysis to identify protein hits alongside gel electrophoresis followed by silver staining.

2.1.1. Sample Collection of Biological Fluids for EV Isolation

Samples of serum, plasma, coelomic fluid and mucus used in this study were kindly gifted from external collaborators as follows:

Purple sea urchin (*Strongylocentrotus purpuratus*) coelomic fluid was provided by Dr. Katherine M. Buckley, Department of Biological Sciences, Auburn University, Auburn, AL 36849, US. Coelomic fluid was isolated from three adult animals by inserting a

chilled, 20-gauge syringe into the peristomal membrane and mixed (1:1) with calcium-magnesium-free sea water (CMFSW, 460 mM NaCl, 10.73 mM KCl, 7.0 mM Na_2SO_4, 2.38 mM $NaHCO_3$, pH= 7.4), containing 30 mM EDTA. The whole coelomic fluid was centrifuged at 5000x g for 5 min to remove coelomocytes from the samples. Cell-free coelomic fluid was collected, aliquoted, and frozen at -80°C until use. All procedures were carried out according to protocols approved by the Auburn University Institutional Animal Care and Use Committee (2020) (see D'Alessio *et al*.,2021 – b).

Reindeer (*Rangifer tarandus*) plasma was kindly provided by Dr. Stefanía Thorgeirsdóttir, Institute for Experimental Pathology at Keldur, University of Iceland, Keldnavegur 3, Reykjavik, Iceland. Plasma was provided from previously isolated blood samples that had been taken from sixteen individual female reindeer – average age approximately seven years (range 1.5-12 years old) – sampled in Iceland as part of research dealing with the general health of Icelandic reindeer with specific emphasis on chronic wasting diseases (CWD) and presence of parasites. Sample collection was under the Icelandic laws and regulations on sampling from wild animals (64/1994) and licenses of the Institute for Experimental Pathology at Keldur, University of Iceland (number #0001 jt-650269-4594), approved by the central animal ethics committee in Iceland (Icelandic Food Regulation Authority, MAST Matvælastofnun). The plasma was isolated from EDTA blood samples according to standard procedures. Plasma was aliquoted at 250µL and stored at -80 °C until further use for the individual experiments (see D'Alessio *et al*.,2021 – a).

Sea lamprey (*Petromyzon marinus*) plasma was kindly provided by Dr. Jonathan P. Rast, Emory University School of Medicine, Pathology & Laboratory Medicine, Atlanta, GA, 30322, USA; Blood was collected from 7 Atlantic coast sea lamprey ammocoete larvae for the isolation of blood plasma, which was diluted in 200 µL 0.66X PBS, 50 mM EDTA.

The diluted plasma aliquots (approximately 250 µL per individual animal) were frozen at -80 °C until used for the experiment in this current study. All procedures were carried out according to protocols approved by the Emory University Institutional Animal Care and Use Committee (PROTO201700387, 2020) (see Rast *et al*.,2021).

Naked mole-rat (*Heterocephalus glaber)* plasma was kindly provided by Dr. Matthew Pamenter, Department of Biology, University of Ottawa. Naked mole rats were group-housed in interconnected multi-cage systems at 30 °C and 21% O_2 in 50% humidity and with a 12L:12D light cycle. Animals were fed fresh tubers, vegetables, fruit, and Pronutro cereal supplement ad libitum. Animals were not fasted before experimental trials. All experimental procedures were approved by the University of Ottawa Animal Care Committee (protocol #3444) under the Animals for Research Act and by the Canadian Council on Animal Care. Animals (1–2-year-old subordinate males and females weighing 40–60 g) were exposed to either 21% O_2 (normoxia) or 7% O_2 (hypoxia) for 4h. Each experimental group was comprised of 10 animals. Following treatment, the animals were sacrificed by cervical dislocation followed by rapid decapitation. Blood was collected in heparinised syringes, and plasma was extracted by spinning whole blood at 1500 rpm for 15 min. In addition to plasma, brain protein extracts from hypoxia and control-treated naked mole rats were provided. Plasma aliquots were then frozen at −80 °C until analysis. In addition to plasma, brain protein extracts from hypoxia and control-treated naked mole rats were provided. Whole brains were rapidly removed on ice, similarly frozen in liquid nitrogen, and stored at −80 °C until analysis (see D'Alessio *et al*.,2022).

Atlantic cod (*Gadus morhua L*.) serum and mucus were kindly provided by Dr. Bergljót Magnadóttir, Institute for Experimental Pathology, University of Iceland, Keldur v. Vesturlandsveg, 112 Reykjavik, Iceland. Samples were derived from experimentally

farmed Atlantic cod, hatched, and kept at the Marine Institute's Experimental Fishfarm Stadur, Grindavik, Iceland. The fish (n = 45 per tank) were reared at 7 °C, which is the average rearing temperature of adult cod. The fish were fed commercial food pellets, and a natural photoperiod (64N) was provided. Serum was obtained from blood samples collected from a caudal vessel. The blood was clotted at room temperature for 2h and then at 4 °C overnight, followed by sera collection by centrifugation at 750g for 10 min. (Magnadóttir *et al.,*2019;2020). The sera were divided into 250µl aliquots to avoid freeze-thawing cycles of individual serum samples and stored at -80 °C until further use for the current study.

2.1.2. EVs Enrichment from Biological Fluids by Differential Centrifugation

The individual purple sea urchin (*Strongylocentrotus purpuratus*) coelomic fluid, sea lamprey (*Petromyzon marinus*) serum, Atlantic Cod (*Gadus morhua L.*) serum and mucus, Naked mole-rat (*Heterocephalus glaber*) plasma and Reindeer (*Rangifer* tarandus) plasma-derived EVs, were collected using the same EV enrichment approach. EVs were prepared according to previously established small-scale preparation protocols (Fig.8) in our laboratory (Magnadóttir *et al.,*2018; Pamenter *et al.,*2019; Bowden *et al.,*2020). Biological sample aliquots from the different species were thawed on ice and diluted 1:5 in Dulbecco Phosphate Buffered Saline (DPBS, no calcium & no magnesium, Fisher Scientific) ultrafiltered using a 0.22 µm filter, before use): 100-250µl of plasma/serum/mucus/coelomic fluid (depending on how many samples and how much samples were available for each species under study) were mixed with 400µl DPBS. EVs isolation was carried out by sequential centrifugation combining low-speed centrifugation and ultracentrifugation; the EVs preparations were first centrifuged for 20 min at 4000× *g* at 4 °C to remove apoptotic bodies and aggregates. Supernatants containing the EVs were then collected and ultra-centrifuged at 100,000× *g* at 4 °C for 1h to isolate

total EVs (50-1000nm). The resulting EV-enriched pellet was resuspended with 500 µL DPBS ("washing step") and then ultra-centrifuged again for one hour at 100,000× *g* at 4 °C. The final EV-enriched pellet was resuspended in 100 µL of DPBS for further analysis. The EVs from each preparation were frozen at −80 °C until used in the procedures described below (all assessments were performed with EV preparations that had not frozen for longer than one week). More details on the EVs isolation from body fluids of each species can be found in Chapter 3, section 3.2 for EVs isolation of sea lamprey serum, purple sea urchin coelomic fluid and reindeer plasma; Chapter 4, section 4.2.2 for the isolation of EVs from naked mole-rat plasma; Chapter 5, section 5.2.1 for details on EVs isolation from Atlantic Cod serum and mucus.

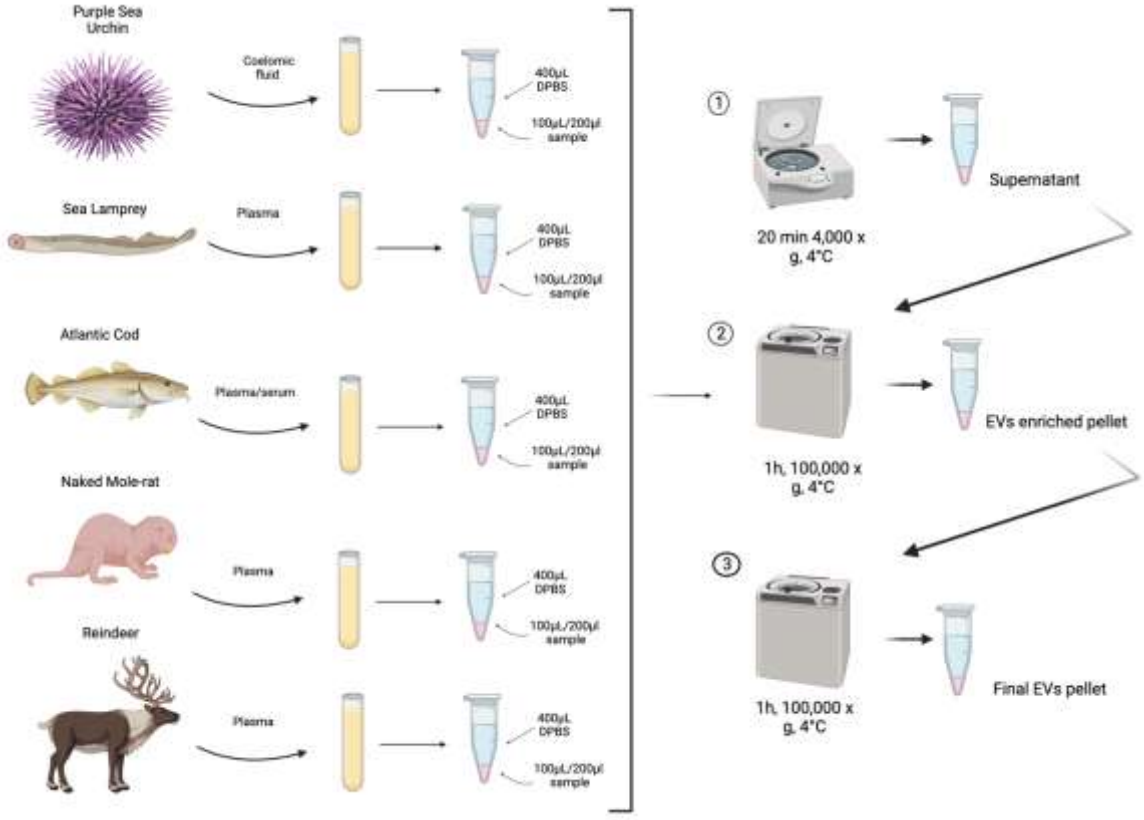

Figure 8. EVs isolation small-scale protocol preparation. Schematic representation of general small-scale EVs isolation protocol from selected taxa investigated: sea lamprey (Petromyzon marinus), purple sea urchin (Strongylocentrotus Purpuratus), reindeer (Rangifer tarandus), naked mole rat (Heterocephalus glaber), and Atlantic cod (*Gadus* morhua)—image created with BioRender.com.

2.1.3. Nanoparticle Tracking Analysis (NTA)

To determine the EV size and distribution profiles, nanoparticle tracking analysis (NTA), which is based on the Brownian motion of particles in suspension (Carr and Wright, 2008), was used and carried out using the NanoSight NS300 system (Malvern Panalytical Ltd., Malvern, UK). Before application on the NanoSight, the EV samples were diluted 1/1000 in DPBS (10 µL of EV preparation diluted in 990 µL of DPBS). The diluted EV samples were applied to the NanoSight NS300 (Malvern Panalytical, UK)

with a continuous flow through the system by a syringe pump (speed setting 50), recording four repetitive reads, 60 sec each. Particle numbers per frame were 40 to 60, and camera settings were adjusted accordingly in the range of 9 to 13, depending on the type of EV sample for recording. For post-analysis, the threshold was set at 3 or 5 but kept consistent for each species under investigation. The same measurement settings were used for EV profiling for each species' samples. Replicate histograms were generated from the recorded videos using the NanoSight software 3.0 (Malvern), representing the mean and confidence intervals of the four recordings for each sample. More details on the NTA analysis of EVs from body fluids of each species can be found in Chapter 3, section 3.2 for sea lamprey, purple sea urchin and reindeer; Chapter 4, section 4.2.2 for the isolation of EVs from naked mole-rat plasma; Chapter 5, section 5.2.1 for details on EVs isolation from Atlantic cod serum and mucus.

2.1.4 Morphological analysis of EVs by transmission electron microscopy

EVs isolates from the species under investigation were assessed for morphology using transmission electron microscopy (TEM) in collaboration with Dr. Igor Kraev from the Electron Microscopy Suite, Faculty of Science, Technology, Engineering and Mathematics, Open University. Following the thawing of isolated EV pellets (stored frozen for one week before imaging), the EVs were resuspended in 100 mM sodium cacodylate buffer (pH 7.4). One drop (~3–5 μL) of the EV suspension was placed onto a grid which held a carbon support film which had been previously glow-discharged. Following partial drying of the EV suspension, the sample was fixed for 1 min at room temperature by placing the grid onto a drop of a fixative solution (2.5% glutaraldehyde in 100 mM sodium cacodylate buffer (pH 7.0)). The grid was applied to the surface of three drops of distilled water to wash the EV sample and remove excess water using filter paper. The EVs were then stained for 1 min with 2% aqueous Uranyl Acetate (Sigma-Aldrich),

removing the excess stain with filter paper and air drying the grid. TEM imaging of EVs was carried out with a JEOL JEM 1400 transmission electron microscope (JEOL, Tokyo, Japan), operated at 80 kV, using a magnification of 30,000× to 60,000×. Recording of digital images was performed with an AMT XR60 CCD camera (Deben, UK) (D'Alessio *et al*.,2021(a)(b); Rast *et al.,*2021; D'Alessio *et al*.,2022).

2.1.5 EVs Characterisation by Western Blotting

For characterisation of serum, coelomic fluid and plasma EVs, respectively, in sea lamprey, purple sea urchin, and reindeer, the EV-specific markers CD63 (ab216130, Abcam, UK) and Flotillin-1 (ab41927) (diluted 1/1000 in TBS-T), which have been previously shown to cross-react with EVs from other taxa, besides human, were assessed here, by Western blotting, to assess putative phylogenetic conservation of these markers and cross-reactivity for these antibodies. PAD isozymes (PAD1,2,3,4 and 6; predominantly PAD2, which is the most conserved pad isozyme) were also assessed by Western blotting on plasma, coelomic fluid and serum-derived EVs as described in this chapter, section 2.2.

2.2. SDS-PAGE and Western Blotting Analysis

Sodium dodecyl sulphate polyacrylamide gel electrophoresis (SDS-PAGE) is a commonly used technique to separate a mixture of proteins, obtaining a high-resolution analytical separation of the proteins (Nowakowski, William and Petering, 2014). In this study, SDS-PAGE was carried out on plasma/serum/coelomic fluid and plasma/serum/coelomic fluid EV samples. The materials and reagents used to carry out the SDS PAGE are listed in Table 1. All samples were diluted 1:1 in denaturing 2× Laemmli sample buffer (BioRad, UK) (containing 5% 2-Mercaptoethanol, BioRad, UK) and heated for 5min at 100 °C. 1x Run buffer for SDS-PAGE was prepared using (50ml of 10x

Tris/Glycine/SDS buffer and 450ml of distilled water (dH_2O)). The samples in 2x Laemmli sample buffer were applied on 4–20% gradient Mini-PROTEAN ® TGX ™ Pre-cast Protein Gels (10 or 15 well gels, BioRad, UK); the protein standard was Precision Plus Protein Dual Color Standards (BioRad, UK; 5-10µl per gel), which is a mixture of 10 recombinant proteins in the size range of 10-250kDa, while for the samples a load-ing volume ranging from 10-30µl per samples were used. The gels were run for 50 minutes at 165 volts (V) for protein separation.

Table 1. Reagents and materials. List of reagents and materials with the respective catalogue number and company of purchase used for SDS-PAGE.

Reagent/Material	**Cat. Number**	**Company**
2x Laemmli Sample Buffer	1610737	Bio Rad UK
2-Mercaptoethanol	1610737	Bio Rad UK
10X Tris/Glycine/SDS Buffer	1610732	Bio Rad UK
4-20% Mini-PROTEAN ® TGX ™ Precast Protein Gels, 10 well, 30µl	4562093	Bio Rad UK
4-20% Mini-PROTEAN® TGX™ Precast Protein Gels, 15 well, 15µl	4561096	Bio Rad UK
Precision Plus Dual Color Standards	1610374	Bio Rad UK

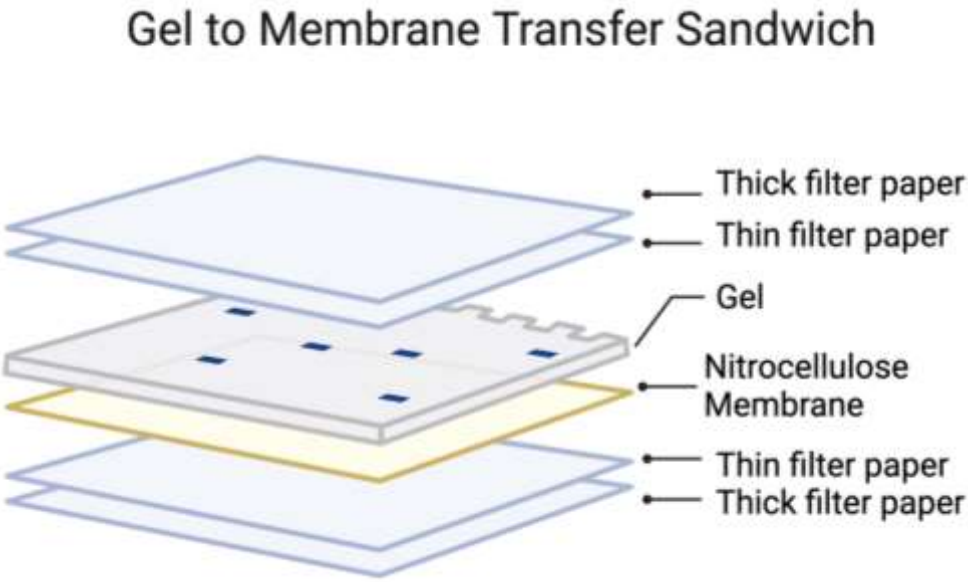

Figure 9. Schematic representation of sandwich assembly with different membranes. (Image created with BioRender.com).

Western blotting was performed at 15 V for 1 h on a Trans-Blot® SD semi-dry transfer cell (BioRad, UK). Material, reagents, and antibodies used to carry out Western blotting analysis are listed in Table 2 below:

Table 2. Materials, reagents, and primary/secondary antibodies used to carry out Western blotting.

Material/Reagents	**Cat. Number**	**Company**	**-**	**-**
10x Tris Glycine buffer	1610734	BioRad, UK		
Nitrocellulose/Filter Paper Sandwiches	1620215	BioRad, UK		
Ponceau S	010M4350	Sigma		

Bovine Serum Albumin (BSA)	SLCG0183	Sigma		
10x Tris Buffered Saline	1706435	BioRad, UK		
Tween 20, 100% Nonionic Detergent	1706531	BioRad, UK		
Amersham ECL Western Blotting Detection reagent – for 1 000cm^2 membrane	RPN2109	Cytivia		

Primary Antibodies	**Cat. Number**	**Company**	**Concentration**	**Dilution in TBS**
CD63 (rabbit-polyclonal)	ab216130	Abcam, UK	1mg/ml	1/1000
Flotillin-1 (rabbit-polyclonal)	ab41927	Abcam, UK	0.9mg/ml	1/1000
PAD1(rabbit-polyclonal)	ab181762	Abcam, UK	1mg/ml	1/1000
PAD2 (rabbit-polyclonal)	ab50257	Abcam, UK	1mg/ml	1/1000
PAD3(rabbit-polyclonal)	ab50246	Abcam, UK	1.832 mg/ml	1/1000

PAD4(rabbit-poly-clonal)	ab50332	Abcam, UK	7.2 mg/ml	1/1000
PAD6(rabbit-poly-clonal)	PA5-72059	Abcam, UK		1/1000

Secondary Anti-bodies	**Cat. Num-ber**	**Company**	**Concentra-tion**	**Dilution in TBS**
Anti-rabbit IgG H&L	ab6721	BioRad	2mg/ml	1/3000
Anti-mouse IgM H&L	ab6728	BioRad	2mg/ml	1/3000

After the proteins had been transferred to the nitrocellulose membrane, the sandwich was disassembled, the membrane stained with PonceauS (Sigma, UK) for 5 min and rinsed with distilled water to assess even protein transfer. The membrane was then blocked with 5% bovine serum albumin (BSA, Sigma, UK) in Tris-buffered saline (TBS) containing 0.1% Tween20 (BioRad, UK; TBS-T) for one hour at room temperature. Primary antibody incubation was carried out overnight at 4 °C on a shaking platform using the following antibodies: anti-human PAD1 (ab181762, Abcam, diluted 1/1000 in TBS-T), PAD2 (ab50257, Abcam, diluted 1/1000 in TBS-T), PAD3 (ab50246, diluted 1/1000 in TBS-T) and PAD4 (ab50332, diluted 1/1000 in TBS-T) PAD6 (PA5-72059, Thermo Fisher Scientific UK, diluted 1/1000 in TBS-T) antibodies, for detection of putative PAD protein homologues in whole sample and sample-derived EVs. For EVs characterisation, EVs markers CD63 (ab216130, Abcam, UK) and Flotillin-1 (ab41927) (diluted 1/1000 in TBS-T) primary antibodies were assessed by incubating the membranes with the respective antibodies overnight at 4 °C on a shaking platform. Following primary antibody incubation, the nitrocellulose membranes were washed at RT in TBS-T

for 3 × 10 min and, after that, incubated with HRP-conjugated secondary antibodies (anti-rabbit IgG, BioRad; diluted 1/3000 in TBS-T) for 1h at RT. The membranes were then washed for 4 × 10 min TBS-T, followed by one wash in TBS without Tween20 and digitally visualised, using enhanced chemiluminescence (ECL, Amersham, UK) in conjunction with the UVP BioDoc-ITTM System (Thermo Fisher Scientific, Dartford, UK).

2.3. Isolation of Deiminated Proteins Using F95 Enrichment

The focus of the study was to assess deiminated EV protein cargoes, besides total protein EV cargo, in some cases. For the identification of deiminated proteins, these were isolated from both EVs and whole biological fluids, such as serum, coelomic fluid, and plasma, depending on the species of interest. Citrullinated/deiminated proteins were enriched using the F95 pan-deimination/citrullination antibody (MABN328, Merck, UK) and the Catch and Release®v2.0 immunoprecipitation kit (Merck). The F95-antibody specifically detects proteins modified by citrullination and has been developed against a deca-citrullinated peptide (Nicholas and Whitaker, 2002). Pools of plasma/coelomic fluid/serum from individual animals (100µL plasma/coelomic fluid/serum pool) and, correspondent, EV isolates from the same individual animals (100 µL EVs pool) were used for F95 enrichment. The spin column, capture tubes and microcentrifuge tubes provided with the kit (Catch and Release®v2.0 immunoprecipitation kit (Merck)) were labelled, and the spin column snap-off bottom plug was removed and placed aside. The spin column was inserted in the capture tube, with the lid loose, and centrifuged at 2000*g* for 30s/1min to remove the resin slurry buffer. The resin was then washed twice with 400µl 1x wash buffer, the content of the capture tube was discarded, and the bottom end of the column was plugged with the snap-off bottom plug. Reagents provided with the kit were added to the column in the following order: 380 µl of 1x wash buffer, 100 µl of EVs pool (from 3-10 individuals), 10 µl of specific

antibody for immunoprecipitation (F95antibody, MAB328, Merck) and 10 µl of antibody capture affinity ligand (as recommended in the manufacturer's instructions (Fig.10 – step 1). The column top was capped with the screw-on cap, secured with parafilm and incubated at 4 C overnight using a rotating platform (Fig.10 - step 2). Thereafter, the snap-off bottom plug was removed and discarded, and the column was placed in the capture tube with a loose cap and centrifuged at 2000*g* for 1min, and the flow-through was discarded. The bound protein was eluted with 4x non-reducing (denaturing) elution buffer (Fig.10 - step 3), and the protein elute was after that diluted 1:1 in 2× reducing (containing 5% beta-mercaptoethanol, Sigma, UK) Laemmli sample buffer (BioRad, Watford, UK) (Fig.10 – step 4). Samples were kept frozen in sample buffer at−20 °C until further use for SDS-PAGE analysis, Western blotting, and in-gel digestion for LC–MS/MS analysis (carried out by service from Cambridge Proteomics, UK) (Fig.10 – step 5).

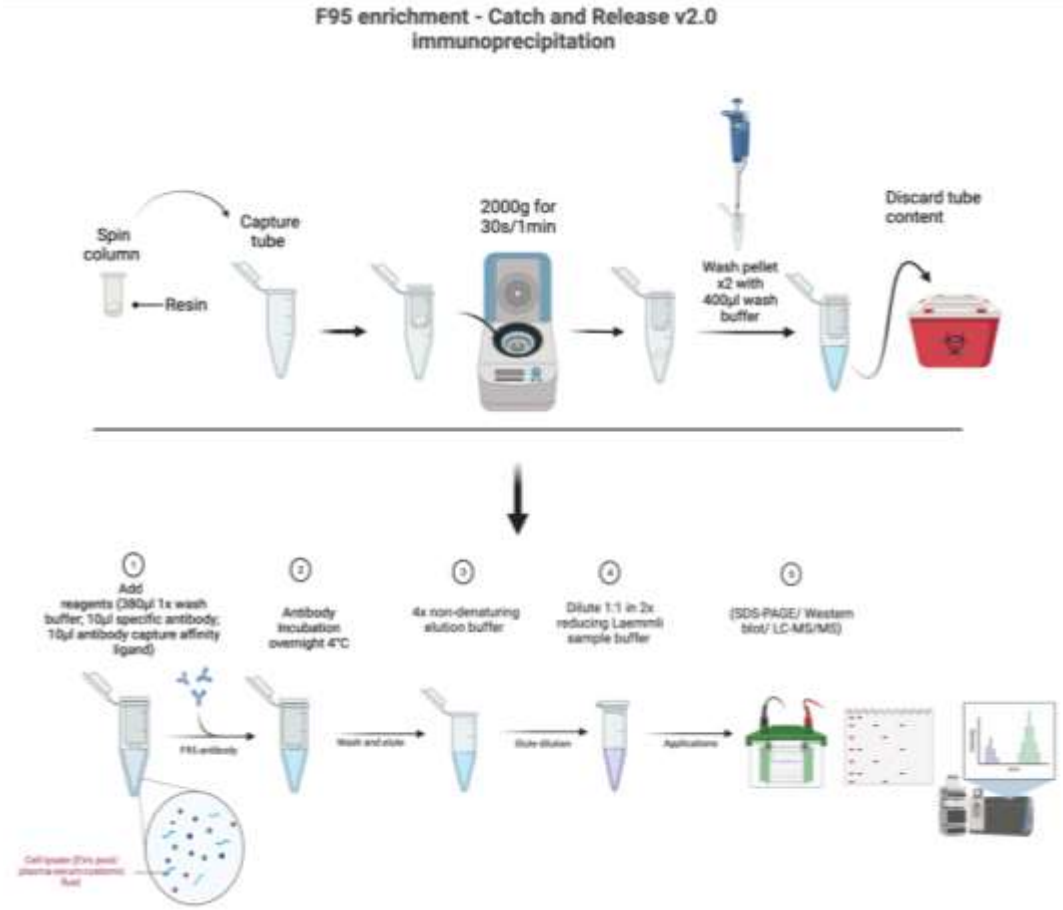

Figure 10. F95 enrichment protocol. Schematic overview of the F95 enrichment protocol (adapted from Catch and Release®v2.0 immunoprecipitation kit protocol; Merck). (Image created with BioRender.com).

2.4. Silver Staining of Total and Deiminated Proteins

SDS-PAGE (using 4–20% gradient TGX gels, BioRad, UK) was carried out under reducing conditions for the F95-enriched protein eluates from both whole plasma/serum/coelomic fluid and plasma/serum/coelomic EVs, as well as total protein cargo from EVs. Samples were diluted in denaturing 2× Laemmli sample buffer (containing 5% beta-mercaptoethanol, BioRad, UK), were heated for 5 min at 100 ˚C and run for 50 min at 165 V. The gels were then silver stained using the BioRad Silver Stain Plus Kit (1610449, BioRad, UK), according to the manufacturer's instructions. To fix two gels, a fixative solution was prepared with 60ml of distilled water, 100ml of methanol, 20 ml

of fixative enhancer and 20 ml of acetic acid. The gels were placed in a container with the fixative solution for 20 min. After the fixative step, the gels were rinsed 2x10 min with 400 ml of distilled water, and 5 min before the staining and development step, a solution of 35 ml of distilled water, 5 ml of silver complex solution, 5 ml of reduction moderator solution, 5 ml of image development reagent and 50 ml of development accelerator solution at RT, were mixed into a beaker in the order as described above. The gels were placed into the staining solution for 20 min (gels were monitored during this step to ensure bands were visible and the gels did not overstain), then transferred into a 5% acetic acid solution to stop the staining reaction for 15 min. The gels were then rinsed with distilled water for 5 minutes and visualised using a lightbox, and images were taken using a digital camera.

2.5. Liquid Chromatography-Tandem Mass Spectrometry (LC-MS/MS) Analysis for the Identification of Deiminated Protein Candidates

2.5.1 LC-MS/ MS

For the LC–MS/MS analysis of deiminated proteins (derived from a pool of 3-10 individuals), the F95-enriched protein preparations (diluted 1:1 in 2× Laemmli buffer and boiled for 5 min at 100 °C) were run 0.5 cm into a 12% TGX gel (BioRad, UK) and cut out as one band each for in-gel digestion. Liquid chromatography with tandem mass spectrometry (LC–MS/MS) (Fig.11) was carried out to identify deiminated proteins from plasma/coelomic fluid and plasma/coelomic fluid EVs (as well as the brain citrullinome enriched fractions (from naked mole-rat – see more detail in Chapter 4), as service carried out by Cambridge Proteomics (University of Cambridge, UK). In summary, the concentrated protein band (containing the F95 eluate) was excised, trypsin digested and subjected to proteomic analysis using a Dionex Ultimate 3000 RSLC

nanoUPLC (Thermo Fisher Scientific Inc., Waltham, MA, USA) system in conjunction with a QExactive Orbitrap mass spectrometer (Thermo Fisher Scientific Inc, Waltham, MA, USA). Peptide separation was performed using reverse-phase chromatography (flow rate 300 nL/min) and a Thermo Scientific reverse-phase nano Easy-spray column (Thermo Scientific PepMap C18, 2 µm particle size, 100 A pore size, 75 µm i.d. × 50 cm length). Peptides were loaded onto a pre-column (Thermo Scientific PepMap 100 C18, 5 µm particle size, 100 A pore size, 300 µm i.d. × 5 mm length) from the Ultimate 3000 autosampler (0.1% formic acid for 3 min, flow rate 10 µL/min). Afterwards, peptides were eluted from the pre-column onto the analytical column. The linear gradient employed was 2–40% solvent B (80% acetonitrile, 20% water + 0.1% formic acid) for 30 min. An Easy-Spray source (Thermo Fisher Scientific Inc.) was used to spray the LC eluant into the mass spectrometer. An Orbitrap mass analyser (set at a resolution of 70,000) was used to measure all m/z values of eluting ions, scanned between m/z 380 and 1500. Fragment ions were automatically isolated and generated using data-dependent scans (Top 20) by higher-energy collisional dissociation (HCD, NCE: 25%) in the HCD collision cell. The resulting fragment ions were measured using the Orbitrap analyser set at a resolution of 17,500. Singly charged ions and ions with unassigned charge states were excluded from selection for MS/MS, employing a dynamic exclusion window of 20 s. In cases where the total protein content of EVs was assessed (for cod EVs from serum and mucus), a similar procedure for protein hits was carried out for total isolated proteins.

2.5.2 Protein Hits Identification

The data were processed post-run using Protein Discoverer (version 2.1., Thermo Scientific). All MS/MS data were converted to mfg files. The files were submitted to the Mascot search algorithm (Matrix Science, London, UK) to identify deiminated protein hits. A search was conducted against a species-specific or a wider tax on specific

UniProt database (Fig.11). Search for protein hits identified in purple sea urchin (*Strongylocentrotus purpuratus*) was conducted against the specific database (CCP_*Strongylocentrotus_purpuratus Strongylocentrotus_purpuratus*_20210510; 34,423 sequences; 23,911,872 residues) and a common Echinoidea UniProt database CCP_Echinidea Echinidea_20210511 (38,194 sequences; 24,939,030 residues). An additional search was conducted against a common contaminant database (cRAP 20,190,401; 125 sequences; 41,129 residues) for all species under investigation. Search for deiminated protein hits identified in lamprey (*Petromyzon marinus*) was conducted against a common UniProt database against Atlantic sea lamprey (CCP_Petromyzon_marinus_20201214 (11407 sequences, 4607059 residues). Deiminated protein hits identified in reindeer (*Rangifer tarandus*) were searched against a common UniProt database against Artiodactyla (CCP_ Artiodactyla Artiodactyla_20201013; 840,112 sequences; 473,198,619 residues). Deiminated protein hits identified in naked mole-rat (Heterocephalus glaber) were searched again in the UniProt database against the naked mole-rat protein database CCP_*Heterocephalus_glaber*_20190911 (21,449 sequences: 10,466,552 residues). In addition, a common contaminant database was also searched (cRAP 20190401; 125 sequences; 41,129 residues). Furthermore, total protein content hits of EVs from cod mucus and sera were assessed against species-specific (*Gadus morhua*) database: Gadus_morhua_20190405 (1283 sequences; 308668 residues), with settings at significant threshold $p < 0.05$ and cut off at Ions score 15; or against all teleost UniProt database. Deiminated protein hits identified in the species under study for each analysis were selected from the raw list of proteins, excluding human proteins, other species proteins and contaminants. Proteins identified in the F95 enrichment and whole protein isolation were organised on a table with the Protein ID and Protein name, species, and common name of the species, matches and sequences and total score ($p<0.05$) - †Ions score was -10*Log(P), where P is the probability that the

observed match is a random event. Individual ions scores > *n* indicate identity or extensive homology (p>0.05). Protein scores are derived from ions scores as a non-probabilistic basis for ranking protein hits.

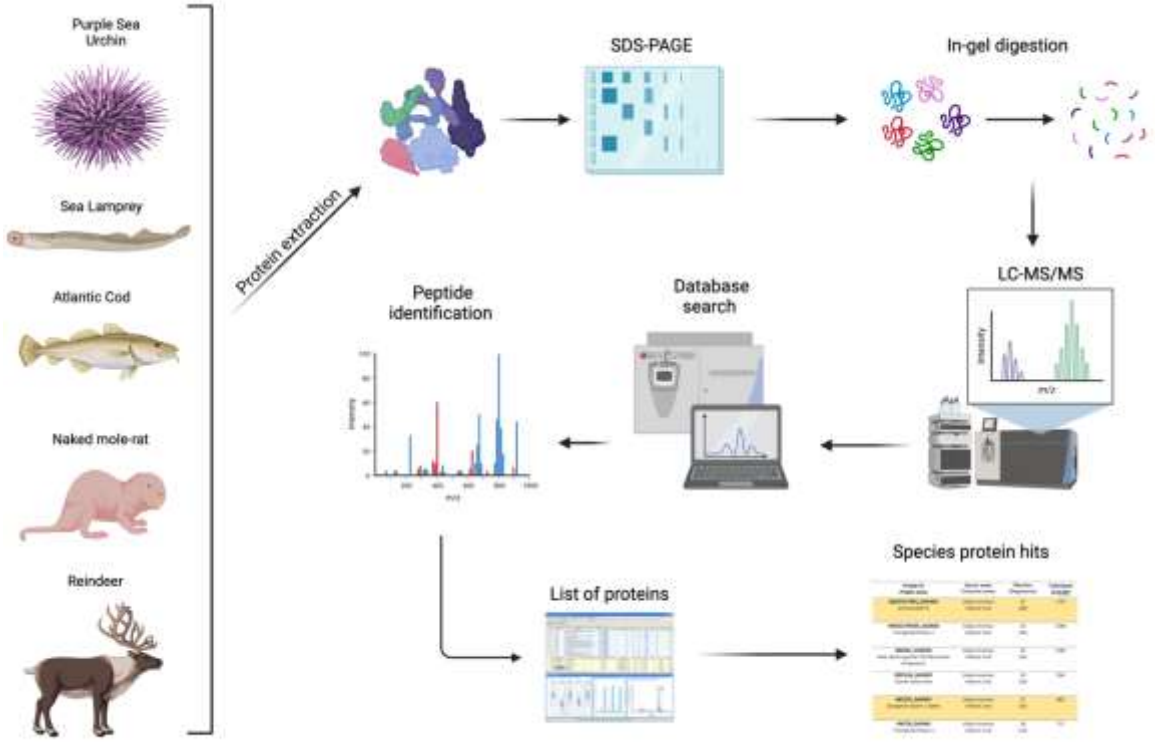

Figure 11. Liquid chromatography-tandem mass spectrometry (LC-MS/MS) analysis flow. Identification of deiminated proteins in purple sea urchin, sea lamprey, Atlantic cod, naked mole-rat, and reindeer. Deiminated proteins were extracted from the animal's whole samples and samples derived from EVs by F95 immunoprecipitation and subjected to LC-MS/MS. Protein hits obtained were reorganised in a table for further analysis. (Image created with BioRender.com).

2.6. Protein-Protein Interaction Network Analysis

To predict and identify putative protein–protein interaction networks associated with the deiminated proteins and total proteomes from the individual species' plasma/coelomic fluid and plasma/serum/coelomic fluid EVs, STRING analysis (Search Tool for the Retrieval of Interacting Genes/Proteins; https://string-db.org/) was performed.

Protein networks were generated based on protein names, and the function of "search multiple proteins" was applied in STRING (https://string-db.org/) using the specific or representative animal under study (where no specific database was available) protein database. Parameters applied in STRING were "basic settings" and "medium confidence". Nodes connected with colour lines represent the following evidence-based interactions for the network edges: "known interactions" (these are based on experimentally determined curated databases), "predicted interactions" (these are based on gene neighbourhood, gene co-occurrence, gene fusion, via text mining, protein homology or co-expression). Gene ontology (GO) and KEGG (Kyoto Encyclopaedia of Genes and Genomes) pathways for the deiminated protein networks were further assessed in STRING and are highlighted by colour coding. STRING was accessed from March 2021 to October 2023.

2.7. Neighbour Joining Tree Analysis of PAD Isozyme Protein Sequences and EVs Surface Markers.

Previously known PAD isozyme protein sequences for Artiodactyla (white-tailed deer (*Odocoileus virginianus texanus)*, red deer (*Cervus elaphus hippelaphus))* and sea lamprey (*Petromyzon marinus)* were used for reconstruction of neighbour joining tree: protein sequences were compared with human (*Homo sapiens)* PAD isozymes, teleost fish (*Dicentrarchus labrax* (Sea Bass) and *Oncorhynchus mykiss* (Rainbow trout)), reptilian (Alligator (*Alligator missippiensis))*, amphibian (African clawed frog (*Xenopus laevis*), and cow (*Bos taurus)*. The sequences used for the neighbour-joining tree using Clustal Omega (**https://www.ebi.ac.uk/Tools/msa/clustalo/)** are listed in Table 3 below:

Table 3. PAD sequences were retrieved from the NCBI (National Centre for Biotechnology Information) database.

Species	**Accession number**
Petromyzon marinus (Lamprey)	PAD2-like (XP_032825570.1)
Xenopus laevis (African clawed frog)	PAD2 homologue NP_001080369.1
Alligator missippiensis (Alligator)	PAD1 XP_006259278.3 PAD2 XP_019355592.1 PAD3 XP_014457295.1
Dicentrarchus labrax (Sea Bass)	PAD protein CBN80708.1
Oncorhynchus mykiss (Rainbow trout)	PAD protein CAX45844.1 PAD type-2isoform X2 XP_021425236.1

Bos taurus (Cow)	PAD1 (NP_001094742.1) PAD2 (NP_001098922.1) PAD3 (XP_010800991.1) PAD4 (NP_001179102.1) PAD6 (XP_002685843.1)
Odocoileus virginianus texanus (White tailed deer)	PAD1 (XP_020733655.1) PAD2 (XP_020733656.1) PAD3 (XP_020733658.1) PAD4 (XP_020754850.1) PAD6 (XP_020754849.1)
Cervus elaphus hippelaphus (Red deer)	PAD1 (OWK12974.1) PAD4 (OWK12644.1)
Homo sapiens (Human)	PAD1 (NP_037490.2) PAD2 (NP_031391.2) PAD3 (NP_057317.2) PAD4 (NP_036519.2) PAD6 (NP_997304.3)

No PAD sequences were reported for *S. purpuratus*; a search for PAD orthologs was conducted using BLAST searches for *S. purpuratus* and other echinoderms on NCBI (https://www.ncbi.nlm.nih.gov/) and Echinobase (https://www.echinobase.org), was conducted. Following this, the *S. purpuratus* genome and the other available echinoderm genome assemblies were further interrogated for PAD/PAD-like genes based on conservation in PAD protein domains using tBLASTn searches (https://blast.ncbi.nlm.nih.gov/Blast.cgi?PROGRAM=tblastn) with human PAD protein sequences (PAD1–4, PAD6). Any resultant scaffold matches were then used to predict PAD/PAD-like sequences using the FGENESH gene finder tool in Softberry (http://www.softberry.com), and predicted PAD/PAD-like protein sequences were checked using BLASTp searches for accuracy of identification. Available Echinodermata transcriptional data (e.g., expressed sequence tag and transcriptome shotgun assembly datasets) were also checked using the same approach to detect any potential expression of PAD/PAD-like protein genes to account for any possible missing data in any of the current echinoderm genome assemblies. One scaffold match for the mottled brittle starfish *Ophionereis fasciata* (GCA_900067615) was found while searching against all other echinoderm genome assemblies, and using the FGENESH gene fold match, we were able to predict protein from *O. fasciata* which revealed identity matches with putative PADs in Cyanobacteria (See section 3.5, Table 5 for more details). This highlights possible horizontal gene transfer from cyanobacteria to Chordata (D'Alessio *et al*., 2021 (b)) and is further analysed in the discussion.

Table 4. EVs markers sequences retrieved from the NCBI database.

EVs Marker	Species	Accession N.
Flotillin-1	• *Strongylocentrotus purpuratus* • *Petromyzon marinus* • *Gadus morhua* • *Heterocephalus glaber* • *Odocoileus virginianus texanus* • *Cervus elaphus* • *Homo Sapiens*	• >XP_0308532323 • >XP_032820327 • >XP_030202492.1 • >XP_004847119.1 • >XP_020744507.1 • >XP_043763965.1 • >AAC35387.1
CD63	• *Strongylocentrotus purpuratus* • *Petromyzon marinus* • *Gadus morhua* • *Heterocephalus glaber* • *Cervus elaphus* • *Odocoileus virginianus texanus* • *Homo sapiens*	• >XP_030851019.1 • >XP_032801945.1 • >XP_030212776.1 • >XP_004861432.1 • >XP_043746766.1 • >XP_020764156.1 • >AHI51903.1(partial)

The protein sequences for extracellular vesicle markers used for the EV characterisation, Flotillin-1 and CD63, were retrieved from NCBI database for the species under study: purple sea urchin (S*trongylocentrotus purpuratus*), sea lamprey (*Petromyzon marinus*), Atlantic cod (*Gadus morhua*), White-tailed deer (*Cervus elaphus*) and Red deer (*Odocoileus virginianus texanus*), as no specific sequence were present for Reindeer (*Rangifer tarandus*) (Table 4). Species sequences were submitted alongside human sequences to Clustal Omega (https://www.ebi.ac.uk/Tools/msa/clustalo/) for the reconstruction of the neighbour-joining tree (See Chapter 3, section 3.5).

2.8 Cell Culture Experiments for Wound Healing Studies

This section reports the different cell lines and cell culture techniques used to assess the role of EVs derived from serum and mucus of Atlantic cod (*Gadus morhua)* in *in-vitro* wound healing models. The different materials and reagents used to perform those techniques are listed in Table 5 below:

Table 5. List of reagents and materials used for cell culture and wound healing experiments.

Reagent/Material	**Cat. Number**	**Company**
10ml Serological Pipette bulks 20 bags of 25	F110127	Gilson
5ml Serological Pipette bulks 20 bags of 25	F110125	Gilson
Biocat 120ml BAMBANKER SERUM-FREE CELL FREEX-ING MEDIUM	13109155	Fisher Scientific
DMEM, high glucose, Gluta-MAX™ Supplement	10566016	Thermo Fisher Scientific
Corning™ Costar™ 12-well Clear TC-treated Multiple Well Plates, Individually Wrapped, Sterile	10253041	Fisher Scientific
Nunc™ 15ml Conical Sterile Polypropylene Centrifuge Tubes	339650	Thermo Fisher Scientific

Nunc™ Cell-culture Treated multidishes	140685	Thermo Fisher Scientific
Nunc™ EasYFlask™ Cell culture Flasks (T25)	156340	Thermo Fisher Scientific
Nunc™ EasYFlask™ Cell culture Flasks (T75)	156499	Thermo Fisher Scientific
Fisherbrand™ Externally and Internally Threaded Cryogenic	117839	Fisher Scientific
Gibco™ Penicillin-Streptomycin-Glutamine (100X)	12090216	Fisher Scientific
Gibco™ Trypsin- EDTA (0.25%) phenol red	11560626	Fisher Scientific
MP Biomedicals Fetal Bovine Serum (FBS)	15799170	Fisher Scientific
Falcon 50ml Conical Centrifuge Tubes	10788561	Fisher Scientific

Overall, three different cell lines were utilised in the current study for pilot assessment of the potential of EVs derived from Atlantic codfish biological fluids (serum and mucus) to enhance wound healing. The initial experiments were performed using mouse fibroblasts, and thereafter, for a more direct translation to humans, experiments were carried out on human keratinocytes and fibroblasts.

3T3-L1 Mouse Fibroblasts cell line (ATCC CL-173) originates from a mouse embryo. It was initially used in this pilot study to assess cod serum-derived EVs' functionality in tissue regeneration. This cell line was obtained by the University of Westminster cell bank, and passage number 1 was started at the initial thawing of the provided aliquot. Cells were cultured in a T75 flask (ThermoFisher Scientific), according to the manufacturer's protocol, in 1x DMEM (Gibco™) containing 10% FBS (MP Biomedical Fetal Bovine Serum, Fisher Scientific) and 1% Penicillin-Streptomycin (Gibco™) until 70-80% confluency was reached. After that, the cells were seeded into a 12-well plate for wound scratch assay in the presence of EVs derived from cod biofluids (more method details in Chapter 5.3.3.1).

The Immortalised Human Keratinocytes (HaCat) cell line was used for an initial pilot study of the potential of cod serum EVs in regeneration translatable into humans, available from the University of Westminster cell bank (ATCC n. PCS-200-011). General cell culture procedures followed the manufacturer's recommendation (Thermo Fisher). Passage number 1 was counted after thawing the initial aliquot. This pilot assessment formed the basis of a more extensive investigation with a newly obtained cell line and culture (human dermal fibroblasts, adult - Cat. No. C-013-5C; GIBCO), where all passages were accurately recorded. Human immortalised Keratinocytes were cultured in a T75 flask (Thermo Scientific) in 1x DMEM (Gibco™) containing 10% FBS (MP Biomedical Fetal Bovine Serum, Fisher Scientific) and 1% Penicillin-Streptomycin (Gibco™) until 70-80% confluency and then seeded into a 12-well plate for optimisation of the wound scratch assay in the presence of EVs derived from cod biofluids (more method details in Chapter 5.3.3.1).

Human Dermal Fibroblast, adult (HDFa)cells (Cat. No. C-013-5C; GIBCO), are primary human dermal fibroblasts isolated from adult skin, purchased from

ThermoFisher Scientific and cultured according to the manufacturer's recommendation. This cell line was used to study the effects of cod EVs in scratch assay mimicking regeneration, as they represent the main functional component of the tissue from which they are derived. Cells were cultured in a T75 flask (Thermo Scientific) in 1x DMEM (Gibco™) containing 10% FBS (MP Biomedical Fetal Bovine Serum, Fisher Scientific) and 1% Penicillin-Streptomycin (Gibco™) until 70-80% confluency and then seeded into a 12-well plate for wound scratch assay in the presence of EVs derived from cod biofluids (more method details in Chapter 5.3.3.1).

Primary cells are cells taken directly from living tissue and established for growth *in vitro*. These cells have undergone very few populations doubling. Therefore, they are more representative of the main functional component of the tissue from which they are derived compared to continuous (immortalised) cell lines, making primary cells a more representative model for the *in vivo* state.

2.8.1 In Vitro Scratch Wound Healing Assay

Migration of mouse fibroblasts (3T3-L1), human immortalised keratinocytes (HaCat), human dermal fibroblasts, and adult (HDFa) cells were assessed using a wound healing scratch assay. Cells were seeded, following optimisation of protocols (See Appendix 1), into a 12-well plate (Thermo Fisher) at a concentration of 2 x 10^6 cells/well and cultured in media containing 10%FBS and 1% penicillin-streptomycin to nearly confluent cell monolayers (90%). Then, a linear scratch was generated in the monolayer with a sterile 200µl plastic pipette tip. Any cellular debris was removed by washing the well with phosphate buffer saline (PBS). Fresh DMEM medium was added to a set of three wells (control group), and EVs isolated from cod (*Gadus morhua*) serum/mucus (for details on EV concentration/quantity, see Chapter 5.2.5) were resuspended with DMEM and added to a set of three wells (treatment group). Images were taken using

EVOS FL Auto Imaging Systems microscopy (Thermo Fisher Scientific) at different time points, following optimisation of time points for the scratch closure, with a 4x objective.

2.8.2 Immunocytochemistry

Immunocytochemistry (ICC) detects and visualises proteins or antigens in cells using antibodies that specifically recognise the target of interest. The antibody is directly or indirectly linked to a reporter, such as a fluorophore or enzyme. The reporter gives rise to a signal, such as fluorescence or colour from an enzymatic reaction, which can be detected under a microscope (The Human Protein Atlas, no date). Reagents and materials used for the ICC technique are reported in Table 6 below, together with primary and secondary antibodies used to assess immunofluorescence protein changes in human dermal fibroblasts and keratinocyte cell lines for *in vitro* wound healing pilot study (more details on the protocol and cell line used are reported in Chapter 5, section 5.2.6).

Table 6. List of reagents, materials and used for immunocytochemistry.

Reagent/Material/Antibodies	**Cat. Number**	**Company**
Gibco™ PBS, pH 7.4	10010023	Thermo Fisher Scientific
Glycine (White Crystals or Crystalline Poweder), Fisher BioReagents™	10467963	Fisher Scientific
Paraformaldehyde Solution 4% in PBS	J19943.K2	Thermo Fisher Scientific
DAPI Solution (1mg/ml)	62248	Thermo Fisher Scientific
Gibco™ PBS, pH 7.4	10010023	Thermo Fisher
Bovine Serum Albumin (BSA)	SLCG0183	SLCG0183

Primary/Secondary Antibodies	**Cat. Number**	**Company**	**Dilution**
Recombinant Anti-FGF2 antibody [EPR20145-219]	ab208687	Abcam	1/500
Recombinant Anti-Vimentin antibody [EPR3776]	ab92547	Abcam	1/500
Goat Anti-Rabbit IgG H&L (Alexa Fluor® 488)	ab150077	Abcam	1/200 – 1/1000

The application of ICC in the current study was used to assess changes in the expression of Vimentin and FGF-2 proteins, which are involved in the process of wound healing in human fibroblasts and keratinocytes after scratch injury in the absence and presence of cod serum/mucus derived-EVs. Human Dermal Fibroblast, adult (HDFa), (Cat. No. C-013-5C; GIBCO), cells were seeded on a 12well plate and once reached confluency, were fixed at room temperature for 10min with 4% Paraformaldehyde in PBS (pH 7.4) (Thermo Fisher), washed three times with ice-cold PBS and then incubated for 10min with PBS containing 0.2% Triton X-100 for permeabilisation. After 10 min, wells containing cells were rinsed with PBS for 5 min x 3 times. Cells were incubated

with blocking buffer (1% BSA + 22.52 mg/ml glycine in PBST) for 30min and after incubated with primary antibodies (Anti-Vimentin and Anti-FGF2, 1/500) diluted in 1%BSA+PBST overnight at 4 °C. Following primary antibody incubation, the blocking solution was removed, and the cells were washed three times, 5 minutes each wash, with PBS. Secondary antibody Goat Anti-Rabbit IgG H&L (Alexa Fluor 488, ab150077) was diluted 1/1000 in 1% BSA in PBST and incubated for 1h at room temperature, left in the dark. After the incubation, cells were washed three times with PBS, in the dark, and incubated for 1min with 0.1/1 mg/ml of DAPI solution. The solution was removed, cells rinsed with PBS and visualised with EVOS. ICC protocol was adapted and optimised for this experiment based on a general ICC protocol.

2.9 Statistical Analysis

The generation of NTA curves was carried out using the Nanosight 3.0 software (Malvern, UK). The NTA curves show the mean (black line) and standard error of the mean (SEM), and the confidence intervals are indicated (red line). Protein–protein interaction networks were generated using STRING (https://string-db.org/), applying basic settings and medium confidence. Images obtained from scratch assays were analysed using ImageJ software. Images at different time points were uploaded to the software, and using the freehand selection function, the gap area was outlined and measured. Data obtained from the wound gap analysis were then inserted into GraphPad Prims 10 to generate histograms, and a one-way ANOVA test was employed for the statistical analysis; significance was considered as $p \leq 0.05$. Graphs presenting EV numbers, modal numbers, and densitometry analysis results from western blots were created in GraphPad Prism 10; densitometry of Western blots was carried out using ImageJ.

Chapter 3 – Extracellular Vesicles Signatures and Deiminated Protein Cargo Across Three Points in the Phylogeny Tree – Insights from Echinoderms, Jawless Vertebrates, and Mammals

3.1. Introduction

In this study, the unique extracellular vesicle signatures and protein cargo, alongside their deimination signatures, are being explored for the first time in three distinct species: the purple sea urchin (*Strongylocentrotus purpuratus*), the sea lamprey (*Petromyzon marinus*), and the reindeer (*Rangifer tarandus*) (D'Alessio et al., 2021(a); D'Alessio et al., 2021(b); Rast et al., 2021). The selected species represent pivotal positions in the phylogenetic tree (the purple sea urchin represents invertebrates (phylum Echinodermata, order Echinoida), the sea lamprey represents an ancient lineage of jawless fish (phylum Chordata, order Petromyzontiformes), and the reindeer represents mammals (phylum Chordata, order Artiodactyla), and their unique immunological characteristics make them compelling model organisms for comparative analysis. This study offers fresh insights into the post-translational regulation of pathways involved in immunity and metabolism across different phylogenetic tree branches. By using these species as reference points, the research seeks to enhance our understanding of the roles of post-translational modifications in the functional diversification of conserved proteins throughout evolution. This research sheds light on the intricate mechanisms of post-translational modifications in various species and underlines their significance in the potential diversification of proteins involved in immunity and metabolism. Thus, this research journey delves into the evolutionary history by examining the signatures of extracellular vesicles, protein cargo, and deimination signatures, providing a deeper understanding of biological processes across diverse species.

Strongylocentrotus purpuratus (Purple Sea urchin)

The purple sea urchin, scientifically known as *Strongylocentrotus purpuratus*, is a marine invertebrate belonging to the phylum Echinodermata. It is primarily found along the eastern side of the Pacific Ocean, spanning from Mexico to Alaska, and is commonly located in intertidal and near-shore subtidal waters (Sodergren *et al.,* 2006; Amir *et al.,* 2020). Unlike many other organisms, echinoderms exhibit an extensive lifespan, ranging from 5 to over 100 years. This peculiarity is attributed to their lack of discernible signs of cellular senescence and their deviation from the conventional ageing process (Amir *et al.,* 2020). Sea urchins hold significant importance as study subjects in developmental biology, particularly in research areas concerning regeneration and ageing. Analysis of their genome sequence has provided valuable insights into their immune responses and further solidified their connection to vertebrates (Sodergren *et al.,* 2006; Smith and Kroh, 2013). The immune system of sea urchin mirrors that of vertebrates, consisting of two lines of defence: a physical/chemical barrier and a secondary barrier composed of humoral factors. This prompts a humoral response, activating phagocytic cells, antimicrobial agents, and an inflammatory reaction (Chiaramonte and Russo, 2015).

Additionally, sea urchins possess an ancient complement activation system like the one possessed by vertebrates. They also feature an expanded repertoire of pattern recognition receptors encoded within their genome and a distinctive array of immune effector proteins. The sea urchin's capacity to thrive in challenging conditions and adapt to diverse marine environments is likely attributed to its intricate and advanced immune system. Consequently, comprehending the role of post-translation deimination facilitated by Peptidylarginine deiminases (PADs) and PAD homologues (such as arginine deiminase, ADI) may shed light on different immune mechanisms, potentially including

those related to symbiosis with bacteria. This became evident during the study, as no homologue of sea urchin PAD was identified (D'Alessio *et al.,* 2021).

Petromyzon marinus (Sea lamprey)

The sea lamprey (*Petromyzon marinus*) is an ancient jawless vertebrate that diverged from the lineage leading to humans approximately 500 million years ago (Kuraku and Kuratani, 2018). Native to the Northern Atlantic, sea lampreys have played a pivotal role as a model in the study of vertebrate developmental evolution (York and McCauley, 2020). Distinguishing itself from jawed vertebrates, the sea lamprey possesses a unique adaptive immune system characterised by the absence of immunoglobulins, instead relying on three types of variable lymphocyte receptors (VLRs) (Bohem et al., 2018). Additionally, its complement system displays distinct features compared to jawed vertebrates (Matshushita, 2018). Due to its phylogenetic position, the lamprey holds significant importance as a model species for evaluating the conservation and divergence of vertebrate traits (Xu *et al.,* 2016; York and McCauley, 2020).

Rangifer tarandus (Reindeer)

The reindeer (Rangifer tarandus), also known as caribou in North America, belongs to the mammalian order Artiodactyla within the family Cervidae. Throughout their evolution, reindeer have developed specific and extraordinary biological traits related to fat metabolism, alterations in their internal biological clock, minimal heat dissipation, and a low resting metabolic rate (Lin *et al.,* 2019). Nevertheless, these features' underlying molecular and genetic mechanisms remain largely unexplored (Lin *et al.,* 2019; Weldenegodguad *et al.,* 2020). The genome of the reindeer has been successfully sequenced (Taylor *et al.,* 2019), and investigations into its genetic diversity and mitochondrial DNA have been conducted among Alaskan, Siberian, Scandinavian reindeer,

and wild caribou populations (Cronin *et al.,* 2006). According to the IUCN Red List of Threatened Species (2016), reindeer have been categorised as a vulnerable species due to a decrease in their numbers, potentially linked to shifts in their habitat and their susceptibility to chronic wasting disease (CWD), a fatal neurodegenerative ailment (William and Young, 1980; Moore *et al.,* 2016). Furthermore, it is notable that *R. tarandus* may serve as a carrier for various zoonotic diseases, including those caused by parasites, bacteria, and viruses (Palmer *et al.,* 2004; Tryland *et al.,* 2018; Pollard *et al.,* 2018; Sanchez Romano *et al.,* 2019; Palmer *et al.,* 2021). Deers have recently been identified as novel reservoir hosts for SARS-CoV-2 (Palmer *et al.,* 2021).

3.2 Extracellular Vesicles Signatures Across Species

Extracellular vesicle characterisation by Nanoparticle Track Analysis (NTA) in purple sea urchin, sea lamprey, and reindeer revealed similar EV size distribution, albeit with some variations between species: EVs isolated from coelomic fluid of purple sea urchin, showed a population of EVs poly-dispersed in the range of 30-300nm, with the majority of small EVs (exosome) in the range of 50-150nm and larger EVs (microvesicles) up to 300nm (Fig.12). Lamprey and reindeer plasmas showed a more similar EV population distribution among the two species, between 40-500nm, with the majority of EVs in the range of 70-300nm for lamprey (Fig.13) and 100-250nm for reindeer (Fig.14). EVs characterisation in the three species was further assessed by transmission electron microscopy and surface markers confirmed by western blotting, which showed positive for the phylogenetically conserved EVs-specific markers CD63 and Flotillin-1(Fig.12,13,14), meeting the minimum requirements for EV characterisation by the International Society for Extracellular Vesicles (ISEV) research (Théry et al.,2018).

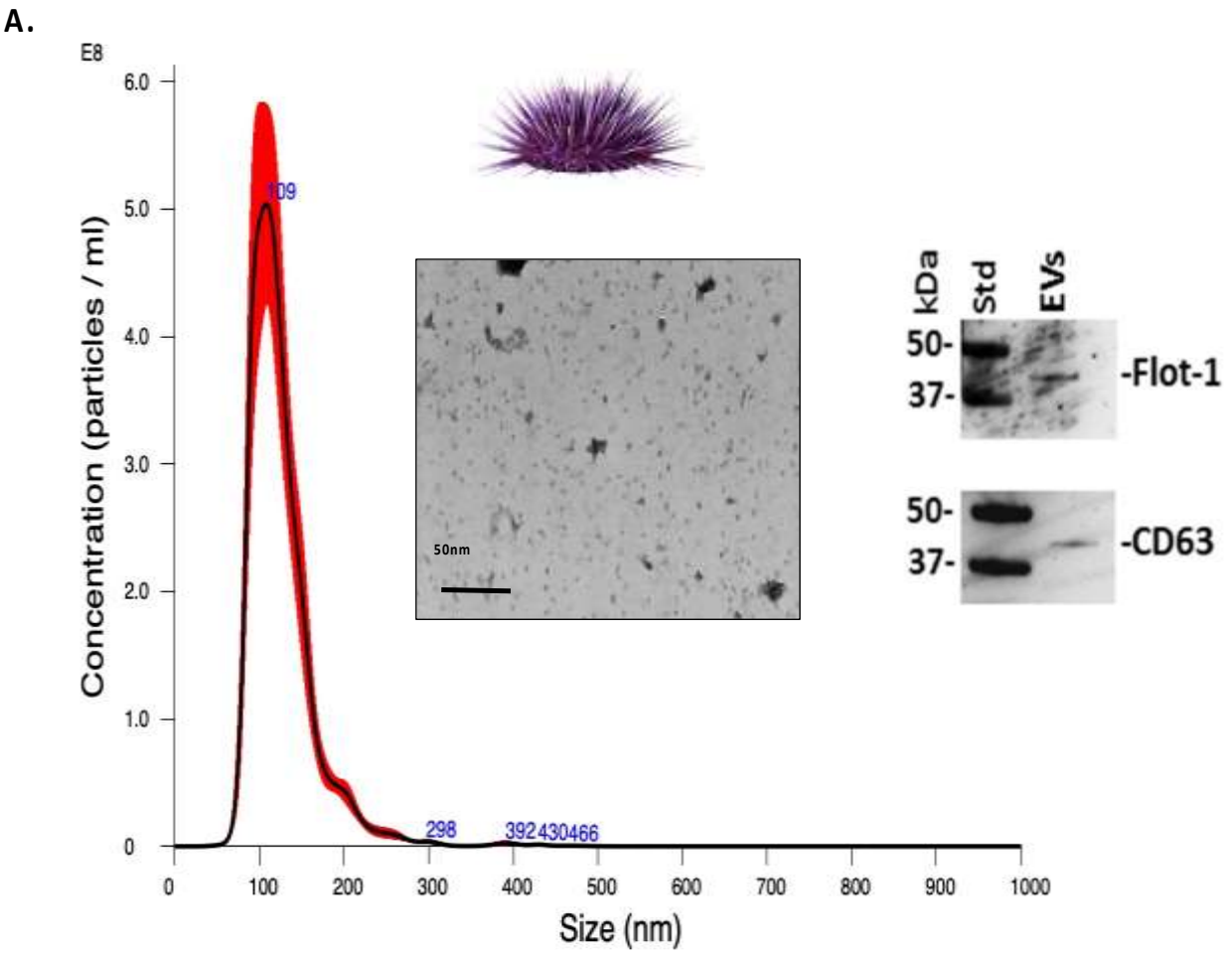

Figure 12. EVs characterisation across phylogeny. Representative NTA curves, Transmission Electron Microscopy for EVs characterisation and Western Blot for phylogenetically conserved EVs-specific markers: CD63 (1/1000) and Flot-1 (1/1000) for purple sea urchin (*Strongylocentrotus purpuratus)*

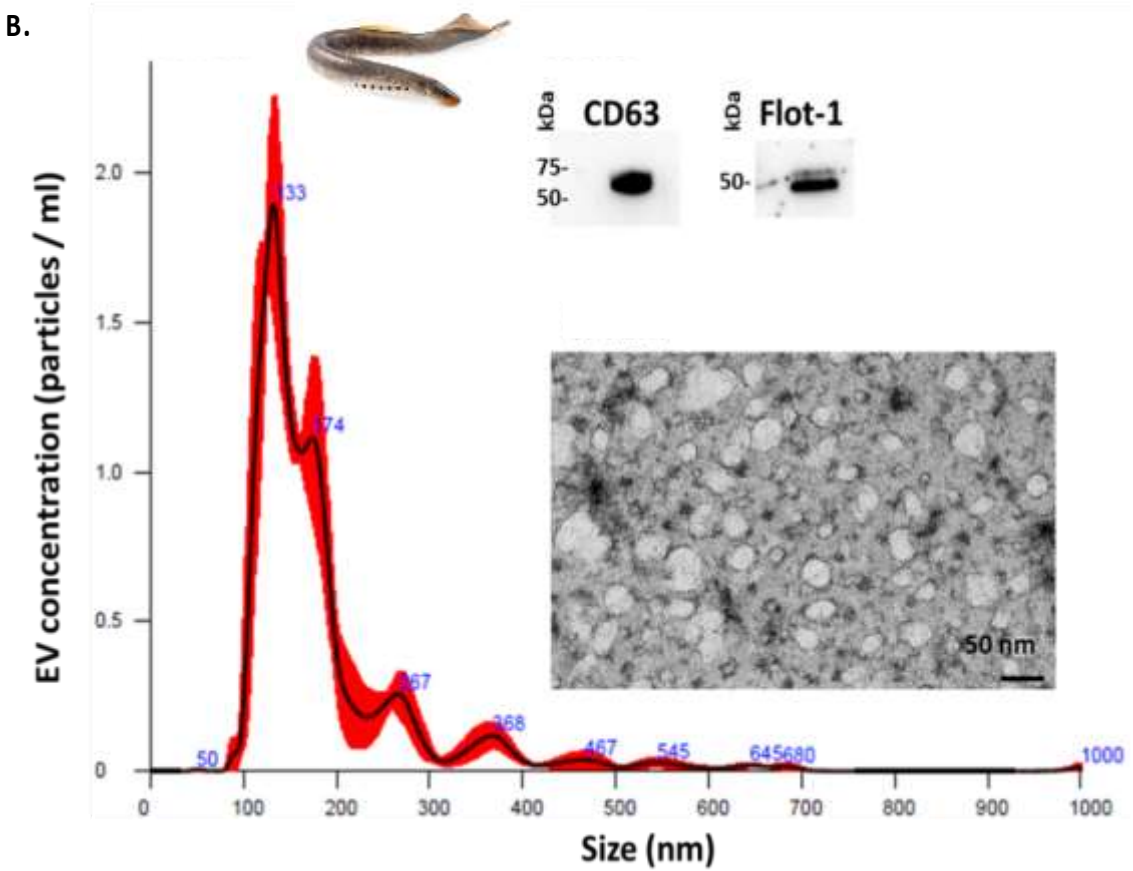

Figure 13. EVs characterisation across phylogeny. Representative NTA curves, Transmission Electron Microscopy for EVs characterisation and Western Blot for phylogenetically conserved EVs-specific markers: CD63 (1/1000) and Flot-1 (1/1000) for lamprey (*petromyzon marinus*).

C.

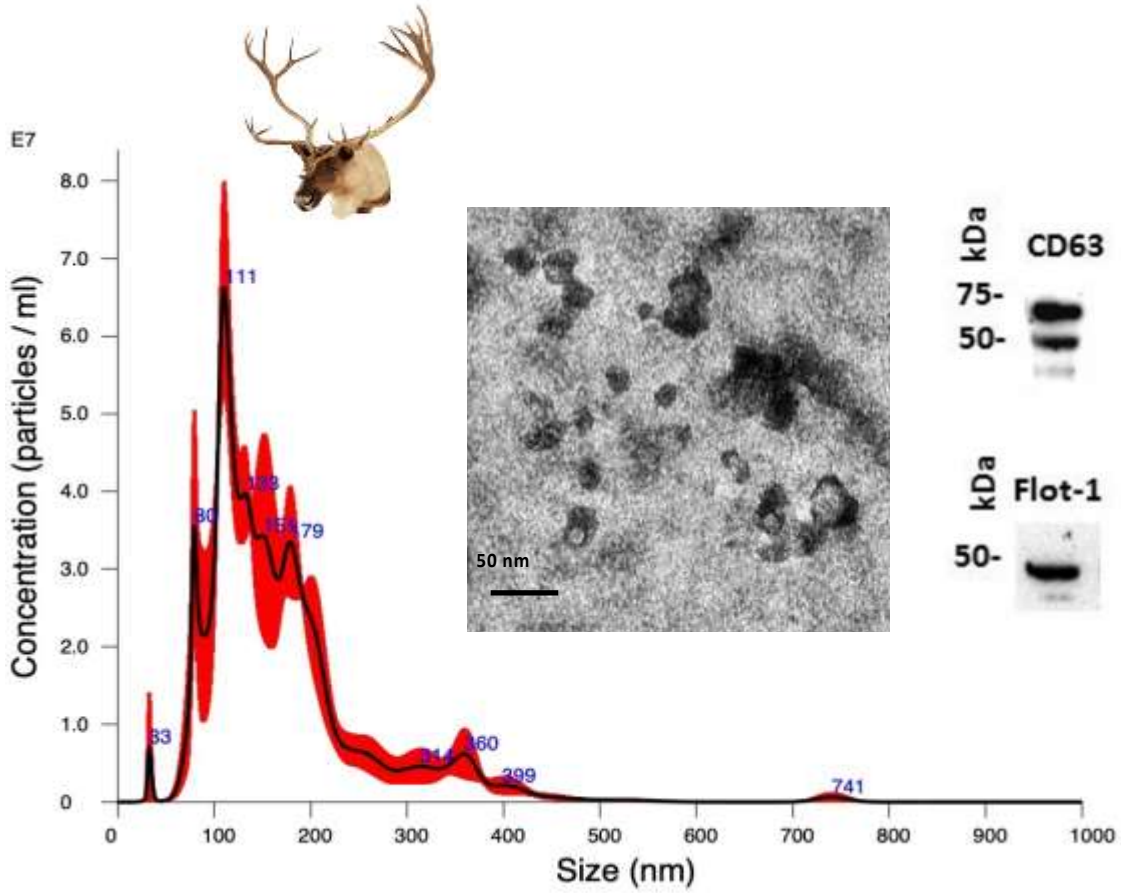

Figure 14. **EVs characterisation across phylogeny.** Representative NTA curves, Transmission Electron Microscopy for EVs characterisation and Western Blot for phylogenetically conserved EVs-specific markers: CD63 (1/1000) and Flot-1 (1/1000) for Reindeer (*Rangifer tarandus)*(C).

3.3 Neighbour-joining tree of EVs markers.

A neighbour-joining tree for EV markers in purple sea urchin (*Strongylocentrotus purpuratus*), sea lamprey (*Petromyzon marinus*) and reindeer (*Rangifer tarandus*) was produced by aligning the sequences for Flotillin-1, CD63, in human (*Homo sapiens*), purple sea urchin (*Strongylocentrotus purpuratus),* lamprey (*Petromyzon marinus*), Atlantic cod (*Gadus morhua*), red deer (*Cervus elaphus*) and white deer (*Odocoileus virginianus texanus*) as species of reference for reindeer (as no sequences for *Rangifer tarandus* was identified), using Clustal Omega – Multiple sequence alignment (**https://www.ebi.ac.uk/Tools/msa/clustalo/**) (Fig.15).

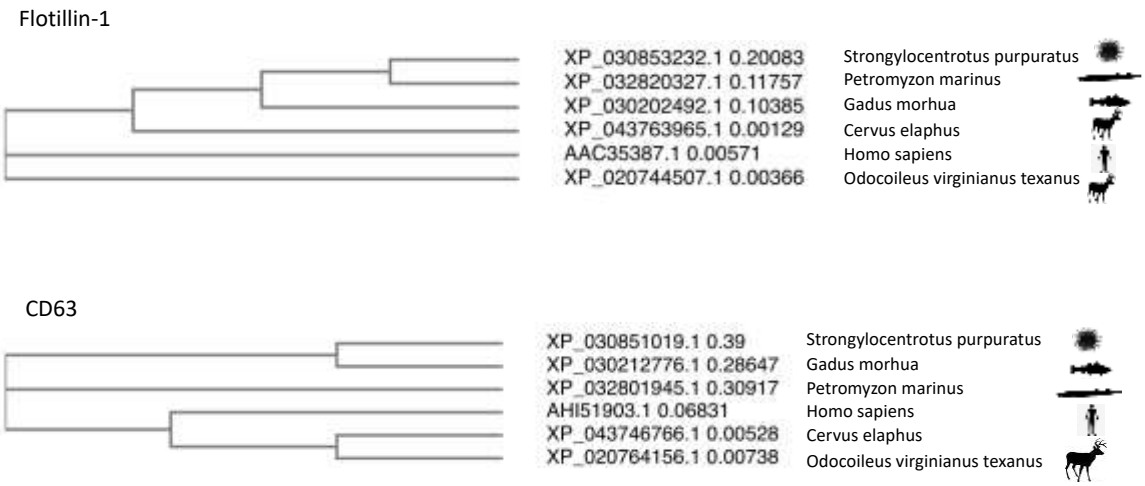

Figure 15. EV-specific markers across phylogeny. Neighbour-joining tree of EV-markers (Flotillin-1, Alix, CD63) for purple sea urchin (*Strongylocentrotus purpuratus)*, sea lamprey (*Petromyzon marinus)*, Atlantic cod (*Gadus Morhua)*, red deer (*Cervus elaphus)*, white deer (*Odocoileus virginianus texanus)* and human (*Homo sapiens)*. Sequences were retrieved from the NCBI database and submitted to Clustal Omega to reconstruct a neighbour-joining tree.

3.4 PAD Isozyme Detection

Putative PAD-like proteins were assessed by western blotting in the coelomic fluid of purple sea urchin and plasma of lamprey and reindeer via cross-reaction using anti-

human PAD isozyme-specific antibodies. While for lamprey and reindeer, the PAD2 antibody showed a protein band at the expected size of 70-75 kDa, as for mammalian PAD2 (Fig 17-B and C, respectively), in purple sea urchin, PAD2 showed a lower cross-reactive band at 65-70 kDa (Fig.17-A).

PADs in Echinodermata – Purple Sea Urchin

Searching the Echinoid database, no PAD-like protein hits were identified as present; also, mining the genome and transcriptome, no PAD/PAD-like protein-coding genes were found in the sea urchin genomes nor across Echinodermata (D'Alessio *et al.,*2021-b). PAD/ADI proteins have been reported in microbiota of Echinoidea, for example, the marine bacterium *Marixanthomonas ophiurae*, family *Flavobacteriaceae* isolated from deep-sea brittle stars and from *Echinicola strongylocentroti*, a bacterium isolated from sea urchin (*Strongylocentrotus intermedius*) (D'Alessio *et al*., 2021- b). ADI is well-known in cyanobacteria (Romanenko et al.,2007), also known as blue-green algae, contributing to the sea urchin diet. Our research found a PAD coding gene identified from an echinoderm genome assembly attributed to a Cyanobacteria (Table 7). We, therefore, cannot exclude that the deiminated protein products observed in purple sea urchins may be generated by ADI activity from microbiota coelomic fluid as a result of symbiosis between commensals and/or pathogens and the host, considering the absence of functional PAD genes across the Echinodermata (D'Alessio *et al.,*2021 - b).

Table 7. Top 5 BLASTp results for the predicted PAD protein from the mottled brittle starfish (*Ophionereis fasciata*) genome (all with 100% query cover).

Hit	Protein Accession No.	Species/Family Name	E-Value	Identity (%)
1	WP_111894244	*Arthrospira* sp.	3e-69	99
2	WP_048895331	*Limnospira indica*	4e-69	100
3	CCE20058	*Limniospira indica*	4e-69	100
4	CDM98608	*Limniospira indica*	4e-69	100
5	WP_006622374	*Microcoleaceae*	5e-69	100

PADs in Jawless Vertebrates – Sea Lamprey

In lamprey, PAD-like proteins were detected in plasma via cross-reaction using human PAD antibodies (Fig.17-B): PAD1 and PAD3 were assessed in plasma, showing bands at the expected size of 70-75kDa. In contrast, in PAD4, a non-specific cross-reaction was observed. In PAD6, a strong reaction was visible, showing a double band at 50 and 75kDa. However, PAD2 antibodies showed the strongest reaction, with a visible band at the expected size of 70-75kDa, accordingly with the PAD2-like protein sequences previously reported in lamprey (XP_032825558.1; XP_032825490.1; XP_032825520.1) (Rast *et al.,*2021). Moreover, analysis of the per cent identity matrix generated by Clustal Omega for lamprey, compared with human PADs 1-6 and sea bass PAD, revealed similarity in amino acid identity between the three lamprey PAD2-like proteins (72-74%), with human PAD2 (50.1-50.6%) and with sea bass PADs (49.8-55.2%) (Fig.16-B) (Rast et al.,2021).

A.

PAD 6 _*H. sapiens*	100.00	38.77	38.55	39.81	45.95	45.43	47.47	45.15	40.94
XP_032825558.1	38.77	100.00	74.47	72.76	49.83	49.84	49.66	50.08	51.17
XP_032825520.1	38.55	74.47	100.00	91.69	49.32	49.23	50.51	50.15	49.77
XP_032825490.1	39.81	72.76	91.69	100.00	50.26	50.00	51.74	50.62	51.63
PAD 3_*H. sapiens*	45.95	49.83	49.32	50.26	100.00	60.14	59.01	55.01	54.07
PAD 1_*H. sapiens*	45.43	49.84	49.23	50.00	60.14	100.00	60.31	52.44	50.46
PAD 4_*H. sapiens*	47.47	49.66	50.51	51.74	59.01	60.31	100.00	53.06	51.87
PAD 2_*H. sapiens*	45.15	50.08	50.15	50.62	55.01	52.44	53.06	100.00	56.69
PAD_*D. labrax*	40.94	51.17	49.77	51.63	54.07	50.46	51.87	56.69	100.00

B.

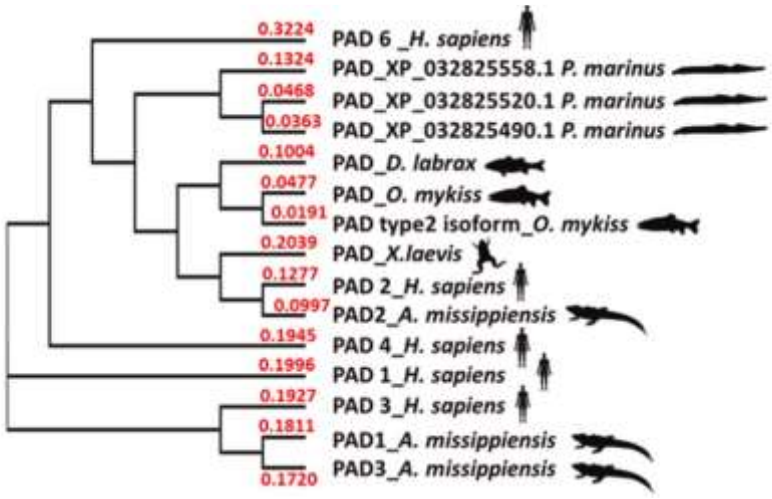

Figure 16. Percent identity matrix as generated by Clustal Omega for lamprey (*P. marinus*) PAD2-like protein sequences reported (XP_0.382558.1; XP_032825520.1; XP_032825490.1), compared with human PADs 1–6 and sea bass (*D.labrax*) PAD (for the percent identity matrix including all sequences in the neighbour-joining tree (A). Neighbour-joining tree shows reported lamprey PAD2-like protein sequences compared with teleost (sea bass (*D. labrax)* and rainbow trout (*O. mykiss*)) PAD-like proteins, amphibian (*X. laevis*) PAD-like protein, reptilian (*A. mississippiensis*) PAD1-3 isozymes and all five human (*H. sapiens*) PAD isozymes (PAD1, 2, 3, 4 and 6, respectively). The closest homology was found with human PAD2, followed by teleost (sea bass) PAD. The red numbers represent a measure of support for the node (B).

PADs in Artiodactyla – Reindeer

In reindeer, PAD2, PAD3, and PAD4 were assessed in both plasma and plasma EVs using anti-human PADs-specific antibodies (Fig.17-C), revealing their presence at the predicted size of 70-75kDa in plasma. At the same time, only PAD4 seemed to be exported in reindeer plasma EVs, showing a strong positive reaction.

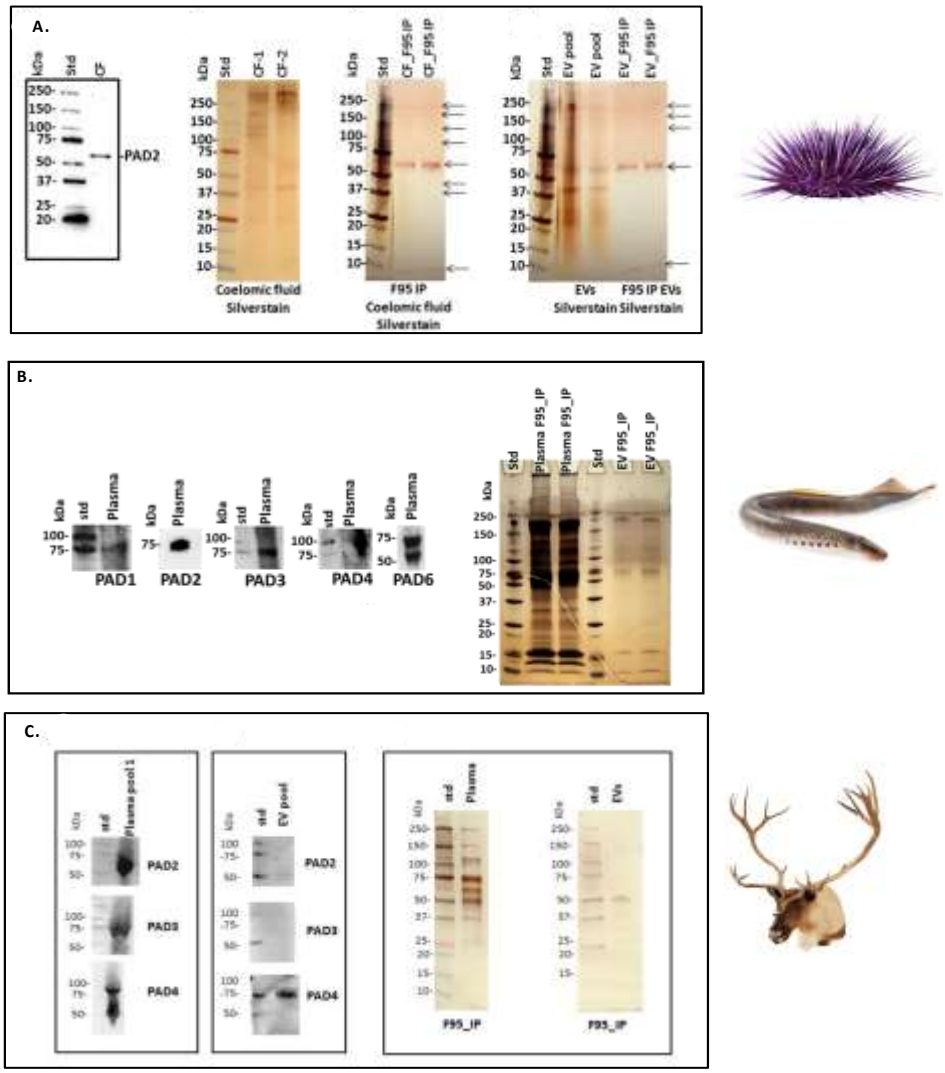

Figure 17. Peptidylarginine deiminase (PAD) isoforms detection by Western blotting and Silverstein detection of total proteins and F95-enriched proteins in (A) purple sea urchin coelomic fluid, (B) lamprey plasma and plasma EVs and (C) reindeer plasma and plasma EVs.

3.5 Neighbour-joining tree of PADs isozymes

The following sequences were used for the neighbour-joining tree (Fig.18) using Clustal Omega (https://www.ebi.ac.uk/Tools/msa/clustalo/): human (*Homo sapiens*) PAD1 (NP_037490.2), PAD2 (NP_031391.2), PAD3 (NP_057317.2), PAD4 (NP_036519.2) and PAD6 (NP_997304.3); *Odocoileus virginianus texanus* PAD1 (XP_020733655.1), PAD2 (XP_020733656.1), PAD3 (XP_020733658.1), PAD4 (XP_020754850.1) and PAD6 (XP_020754849.1) isozymes; *Bos taurus* PAD1 (NP_001094742.1), PAD2 (NP_001098922.1), PAD3 (XP_010800991.1), PAD4 (NP_001179102.1), and PAD6 (XP_002685843.1) isozymes; *Cervus elaphus hippelaphus* PAD1 (OWK12974.1), PAD4 (OWK12644.1) isozymes; *Petromyzon marinus* (lamprey) PAD2-like (XP_032825570.1); teleost fish (sea bass – *Dicentrarchus labrax* CBN80708.1; rainbow trout – *Oncorhynchus mykiss* PAD protein CAX45844.1 and PAD type-2isoform X2 XP_021425236.1), reptilian (*Alligator missippiensis* PAD1 XP_006259278.3, PAD2 XP_019355592.1 and PAD3 XP_014457295.1), amphibian (*Xenopus laevis* PAD2 homologue NP_001080369.1).

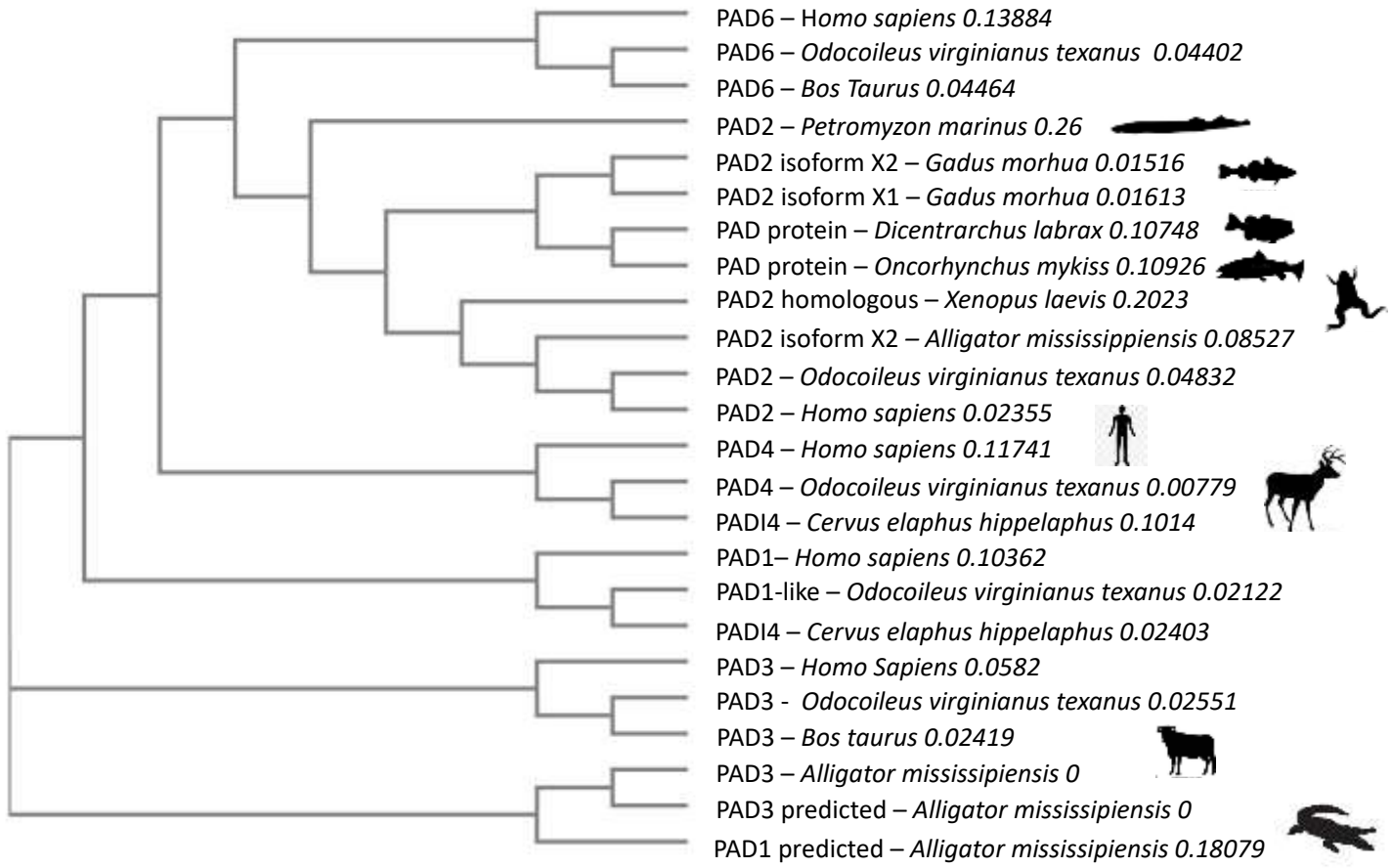

Figure 18. Neighbour-joining tree of known PADs from Artiodactyla, lamprey and Atlantic cod compared with teleost, amphibians, reptiles, and human PAD sequences**.**

The numbers following the species names represent a measure of support for the node.

3.6 Analysis of Deiminated Protein Cargo and Associated Protein-Protein Interaction Network Identification in Purple Sea Urchin, Sea Lamprey, and Reindeer

Identification of deiminated proteins in purple sea urchin coelomic fluid and EVs, lamprey plasma and plasma EVs and reindeer plasma and plasma EVs was carried out following F95 -enrichment, using protein hits identified by LC-MS/MS analysis. For each species, deiminated protein hits were identified using specific or common UniProt databases (Echinoidea database for purple sea urchin, lamprey-specific database and *R.tarandus* and Artiodactyla database for reindeer).

***Strongylocentrotus purpuratus* – Purple Sea Urchin**

In purple sea urchin's coelomic fluid were identified a total of 41 deiminated proteins (including uncharacterised proteins), of which six were overlapping with EVs deiminated protein hits: two annotated target proteins (Major yolk protein and 60S ribosomal protein L40) and four uncharacterised proteins with a secondary annotation (Cytoskeletal Actin-1A, -2A, -1B, and -2B; Histone H2B; Histone H4 and Tubulin beta chain). Seven annotated deiminated target proteins were identified to be unique for coelomic fluid (Complement C3; Late histone H2B.2.1; Tubulin alpha chain, Fascin; Elongation factor alpha-1; Glyceraldehyde-3-phosphate dehydrogenase and Cell surface protein). Furthermore, 31 (including non-annotated hits) deiminated protein hits were identified in EVs, and four of those were identified as unique for EVs (Beta actin, Cytoplasmic actin CyII, gp96 heat shock protein, and 98K protein) (Table 8,Fig 17- A). In addition to deiminated proteins in coelomic fluid and EVs, LC-MS/MS analysis was carried out for total protein cargo of sea urchin EVs: 182 protein hits were identified, whereof eight overlapped with deiminated hits from EVs (Major yolk protein, Beta-actin, Actin, Tubulin beta chain, Histones H2B and H4, Heat shock protein gp96, and

60S ribosomal protein L40). Protein found as deiminated in coelomic fluid were found amongst the total protein cargo in EVs (Complement C3, Actin cytoskeletal 1A-1B, Tubulin alpha chain, Tubulin beta chain, Histone H4, Histone H2B and Glyceraldehyde-3-phosphate dehydrogenase), indicating differences in deimination targets between EVs and coelomic fluid and showing a large number of proteins relating to many vital cellular functions are exported as EVs cargo, although only some of these proteins are deiminated in EVs (Table 8, Fig.19– B).

Table 8. Deiminated protein hits identified by F95 enrichment in conjunction with LC-MS/MS. Hits identified in coelomic fluid derived-EVs, coelomic fluid (CF), or both are indicated by a tick (v). Uncharacterised hits with an annotated secondary hit are included and shown in brackets.

Protein ID **Protein name**	***Species name*** **Common name**	**EVs**	**CF**
P19615/MYP_STRPU Major yolk protein	*Strongylocentrotus purpuratus* Purple sea urchin	**v**	**v**
A0A7M7HL75_STRPU Uncharacterized protein *(*Actin, cytoskeletal 2A; Actin, cytoskeletal 1A; Actin, cytoskeletal 1B; Actin, cytoskeletal 2B)	*Strongylocentrotus purpuratus* Purple sea urchin	**v**	**v**
A0A7M7PME7_STRPU Uncharacterized protein (Major yolk protein)	*Strongylocentrotus purpuratus* Purple sea urchin	**v**	**v**
A0A1L3KPZ4_MESNU Beta actin	*Mesocentrotus nudus* Sea urchin	**v**	

O18555_HELER Cytoplasmic actin CyII	*Heliocidaris erythrogramma* Sea urchin	**v**	
A0A7M7NNT8_STRPU Uncharacterized protein (Histone HB2)	*Strongylocentrotus purpuratus* Purple sea urchin	**v**	**v**
H3IPI3_STRPU Uncharacterized protein (Histone H4)	*Strongylocentrotus purpuratus* Purple sea urchin	**v**	**v**
A0A7M7SSL0_STRPU Uncharacterized protein (Heat shock protein gp96)	*Strongylocentrotus purpuratus* Purple sea urchin	**v**	
A0A7M7GHQ8_STRPU Uncharacterized protein (Tubulin beta chain)	*Strongylocentrotus purpuratus*	**v**	**v**

	Purple sea urchin		
D5H3J3_PSAMI 60S ribosomal protein L40	*Psammechinus miliaris* Green sea urchin	**v**	**v**
Q7M4J9_HEMPU 98K protein	*Hemicentrotus pulcherrimus* Sea urchin	**v**	
O443344_STRPU Complement C3	*Strongylocentrotus purpuratus* Purple sea urchin		**v**
A0A7M7NRQ3_STRPU Uncharacterized protein (Tubulin beta chain)	*Strongylocentrotus purpuratus* Purple sea urchin		**v**
P07794/H2BL1_PSAMI Late histone H2B.2.1	*Strongylocentrotus purpuratus*		**v**

	Purple sea urchin		
A0A7M7RBS6_STRPU Uncharacterized protein (Histone H2B)	*Psammechinus miliaris* Green sea urchin		
D5H3J3_PSAMI 60S ribosomal protein L40	*Strongylocentrotus purpuratus* Purple sea urchin	**v**	**v**
A0A7M6UC80_STRPU Uncharacterized protein (Histone H2A.V; Histone H2A-bta, sperm)	*Psammechinus miliaris* Green sea urchin		**v**
A0A7M7MZP4_STRPU Uncharacterized protein (Tubulin alpha chain)	*Strongylocentrotus purpuratus* Purple sea urchin		**v**
A0A7M7NVJ2_STRPU Uncharacterized protein (Fascin)	*Strongylocentrotus purpuratus* Purple sea urchin		**v**

A0A7M6UMT5_STRPU Uncharacterized protein (Elongation factor alpha-1)	*Strongylocentrotus purpuratus* Purple sea urchin	**v**
A0A1DB8I2L3_STENE Glyceraldehyde-3-phosphate dehydrogenase	*Strongylocentrotus purpuratus* Purple sea urchin	**v**
Q26049_PARLI Cell surface protein	*Paracentrotus lividus* Mediterranean purple sea urchin	**v**

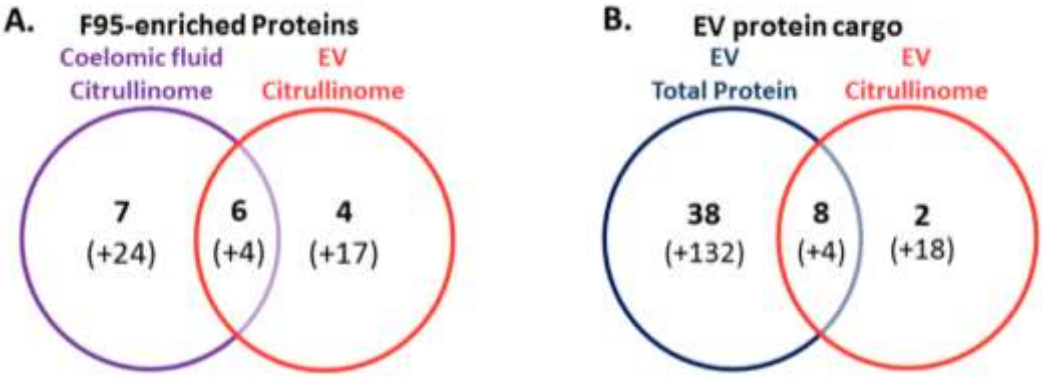

Figure 19. Shared deiminated protein hits in Purple Sea Urchin. Venn diagrams showing unique and shared deiminated protein hist identified in purple sea urchin coelomic fluid and coelomic fluid- EVs (A); unique and shared protein hits identified in total EV protein cargo and EV citrullinome in purple sea urchin (B).

***Petromyzon marinus* – Sea Lamprey**

In lamprey total plasma, 72 annotated hits were identified, 48 of which were specific to plasma only, 24 hits were shared between plasma and plasma EVs, and 13 protein hits were identified to be specific for EVs only (Table 9- Fig.20). Common deiminated protein targets in plasma and plasma-EVs included: Fibrinogen C-terminal-domain containing protein, C1q domain-containing protein, C1q and TNF related 9, Anaphylatoxin-like domain-containing protein, SERPIN domain-containing protein, DUF1081 domain-containing protein, Blood plasma apolipoprotein LAL2, Serum albumin, Plastocyanin-like domain-containing protein, Beta-actin; Actin gamma 2, Elongation factor 1-alpha, Pyruvate kinase, Histone H2A, Histone H2B, Histone H3, Histone H4, 2-phospho-D-glycerate hydrolyse, Heat shock protein 90, Glyceraldehyde-3-phosphate dehydrogenase, Tyrosine 3-monooxygenase/tryptophan 5-mono- oxygenase activation protein eta, 60S ribosomal protein L18a, CRALTRIO domain-containing protein, Peptidase S1 domain-containing protein. Deiminated proteins identified in EVs only included Desmin, 60 kDa chaperonin, 78 kDa glucose-regulated protein, Septin 7, 160 kDa neurofilament protein, 60S acidic ribosomal protein P0, 60S ribosomal protein L8, 60S ribosomal protein L23, Ribosomal protein L3 like, 75 kDa glucose-regulated protein, OTU deubiquitinase with linear linkage specificity b, FACT complex subunit and Spartin b. Deiminated proteins identified in whole plasma only included: Activation peptide fragment 1, Angiotensinogen, Serpin peptidase inhibitor (heparin cofactor), Ferritin, Fibrinogen (alpha, beta and gamma-chain), Fibronectin, Fibrinopeptide A, Albumin domain- containing protein, Trypsinogen b2, Adiponectin, TED_complement domain-containing protein, Tubulin beta chain, L-lactate dehydrogenase, Jacalin-type lectin domain-containing protein, Cytoglobin, M20_dimer domain-containing protein, Alpha-1,4 glucan phosphorylase, Triosephosphate isomerase, AMP deaminase, Fructose- bisphosphate aldolase, Carnosine dipeptidase 2, Ribosomal protein L7,

60S ribosomal protein L13a, Ribosomal protein L4, Ribosomal protein L23a, 40S ribosomal protein S9 and S11, 60S ribosomal protein L21, 40S ribosomal protein S26, Carbonic anhydrase, 3-hydroxyacyl-[acyl-carrier-protein] dehydratase, H15 domain-containing protein, Erythrocyte membrane protein band 4.1 like 2, Cap methyltransferase 1, Olfactomedin 4, PLAT domain-containing protein, Ankyrin repeat domain 28, Centromere protein S, Kringle domain-containing protein, Glutamine-fructose-6-phosphate transaminase, Palmitoyltransferase, Protein kinase domain-containing protein, KIF-binding protein, DDE_Tnp_1_7 domain-containing protein, LRRNT domain-containing protein, Anoctamin, Vesicle-fusing ATPase and Myosin motor domain-containing protein.

Table 9. Deiminated protein hits by F95-enrichment in conjunction with LC-MS/MS. Hits identified in sea lamprey plasma-EVs and whole plasma, or both, are indicated by a thick (v). Uncharacterised hits with an annotated secondary hit are included and indicated in brackets.

Protein ID **Protein name**	***Species name*** **Common name**	**Plasma-EVs**	**Plasma**
S4RH70_PETMA DUF1081 domain-containing protein	*Petromyzon marinus* Sea lamprey	**v**	**v**
ALBU_PETMA Serum albumin SDS-1	*Petromyzon marinus* Sea lamprey	**v**	**v**
S4RBZ1_PETMA SERPIN domain-containing protein	*Petromyzon marinus* Sea lamprey	**v**	

S4RVP0_PETMA Anaphylatoxin-like domain-containing protein	*Petromyzon marinus* Sea lamprey	**v**	**v**
S4RPC4_PETMA Fibrinogen beta chain	*Petromyzon marinus* Sea lamprey		**v**
S4RP12_PETMA Plastocyanin-like domain-containing protein	*Petromyzon marinus* Sea lamprey	**v**	**v**
FIBG_PETMA Fibrinogen gamma chain	*Petromyzon marinus* Sea lamprey		**v**
S4REY0_PETMA Activation peptide fragment 1	*Petromyzon marinus* Sea lamprey		**v**
K7N848_PETMA Angiotensinogen	*Petromyzon marinus* Sea lamprey		**v**
S4RUQ3_PETMA SERPIN domain-containing protein	*Petromyzon marinus* Sea lamprey		**v**
S4RPV0_PETMA Fibrinogen C-terminal domain-containing protein	*Petromyzon marinus* Sea lamprey	**v**	**v**

S4RUS7_PETMA Serpin peptidase inhibitor, clade D (heparin cofactor), member 1	*Petromyzon marinus* Sea lamprey		**v**
S4RC14_PETMA Fibronectin	*Petromyzon marinus* Sea lamprey		**v**
S4RSU9_PETMA Albumin domain-containing protein	*Petromyzon marinus* Sea lamprey		**v**
S4R8Z6_PETMA C1q and TNF related 9	*Petromyzon marinus* Sea lamprey	**v**	**v**
S4RSZ0_PETMA Fibrinogen C-terminal domain-containing protein	*Petromyzon marinus* Sea lamprey		**v**
O42160_PETMA Trypsinogen b2	*Petromyzon marinus* Sea lamprey		**v**
S4RVH9_PETMA Peptidase S1 domain-containing protein	*Petromyzon marinus* Sea lamprey		**v**
S4RH85_PETMA Uncharacterized protein (Beta-actin; Actin gamma 2, smooth muscle)	*Petromyzon marinus* Sea lamprey		**v**
FIBA1_PETMA Fibrinogen alpha-1 chain	*Petromyzon marinus* Sea lamprey		**v**

S4RT32_PETMA Adiponectin, C1Q and collagen domain containing	*Petromyzon marinus* Sea lamprey		**v**
S4R568_PETMA Tubulin beta chain	*Petromyzon marinus* Sea lamprey		**v**
S4S1D7_PETMA Glyceraldehyde-3-phosphate dehydrogenase	*Petromyzon marinus* Sea lamprey		**v**
S4RL04_PETMA Tyrosine 3-monooxygenase/tryptophan 5-monooxygenase activation protein eta	*Petromyzon marinus* Sea lamprey	**v**	**v**
APL2_PETMA Blood plasma apolipoprotein LAL2	*Petromyzon marinus* Sea lamprey	**v**	**v**
S4RW10_PETMA Ferritin	*Petromyzon marinus* Sea lamprey		
LDH_PETMA L-lactate dehydrogenase	*Petromyzon marinus* Sea lamprey		**v**
S4RJ23_PETMA C1q and TNF related 9	*Petromyzon marinus* Sea lamprey		**v**
S4S0L1_PETMA Jacalin-type lectin domain-containing protein	*Petromyzon marinus* Sea lamprey		**v**

S4R963_PETMA Cytoglobin	*Petromyzon marinus* Sea lamprey		**v**
S4RB03_PETMA Histone H2B	*Petromyzon marinus* Sea lamprey		**v**
S4RUX0_PETMA Ferritin	*Petromyzon marinus* Sea lamprey		**v**
S4R4V3_PETMA Pyruvate kinase	*Petromyzon marinus* Sea lamprey		**v**
S4RR00_PETMA TED_complement domain-containing protein	*Petromyzon marinus* Sea lamprey		**v**
S4RWE8_PETMA M20_dimer domain-containing protein	*Petromyzon marinus* Sea lamprey		**v**
S4RAY0_PETMA Histone H4	*Petromyzon marinus* Sea lamprey		**v**
S4S1N9_PETMA Elongation factor 1-alpha	*Petromyzon marinus* Sea lamprey		**v**
S4RMH3_PETMA Ferritin	*Petromyzon marinus* Sea lamprey		**v**
S4S090_PETMA C1q domain-containing protein	*Petromyzon marinus* Sea lamprey		**v**
S4RAZ5_PETMA Histone H2A	*Petromyzon marinus* Sea lamprey	**v**	**v**

S4RLF1_PETMA Alpha-1,4 glucan phosphorylase	*Petromyzon marinus* Sea lamprey		**v**
S4S088_PETMA C1q domain-containing protein	*Petromyzon marinus* Sea lamprey		**v**
S4RFY7_PETMA Jacalin-type lectin domain-containing protein	*Petromyzon marinus* Sea lamprey		**v**
S4RDV2_PETMA Heat shock protein 90, alpha (cytosolic), class A member 1, tandem duplicate 2	*Petromyzon marinus* Sea lamprey	**v**	**v**
S4R694_PETMA Triosephosphate isomerase	*Petromyzon marinus* Sea lamprey		**v**
S4R691_PETMA AMP deaminase	*Petromyzon marinus* Sea lamprey		**v**
S4RTN2_PETMA Zgc:152830	*Petromyzon marinus* Sea lamprey		**v**
S4RGR5_PETMA Fructose-bisphosphate aldolase	*Petromyzon marinus* Sea lamprey		**v**
S4RXJ5_PETMA Carnosine dipeptidase 2	*Petromyzon marinus* Sea lamprey		**v**

S4RG79_PETMA C1q domain-containing protein	*Petromyzon marinus* Sea lamprey		**v**
S4RG79_PETMA 2-phospho-D-glycerate hydro-lyase	*Petromyzon marinus* Sea lamprey	**v**	**v**
S4RX00_PETMA N-glycanase_N domain-containing protein	*Petromyzon marinus* Sea lamprey	**v**	**v**
S4RQ44_PETMA PFK domain-containing protein	*Petromyzon marinus* Sea lamprey	**v**	**v**
S4RWR0_PETMA 60S ribosomal protein	*Petromyzon marinus* Sea lamprey	**v**	**v**
S4S092_PETMA C1q domain-containing protein	*Petromyzon marinus* Sea lamprey	**v**	**v**
S4RQL1_PETMA Ribosomal protein L7	*Petromyzon marinus* Sea lamprey		**v**
S4S165_PETMA Histone H2A	*Petromyzon marinus* Sea lamprey	**v**	**v**
S4R6W7_PETMA C1q domain-containing protein	*Petromyzon marinus* Sea lamprey		**v**

S4RPI3_PETMA 0S ribosomal protein L13a	*Petromyzon marinus* Sea lamprey		**v**
S4RE39_PETMA Peptidase S1 domain-containing protein	*Petromyzon marinus* Sea lamprey		**v**
S4R718_PETMA Ribosomal protein L4	*Petromyzon marinus* Sea lamprey		**v**
S4RXD9_PETMA Carbonic anhydrase	*Petromyzon marinus* Sea lamprey		**v**
S4RFI6_PETMA Ribosomal protein L23a	*Petromyzon marinus* Sea lamprey		**v**
S4R5M7_PETMA -hydroxyacyl-[acyl-carrier-protein] dehydratase	*Petromyzon marinus* Sea lamprey		**v**
S4RW50_PETMA C1q and TNF related 9	*Petromyzon marinus* Sea lamprey		**v**
S4RAY9_PETMA H15 domain-containing protein	*Petromyzon marinus* Sea lamprey		**v**
S4RZ58_PETMA CRAL-TRIO domain-containing protein	*Petromyzon marinus* Sea lamprey	**v**	**v**
S4RAY6_PETMA Histone H3	*Petromyzon marinus* Sea lamprey	**v**	**v**

S4R900_PETMA Erythrocyte membrane protein band 4.1 like 2	*Petromyzon marinus* Sea lamprey	**v**
S4R4U3_PETMA 40S ribosomal protein S9	*Petromyzon marinus* Sea lamprey	**v**
S4RLF4_PETMA Cap methyltransferase 1	*Petromyzon marinus* Sea lamprey	**v**
S4RZY7_PETMA Olfactomedin 4	*Petromyzon marinus* Sea lamprey	**v**
S4RV41_PETMA PLAT domain-containing protein	*Petromyzon marinus* Sea lamprey	**v**
S4RFJ2_PETMA Ankyrin repeat domain 28	*Petromyzon marinus* Sea lamprey	**v**
S4RFF9_PETMA 60S ribosomal protein L18a	*Petromyzon marinus* Sea lamprey	**v**
***S4RXZ4_PETMA** Centromere protein S	*Petromyzon marinus* Sea lamprey	**v**
S4RIK4_PETMA Kringle domain-containing protein	*Petromyzon marinus* Sea lamprey	**v**
S4RVF7_PETMA 40S ribosomal protein S26	*Petromyzon marinus* Sea lamprey	**v**

S4RU19_PETMA Protein kinase domain-containing protein	*Petromyzon marinus* Sea lamprey	**v**
S4RZ42_PETMA 60S ribosomal protein L21	*Petromyzon marinus* Sea lamprey	
S4RCX7_PETMA Fibrinopeptide A	*Petromyzon marinus* Sea lamprey	**v**
S4RHB4_PETMA KIF-binding protein	*Petromyzon marinus* Sea lamprey	**v**
***S4R9C6_PETMA** DDE_Tnp_1_7 domain-containing protein	*Petromyzon marinus* Sea lamprey	**v**
S4RH55_PETMA LRRNT domain-containing protein	*Petromyzon marinus* Sea lamprey	**v**
S4R9Z3_PETMA Anoctamin	*Petromyzon marinus* Sea lamprey	**v**
S4RDD9_PETMA Vesicle-fusing ATPase	*Petromyzon marinus* Sea lamprey	**v**
S4RUU5_PETMA Myosin motor domain-containing protein	*Petromyzon marinus* Sea lamprey	**v**

S4RH85_PETMA		
Uncharacterized protein (Beta-actin; Actin gamma 2, smooth muscle)	*Petromyzon marinus* Sea lamprey	**v**
S4RE82_PETMA	*Petromyzon marinus*	
Desmin b	Sea lamprey	**v**
S4RBJ3_PETMA	*Petromyzon marinus*	
60 kDa chaperonin	Sea lamprey	**v**
S4RB03_PETMA	*Petromyzon marinus*	
Histone H2B	Sea lamprey	**v**
S4RAY0_PETMA		
Histone H4	*Petromyzon marinus* Sea lamprey	**v**
S4S091_PETMA		
C1q domain-containing protein	*Petromyzon marinus* Sea lamprey	**v**
S4RIP9_PETMA		
78 kDa glucose-regulated protein	*Petromyzon marinus* Sea lamprey	**v**
S4R4V3_PETMA	*Petromyzon marinus*	
Pyruvate kinase	Sea lamprey	**v**

S4RFB7_PETMA 60S ribosomal protein L23	*Petromyzon marinus* Sea lamprey	**v**
S4S1N9_PETMA Elongation factor 1-alpha	*Petromyzon marinus* Sea lamprey	**v**
S4RX19_PETMA Septin 7	*Petromyzon marinus* Sea lamprey	**v**
S4RRG5_PETMA 160 kDa neurofilament protein	*Petromyzon marinus* Sea lamprey	**v**
S4RNE3_PETMA 60S ribosomal protein L18a	*Petromyzon marinus* Sea lamprey	**v**
S4S171_PETMA 60S acidic ribosomal protein P0	*Petromyzon marinus* Sea lamprey	**v**
S4RID2_PETMA Uncharacterized protein (Fibrinogen C-terminal domain-containing protein)	*Petromyzon marinus* Sea lamprey	**v**
S4R4R6_PETMA Ribosomal protein L3 like	*Petromyzon marinus* Sea lamprey	**v**
S4RPS8_PETMA 75 kDa glucose-regulated protein	*Petromyzon marinus* Sea lamprey	**v**

S4RCL1_PETMA OTU deubiquitinase with linear linkage specificity b	*Petromyzon marinus* Sea lamprey	**v**
S4RDI0_PETMA FACT complex subunit	*Petromyzon marinus* Sea lamprey	**v**
S4R9Q9_PETMA Peptidase S1 domain-containing protein	*Petromyzon marinus* Sea lamprey	**v**
S4RYF8_PETMA Gp_dh_N domain-containing protein	*Petromyzon marinus* Sea lamprey	**v**
S4S068_PETMA Spartin b	*Petromyzon marinus* Sea lamprey	**v**

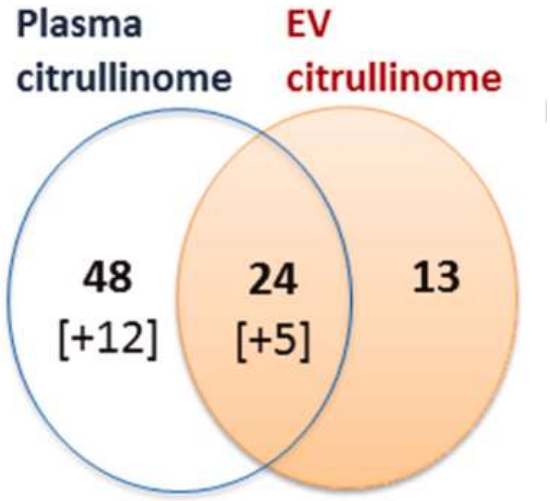

Figure 20. Shared deiminated protein hits in Sea Lamprey. The Venn diagram represents the number of deiminated protein hits identified by LC-MS/MS from the F95-enriched fractions in plasma (plasma citrullinome) and plasma-EVs (EV citrullinome); uncharacterised protein hits are indicated in brackets.

Rangifer Tarandus – Reindeer

110 hits were identified as specific for reindeer whole plasma, while 14 deiminated protein hits were identified as specific to EVs only. EV-specific hits included keratins (KRT5, KRT17, KRT19), collagen (type I alpha-1 and alpha 2 chain; type III alpha-1 chain and isoform X1), SH3 domain-containing protein, cytoplasmic actin 1, endoplasmic reticulum chaperone BiP, HATPase c domain-containing protein, ubiquitin-60S ribosomal protein L40, lysozyme, and histone H2B (although a H2B-like protein did also come up as a possible secondary hit for an uncharacterised hit in whole plasma). Fifteen shared deiminated hits identified between plasma and plasma EVs were albumin, serum albumin, IF rod domain, keratin, keratin 75, keratin, type I cytoskeletal 15, bradykinin, TAF domain-containing protein, histone H4, annexin, junction plakoglobin, VH region, Ig-like domain, endoplasmic reticulum chaperone and obscurin. (Table 10, Fig.21)

Table 10. Deiminated proteins identified by F95 enrichment and liquid chromatography with tandem mass spectrometry (LC-MS/MS) analysis. Hits identified in reindeer plasma-EVs and whole plasma, or both, are indicated by a thick (v). Uncharacterised hits with an annotated secondary hit are included and indicated in brackets.

Protein ID **Protein name**	***Species name*** **Common name**	**Plasma-EVs**	**Plasma**
A0A140T897_BOVIN Albumin	*Bos taurus* Cow	**v**	**v**
L8ISP4_9CETA Serum Albumin	*Bos mutus* Domestic Yak	**v**	**v**

A0A4W2GW83_BOBOX Uncharacterized protein (ALB protein)	*Bos indicus x Bos taurus* Zebu x Cow	**v**	**v**
A0A5N3XZ04_MUNRE IF rod domain-containing protein	*Muntiacus reevesi* Chinese muntjac	**v**	**v**
A0A212DF80_CEREH KRT5	*Cervus elaphus hippelaphus* European red deer	**v**	
A0A6J0WT46_ODOVR serum albumin	*Odocoileus virginianus texanus* White-tailed deer	**v**	**v**
A0A5N4DHW9_CAMDR Keratin	*Camelus dromedarius* Dromedary	**v**	**v**
A0A4W2C021_BOBOX Uncharacterized protein (Collagen alpha-1(I) chain)	*Bos indicus x Bos taurus* Zebu x Cow	**v**	**v**
A0A452FHU9_CAPHI Uncharacterized protein (Collagen type I alpha 1 chain)	*Capra hircus* Goat	**v**	**v**

A0A5N3WTF4_MUNMU Uncharacterized protein (collagen alpha-1(I) chain isoform X1)	*Muntiacus muntjac* Barking deer	**v**	**v**
A0A5N4D320_CAMDR Keratin	*Camelus dromedarius* Dromedary	**v**	**v**
A0A6J0WBI9_ODOVR histidine-rich glycoprotein isoform X1	*Odocoileus virginianus texanus* White-tailed deer	**v**	**v**
A0A212D793_CEREH KRT19	*Cervus elaphus hippelaphus* European red deer	**v**	
A0A287B5W2_PIG Trypsinogen isoform X1	*Sus scrofa* Wild boar	**v**	**v**
A0A4W2D3K5_BOBOX Keratin 75	*Bos indicus x Bos taurus* Zebu x Cow	**v**	**v**
A0A4W2DIS9_BOBOX Keratin 75	*Bos indicus x Bos taurus* Zebu x Cow	**v**	**v**

A0A6B0R6W5_9CETA Uncharacterized protein (IF rod domain-containing protein; Glial fibrillary acidic protein)	*Bos mutus* Domestic yak	**v**	**v**
9XAP9_CAMFR Keratin, type I cytoskeletal 14-like protein	*Camelus ferus* Wild Bactrian camel	**v**	**v**
A0A452FN18_CAPHI IF rod domain-containing protein	*Capra hircus* Goat	**v**	**v**
A0A5N4DGN6_CAMDR Keratin	*Camelus dromedarius* Dromedary	**v**	**v**
A0A4W2IN22_BOBOX IF rod domain-containing protein	*Bos indicus x Bos taurus* Zebu x Cow	**v**	**v**
A0A6I9IRH0_VICPA keratin, type I cytoskeletal	*Vicugna pacos* Alpaca	**v**	**v**
A0A5G2QXD3_PIG IF rod domain-containing protein	*Sus scrofa* Wild boar	**v**	**v**

A0A3Q1LZN8_BOVIN Collagen alpha-2(I) chain	*Bos taurus* Cow	**v**	
A0A287BLD2_PIG Uncharacterized protein (Collagen alpha-1(I) chain preproprotein. Alpha1 chain of type I collage)	*Sus scrofa* Wild boar	**v**	**v**
A0A212D6S5_CEREH KRT17	*Cervus elaphus hippelaphus* European red deer	**v**	
A0A5N4DFY6_CAMDR Keratin	*Camelus dromedarius* Dromedary	**v**	**v**
A0A212CMY9_CEREH Uncharacterized protein (Immunoglobulin heavy constant; Beta-2-microglobulin)	*Cervus elaphus hippelaphus* European red deer	**v**	**v**
A0A6J3QLJ4_TURTR collagen alpha-1(I) chain	*Tursiops truncates* Common bottlenose dolphin	**v**	
A0A2Y9SJP9_PHYMC Keratin, type II cytoskeletal 6A	*Physeter macrocephalus* Sperm Whale	**v**	**v**

A0A452EP10_CAPHI IF rod domain-containing protein	*Capra hircus* Goat	**v**	**v**
A0A6B0R542_9CETA Uncharacterized protein (Bradykinin; Kininogen-1; Kininogen-2; Isoform LMW of Kininogen-1;Isoform LMW of Kininogen-2)	*Bos mutus* Wild yak		
A0A5N4DG47_CAMDR Keratin	*Camelus dromedarius* Dromedary	**v**	**v**
A0A5N3WDS4_MUNMU Bradykinin	*Muntiacus muntjac* Barking deer	**v**	**v**
A0A1S7J1Y9_PIG Alpha2 chain of type I collagen	*Sus scrofa* Wild boar	**v**	
A0A5N4DFY1_CAMDR Keratin	*Camelus dromedarius* Dromedary	**v**	**v**
A0A383ZWF6_BALAS keratin, type II cytoskeletal 6A-like isoform X2	*Balaenoptera acutorostrata scammoni* Minke whale	**v**	**v**

W5Q4S0_SHEEP Uncharacterized protein (Collagen alpha-1(III) chain; Collagen type III alpha 1 chain; Fibrillar collagen NC1 domain-containing protein)	*Ovis aries* Sheep	**v**	**v**
A0A2F0AVL6_ESCRO Keratin, type II cytoskeletal 4	*Eschrichtius robustus* Gray whale	**v**	**v**
A0A5N3W3N9_MUNRE SH3 domain-containing protein	*Muntiacus reevesi* Chinese muntjac	**v**	
A0A340XVM8_LIPVE keratin, type I cytoskeletal 15	*Lipotes vexillifer* Baiji	**v**	**v**
A0A5N4CT25_CAMDR Histone H4	*Camelus dromedarius* Dromedary	**v**	**v**
A0A5N3XAC4_MUNRE Uncharacterized protein (Ig-like domain-containing protein)	*Muntiacus reevesi* Chinese muntjac	**v**	**v**
A0A6J0ZDI0_ODOVR serotransferrin	*Odocoileus virginianus texanus* White-tailed deer	**v**	**v**
ACTB_BOSMU Actin, cytoplasmic 1	*Bos mutus grunniens* Wild yak	**v**	

A0A5N3WEA4_MUNMU Beta-1 metal-binding globulin	*Muntiacus muntjac* Barking deer	**v**	**v**
A0A6J0XRB4_ODOVR keratin, type II cytoskeletal 2 oral-like	*Odocoileus virginianus texanus* White-tailed deer	**v**	**v**
A0A2C9F3E9_PIG Junction plakoglobin	*Sus scrofa* Pig	**v**	**v**
A0A212DB90_CEREH Ig-like domain-containing protein	*Cervus elaphus hippelaphus* European red deer	**v**	**v**
0A6I9IE32_VICPA collagen alpha-1(III) chain isoform X1	*Vicugna pacos* Alpaca	**v**	
A0A212D5P4_CEREH TAF domain-containing protein	*Cervus elaphus hippelaphus* European red deer	**v**	**v**
A0A643C4S8_BALPH Uncharacterized protein (IF rod domain-containing protein; KRT81; Keratin 85)	*Balaenoptera physalus* Fin Whale	**v**	**v**
A0A5N3W8P2_MUNMU Uncharacterized protein (Ig-like domain-containing protein)	*Muntiacus muntjac* Reeves's muntjac	**v**	**v**

A0A212D7J2_CEREH Fibrinogen beta chain	*Cervus elaphus hippelaphus* European red deer	**v**	**v**
A0A287B7K6_PIG IF rod domain-containing protein	*Sus scrofa* Wild boar	**v**	**v**
A0A212DFA6_CEREH IF rod domain-containing protein	*Cervus elaphus hippelaphus* European red deer	**v**	**v**
A0A6J0XD83_ODOVR fibrinogen alpha chain	*Odocoileus virginianus texanus* White-tailed deer	**v**	**v**
A0A2Y9MPQ9_DELLE collagen alpha-1(III) chain	*Delphinapterus leucas* Beluga whale	**v**	
A0A452E8D3_CAPHI Ig-like domain-containing protein	*Capra hircus* Goat	**v**	**v**
W5P2K5_SHEEP IF rod domain-containing protein	*Ovis aries* Sheep	**v**	**v**
A0A5N3UHT3_MUNRE Ig-like domain-containing protein	*Muntiacus reevesi* Chinese muntjac	**v**	**v**

A2P2I1_SHEEP VH region	*Ovis aries* Sheep	**v**	**v**
Q0VCX2|BIP_BOVIN Endoplasmic reticulum chaperone BiP	*Bos taurus* Cow	**v**	
A0A212CAL2_CEREH Elongation factor 1-alpha	*Cervus elaphus hippelaphus* European red deer	**v**	**v**
A0A5N3UV43_MUNMU IF rod domain-containing protein	*Muntiacus muntjac* Barking deer	**v**	**v**
A0A3Q1LUE9_BOVIN Ig-like domain-containing protein	*Bos taurus* Cow	**v**	**v**
A0A6B9SDT6_BOVIN Ig lambda chain variable region	*Bos taurus* Cow	**v**	**v**
A0A212CSZ9_CEREH Ig-like domain-containing protein	*Cervus elaphus hippelaphus* European red deer	**v**	**v**
A0A2F0B9E6_ESCRO Trypsin	*Eschrichtius robustus* Gray whale	**v**	**v**

A0A286ZKC5_PIG HATPase_c domain-containing protein	*Sus scrofa* Wild boar	**v**	
A0A1L6BP13_BUBBU Beta-casein	*Bubalus bubalis* Water buffalo	**v**	**v**
A0A6B0S2F2_9CETA Fibrinogen C-terminal domain-containing protein	*Bos mutus* Wild yak	**v**	**v**
P0C276|RL40_SHEEP Ubiquitin-60S ribosomal protein L40	*Ovis aries* Sheep	**v**	
A0A2Y9SBW8_PHYMC Histone H2B	*Physeter macrocephalus* Sperm Whale	**v**	
A0A6B0RTH8_9CETA Uncharacterized protein (Obscurin)	*Bos mutus* Wild yak	**v**	**v**
A0A6J3S691_TURTR keratin, type II cytoskeletal 78	*Tursiops truncates* Common bottlenose dolphin	**v**	**v**
A0A383ZRF2_BALAS keratin, type I cytoskeletal 24	*Balaenoptera acutorostrata scammony* Minke whale	**v**	**v**

A0A0C5AGQ3_BUBBU Lysozyme	*Bubalus bubalis* Water buffalo	**v**	
A2P2I3_SHEEP VH region	*Ovis aries* Sheep		
A0A075B7I6_PIG Ig-like domain-containing protein	*Sus scrofa* Wild boar		
A0A0R4I993_SUSBA Tubulin alpha chain	*Sus barbatus* Bornean bearded pig		
A0A5N4EAI9_CAMDR Annexin	*Camelus dromedarius* Dromedary		
A0A2Y9EH04_PHYMC fer-1-like protein 4	*Physeter macrocephalus* Sperm Whale		
A0A5J5N0U1_MUNRE Uncharacterized protein (small proline-rich protein 2I-like; Type II small proline-rich protein; small proline-rich protein 2E-like)	*Muntiacus reevesi* Chinese muntjac	**v**	
A0A6B0R269_9CETA Ig-like domain-containing protein	*Bos mutus* Wild yak	**v**	**v**

A0A452E907_CAPHI Uncharacterized protein (skin-specific protein 32; Chromosome 3 C1orf68 homolog; Chromosome 1 open reading frame 68)	*Capra hircus* Goat	**v**	**v**
A0A4W2E476_BOBOX Ig-like domain-containing protein	*Bos indicus x Bos taurus* Zebu x Cow	**v**	**v**
A0A212CS30_CEREH Ig-like domain-containing protein	*Cervus elaphus hippelaphus* European red deer	**v**	**v**
A0A6J0ZEI2_ODOVR complement C3	*Odocoileus virginianus texanus* White-tailed deer		**v**
A0A6J0Y2W1_ODOV fibronectin isoform X5	*Odocoileus virginianus texanus* White-tailed deer		**v**
A0A5N3WRA9_MUNMU C3-beta-c	*Muntiacus muntjac* Barking deer		**v**
A0A6J0YF65_ODOVR alpha-2-macroglobulin	*Odocoileus virginianus texanus* White-tailed deer		**v**

A0A6J0YGQ5_ODOVR pregnancy zone protein-like isoform X1	*Odocoileus virginianus texanus* White-tailed deer	**v**
A0A212D8V0_CEREH FGG	*Odocoileus virginianus texanus* White-tailed deer	**v**
A0A6J0YZJ7_ODOVR ceruloplasmin isoform X2	*Odocoileus virginianus texanus* White-tailed deer	**v**
A0A6J0XY06_ODOVR thrombospondin-1 isoform	*Odocoileus virginianus texanus* White-tailed deer	**v**
A0A6J0XUD5_ODOVR complement C4-A-like	*Odocoileus virginianus texanus* White-tailed deer	**v**
A0A6J0WY92_ODOVR complement factor H-like	*Cervus elaphus hippelaphus*	**v**
A0A6J0W0N0_ODOVR inter-alpha-trypsin inhibitor heavy chain H1	*Odocoileus virginianus texanus* European red deer	**v**
A0A4W2C0F6_BOBOX C4a anaphylatoxin	*Odocoileus virginianus texanus* White-tailed deer	**v**

A0A212CJ19_CEREH CP	*Odocoileus virginianus texanus* White-tailed deer	**v**
A0A6J0XUP5_ODOVR complement C4-A-like	*Odocoileus virginianus texanus* White-tailed deer	**v**
E1BH06_BOVIN C4a anaphylatoxin	*Odocoileus virginianus texanus* White-tailed deer	**v**
A0A6J0WIC5_ODOVR inter-alpha-trypsin inhibitor heavy chain H2	*Bos indicus x Bos taurus* Zebu x Cow	**v**
A0A6J0YC26_ODOVR heparin cofactor 2	*Cervus elaphus hippelaphus* European red deer	**v**
A0A6J0ZDS1_ODOVR C4b-binding protein alpha chain	*Odocoileus virginianus texanus* White-tailed deer	**v**
A0A5N3XTJ5_MUNRE Antithrombin-III	*Bos taurus* Cow	**v**
A0A220IGA4_RANTA Adult beta-globin	*Odocoileus virginianus texanus* White-tailed deer	**v**

A0A6J0WIA8_ODOVR Prothrombin	*Odocoileus virginianus texanus* White-tailed deer	**v**
A0A6J0Y9J4_ODOVR apolipoprotein A-I	*Odocoileus virginianus texanus* White-tailed deer	**v**
Q9TS85_BOVIN Histidine-rich GLYCOPRO-TEIN=FACTOR XIIIA sub-strate	*Muntiacus reevesi* Chinese muntjac	**v**
A0A212DHP9_CEREH APOA1	*Rangifer tarandus* Reindeer	**v**
A0A0B8RTA2_PIG Actin, gamma 1	*Odocoileus virginianus texanus* White-tailed deer	**v**
A0A212D467_CEREH C1QB	*Odocoileus virginianus texanus* White-tailed deer	**v**
A0A5N3VLU1_MUNMU Prothrombin	*Bos taurus* Cow	**v**
S9Y253_CAMFR Kininogen-2 isoform I	*Cervus elaphus hippel-aphus* European red deer	**v**

A0A6J0XQV8_ODOVR Hemopexin	*Sus scrofa* Wild boar	**v**
A0A6J0WWF4_ODOVR vitronectin isoform X1	*Cervus elaphus hippelaphus* European red deer	**v**
A0A6J0W8S2_ODOVR plasminogen isoform X1	*Muntiacus muntjac* Barking deer	**v**
A0A6J0Z5Q2_ODOVR transcobalamin-2	*Camelus ferus* Wild Bactrian camel	**v**
A0A5N3X8Z5_MUNRE Hemopexin	*Odocoileus virginianus texanus* White-tailed deer	**v**
A0A212CJF4_CEREH C1q domain-containing protein	*Odocoileus virginianus texanus* White-tailed deer	**v**
C0LXP2_ODOVR Complement 1 subcomponent q polypeptide gamma	*Odocoileus virginianus texanus* White-tailed deer	**v**
A0A286ZIC1_PIG Actin-depolymerizing factor	*Odocoileus virginianus texanus* White-tailed deer	**v**
A0A5N3VK90_MUNMU Actin-depolymerizing factor	*Muntiacus reevesi* Reeves's muntjac	**v**

A0A212DHZ3_CEREH HPX	*Cervus elaphus hippel-aphus* European red deer	**v**
A0A5N3V774_MUNMU Uncharacterized protein	*Odocoileus virginianus texanus* White-tailed deer	**v**
A0A6J0X6J4_ODOVR selenoprotein P	*Sus scrofa* Wils boar	**v**
A0A6J0Y2T5_ODOVR hemoglobin subunit alpha	*Muntiacus muntjac* Barking deer	**v**
A0A480Y2E3_PIG Kininogen-1 isoform 1	*Cervus elaphus hippel-aphus* European red deer	**v**
A0A6J0YKX8_ODOVR protein AMBP	*Muntiacus muntjac* Barking deer	**v**
A0A5J5MM09_MUNRE Plasminogen	*Odocoileus virginianus texanus* White-tailed deer	**v**
A0A212C7P2_CEREH PLG	*Odocoileus virginianus texanus* White-tailed deer	**v**

A0A5N3WQN5_MUNMU Vitellogenin domain-containing protein	*Sus scrofa* Wild boar	**v**
A0A5N3X9D4_MUNRE SERPIN domain-containing protein	*Odocoileus virginianus texanus* White-tailed deer	**v**
A0A6J0YIK3_ODOVR vitamin D-binding protein	*Muntiacus reevesi* Chinese muntjac	**v**
A0A6J0XXC2_ODOVR apolipoprotein B-100 isoform X1	*Cervus elaphus hippelaphus* European red deer	**v**
A0A6J0Y0A8_ODOVR serpin A3-7-like	*Muntiacus muntjac* Barking deer	**v**
A0A212CS37_CEREH SERPIN domain-containing protein	*Muntiacus reevesi* Chinese muntjac	**v**
A0A6J0VV77_ODOVR CD5 antigen-like	*Odocoileus virginianus texanus* White-tailed deer	**v**
A0A5N3WVG9_MUNMU Apolipoprotein H	*Odocoileus virginianus texanus* White-tailed deer	**v**

A0A212D5I5_CEREH DSP	*Odocoileus virginianus texanus* White-tailed deer	**v**
A0A6B0SDR2_9CETA Glyceraldehyde-3-phosphate dehydrogenase	*Cervus elaphus hippelaphus* European red deer	**v**
A0A5N3V0U6_MUNMU Peptidase_M14 domain-containing protein	*Odocoileus virginianus texanus* White-tailed deer	**v**
A0A2U4C7Y7_TURTR histidine-rich glycoprotein	*Muntiacus reevesi* Chinese muntjac	**v**
A0A452FXZ3_CAPHI Apolipoprotein H	*Cervus elaphus hippelaphus* European red deer	**v**
A0A5N3WZL8_MUNMU Complement C1q subcomponent subunit A	*Bos mutus* *W*ild yak	**v**
A0A6J0XZP9_ODOVR alpha-1-antitrypsin	*Muntiacus muntjac* Barking deer	**v**
A0A452E7A0_CAPHI Plasminogen	*Tursiops truncates* Common bottlenose dolphin	**v**

A0A452F014_CAPHI SERPIN domain-containing protein	*Capra hircus* Goat	**v**
A0A2Y9LVH2_DELLE Amine oxidase	*Muntiacus muntjac* Barking deer	**v**
A0A088Q0F1_9CETA Heat shock protein 90kDa alpha	*Odocoileus virginianus texanus*	**v**
A0A6B0R457_9CETA Activating signal cointegrator 1 complex subunit 3	*Capra hircus* Goat	**v**
A0A212DB97_CEREH SERPINF2	*Capra hircus* Goat	**v**
A0A6J3PT56_TURTR immunoglobulin lambda-1 light chain-like isoform X1	*Delphinapterus leucas* Beluga whale	**v**
A0A212CSZ1_CEREH SERPINA5	*Bos grunniens x Bos taurus* Domestic yak x Cow	**v**
A0A6J0XAN1_ODOVR complement component C9	*Bos mutus* Wild yak	**v**
A0A6J0Y2I3_ODOVR alpha-1B-glycoprotein	*Cervus elaphus hippelaphus* European red deer	**v**

A0A1L6BNZ0_BUBBU Alpha-S1-casein	*Tursiops truncates* Common bottlenose dolphin	**v**
A0A212D4C7_CEREH Ribosomal protein	*Cervus elaphus hippel-aphus* European red deer	**v**
A0A212CIC4_CEREH FETUB	*Odocoileus virginianus texanus* White-tailed deer	**v**
A0A6J0WSX6_ODOVR tubulin beta-3 chain	*Odocoileus virginianus texanus* White-tailed deer	**v**
A0A340WKS1_LIPVE Selenoprotein P	*Bubalus bubalis* Water buffalo	**v**
A0A4W2BXS4_BOBOX Kallikrein B1	*Cervus elaphus hippel-aphus* European red deer	**v**
A0A6J0Z7P6_ODOVR apolipoprotein R-like	*Cervus elaphus hippel-aphus* European red deer	**v**
A0A5N3WWG2_MUNMU SERPIN domain-containing protein	*Odocoileus virginianus texanus* White-tailed deer	**v**

A0A2Y9EXF5_PHYMC 2-phospho-D-glycerate hydro-lyase	*Lipotes vexillifer* Baiji	**v**
A0A212D4I5_CEREH C3/C5 convertase	*Bos indicus x Bos taurus* Zebu x Cow	**v**
A0A212CM12_CEREH 40S ribosomal protein S18	*Odocoileus virginianus texanus* White-tailed deer	**v**
A0A212CI11_CEREH Alpha-2-HS-glycoprotein	*Muntiacus muntjac* Barking deer	**v**
A0A5J5MZJ4_MUNRE MACPF domain-containing protein	*Physeter macrocephalus* Sperm whale	**v**
A0A212C6Y8_CEREH Transthyretin	*Cervus elaphus hippelaphus* European red deer	**v**
A0A212D5R7_CEREH JCHAIN	*Cervus elaphus hippelaphus* European red deer	**v**
A0A480MMJ7_PIG Heat shock 70 kDa protein	*Cervus elaphus hippelaphus* European red deer	**v**

A0A6J0Y8N1_ODOVR angiopoietin-related protein 6 isoform X2	*Muntiacus reevesi* Chinese muntjac	**v**
A0A5N4EH44_CAMDR Biorientation of chromosomes in cell division protein 1-like 1	*Cervus elaphus hippelaphus* European red deer	**v**
S9WER1_CAMFR Biorientation of chromosomes in cell division protein 1-like protein	*Cervus elaphus hippelaphus* European red deer	**v**
A0A3Q1LUP1_BOVIN Uncharacterized protein (cilia- and flagella-associated protein 54)	*Sus scrofa* Wild boar	**v**
A0A2Y9EUI8_PHYMC arachidonate 15-lipoxygenase	*Odocoileus virginianus texanus* White-tailed deer	**v**
A0A0B8RZA9_PIG (Proliferation-associated 2G4, 38kDa)	*Camelus dromedarius* Dromedary	**v**
A0A286ZRK7_PIG 60S ribosomal protein L11	*Camelus ferus* Wild Bactrian camel	**v**

A0A287BDT6_PIG Ubiquitin carboxyl-terminal hydrolase	*Bos taurus* Cow	**v**
A0A287AFA5_PIG Endoplasmin	*Physeter macrocephalus* Sperm whale	**v**
BIP_BOVIN Endoplasmic reticulum chaperone BiP	*Sus scrofa* Wild boar	**v**
A0A2Y9M486_DELLE protein PRRC2C isoform X8	*Sus scrofa* Wild boar	**v**
A0A383Z8A9_BALAS putative SEC14-like protein 6	*Sus scrofa* Wild boar	**v**
A0A212D225_CEREH TMED9	*Sus scrofa* Wild boar	**v**
A0A0B8RSX6_PIG Filamin A, alpha	*Bos taurus* Cow	**v**
A0A452E6D4_CAPHI Uncharacterized protein (complement C5-like)	*Delphinapterus leucas* Beluga whale	**v**
A0A212CJY0_CEREH Transferrin receptor protein 1	*Balaenoptera acutorostrata scammony* Minke whale	**v**

A0A4W2F326_BOBOX Anaphylatoxin-like domain-containing protein	*Cervus elaphus hippelaphus* European red deer	**v**
A0A212CKA1_CEREH Peptidyl-prolyl cis-trans isomerase	*Sus scrofa* Wild boar	**v**
A0A4W2F827_BOBOX 60 kDa poly(U)-binding-splicing factor	*Capra hircus* Goat	**v**
A0A212CT53_CEREH Lactadherin	*Cervus elaphus hippelaphus* European red deer	**v**

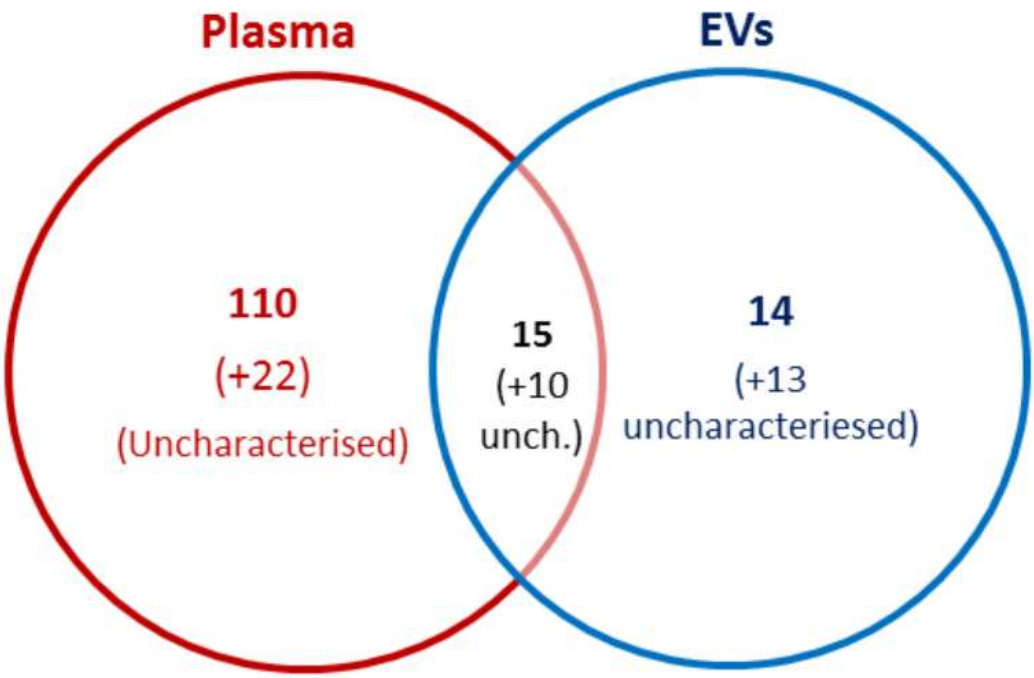

Figure 21. Shared deiminated protein hits in reindeer. Venn diagram showing deiminated protein hits identified in *R. tarandus* whole plasma and plasma EVs, representing shared and unique proteins hits (uncharacterized hits are indicated in brackets).

3.6.1 Discussion: Deiminated Protein Hits in Whole Body fluids and EVs Commonly Identified in Purple Sea urchin, Sea lamprey and Reindeer

In Table 11 below are listed the four common deiminated protein targets across the three species: Histone H2A, H2B, H3, H4, Elongation factor 1 alpha, Ribosomal proteins, and Complement C. These proteins were observed in either the entire biofluid samples and the biofluid-derived extracellular vesicles (EVs), or exclusively in either the whole biofluid sample or the biofluid-derived EVs sample of purple sea urchin, sea lamprey, and reindeer.

Table 11. Common deiminated proteins identified in Purple sea urchin coelomic fluid and coelomic fluid-EVs, Sea lamprey plasma and plasma-EVs and Reindeer plasma and plasma-EVs.

Deiminated Proteins	**Species**					
	Purple sea urchin EVs	**Purple sea urchin CF**	**Sea lamprey plasma-EVs**	**Sea Lamprey plasma**	**Rein-deer plasma -EVs**	**Rein-deer Plasma**
Histone H2A, H2B, H3, H4	✓	✓	✓	✓	✓	✓
Elongation factor alpha 1		✓	✓	✓	✓	✓
Ribosomal proteins		✓	✓	✓	✓	

Complements components		✓	✓	✓		✓

Histone H2A, H2B, H3, H4 were identified to be deiminated in either coelomic fluid and coelomic fluid-EVs in purple sea urchin, also in plasma and plasma-EVs of lamprey and in plasma and plasma-EVs of reindeer. These histones are known deiminated target with roles in epigenetic regulation and antipathogenic responses in a range of taxa (Pamenter et al.,2019; Criscitiello et al.,2020 a,b,c) as well as in relation to gene regulation in human pathologies, including cancer (Lange *et al*.,2017; Fuhrmann and Thompson,2016, Beato and Sharma,2020). In sea urchin histones are reported in embryos, larva, and adults (Marzluff et al.,2006), and their modifications such as phosphorylation and ubiquitination have been widely studied in development (Green et al.,1995; Jasinskiene et al.,1995). In lamprey, histones have been assessed in sperm (Saperas et al.,1994) and histone acetylation has been related to neural regeneration (Chen et al., 2016), however, deimination of histone has never been reported before. The role of deiminated histone H3 has been studied in anti-pathogenic responses in relation to extracellular trap formation (NETosis/ ETosis) (Burgener and Schroder, 2020) and their role as antimicrobial compound has been reported in humans (Lee et al.,2009) and various taxa including molluscs (Li et al., 2007; De Zoysa et al., 2009; Seo et al., 2011; Dorrington et al., 2011), crustaceans (Smith and Dyrynda, 2015; Sruthy et al.,2019), amphibians (Cho et al.,2009), teolosts (Fernandes et al.,2002), reptiles (Kozlowoski et al.,2016), and pinnipeds (Villagra-Blanco et al.,2019). Also, histones have been related to neural regeneration (Lange *et al*.,2011,2014) and neurodegenerative diseases (Sancandi et al.,2021).

Elongation factor 1 alpha was detected in coelomic fluid of purple sea urchin, which has previously found to undergo transcriptional and translational modification in early developmental processes (Peeler et al.,1990). In lamprey, was identified to be deiminated in plasma and plasma-EVs. In reindeer, elongation factor 1 alpha was identified in its deiminated form in whole plasma and exported in plasma-EVs. Elongation factor 1 alpha has multiple roles in metabolic function, cell growth, cytoskeleton organisation, apoptosis, nuclear export of proteins and immune response (Khacho et al.,2009, Talapatra et al.,2002, Vera et al., 2014). Previously, it has been identified as a deiminated candidate in teleosts (Magnadottir et al.,2018) and Crustacea (Bowden et al.,2020).

A range of **ribosomal proteins** were found to be deiminated in coelomic fluid (60 ribosomal protein L40); in lamprey, 60S ribosomal protein L18 was found to be deiminated in both plasma and plasma-EVs, while 60S ribosomal protein L23, ribosomal protein L3 like, 60S acidic ribosomal protein P0 were found to be deiminated in plasma EVs only. In reindeer, ubiquitin-60S ribosomal protein L40 was identified in plasma-EVs only. Ribosomal proteins are structural components of the protein synthesis machinery and play multifaceted roles in protein synthesis (Gerst, 2018; Baßler and Hurt, 2019); they also have been related to innate, including mucosal, immune responses and can act as antimicrobials (Moon,2011,2014; Seo,2017). Ribosomes have been identified as deimination candidates in other taxa, including humans (Guo et al.,2011), teleost (Magnadottir et al.,2018) and Mollusca (Bowden et al.,2020).

Complement C3 was identified as deiminated in coelomic fluid but not deiminated in EVs; however, it was presented in its normal form as part of the EV cargo, thus indicating that it plays different roles in cellular communication in deiminated form and that export of its unmodified versus deiminated form in EVs may differ between animal species. C3 is a key component of the complement system and has been well-described

in sea urchins (Hibino et al., 2006; Smith *et al.,*2010; Chiaramonte and Russo, 2015). A complement system that resembles and has a similar response to the vertebrate's complement system: the complement system is called prophenoloxidase, and its function is to facilitate wound healing by promoting the production of melanin at the site of injury (Chiaramonte and Russo, 2015). In lamprey, the C1q domain-containing protein and C1q-TNF-related protein-9 were identified as deimination candidates in plasma and plasma-EVs. C1q forms part of the lamprey complement system, acting as lectin (Matsushita et al.,2004), activating C3 in association with MASP via the lectin pathway (Dodds and Matsushita, 2007; Matsushita 2018). Lamprey C1q can furthermore interact with a secreted type of VLR (VLRB) in a complex with antigens and may, via MASP, mediate the activation of C3, resulting in cytolysis. The C1q/TNF-related superfamily proteins (CTRPs) are involved in diverse processes, including inflammation, apoptosis, host defence, autoimmunity, organogenesis, cell differentiation, insulin resistance and hibernation (Chen et al., 2016b). Several C1Q/TNF-related proteins have been identified in river lamprey (*Eudontomyzon morii*) and are related to immune response or injury repair processes (Chen et al., 2016b). The deimination of C1q has previously been identified in several taxa, including in mammals (Criscitiello et al., 2020a) and reptiles (Criscitiello et al., 2020c) and C1q domain-containing proteins were also identified to be deiminated in Mollusca (Bowden et al., 2020c). Complement components of the complement system, including C1q, C3, C4, C5, and C9, as well as factor H and the C3/C5 convertase, have also been identified to be deiminated in the whole plasma of reindeer.

The identification of deiminated histones H2A, H2B, H3, and H4 in coelomic fluid and coelomic fluid-derived extracellular vesicles (EVs) of purple sea urchins, as well as in the plasma and plasma-derived EVs of lamprey and reindeer, highlights the conservation of histone deimination across diverse taxa. These modified histones are known to

play crucial roles in epigenetic regulation, antipathogenic responses, and gene regulation, including associations with human pathologies such as cancer. The study also sheds light on the previously unreported deimination of histones in lamprey, specifically in sperm, and emphasises the potential relevance of histone deimination in neural regeneration, a phenomenon observed in lamprey. Furthermore, the role of deiminated histone H3 in anti-pathogenic responses, such as extracellular trap formation, has implications for innate immune defence in various organisms, including humans and different animal taxa. Elongation factor 1 alpha, detected in the coelomic fluid of purple sea urchin and found to be deiminated in lamprey and reindeer, emerges as a multifunctional protein with roles in metabolic function, cell growth, cytoskeleton organisation, apoptosis, nuclear export of proteins, and immune response. The identification of deiminated elongation factor 1 alpha in teleosts and crustaceans further supports the conservation of this post-translational modification across different species. The study also uncovered deimination events in various ribosomal proteins across the studied organisms, highlighting the potential impact of deimination on the structural components of the protein synthesis machinery. Ribosomal proteins, known for their roles in protein synthesis, also exhibit antimicrobial properties and have been associated with innate immune responses. Complement C3, identified as deiminated in the coelomic fluid of purple sea urchins, suggests a unique role for deimination in cellular communication, as the deiminated form of C3 was not detected in EVs. The intricate involvement of complement components, including C1q, C3, C4, C5, C9, factor H, and the C3/C5 convertase, in the complement system of reindeer further emphasises the potential impact of deimination on immune-related processes across species.This comprehensive analysis of deiminated proteins in diverse organisms highlights the broad implications of protein deimination in various biological processes, including epigenetic regulation, immune response, and cellular communication. The conservation of

deimination events across different species suggests evolutionary significance and opens avenues for further exploration of the functional consequences of this post-translational modification in health and disease.

3.6.2 Protein interaction networks identification for deiminated protein hits from body fluids and EVs

Deiminated candidate proteins identified in purple sea urchin coelomic fluid and EVs, lamprey plasm a and plasma EVs and reindeer plasma and plasma EVs were submitted to STRING (Searching Tool for the Retrieval of Interacting Genes/Proteins) (https://string-db.org/) for the prediction of protein-protein interaction networks as shown in Fig.22:Protein-protein interaction networks of deiminated proteins identified in purple sea urchin coelomic fluid (PPI enrichment p-value for the protein network is 5.31 × 10^(-5)) and EVs (PPI enrichment p-value for the protein network is 1.11 × 10-6) based on known and predicted interactions in Echinoidea; Fig.23 Protein-protein interaction networks of deiminated proteins identified in sea lamprey whole plasma (PPI enrichment p-value: 2.78 × 10-15) and plasma EVs (PPI enrichment p-value: 1.28 × 10-11); Fig.24 Protein-protein interaction networks of deiminated proteins identified in reindeer plasma and plasma-EVs based on known and predicted interaction in Bos Taurus as a representative species for Artiodactyla (Reindeer (Rangifer tarandus))(PPI enrichment p-value for both networks is $p < 1.0 \times 10\text{-}16$). Coloured nodes represent query proteins only. Coloured lines connecting nodes show the type of interactions between the nodes of the networks based on known interactions, predicted interactions, show the type of interactions between the nodes.

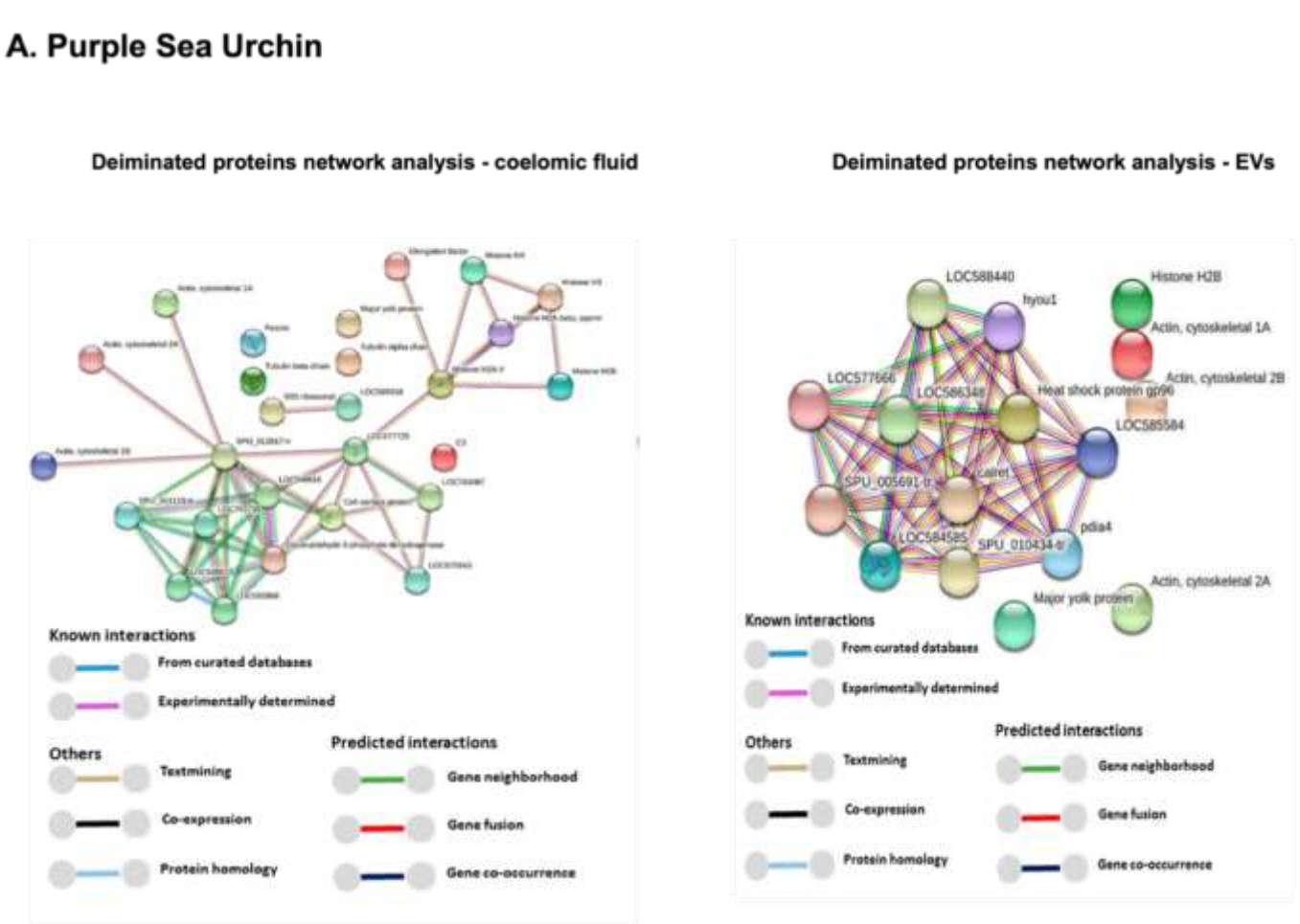

Figure 22. STRING analysis across phylogeny. Protein-protein interaction networks of deiminated proteins identified in *Strongylocentrotus purpuratus* (purple sea urchin).

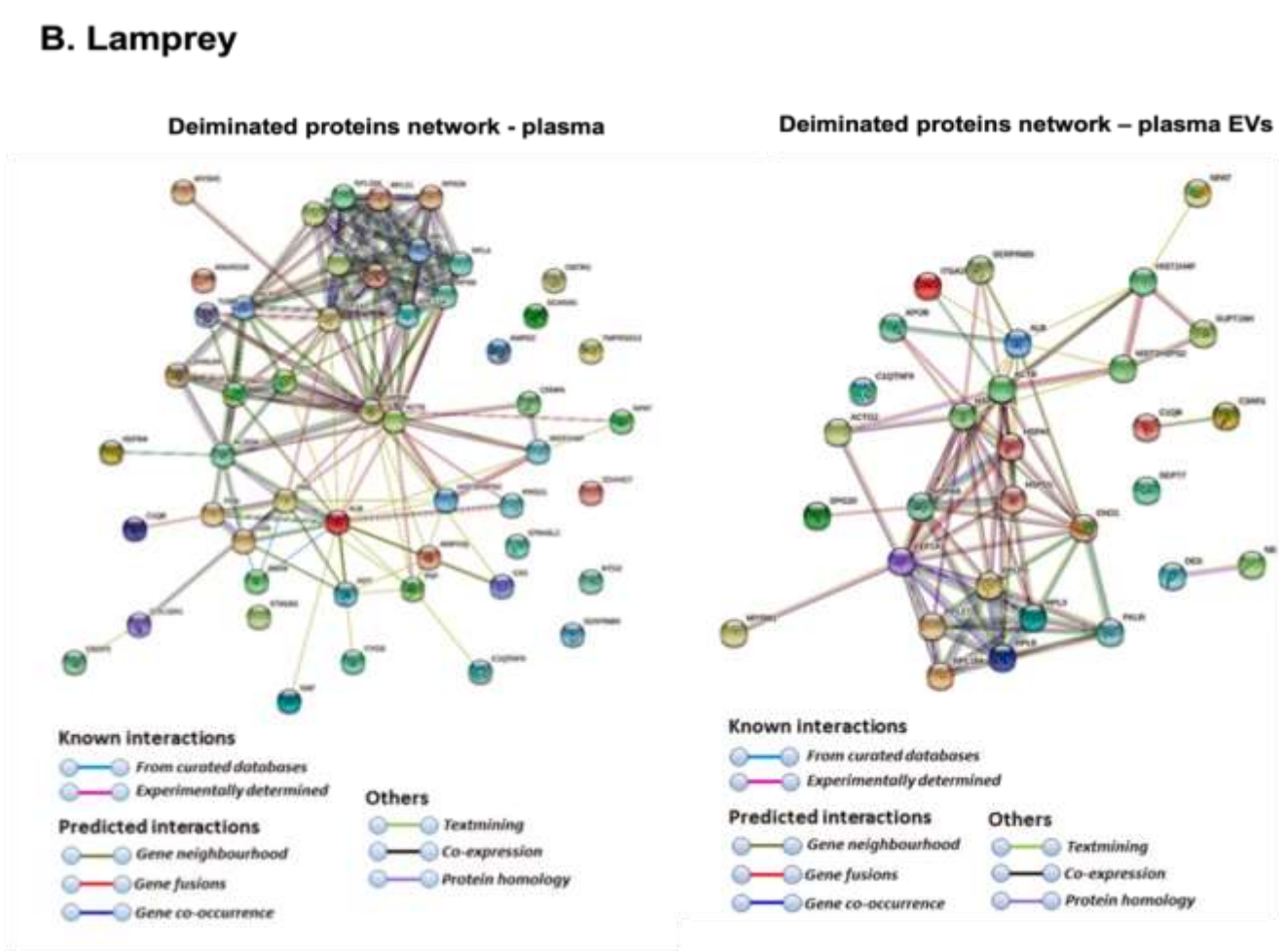

Figure 23. STRING analysis across phylogeny. Protein-protein interaction networks of deiminated proteins identified in *Petromyzon marinus* (sea lamprey).

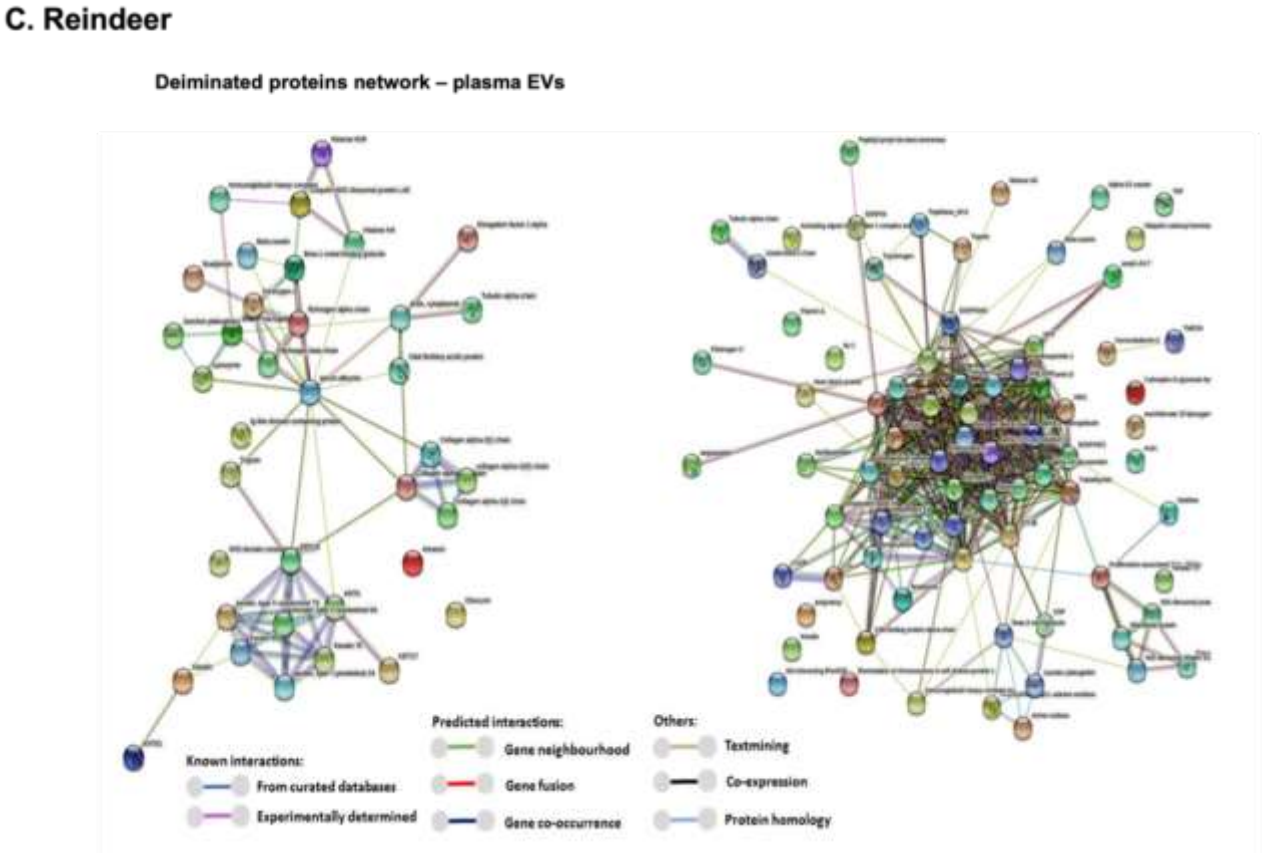

Figure 24. STRING analysis across phylogeny. Protein-protein interaction networks of deiminated proteins identified in *Rangifer tarandus* (reindeer).

3.6.3 Discussion on KEGG Pathway Identification by STRING Analysis for Deiminated Proteins in Purple Sea Urchin, Sea Lamprey and Reindeer

STRING analysis for deiminated proteins in purple sea urchin coelomic fluid revealed nine KEGG pathways (Fig.25): phagosome, glycolysis gluconeogenesis, pentose phosphate pathway, related to immune functions; biosynthesis of amino acids, fructose and mannose metabolism, carbon metabolism, ribosome biogenesis, protein processing in ER and metabolic pathways, all related to metabolic functions. Two of these pathways (phagosome and protein processing in endoplasmic reticulum) were exported and identified also in coelomic fluid EVs (Fig.25). KEGG pathways identified for deiminated proteins in lamprey whole plasma were HIF-1 signalling pathway, Platelet activation, Influenza A, Fructose and mannose metabolism, Carbon metabolism and Type II diabetes mellitus. In contrast, KEGG pathways identified in lamprey plasma-EVs were Antigen processing and presentation, *Staphylococcus aureus* infection, Legionellosis, Prion diseases, Fluid shear stress and atherosclerosis, RNA degradation, Thyroid hormone synthesis, Arrhythmogenic right ventricular cardiomyopathy ARVC), Hypertrophic cardiomyopathy, Dilated Cardiomyopathy (Fig 26). In reindeer, KEGG pathways identified in whole plasma were pertussis, ferroptosis, phagosome, Staphylococcus aureus infection, systemic lupus erythematosus (SLE), prion disease, thyroid hormone synthesis, vitamin digestion and absorption, and complement and coagulation pathways which are also found in reindeer plasma EVs. Specific pathways for reindeer plasma EVs were ECM receptor interaction, platelet activation, amoebiasis, the estrogen signalling pathway, the AGE–RAGE signalling pathway in diabetic complications, the relaxin signalling pathway, as well as in protein digestion and absorption (Fig.27).

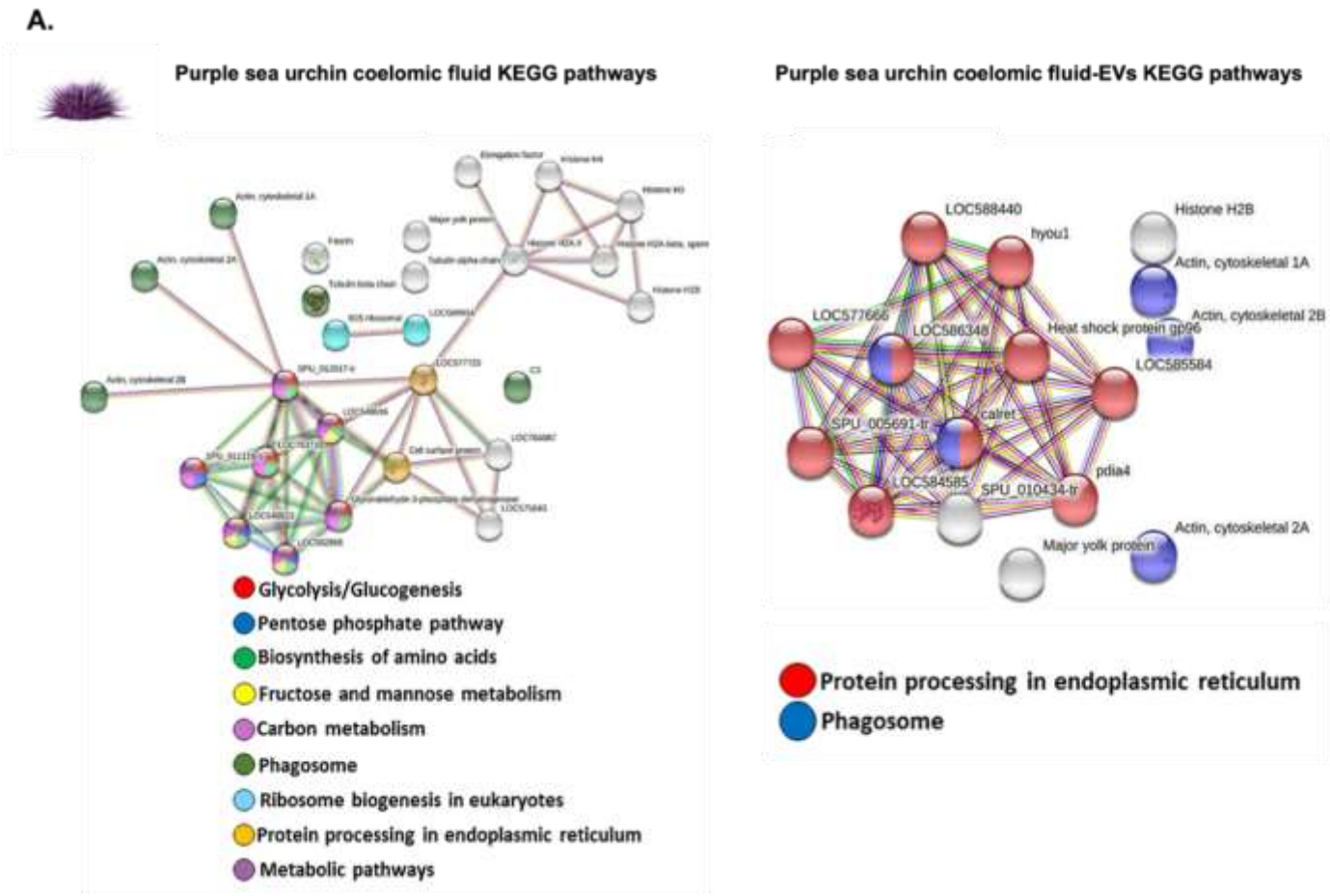

Figure 25. KEGG pathways identified from STRING analysis for deiminated protein candidates across phylogeny. *Strongylocentrotus purpuratus* (purple sea urchin) coelomic fluid and coelomic fluid EVs;

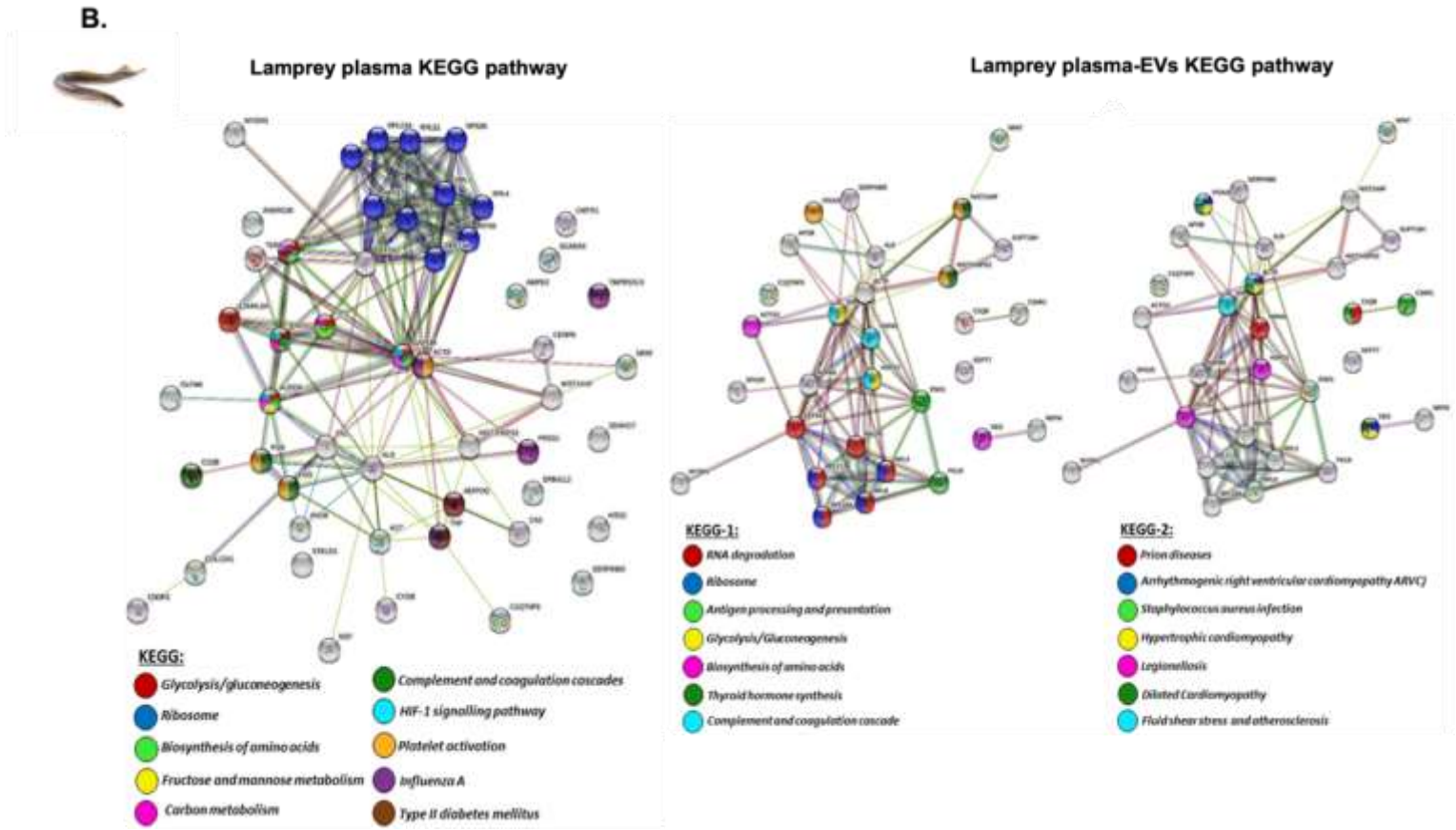

Figure 26. KEGG pathways identified from STRING analysis for deiminated protein candidates across phylogeny. *Petromyzon marinus* (sea lamprey) plasma and plasma EVs;. KEGG pathways identified are highlighted by the colour-coded nodes in (A), (B) and (C), respectively.

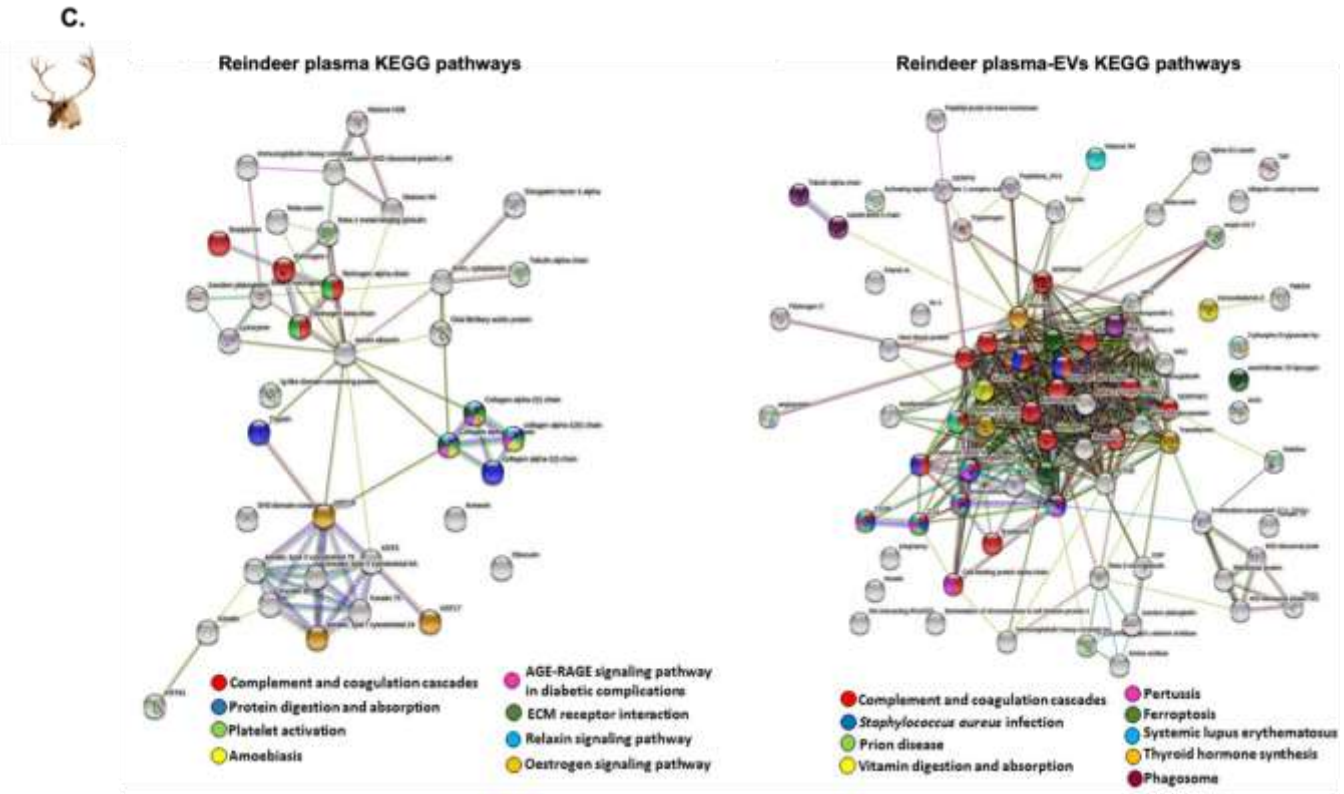

Figure 27. KEGG pathways identified from STRING analysis for deiminated protein candidates across phylogeny. *Rangifer tarandus* (reindeer) plasma and plasma EVs. KEGG pathways identified are highlighted by the colour-coded nodes in (A), (B) and (C), respectively.

Ten KEGG pathways were found to be shared after STRING analysis for deiminated proteins in *Strongylocentrotus purpuratus* (purple sea urchin), *Petromyzon marinus* (sea lamprey) and *Rangifer tarandus* (reindeer); they are illustrated in Fig.28,29 and 30 respectively, and summarised in Table 12 below. Common proteins identified between species are highlighted with coloured boxes (red boxes highlight KEGG pathways common to purple sea urchin and sea lamprey; purple boxes highlight common KEGG pathways between sea lamprey and reindeer; yellow boxes highlight KEGG pathways common to purple sea urchin and reindeer

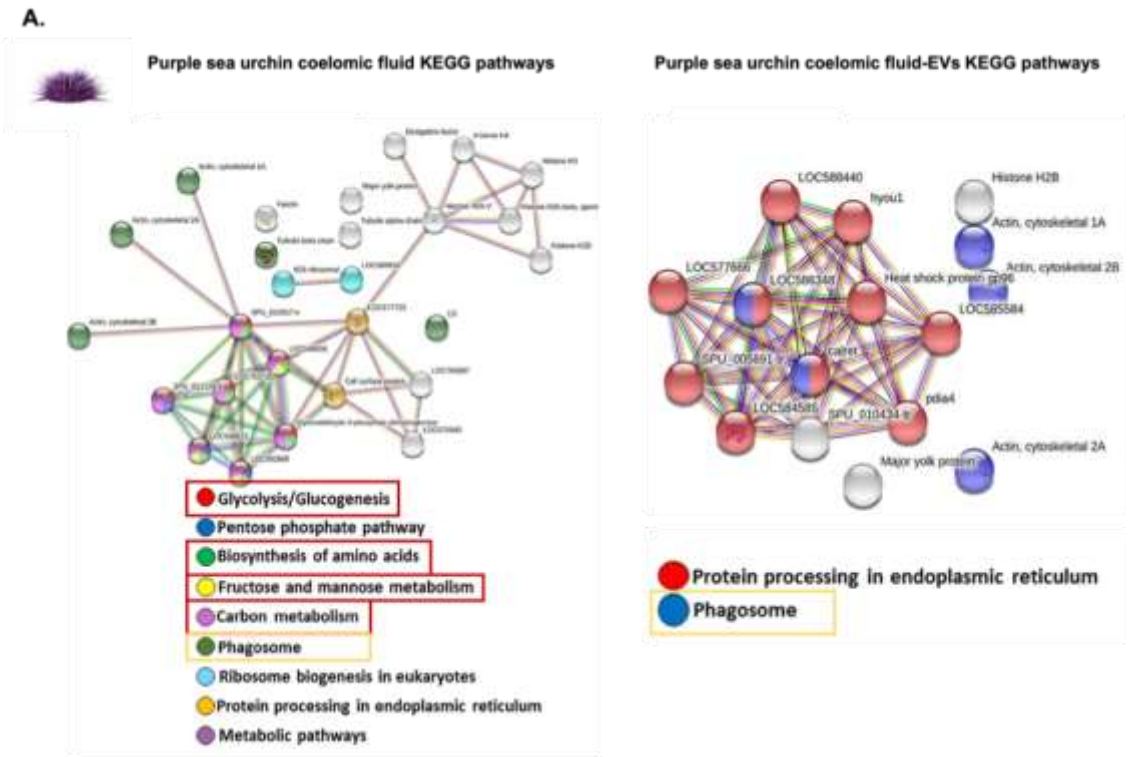

Figure 28. Common KEGG pathways identified from STRING analysis for deiminated protein candidates in purple sea urchin (*Strongylocentrotus purpuratus*). Common pathways are identified by colour-coded boxes: yellow boxes for pathways common to purple sea urchin and reindeer, purple boxes for pathways common sea lamprey and reindeer, and red boxes for common pathways between purple sea urchin and lamprey.

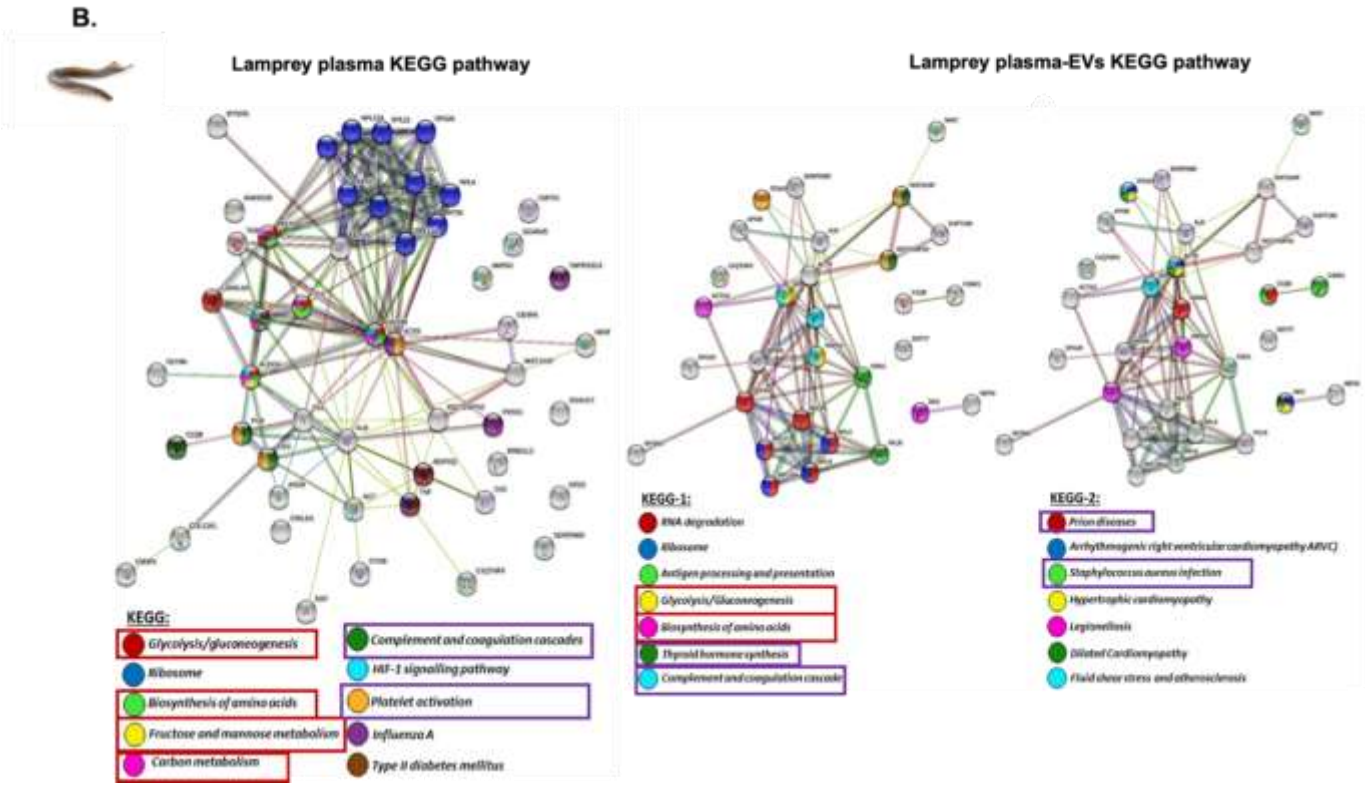

Figure 29.Common KEGG pathways identified from STRING analysis for deiminated protein candidates in lamprey (*Petromyzon marinus*). Common pathways are identified by colour-coded boxes: yellow boxes for pathways common to purple sea urchin and reindeer, purple boxes for pathways common sea lamprey and reindeer, and red boxes for common pathways between purple sea urchin and lamprey.

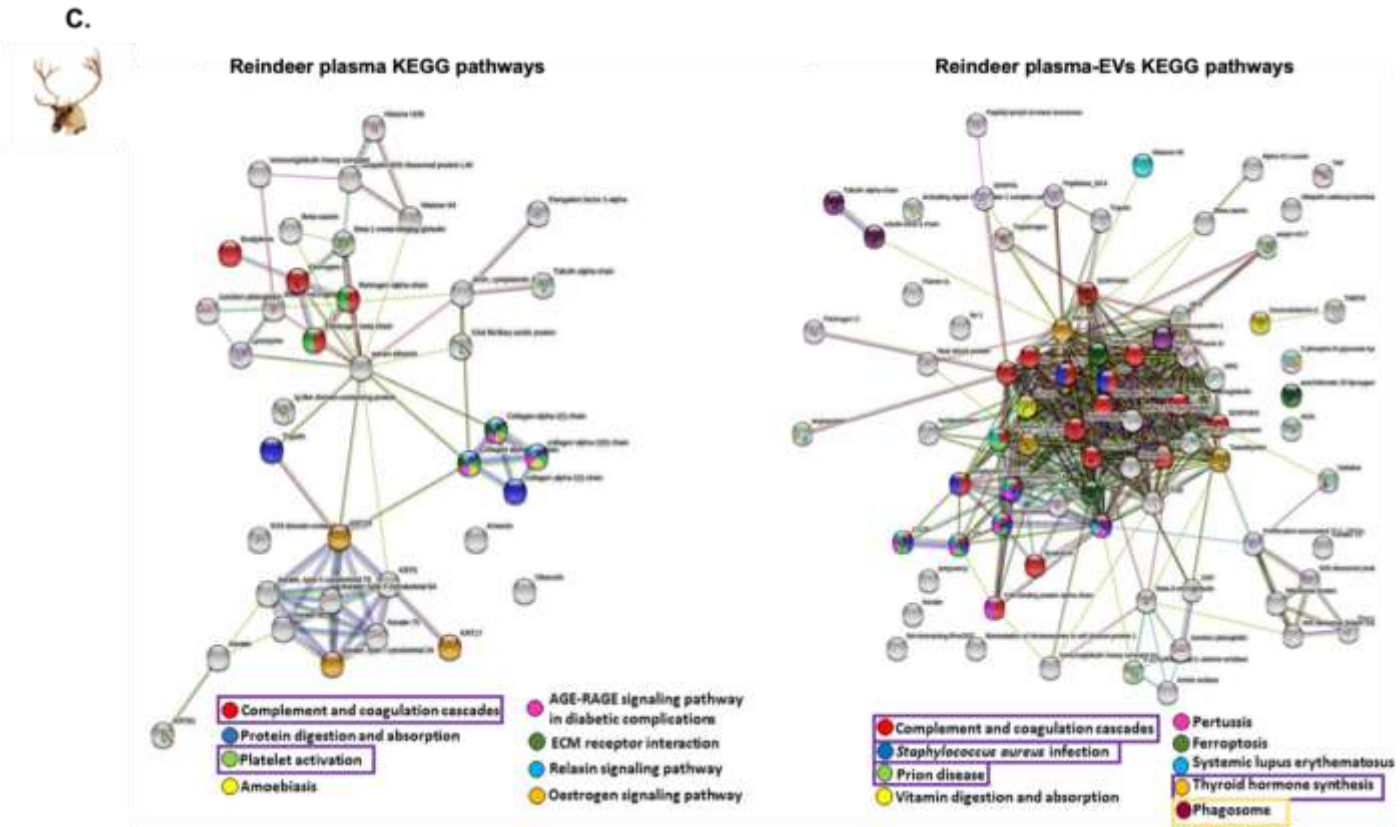

Figure 30. Common KEGG pathways identified from STRING analysis for deiminated protein candidates in reindeer (*Rangifer tarandus*). Common pathways are identified by colour-coded boxes: yellow boxes for pathways common to purple sea urchin and reindeer, purple boxes for pathways common sea lamprey and reindeer, and red boxes for common pathways between purple sea urchin and lamprey

Table 12. Common KEGG pathways identified in whole plasma/coelomic fluid and plasma/coelomic fluid EVs of purple sea urchin, lamprey, and reindeer.

Common/shared KEGG pathways	**Purple Sea Urchin coelomic fluid**	**Purple Sea Urchin coelomic fluid-EVs**	**Sea lamprey whole plasma**	**Sea lamprey plasma-EVs**	**Reindeer whole plasma**	**Reindeer plasma-EVs**
Glycolysis and Gluconeogenesis	✓		✓	✓		
Biosynthesis of amino acids	✓		✓	✓		
Fructose and mannose metabolism	✓		✓			
Carbon metabolism	✓		✓			
Phagosome	✓	✓				✓
Complement and coagulation cascades			✓	✓	✓	✓
Platelet activation			✓		✓	

Thyroid hormones synthesis				✓		✓
Staphylococcus aureus infection				✓		✓
Prion disease				✓		✓

Glycolysis and gluconeogenesis KEGG pathway were found to be commonly present in purple sea urchin coelomic fluid but not exported in coelomic fluid EVs and in sea lamprey plasma and plasma-derived EVs. Also, glycolysis and gluconeogenesis have been identified in cetacean sera (whales and orca) (Magnadóttir *et al*.,2020), in alligator plasma-EVs (Criscitiello *et al*.,2020 c), in lobster and horseshoe crab haemolymph (Bowden *et al*.,2020), in alveolates (Kristmundsson *et al*.,2021) and in plasma-EVs from naked mole-rat (Pamenter *et al*.,2019). **Biosynthesis of amino acids** pathway was identified to be commonly present in sea urchins and lamprey. In purple sea urchins, biosynthesis of the amino acids pathway is present only in coelomic fluid, while in lamprey, this pathway is also exported in plasma-EVs. **Fructose and mannose metabolism** pathways are identified in sea urchin coelomic fluid and lamprey plasma but not in lamprey plasma-EVs. **Carbon metabolism** was commonly identified in coelomic fluid and lamprey plasma. **Phagosome** was the only KEGG pathway identified to be common to purple sea urchins and reindeer. **Complement and coagulation cascade** was found to be common to sea lamprey and reindeer plasma and plasma EVs. The complement system is a proteolytic cascade in blood plasma and a mediator of innate immunity, a nonspecific defence mechanism against pathogens. The main

consequences of complement activation are the opsonisation of pathogens, the recruitment of inflammatory and immunocompetent cells, and the direct killing of pathogens. Complement and coagulation cascade has been found to be deiminated in both plasma and plasma-EVs in reindeer; however, deiminated target proteins which participate in these cascades showed some difference in plasma and plasma-EVs: in reindeer, plasma-EVs deiminated candidates connected to complement and coagulation system were fibrinogen, kininogen and bradykinin, while in whole plasma, C1q, C3, C4, C5, C9 as well as factor H and the C3/C5 convertase were identified as deiminated (D'Alessio *et al.,*2021). **Platelet activation** was commonly identified in lamprey whole plasma and reindeer whole plasma. Still, it was not exported in lamprey and reindeer plasma-EVs. At the same time, **Thyroid hormones synthesis, *Staphylococcus aureus* infection** and **Prion disease** KEGG pathways were found only plasma-EVs of both lamprey and reindeer.

In conclusion, the comparative analysis of metabolic pathways in diverse organisms and their extracellular vesicles (EVs) reveals intriguing patterns of selective presence and absence. Glycolysis, gluconeogenesis, and carbon metabolism are fundamental pathways commonly found in various species, underscoring their essential roles in cellular energetics. The observed differences in pathway distribution between purple sea urchin coelomic fluid, lamprey plasma, and their related EV cargoes suggest intricate regulatory mechanisms and selective packaging of molecular cargo. The distinct presence of amino acid biosynthesis solely in the coelomic fluid of purple sea urchins and its export in lamprey plasma-EVs highlight the nuanced nature of pathway localisation. Fructose and mannose metabolism, identified in sea urchin coelomic fluid and lamprey plasma but absent in lamprey plasma-EVs, further accentuates the dynamic nature of pathway distribution. Notably, the complement and coagulation cascade's commonality in sea lamprey and reindeer, coupled with deimination in both plasma and plasma-

EVs of reindeer, unveils potential regulatory roles in innate immunity. Identifying specific deiminated candidates in different cellular compartments suggests intricate regulation within the complement and coagulation system. Platelet activation's exclusive identification in lamprey and reindeer whole plasma, but not in their plasma-EVs, underscores the selectivity in EV cargo and its potential implications for intercellular communication. The discovery of unique KEGG pathways, such as thyroid hormone synthesis, *Staphylococcus aureus* infection, and Prion disease, solely in plasma-EVs of lamprey and reindeer, suggests a specialised role for EVs in conveying specific signalling information. This comparative analysis sheds light on the sophisticated regulation of metabolic pathways and immune-related processes in different organisms and their extracellular vesicles. The findings underscore the importance of considering both cellular and vesicular components when interpreting the intricate language of intercellular communication. Further exploration of the molecular cargo within EVs holds promise for unravelling novel mechanisms governing systemic responses and cellular crosstalk in diverse biological systems.

Chapter 4. Exploring the Potential Correlation Between Circulating EV Citrullinome and Brain Citrullinome in a Hypoxia Resistant Species, the Naked Mole-Rat (Heterocephalus glaber)

4.1 Introduction

Extracellular vesicles are circulatory membrane vesicles in body fluids and play important roles in cell communication and pathological processes via the transport of various EV cargo, including modified protein cargo. EVs can be indicative of various physiological and pathological responses (Bister *et al*.,2020), and changes in circulating EV signatures have been linked to a range of hypoxia-related diseases, such as cancer and inflammation (Bister *et al*.,2020; Yaghoubi *et al*.,2020; Venturella *et al*.,2021; Zhang *et al*.,2021; Zhang *et al*.,2022). Therefore, it is of great interest to explore whether circulatory EVs signatures, including those of the brain, may indicate a wider physiological response to acute hypoxia. The optimal animal model chosen for the study is a hypoxia-tolerant specie, the naked mole-rat. *Heterocephalus glaber,* naked mole-rats are eusocial mammals that have been recognised recently as an important non-traditional animal model for understanding how evolutionary processes, due to challenging habitats, may optimise mechanisms mechanism for survival under adverse conditions, and lead to unusual characteristics such as tolerance against hypoxia, cancer, and ageing (Cheng *et al*.,2021; Pamenter *et al*.,2022). Such animal models may allow a better understanding of the mechanistic aspects of several human diseases that share features in common with the subterranean eco physiological stressors to which this species is exposed (Buffenstein & Ruby, 2021; Buffenstein *et al*.,2022). Indeed, naked mole rats are one of the most hypoxia-tolerant adult mammals and can tolerate

minutes to hours of anoxia (3% O_2) and days to weeks at 8%O_2 (Park *et al*.,2017); they respond to hypoxia with a suit of metabolic modifications to reduce energy demand and maximise the efficiency of metabolic pathways, by decreasing as much as 85% of resting metabolism, while still retaining consciousness and staying active. This shift to hypometabolic state is supported in part by a decrease in behaviour (Ilacqua *et al*.,2017; Kirby *et al*.,2018; Pamenter *et al*.,2019) and thermogenesis (Vandewint *et* al.,2019; Cheng *et al*., 2021;), and in energy-consuming cellular processes (Nguyen *et al*.,2019; Logan *et al*.,2020; Al-Attar *et al*.,2020; Farhat *et al*.,2020; Hadj-Moussa *et al*.,2021; Reznick *et al*.,2021). Moreover, in hypoxia state, blood glucose increases, metabolic pathways are reorganised to favour carbohydrate metabolism (Pamenter *et al.,*2019; Dzal *et al.,*2019), and mitochondrial respiration becomes more efficient by increasing the coupling of ATP generation to O_2 consumption, decreasing proton leaks (Pamenter *et al*.,2018; Lau *et al.*, 2020; Cheng *et al*.,2021). Therefore, part of this thesis focussed on assessing EV signatures and correlating these to the brain citrullinome following acute hypoxia treatment in the naked mole-rat, have been assessed (D'Alessio *et al.,*2022; Paper 4). This is the first work to assess the roles of EVs in systemic and cellular responses to hypoxia in a hypoxia-resistant species and to assess possible correlation with brain citrulline changes following the hypoxia challenge. Findings may thus be relevant for understanding changes in the brain citrullinome in various neurodegenerative diseases, where part of the injury is caused by hypoxic stress, as well as in acute CNS injury where hypoxia also occurs (Kell & Pretorius, 2022). Indeed, a role for PADs is increasingly being recognised in such scenarios (Lange *et al.,*2011, 2014), and the potential for EV-citrulline signatures has been highlighted (Sancandi *et al*.,2020; Mercer *et al*.,2022).

4.2 Extracellular Vesicles Profiles and Related Citrullinome Changes Under Normoxic and Hypoxic Conditions in Naked Mole-rat

4.2.1 EVs Isolation and Characterisation by NTA Analysis, Western blotting, and Transmission Electron Microscopy

Naked mole rats of 1–2-year-old subordinate males and females weighing 40-60g were exposed to either 21% O_2 (normoxia) or 7% O_2 (hypoxia) for 4h; each experimental group was comprised of 10 animals. Following treatment, the animals were sacrificed by cervical dislocation followed by rapid decapitation: blood was collected, and plasma was extracted by spinning the blood at 1500rpm for 15min, plasma aliquots were frozen at -80C until further analysis, and whole brains were rapidly extracted on ice and similarly frozen in liquid nitrogen, and then stored at -80C until further analysis. Dr Matthew Pamenter kindly carried out the experiments relating directly to the animal model at the University of Ottawa, and all experimental procedures were approved by the University of Ottawa Animal Care Committee (protocol #3444) in accordance with the Animals for Research Act and by the Canadian Council on Animal Care.

Naked Mole-Rat plasma EVs isolation

For assessment of EVs signatures, were isolated from individual naked mole-rat plasma from the experimental groups either exposed to normoxia (control) or hypoxia (10 animals per group), using differential centrifugation as previously described in Pamenter *et al*. (2019). 100µl of plasma of each animal was added to 400µl DPBS and then centrifuged at 4000 x g for 30min. The supernatant was collected and spun at 100,000 x *g* for 1 h at 4°C for collection of total EVs. The EVs enriched pellet was resuspended in 500µl DPBS and centrifuged again at 100,000 x *g* for 1h at 4 °C. The supernatant was discarded, and the EVs pellet was diluted in 100µl DPBS for further analysis.

EVs Quantification by NTA Analysis

EVs isolates from individual plasma samples were quantified by nanoparticle tracking analysis (NTA) by diluting 10µl of EVs pellet with 900µl DPBS and applied to NS300 Nanosight (Malvern Panalytical Ltd. Malvern, UK) at syringe pump speed 50. Particles per sample were recorded four times for 1min at camera level 9, and the post-analysis threshold was set at level 5 with 40-60 particles per window. Replicate histograms were generated from the recorded videos using the NanoSight software 3.0 (Malvern), representing the mean and confidence intervals of the four recordings for each sample (Fig 31-B). Circulating plasma EVs from naked mole-rats hypoxia and normoxia groups were profiled by NTA for assessment of changes in total EV (0-1000nm) numbers, as well as for EV subgroups based on size, separately counted in the size range of 0-100nm ("small EVs"); 101-200nm ("medium-sized EVs") and >200nm ("large EVs"), based on NTA measurements (Fig.31-A). Changes in plasma extracellular vesicle (EV) profiles were noted when comparing normoxia-treated animals to those subjected to hypoxia. Overall, there was a significant decrease in plasma EVs after hypoxia, particularly for smaller and medium-sized EVs (<100 nm; 101–200 nm). A tendency toward reduced levels of larger EVs (201–1000 nm) was also observed in the hypoxia-treated group, albeit not significant.

Elevated extracellular vesicle (EV) release is commonly associated with hypoxia in various models, including humans (Venturella *et al*.,2021; Zhang *et al*.,2021), and there is a suggestion that an increase in larger EVs is linked to inflammatory responses in human diseases (Słomka *et al*.,2018). Notably, our observations reveal a trend toward a decrease in the number of EVs, including those larger than 201 nm. The alterations in plasma EVs of naked mole rats under hypoxic conditions may signify changes in cargo export and the modulation of inflammatory responses to hypoxia. Additionally, it could

point to protective anti-inflammatory systemic responses in this species, known for its remarkable hypoxic tolerance.

EVs Characterisation by Western Blotting and Transmission Electron Microscopy

EVs were also assessed by Western blotting for two EV surface markers, CD63 and Flotillin-1, following the MISEV2018 guidelines for the minimum requirements for EV characterisation: 100 µL aliquot per sample was diluted with 100 µL 2× reducing Laemmli sample buffer (BioRad; containing 5% β-mercaptoethanol, Sigma-Aldrich) and boiled for 5 min at 100 °C. 5 µL aliquot per sample was then applied to 4–20% TGX gels (BioRad, Watford, UK). SDS-PAGE was carried out at 165 V for 52 min. Gels were then transferred for Western blotting analysis using semi-dry transfer (1h at 15V), and even protein transfer was assessed by PonceauS red stain (Sigma-Aldrich). The membranes were blocked in 5% bovine serum albumin (BSA, Sigma-Aldrich) in TBS-T for 1 h at room temperature (RT) and incubated in primary antibodies (CD63 (ab216130) and Flotillin-1 (ab41927) all 1/1000) overnight at 4°C on a shaking platform. Following primary incubation, membranes were washed with TBS-T 3x, 10min each time, and secondary antibody HRP-labelled anti-rabbit IgG diluted 1/3000 TBS-T, incubated for 1h at RT. Membranes were washed 5x 10min each time in TBS-T before proceeding with visualisation, using ECL (Amersham Biosciences, Buckinghamshire, UK) and the UVP BioDoc-ITTM System (Thermo Fisher Scientific, Dartford, UK) (Fig 31-C). In addition, EVs were characterised by transmission electron microscopy (TEM) to assess the EVs morphology (Fig 31-D), as previously described in Chapter 2, Section 2.1.4

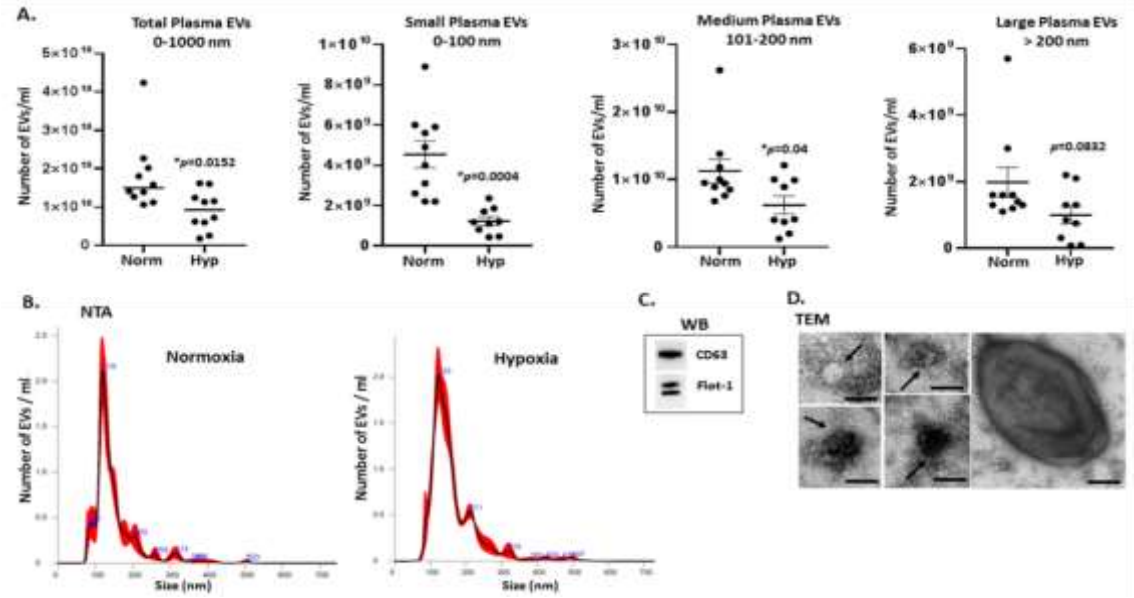

Figure 31. EVs profile trends from plasma of naked mole-rats treated for 4h in normoxia (control)or hypoxia. (A) Number of EVs isolated from naked mole-rat plasma, comparing normoxia and hypoxia conditions. Changes were assessed in release profiles of total EVs (0-1000nm), small EVs (<100nm), medium-sized EVs (101-200nm) and large EVs (201-1000nm) based on NTA measurements of plasma EVs from 10 animals per groups; error bars represent standard error of the mean (SEM); *t*-test, exact *p*-values are shown, $p < 0.05$ considered statistically significant (indicated by *). (B) Representative NTA curves of plasma EVs from naked mole rats following hypoxia or treatment, respectively. (C) Western blotting analysis of EVs markers for naked mole-rat plasma EVs, showing positive bands for CD63 and Flotillin-1; (D) Transmission electron microscopy (TEM) of plasma-EVs from naked mole rats, showing representative images of differently sized EVs: scale bar indicates 100nm, black arrows highlight individual EVs. (D'Alessio *et al.*,2022).

4.2.2 Protein-citrullination EV cargo Profiles Naked Mole-Rat Plasma Under Normoxic (Control) Versus Hypoxic Conditions and Associated KEGG Pathway

Protein-citrullination EV cargo identification

EVs were isolated and pooled from the plasma of the two experimental groups (normoxia and hypoxia) and subjected to F95 enrichment for isolation of citrullinated/deiminated proteins (as described in Chapter 2, Section 2.4 – Isolation of Deiminated Proteins using F95 enrichment), to identify deiminated/citrullinated protein hits in plasma-EV cargo. The F95-enriched proteins isolated by immunoprecipitation from the plasma EVs of the two groups were first analysed by SDS-PAGE and silver staining (Fig.32-A) and then subjected to LC-MS/MS analysis for identification of protein hits (as described in Chapter 2, Section 2.5.1 – LC-MS/MS) to compare citrullinated proteins from naked mole-rat plasma-EVs cargo under normoxia and hypoxia conditions. Deiminated protein hits identified in plasma EVs of normoxia- and hypoxia-treated naked mole-rats were next assessed by STRING analysis https://string-db.org/, accessed on 10 March 2022) for protein-protein interaction analysis (Fig32-B).

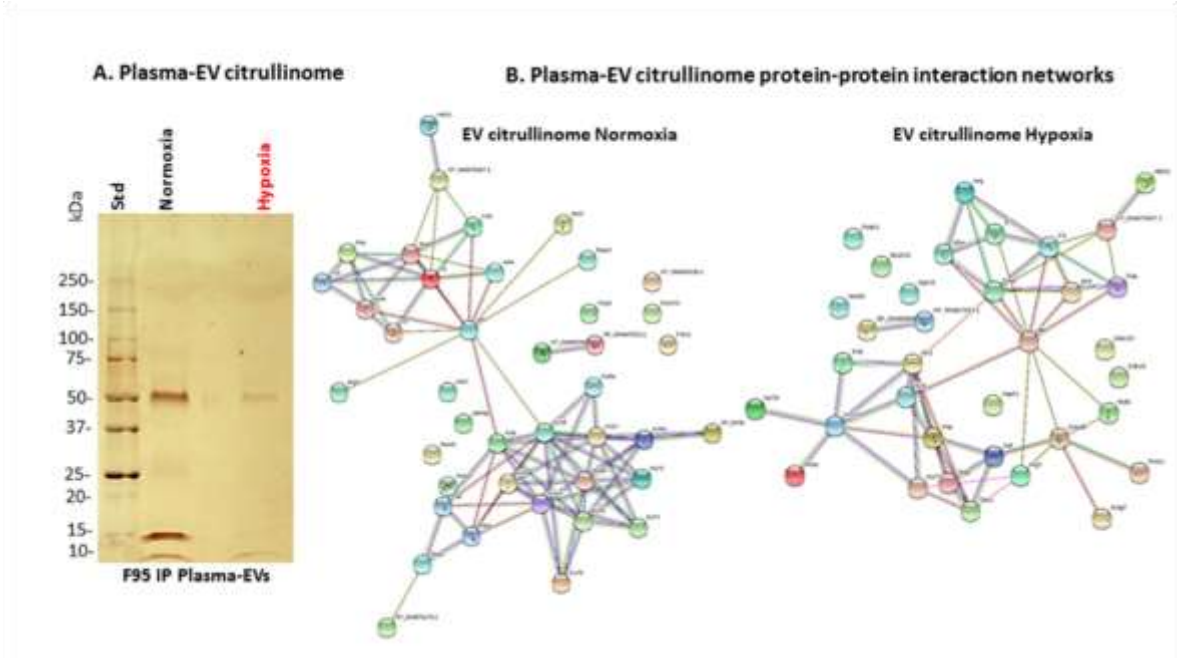

Figure 32. F95-enriched protein cargo of plasma EVs citrullinome from normoxia- and hypoxia-treated naked mole-rats. (A) SilverGel showing citrullinated fractions from EVs, then subjected to LC-MS/MS analysis. (B) STRING protein-protein interaction networks of plasma-EV citrullinome of normoxia- and hypoxia-treated naked mole-rats.

Table 13 below lists the protein hits identified as deiminated specific to the normoxia group and hypoxia group, respectively, and protein hits commonly shared between both groups. Overall, a total of 29 protein hits were identified in both plasma EVs groups, whereas 21 deiminated hits were specific for the normoxia plasma EVs group, and 15 deiminated hits were identified to be specific to the hypoxia plasma EVs group.

Table 13. F95-enriched deiminated proteins identified in plasma EVs from normoxia- and hypoxia-treated naked mole-rats. Common and specific hits per group are highlighted in the table, and deiminated protein hits identified in normoxia or hypoxia plasma EVs, or both, are indicated with a tick (v). Protein hits identified in the normoxia group only, are highlighted in blue, and protein hits specific to the hypoxia group are highlighted in pink.

Protein ID	Protein Name	Normoxia	Hypoxia
G5B5P2	Serum Albumin	v	v
G5BT87	Histidine-reach glycoprotein	v	v
G5ALS3	Keratin, type II cytoskeletal	v	v
G5ALS1	Keratin, type II cytoskeletal 6B	v	v
G5B3Q0	Keratin, type II cuticular Hb5	v	v
G5BPM1	Alpha-2-macroglobulin	v	v
G5BT86	Kininogen-1	v	v
G5BS33	Hemoglobin subunit beta	v	v
G5BQA9	Serotransferrin	v	v
G5B0M6	Keratin, type II cytoskeletal 14	v	v
G5BXY1	Hemoglobin subunit alpha	v	v

G5BJ37	Keratin, type II cytoskeletal 79	v	v
G5BAT4	Desmoplakin	v	v
G5C776	Arginase	v	v
G5B0M4	Keratin, type I cytoskeletal 17	v	v
G5BJ39	Keratin, type II cytoskeletal 8	v	v
G5BYJ8	Hemoglobin subunit beta	v	v
G5BUN4	Inter-alpha-trypsin inhibitor heavy chain H4	v	v
G5C0N5	Complement C3	v	v
G5BSE8	Histone H2A	v	v
G5BV28	Histone H3	v	v
G5C3H6	Complement C4-A	v	v
G5BRJ4	Induced myeloid leukemia cell differentiation protein Mcl-1-like protein	v	v
G5ARW1	Peroxidredoxin-1	v	v
G5BC311	Desmoglein-1	v	v
G5AWC0	Annexin	v	v

G5AXH0	Actin, gamma-enteric smooth muscles	v	v
G5BFU9	N6-adenosine-methyltransferase 70kDa subunit	v	v
G5BG61	SRRM2-like protein	v	v
G5B0N6	Keratin, type I cuticular Ha30-I	v	
G5B0N5	Keratin, type I cuticular Ha4	v	
G5B3P5	Keratin, type II cytoskeletal 75	v	
G5AX68	Keratin, type I cytoskeletal 27	v	
G5B0N2	Keratin, type I cuticular Ha5	v	
G5ALS4	Keratin, type II cytoskeletal 71	v	
G5B3P8	Keratin, type II cuticular Hb4	v	
G5BL99	Keratin, type II cuticular Hb6	v	

G5BJ40	Keratin, type I cytoskeletal 18	v	
G5AX70	Keratin, type cytoskeletal 25	v	
G5AYD5	Dedicator of cytokinesis protein 10	v	
G5BQ09	Coagulation factor XII	v	
G5AYL5	Integrator complex subunit 7	v	
G5B319	Janus kinase and microtubule-interacting protein 1	v	
G5B3A4	Plakophilin-1	v	
G5BV47	Histone H3.3	v	
G5BI06	Skin-specific protein 32	v	
G5C656	Puratrophin-1	v	
G5APA7	Selenoprotein P	v	
G5BH20	Histone H2B	v	
G5BKL1	Histone H2B		v
G5ALS8	Keratin, type II cytoskeletal 1 (fragment)		v

G5ALS9	Keratin, type II cytoskeletal 1b (fragment)	v
G5B0M0	Junction plakoglobin	v
G5CAP7	Glyceraldheyde-3-phosphate dehydrogenase (fragment)	v
G5C5U7	Plectin-1	v
G5BYG4	Apoptosis facilitator Bcl-2-like protein 14	v
G5BNM3	Multidrug resistance-associated protein 7	v
G5BAK9	Fatty acid-binding protein, epidermal	v
G5BX43	Serine/threonine-protein kinase PCTAIRE-3	v
G5C312	Desmocollin-1 (fragment)	v

G5AQ00	Tubulin-alpha-1C chain	v
G5AUQ5	Serine/threonine-protein kinase PDIK1L	v
G5BYF7	Putative G-protein coupled receptor 19	v
G5B253	Ventricular zone-expressed PH domain containing protein-like protein 1	v

KEGG Pathways Identification

STRING analysis was used to identify Kyoto Encyclopedia of Genes and Genomes (KEGG) pathways for deiminated proteins from naked mole-rat derived EVs (https://string-db.org/, accessed on 10 March 2022). Based on hits identified from the LC-MS/MS analysis, predicted protein interaction networks were built using the protein IDs and organism of choice, Heterocephalus glaber, in the STRING software. KEGG pathway analysis for the normoxia-treated naked mole-rat plasma-EV citrullinome (Fig.33-A) and KEGG pathway analysis for the hypoxia-treated naked mole-rat plasma-EV citrullinome (Fig.33-B), revealed four shared pathways between the groups (Complement and coagulation cascades, African trypanosomiasis, *S.aureus* infection and systemic lupus erythematosus), all related to immune functions, and one specific pathway for the normoxia group (oestrogen signalling pathway), thus indicating that some main pathways in immune responses are influenced by deimination in circulatory EV cargo transport, both in hypoxia and normoxia conditions. Notably, the estrogen signalling pathway, known for its diverse functions in health and disease, including the regulation of epigenetic mechanisms, was specifically associated with the normoxia EV citrullinome. (D'Alessio *et al*.,2022 – Paper - 3).

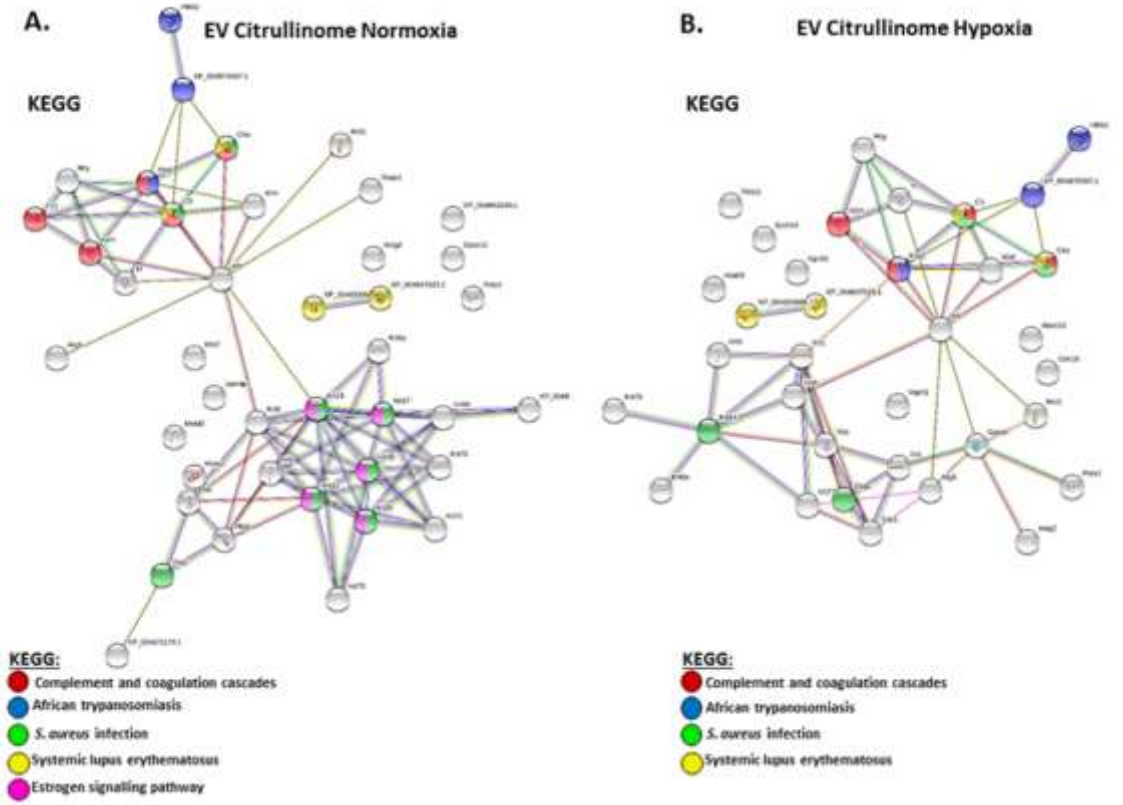

Figure 33. STRING analysis of plasma EV citrullinome for (A) normoxia-treated naked mole-rat and (B) hypoxia-treated naked mole-rats, showing predicted protein networks and associated KEGG pathways.

4.3 The Brain Citrullinome and Related Citrullinome Changes Under Normoxic and Hypoxic Conditions in Naked Mole-rat

4.3.1 Protein Isolation from Brain Tissue and Western Blotting

Proteins were extracted from brain tissue of naked mole-rats exposed to 21% O_2 (normoxia) or 7% O_2 (hypoxia) (*n*=5 animals per treatment group). Whole brains were homogenised in RIPA+ buffer (Sigma-Aldrich, Gillingham, UK, containing 10% protease inhibitor cocktail, Sigma-Aldrich) in 2ml Eppendorf tubes on ice, using a Mini Handled Homogeniser (Kimble, DWK, Life Sciences, VWR International). The homogenate was then gently pressed through a 23G needle into fresh Eppendorf tubes on ice, followed by gently pipetting up and down to eliminate any tissue clots. For each brain (400mg tissue), 2 ml of RIPA+ buffer was used. The homogenates were then incubated on a roller for 1.5h at 4°C for collection of isolated protein. The extracted proteins were aliquoted and immediately frozen at -80 °C. For SDS-PAGE and Western blotting 100µl of each extracted protein sample were diluted with 100µL 2x reducing Laemmli sample buffer (BioRad; containing 5% ß-mercaptoethanol, Sigma-Aldrich) and boiled for 5min at 100 ºC. For each sample, 5µL of the aliquots was applied to 4-20% TGX gels (BioRad, Watford, UK), and SDS-PAGE analysis was carried out at 165 V for 52min; the gels were thereafter transferred for Western Blotting analysis using semi-dry transfer (1h at 15 V) and assessed for even protein transfer by PonceauS red stain (Sigma-Aldrich). The membranes were blocked in 5% bovine serum albumin (BSA, Sigma-Aldrich) in TBS-T for 1h at room temperature (RT) and incubated in primary antibodies overnight at 4ºC on a shaking platform. The primary antibodies used were anti-human PAD1 (ab181762, Abcam Cambridge, UK), PAD2 (ab50257), PAD3 (ab50246), PAD4 (ab50247), PAD6 (PA5–72059, Thermo Fisher Scientific, Hemel Hempstead, UK), and pan-citrulline F95 (MABN328, Merck, Feltham UK, as well as citrullinated histone H3

(citH3, ab5103) antibodies, all diluted 1/1000 in TBS-T. Washing was carried out with TBS-T (3 × 10 min). Secondary antibody incubation was completed for 1h at RT (using HRP-labelled anti-rabbit IgG or anti-mouse IgM antibodies; BioRad, diluted 1/3000 in TBS-T). Following washing (5 × 10 min in TBS-T), visualisation was carried out using ECL (Amersham Biosciences, Buckinghamshire, UK) and the UVP BioDoc-ITTM System (Thermo Fisher Scientific, Dartford, UK). Blots were stripped and re-probed for beta-actin (Abcam, 1/5000 in TBS-T). Protein densitometry analysis was conducted using ImageJ software. Results from the western blotting analysis confirmed the presence of all PAD isozymes in whole brain protein extracts, with increase in PAD1, PAD3 and PAD6 levels observed in response to hypoxia (albeit not statistically significant) (Fig.34 -A, Cand E), while PAD2 levels did not change (Fig.34-B) and PAD4 levels were significantly (p=0.0031) reduced in the hypoxia brains (Fig.34-D). Histone H3 citrullination did not change significantly (Fig.34-F). Overall, considerable individual variability was also observed; 5 brains were assessed per group.

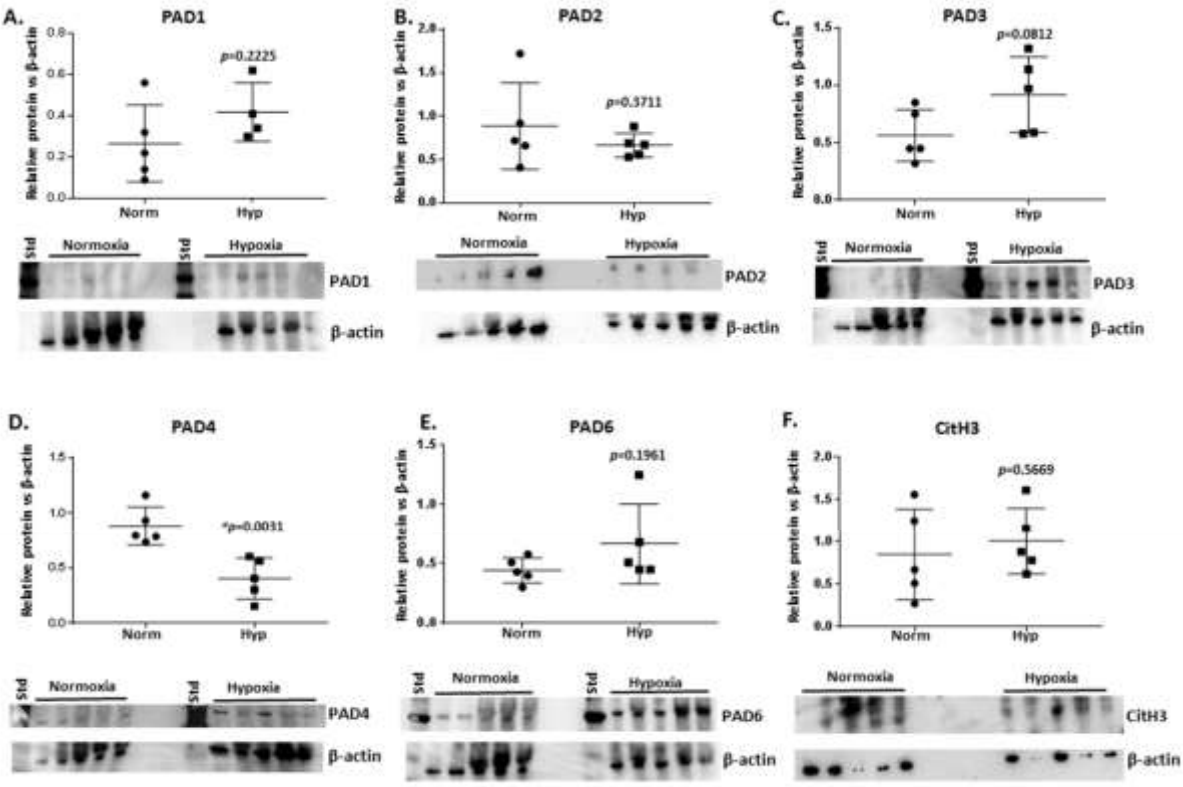

Figure 34. PAD isozyme and CitH3 protein level in brains of naked mole-rats following normoxia and hypoxia treatment, showing (A) PAD1, (B) PAD2, (C) PAD3, (D) PAD4, (E) PAD6, and (F) CitH3. Protein levels were assessed in *n = 5* brains per group and normalised against beta-actin protein levels: exact *p*-values are indicated (*t*-test; *indicates significance at $p < 0.05$; circles represent normoxia and squares hypoxia brains samples, respectively), and the error bar represents SD.

4.3.2 F95-Enrichment, Silver Staining and LC-MS/MS of Deiminated Proteins from Brain Tissue of Naked Mole-Rat

Protein extractions from naked mole-rat brain tissue were enriched using F95 pan-citrulline antibody (MAB328, Merck) in conjunction with the Catch-and-Release Immunoprecipitation Kit (Merck) following the protocol as described in Chapter 2, Section 2.3 – Isolation of Deiminated Proteins using F95 enrichment. Protein extracts from 5 brains were pooled per experimental group (normoxia and hypoxia) and subjected to SDS-PAGE and silver staining (as described in Chapter 2, Section 2.2 – SDS-PAGE and

Western Blotting - and Section 2.4 – Silver Staining of Total Deiminated Proteins)(Fig.27- A); protein elutes from brain tissue were diluted in 1:1 in 2x reducing Laemmli sample buffer, boiled for 5min at 100 °C, and separated on 4-20% TGX gels (BioRad) for 52min at 165V. Following electrophoresis, the gels were silver stained using the BioRad Silver Stain Plus Kit according to the manufacturer's instructions. Protein extracts from normoxic and hypoxic naked mole-rat brain tissue (*n*=5 brain tissue for treatment group), were also subjected to in-gel digestion for LC-MS/MS analysis, carried out by the Cambridge Centre for Proteomics (University of Cambridge, Cambridge, UK), as previously (as described in Chapter 2, Section 2.5.1 – LC-MS/MS). The samples were prepared 1:1 in reducing Laemmli sample buffer, boiled and run 0.5 cm into a 10% TGX gel (BioRad), and then cut out as one whole band per sample for in-gel analysis (whole EV protein, F95-enriched EV proteins, F95-enriched brain proteins for normoxia versus hypoxia groups). The Cambridge Centre carried out proteomic analysis for Proteomics (Cambridge, UK) according to previously described methods (Pamenter *et al*.,2019 and as described in Chapter 2, Section 2.5.2), and protein hits were assessed against the naked mole-rat protein database CCP_*Heterocephalus_glaber*_20190911 (21,449 sequences; 10,466,552 residues). In addition, a common contaminant database was also searched (cRAP 20190401; 125 sequences; 41,129 residues). Protein scores are derived from ion scores as a non-probabilistic basis for ranking protein hits; individual ion scores > 30 indicated identity or extensive homology ($p < 0.05$). Naked mole-rat brain citrullinome for hypoxia versus control brains was assessed by Silverstaining (Fig.35-A) and then subjected to protein network analysis by STRING (https://string-db.org/, accessed on 10 March 2022) (Fig.35-B). 852 protein hits were detected in the normoxic brains, while the hypoxic brains exhibited 1222 hits. Among these, 34 deiminated hits were exclusive to normoxic brains, and 245 hits were exclusive to hypoxic brains.

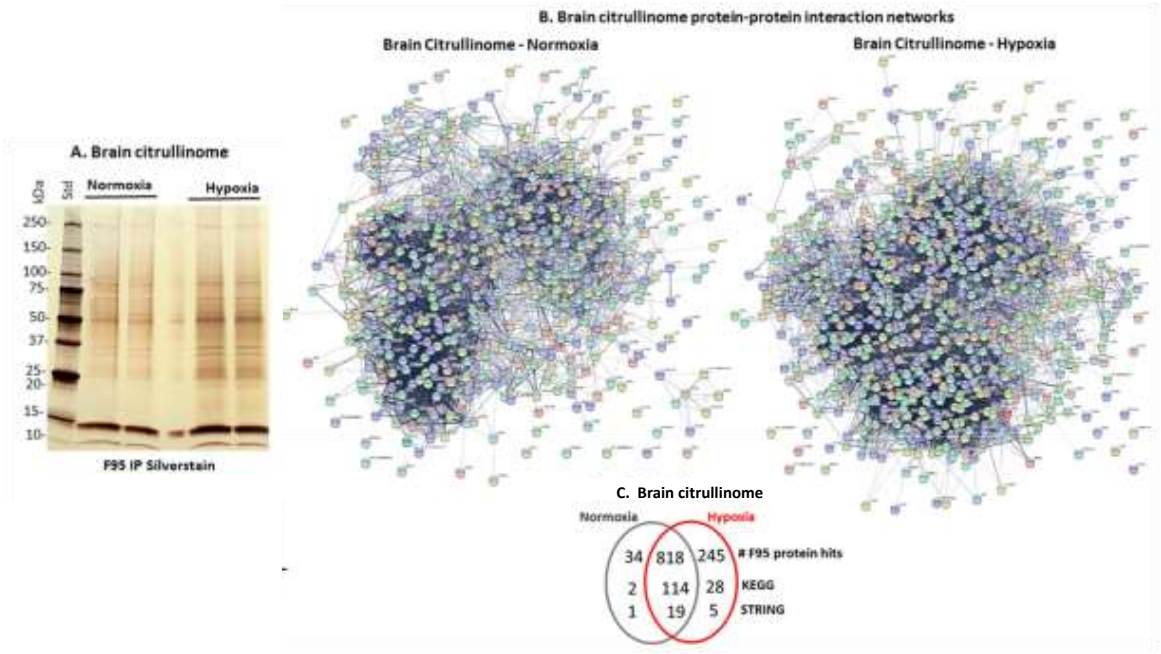

Figure 35. The brain citrullinome of naked mole-rats following normoxia or hypoxia treatment. (A) SilverGel showing F95-enriched proteins from brains (normoxia) and brains taken from animals after a hypoxia challenge; *n* = 5 (pool of 5 brains per group; 2 experimental replicates). (B) Protein-interaction networks for all deiminated protein candidates identified in naked mole-rat brains following normoxia or hypoxia (brain citrullinome). The PPI enrichment *p*-value for both networks was $<1.0 \times 10^{-16}$, indicating hits and pathways are presented in Figure 7D. The PPI enrichment p-value for both networks was $<1.0 \times 10^{-16}$, indicating more interactions than expected for a random set of genomes, indicating that the proteins are at least partially biologically connected as a group. (C) Venn diagram summarising deimination/citrullinome hits (F95) and shared and specific pathways for the citrullinome between normoxic and hypoxic brains (n = 5 brains per group in all experiments).

4.4 Protein-Protein Interaction Network Analysis of Naked Mole-Rat Brain Citrullinome Compared to Naked Mole-Rat EVs Citrullinome

Observed changes in PAD regulation may be reflected in brain citrullinome changes. The brain citrullinome revealed 107 KEGG pathways common to the normoxic (control) and hypoxic brain groups. 28 KEGG pathways were unique to the hypoxic brain citrullinome: pathways identified were related to a range of physiological,

pathobiological mechanisms, hemostasis, and immunological/inflammatory pathways (D'Alessio *et al.,*2022). Normoxic brain citrullinome revealed only 2 KEGG pathways (Phenylalanine, tyrosine, and tryptophan biosynthesis; Nitrogen metabolism). Furthermore, protein-protein interaction between deiminated protein hits, identified as specific to hypoxia brains, revealed 50 KEGG pathways. On the contrary, no KEGG pathways were identified from the protein interaction network analysis, and deiminated protein hits were identified to be specific to normoxia brains (control group), excluding any overlapping targets between the groups from the protein network analysis.

The investigation into the estrogen signalling pathway has revealed an intriguing connection between the hypoxic brain and extracellular vesicles (EVs) in normoxia. The estrogen signalling pathway is evident in the hypoxic brain, suggesting a potential role in cellular responses to low oxygen levels; activation or modulation of this pathway in the hypoxic brain may be associated with adaptive mechanisms or responses to oxygen deficiency (Chaltel-Lima,2023). Simultaneously, when exploring the EV citrullinome in the normoxia (control) group, a surprising recurrence of the estrogen signalling pathway was observed. Unlike its presence in the hypoxic brain, the estrogen-related proteins found in the EV citrullinome were exclusive to the normoxia condition, indicating a distinct regulatory role for citrullination in the extracellular vesicle environment under normal oxygen levels. The presence of the estrogen signalling pathway in both the hypoxic brain and EVs under normoxia implies a potential interplay between the cellular response to oxygen levels and extracellular communication through EVs. This connection prompts further investigation into the mechanisms governing estrogen signalling in diverse cellular compartments and its implications for intracellular adaptations to hypoxia and intercellular communication via EVs in normoxia. Unravelling this intricate relationship may offer valuable insights into the broader regulatory network governing estrogen signalling across different physiological conditions.

Moreover, analysis of comparative network of the EV citrullinome and brain citrullinome of hypoxia and normoxia naked mole-rat groups, has revealed intriguing connections. Notably, the identified KEGG pathway, African trypanosomiasis, emerges as a commonality in both the EVs citrullinome and the brain citrullinome across the normoxia (control) and hypoxia-exposed animal groups. This surprising connection suggests that there might be communication or shared reactions at the molecular level between EVs and the brain, highlighting how important citrullination is for cells to adapt to different oxygen levels (Albanese *et al*.,2021). The implication of African trypanosomiasis in both normoxia and hypoxia EVs and brain citrullinome, raises questions about its specific role in the cellular response to oxygenation stress. This connection in the citrullinome networks prompts further investigation into the molecular mechanisms linking African trypanosomiasis to normoxic and hypoxic conditions. A recent study by Saraiva *et al.,* (2022), investigate the hypoxia effects on *Trypanosoma cruzi*, the causative agent of African trypanosomiasis, also known as Chagas diseases. The study shows that hypoxic conditions trigger a shift in the bioenergetic metabolism of *T. cruzi* epimastigote, showing an increased production of ROS and fermentation to sustain ATP production, that allow the parasite to survive and proliferate (Saraiva *et al*.,2022). This connection in the citrullinome networks of naked mole-rat prompts further investigation into the molecular mechanisms linking African trypanosomiasis to normoxic and hypoxic conditions.

Chapter 5 – Pilot Investigation on the Potential of Atlantic Cod (Gadus morhua) Serum/Mucus Derived Extracellular Vesicles for In-Vitro Application in Tissue Regeneration Models.

5.1. Introduction

Wound healing research often relies on animal models to better understand the mechanisms and processes involved in tissue regeneration. Various animal species, such as mice, rats, rabbits, guinea pigs, pigs, and zebrafish, have been used as models for wound healing (Grada *et al*., 2018). Importantly, cod-derived products have shown promising results in wound healing and tissue regeneration. Fish skin collagen, and in particular Atlantic codfish (*Gadus morhua)* skin-derived collagen, has been investigated as an innovative, sustainable, and efficacious product to produce new cosmetic formulations (Alves *et al*.,2017), in tissue regeneration and drug delivery (Furtado *et al*.,2022). Another study investigated the properties of *Gadus morhua* (Atlantic cod) liver oil in diabetic wound healing *in vivo* (Kahzaeli *et al*., 2020). The researchers found that encapsulating certain concentrations of cod liver oil with poly lactic acid/chitosan nano scaffolds significantly reduced wound area and improved healing compared to rats treated only with nanofibers. Additionally, another study compared human amnion/chorion membrane allografts with skin xenografts from cod in acute wound healing (Kirsner et al., 2020). Importantly, wounds treated with cod skin graft healed significantly faster than that treated with human amnion/chorion membrane. The cod skin exhibited a unique molecular composition, including high Omega-3 polyunsaturated fatty acids (PUFAs), promoting wound healing (Kotronoulas *et al*., 2019). The preservation of the cod skin's integrity and molecular composition during viral deactivation, typically employed for xenograft materials to reduce the risk of viral infection,

greatly influenced the wound healing process (Kirsner *et al.,* 2020). As cod-derived products have shown such promising results in the context of wound healing and tissue regeneration, and since extracellular vesicles (EVs) have gained attention as potential therapeutic agents due to their ability to transfer bioactive molecules and participate in intercellular communication, it is of great interest to further investigate other cod-derived products, including cod-EVs isolated from different biological fluids such as serum and mucus. This may be of considerable interest as to date, there have mainly been comprehensive studies carried out on mesenchymal stem cell-derived extracellular vesicles (EVs) and their role in wound healing (De Jong *et al*.,2014; Lamichhane *et al*., 2015; Rani and Ritter,2016; Keshktar, Azarpira and Ghahremani,2018; Ferreira and Gomes, 2018; Casado-Diaz et al, 2020; Zhang *et al.*,2020). In comparison, minimal studies have focused on EVs derived from fluids of various species across phylogeny (Wu *et al*.,2022) or from plants and animal derivates, such as aloe vera or royal jelly (Kim *et al*.,2021; Alvarez *et al*.,2023). Therefore, a specific focus of the current study was to assess any potential for cod serum and mucus-derived EVs in wound healing models *in vitro*. This part of the study utilised three cell lines: 1) 3T3.L1 - mouse fibroblasts, 2) HaCat – Immortalized Human keratinocytes, 3) HDFa – Human Dermal Fibroblasts, Adult, to assess wound closure at different time points (0h,6h,24h), upon EVs treatment, derived from Atlantic cod serum and mucus. Wound closure was carried out by measuring differences in scratch closure/migration speed. In addition, Fibroblast Growth Factor 2 (FGF2), a marker of fibroblasts implicated in different biological processes both *in vivo* and *in vitro,* including cell migration, differentiation, angiogenesis, and wound healing (Yun *et al*.,2010; Koike *et al*.,2020), and Vimentin, an intermediate filament, marker of fibroblasts and wound healing (Cheng *et al*.,2016; Ostrowska-Podhorodecka *et al.,*2022), were assessed in different assays by immunocytochemistry.

Atlantic Cod – Gadus morhua

The Atlantic cod genome has been sequenced, revealing a unique immune system with distinct properties that differ from other teleost fish species (Star *et al*., 2011). The cod exhibits high levels of IgM and a minimal antibody immune response after pathogen exposure (Magnadóttir *et al.*,2001; Magnadóttir *et al*.,2011). Furthermore, its peripheral blood contains abundant phagocytic neutrophils. Interestingly, while most genes involved in the vertebrate immune response are present in the Atlantic cod genome, it lacks major histocompatibility complex (MHC) II isoforms, the assembly and trafficking chaperone Invariant chain (Ii), and the MHCII interacting protein CD4, which are essential for adaptive immunity against bacterial and parasitic infections (Star *et al*., 2011). The cod genome also reveals an unusual composition of Toll-like receptors (TLRs), which play a fundamental role in the innate immune response and initial pathogen detection. The cod genome predominantly includes teleost-specific TLR14/18 from the TLR1 family and families of nucleic acid-recognizing TLRs (TLR7, -8, -9, and -22), suggesting that the cod immune response relies on nucleic acid-detecting TLRs for the recognition of bacterial pathogens (Sundaram *et al*., 2012). Importantly, EVs have recently been isolated and characterized for the first time from cod mucus and serum (Magnadóttir *et al*., 2019a, 2020), verifying their presence in these biofluids. Nanoparticle tracking analysis revealed a poly-dispersed population of EVs ranging from 30 to 500 nm in cod mucosa, with an approximate yield of $5.8x10^9$ particles/ml. Further characterization using transmission electron microscopy confirmed the morphology of these EVs, and western blot analysis detected the presence of phylogenetic-conserved specific markers CD63 and Flotillin-1, confirming their identity as EVs (Magnadóttir *et al.,* 2019a). Similarly, cod serum-derived EVs displayed a similar size distribution (30-600 nm) and were positive for CD63 and Flotillin-1 markers (Magnadóttir *et al.,* 2019b). Notably, the analysis of cod mucosal EVs cargo revealed the presence of innate

immune factors such as C3 and C-reactive proteins I and II (CRP-1 and CRP-II), which were also found to be deiminated in mucosal EVs. Other deiminated proteins, including tubulin beta chain, elongation factor 1-alpha, Beta-actin, fast skeletal muscle alpha-actin, galectin, and profilin, were also identified in mucosal EVs (Magnadóttir *et al.,* 2019a). The deimination of complement C3 was also observed in cod serum and serum-derived EVs, marking the first identification of deiminated complement C3 in cod EVs (Magnadóttir *et al.,* 2019b). Complement component C3 plays a crucial role in all pathways of complement activation, which is essential for the first line of immune defence against invading pathogens. Additionally, C3 has been implicated in tissue regeneration and remodelling during cod ontogeny (Lange *et al.,* 2004a, 2005) The unique immune system and composition of EVs in cod suggest that these vesicles may have specific properties and functions contributing to tissue regeneration. Therefore, studying the effects of Atlantic cod serum and mucus-derived EVs in tissue regeneration and exploring their whole protein cargo content and mechanisms of action could provide valuable insights for the development of novel therapeutic strategies in regenerative medicine.

5.2. Material and Methods

5.2.1. Cod Serum and Mucus Extracellular Vesicles Preparation, Isolation, Characterisation, and Protein Content Analysis

Cod serum EVs were isolated from cod serum and mucus using sequential centrifugation and ultracentrifugation according to previously standardized and described protocols (Fig.36) (Criscitiello *et a*l.,2020 – a,b,c; Bowden *et al.*,2020; Lange *et al*.,2019) and following recommendations of MISEV2018 (the minimal information for studies of extracellular vesicles) (Théry *et al*.,2018). For each EV isolation, 250µl of cod serum and mucus aliquots were diluted 1:5 in (750µl) Dulbecco's PBS (DPBS, ultrafiltered

using a 0.22 μm filter before use). Serum and mucus aliquots were centrifuged for 20 min at 4000×*g* at 4 ºC to remove apoptotic bodies and aggregates, and the obtained supernatants were then collected and ultra-centrifuged at 20,000×*g* at 4 ºC for 1h. The obtained supernatants were discarded, and the EV-enriched pellets were resuspended each in 500μl DPBS and thereafter ultra-centrifuged again for 1h at 20,000 x*g* at 4 ºC. The final resulting total EV pellets were resuspended each in 50μl of DPBS and stored at -80C for further experiments and analysis (Fig.36). For the characterisation with nanoparticle tracking analysis (NTA), based on Brownian motion of particles in suspension, cod serum and mucus EVs samples were diluted 1/1000 in DPBS (10μl of EV preparation diluted in 990μl of DPBS). The diluted EV sample was applied to the NanoSight NS300 system (Malvern Panalytical Ltd., Malvern, UK), recording four repetitive reads, 60 seconds each and camera setting level 13. Post-analysis threshold setting was set at level 3. Replicate histograms were generated from these videos using the NanoSight software 3.0 (Malvern), representing the mean and the confidence intervals of the three sample recordings. EV size distribution profiles generated by the three recordings showed a poly-dispersion of EVs in the 50-350nm range comprising both small and medium/large EVs (further details in section 5.3.1). The concentration of EVs was determined based on the NTA quantification of particles per ml and estimated as $1.55x10^{10}$ +/- $9.17x10^{8}$ particles/ml EVs per 1ml Cod serum and $1.29x10^{10}$ +/- $1.22x10^{2}$ particles/ml in EVs per 1ml of cod mucus respectively.

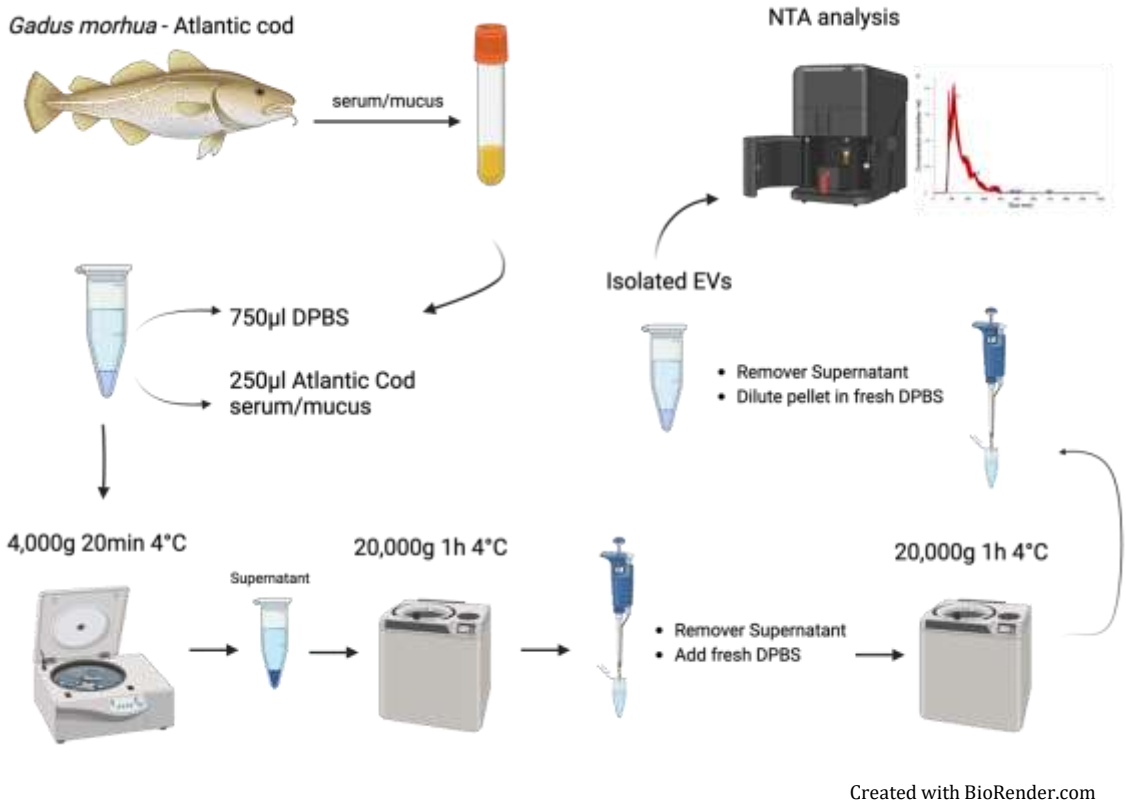

Figure 36. Atlantic Cod Extracellular vesicles small scale isolation protocol and NTA analysis. (Image created with BioRender.com)

5.2.2. Western blotting

For the characterisation of surface markers on Atlantic cod serum- and mucus-derived EVs, SDS-PAGE was carried out, followed by Western Blotting. Cod EVs samples were diluted 1:1 in denaturing 2× Laemmli sample buffer (containing 5% beta-mercaptoethanol, BioRad, UK) and heated for 5min at 100 °C. Protein separation was carried out using 4–20% gradient TGX gels (BioRad UK) for 50min at 165 V, followed by Western blotting at 15 V for 1 h on a Trans-Blot® SD semi-dry transfer cell (BioRad, UK). Membranes were stained with PonceauS (Sigma, UK) for 5 min and rinsed with distilled water to assess even protein transfer, and then blocked with 5% bovine serum albumin (BSA, Sigma, UK) in Tris-buffered saline (TBS) containing 0.1% Tween20 (BioRad, UK; TBS-T) for 1 h at room temperature. Primary antibody incubation was carried out

overnight at 4 °C on a shaking platform using antibodies against the following EV markers: CD63 (ab216130, Abcam, UK) Flotillin-1 (ab41927, Abcam) and Alix (ab117600, Abcam) (Table 11); diluted 1/1000 in TBS-T, previously shown to cross-react with EVs from other taxa, besides humans. Following primary antibody incubation, the nitrocellulose membranes were washed at RT in TBS-T for 3 × 10 min and thereafter incubated with HRP-conjugated secondary antibodies (anti-rabbit IgG, BioRad, diluted 1/3000 in TBS-T) (Table 11), for 1h at RT. The membranes were then washed for 4 × 10 min with TBS-T, followed by one wash in TBS without Tween20, and digitally visualised, using enhanced chemiluminescence (ECL, Amersham, UK) in conjunction with the UVP Bio-Doc-ITTM System (Thermo Fisher Scientific, Dartford, UK).

Table 14. List of primary and secondary antibodies used for WB for EVs characterisation.

Primary Antibodies	**Cat. Number**	**Company**	**Dilution in TBS**
CD63	ab216130	Abcam, UK	1/1000
Flotillin-1	ab41927	Abcam, UK	1/1000
Secondary antibodies	**Cat. Number**	**Company**	**Dilution in TBS**
Anti-rabbit IgG H&L	ab6721	BioRad	1/3000

5.2.3. Liquid Chromatography with Tandem Mass Spectrometry LC-MS/MS Analysis

Liquid chromatography with tandem mass spectrometry (LC–MS/MS) was carried out to identify whole cod serum-EV and mucus-EVs proteome, as a service carried out by

Cambridge Proteomics (University of Cambridge, UK). In summary, the concentrated protein band (containing whole proteome extract) was excised for in-gel digestion, trypsin digested and subjected to proteomic analysis using a Dionex Ultimate 3000 RSLC nanoUPLC system (Thermo Fisher Scientific Inc., Waltham, MA, USA), in conjunction with a QExactive Orbitrap mass spectrometer (Thermo Fisher Scientific Inc, Waltham, MA, USA). Peptide separation was performed using reverse-phase chromatography (flow rate 300 nL/min) and a Thermo Scientific reverse-phase nano Easy-spray column (Thermo Scientific PepMap C18, 2 µm particle size, 100 A pore size, 75 µm i.d. × 50 cm length). Peptides were loaded onto a pre-column (Thermo Scientific PepMap 100 C18, 5 µm particle size, 100 A pore size, 300 µm i.d. × 5 mm length) from the Ultimate 3000 autosampler (0.1% formic acid for 3 min, flow rate 10 µL/min). Thereafter, peptides were eluted from the pre-column onto the analytical column. The linear gradient employed was 2–40% solvent B (80% acetonitrile, 20% water + 0.1% formic acid) for 30 min. An Easy-Spray source (Thermo Fisher Scientific Inc.) was used to spray the LC eluant into the mass spectrometer. An Orbitrap mass analyser (set at a resolution of 70,000) was used to measure all m/z values of eluting ions, scanned between m/z 380 and 1500. Fragment ions were automatically isolated and generated using data-dependent scans (Top 20) by higher-energy collisional dissociation (HCD, NCE: 25%) in the HCD collision cell. The resulting fragment ions were measured using the Orbitrap analyser set at a resolution of 17,500. Singly charged ions and ions with unassigned charge states were excluded from selection for MS/MS, employing a dynamic exclusion window of 20 s. The data were processed post-run using Protein Discoverer (version 2.1., Thermo Scientific). All MS/MS data were converted to mgf files. The files were submitted to the Mascot search algorithm (Matrix Science, London, UK) to identify protein hits. Protein hits search identified from cod serum EVs and whole mucus was conducted against a species-specific (*Gadus morhua*),

(Gadus_morhua_20190405; 1283 sequences; 308668 residues), with significance threshold set at p<0.05 and cut-off ion score at 15, or against all teleost UniProt database (CCP_Teleostei Teleostei_20201009; 4085639 sequences; 2121030378 residues), with significance threshold set at p<0.05 and cut-off ion score at 53.

5.2.5. In-vitro Application of Atlantic Cod Serum and Mucus-Derived EVs to an in-vitro Scratch Wound Healing Model.

5.2.5.1 Mouse Fibroblasts (3T3-L1)

Mouse fibroblast cells (ATCC 3T3-L1 cell line) were cultured in a T75 flask (Thermo Scientific) in 1x DMEM (Gibco™) containing 10% FBS (MP Biomedical Fetal Bovine Serum, Fisher Scientific) and 1% Penicillin-Streptomycin (Gibco™) until 70-80% confluency, cells were trypsinized with 3ml of 0.25% trypsin-EDTA, incubated for 10min and thereafter neutralised with 5ml of DMEM and spin down at 1000*g* for 5min. The cell pellet was resuspended in 1ml DMEM and seeded first into a 6-well plate (ThermoFisher) at a concentration of $3x10^2$ cells/well to assess cell growth and perform the first assessment of wound scratch assay. Thereafter, cells were plated in a 12-well plate (ThermoFisher) at a concentration of $2x10^2$ cells/well and cultured in complete medium (DMEM) containing 10%FBS and 1% Penicillin-Streptomycin to nearly confluent cell monolayers for about 24h/36 h. The 6-well and 12-well plates were incubated until 90% confluency was reached to obtain a full fibroblast monolayer to perform a linear scratch with a sterile 200ul plastic pipette tip. Any cellular debris was removed by washing the wells with phosphate buffer saline (PBS). Fresh DMEM medium was added to a set of three wells (control group), and isolated EVs from 1ml Atlantic cod serum, containing approximately $1.55x10^{10}$ +/- $9.17x10^8$ particles/ml EVs, were diluted in 1ml DMEM and added to a set of three wells per treatment group. Images were taken

using EVOS FL Auto Imaging Systems (Thermo Fisher Scientific) at time points of 0h and 24h, following optimisation of assessment of wound closure time, using the 4x objective.

5.2.5.2 Immortalized Human Keratinocytes (HaCat)

Human immortalised keratinocytes (HaCat) migration was assessed using a scratch wound assay. After reaching 80% confluency, the cells were trypsinized with 3ml of 0.25% trypsin-EDTA, incubated for 7-10min and thereafter neutralised with 5ml of DMEM and spun down at 1000*g* for 5min. Cell pellets were resuspended in 1ml DMEM, and then the cells were seeded into 12-well plates (ThermoFisher) at a concentration of $2x10^2$ cells/well and cultured in media containing 10%FBS and 1% Penicillin-Streptomycin to nearly confluent cell monolayers for about 24h/36 h. The selection of seeding density was based on general cell culture recommendations, the cells' doubling time and the necessity of obtaining an 80 % confluency in a short time to conduct scratch assay analysis. Several trials were required to achieve the right seeding density (more information is provided about the protocol optimisation in Appendix 1, section 1.2). A linear scratch was generated in the monolayer using a sterile 200µl plastic pipette tip. Any cellular debris was removed by washing the well with phosphate buffer saline (PBS). Fresh DMEM medium was added to a set of three wells (control group), and isolated EVs obtained from 250µl Atlantic cod serum (3,88x109 particles/ml) were diluted in 1ml DMEM and added to a set of three wells (treatment group) while control wells only received medium. Images were taken using EVOS FL Auto Imaging Systems (Thermo Fisher Scientific) at 0h and 24h using the 4x objective.

5.2.5.3 Human Dermal Fibroblasts Adult (HDFa)

The HDFa primary cell line migration was assessed using the same scratch wound assay protocol described above. After reaching 80% confluency, cells were trypsinized

with 3ml of 0.25% trypsin-EDTA, incubated for 2-3min, neutralised with 5ml of DMEM, and spun down at 1000g for 5min. Cell pellets were resuspended in 1ml DMEM, and the cells were seeded into a 12-well plate (ThermoFisher) at a concentration of $2x10^2$ cell/well and cultured in media containing 10%FBS and 1% Penicillin-Streptomycin to nearly confluent cell monolayers. The rationale behind the choice of seeding density was, as before, based on the general cell culture recommendations, cell doubling time and the necessity to obtain an 80 % confluency in an optimal time window to conduct the scratch assay analysis. Several trials were required to achieve the right seeding density. A linear scratch was generated in the cell monolayer of each well with a sterile 200µl plastic pipette tip. Any cellular debris was removed by washing the wells with phosphate buffer saline (PBS). Fresh DMEM medium was added to a set of three wells (control group), and isolated EVs from 250µl ($3,88x10^9$ particles/ml) Atlantic cod serum was diluted in 1ml DMEM and added to a set of three wells (treatment group). In contrast, control wells were treated with medium only as before. Images were taken using EVOS FL Auto Imaging Systems (Thermo Fisher Scientific) at 0h, 6h and 24h with a 4x objective.

5.2.6. Immunocytochemistry (ICC)

Human Derma Fibroblasts, adult cells (HDFa) (Cat. No. C-013-5C; GIBCO) were cultured in a T75 flask until confluency was reached; cells were then trypsinised with 3ml of 0.25% trypsin-EDTA and incubated for 2-3min; trypsin was then neutralised with 5ml of DMEM, spun down at 1000 *g* for 5min and cell pellet resuspended in 1ml DMEM. Cells were seeded onto a 12 well plate at a concentration of $3x10^2$ cells/well and cultured until 80% confluency was reached. Once HaCat reached confluency (about 12-18h later the day were seeded), the media was replaced with fresh media for the control group (x3 well), which received 1ml of fresh DMEM only, while the treatment

group (x3 well) received 250 µl of cod serum and/or mucus derived EVs diluted in 750µl of fresh medium and apply to a set of three wells. Cells were incubated for 4h, and ICC protocol was applied thereafter. Media was removed from each seeded well, and cells were rinsed with PBST (1x PBS + 0.1% Tween20). Cells were fixed at room temperature for 10 min with 4% Paraformaldehyde in PBS (pH 7.4) (Thermo Fisher), washed three times with ice-cold PBS and then incubated for 10 min with PBS containing 0.2% Triton X-100 for permeabilization, and after 10 min rinsed three times, 5 min each time, with PBS. Cells were incubated with blocking buffer (1% BSA + 22.52mg/ml glycine in PBST) for 30min and after incubated with primary antibodies (Anti-Vimentin and Anti-FGF2, 1/500) diluted in 1% BSA+PBST overnight at 4ºC. Following primary antibody incubation, the blocking solution was removed, and the cells were washed three times, 5 minutes each wash, with PBS and secondary antibody incubated for 1h at room temperature in 1% BSA, left in the dark. After the incubation, cells were washed three times with PBS and incubated for 1 minute with 0.1/µg/ml of DAPI solution. The DAPI counterstain solution was removed, cells rinsed with PBS and visualised using the EVOS FL Auto Imaging Systems (Thermo Fisher Scientific). The ICC protocol was adapted and optimised for this experiment based on a general ICC protocol. In the first instance, the ICC protocol was optimised on control scratch injuries (See Appendix 2) to assess the staining quality before carrying out the ICC-optimized protocol on the full experiment setup, including EV treatment. Mouse fibroblasts were mainly used to optimise scratch injuries (including time windows for wound closure), and ICC was not applied in this model; when moving into human cellular models, HDFa cells were stained for anti-Vimentin and anti-FGF2 to assess changes in expression of those two proteins, when treated with Atlantic cod serum- and mucus-derived EVs. EVs applied from Atlantic cod were either from serum or mucus and in some instances, both sources were assessed; this was somehow restricted to various pilot attempts due to

restrictions in the availability of cod serum and mucus. Findings provide some preliminary insights into the potential of cod EVs to promote wound healing.

5.2.7. Statistical Analysis

Images obtained from the scratch assays at different time points were imported to PowerPoint, and images were organised to ensure that image size was consistent; the scratch was manually delineated with a red line. The images were then grouped and copied in ImageJ software (https://imagej.nih.gov/ij/), where the area of the scratches volume was measured using the function of freehand selection, tracing the wound edges previously manually traced in PowerPoint. Results were recorded in GraphPad Prism 9, and histograms were generated, representing differences in gap closure/changes in gap size of the EV treated versus control scratch injuries at different time points.

5.3. Results

5.3.1. Characterization of Gadus morhua (Atlantic Cod) Serum and Mucus EVs

EVs from cod serum were characterised by size distribution based on the Brownian motion of particles in suspension using nanoparticle tracking analysis (NTA), morphological analysis using transmission electron microscopy (TEM; kindly imaged by Dr Igor Kraev, Open University) and Western blotting using the EV-specific markers CD63 and Flotillin-1 (Fig.37). NTA results showed a poly-dispersed population consisting mainly of approximately 70-500nm sized vesicles (small/EVs and medium/EVs), with the majority of EVs being 90-400nm, with main peaks around 100-120nm and smaller peak at 300-400nm size range (Fig.37). The concentration of EVs was determined based on the NTA quantification of particles per ml and estimated as $1.55x10^{10}$ +/- $9.17x10^{8}$ particles/ml EVs per 1ml cod serum. Western blotting showed a positive band for the specific EV markers CD63 at the predicted size of 26kDa and Flotillin-1 at the predicted size of 47kDa (Fig.37). Transmission electron microscopy confirmed the EVs morphology and verified the size range observed by NTA (Fig.37).

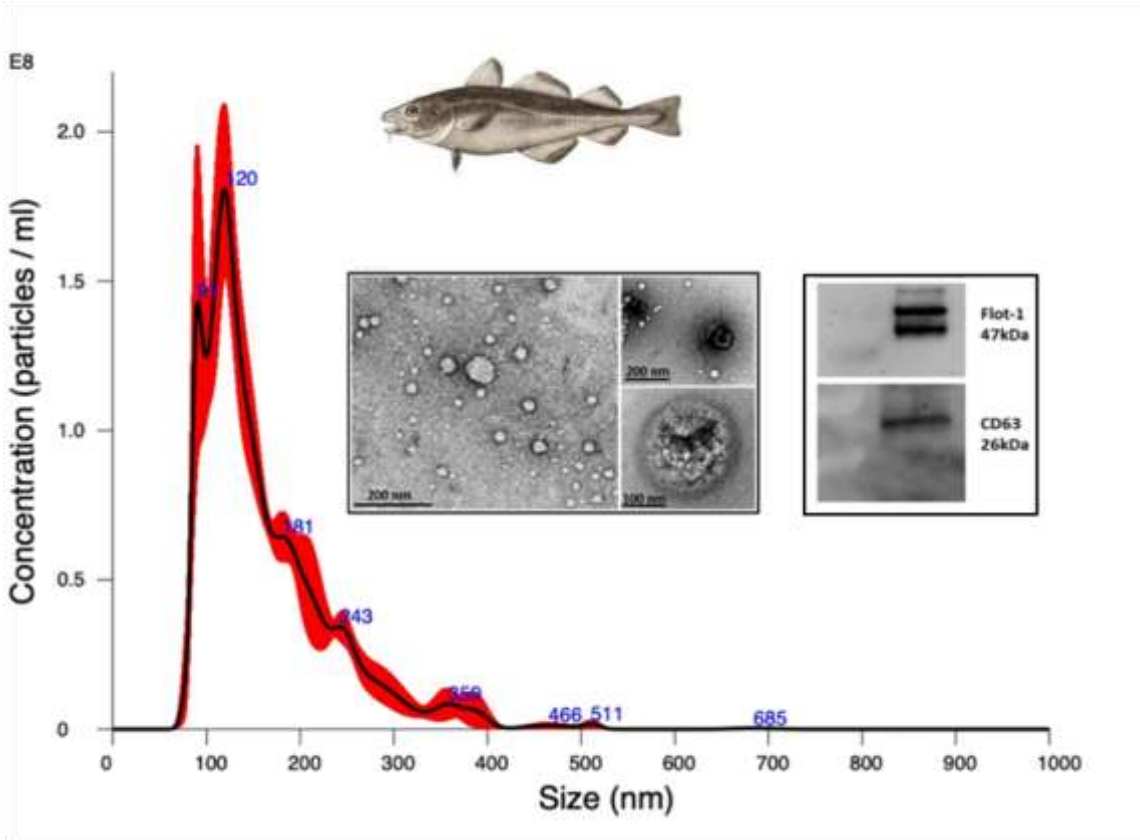

Figure 37. Cod serum EVs characterisation. Characterisation of EVs isolated from cod serum by NTA (Nanoparticle tracking analysis) for size distribution (a representative NTA histogram is shown, black line representing the mean and the red line (broad lone) represents the standard error for the mean (SEM), based on four 60s replicate video recordings of the same sample), by TEM (Transmission electron microscopy) for EVs morphology and by Western blotting for EV-specific markers CD63, Flot-1 and Alix (all antibodies diluted 1/1000).

Atlantic cod mucus-derived EVs have been previously characterised by Magnadóttir *et al*., (2019a): EVs from cod mucus were characterised by size exclusion using NTA, by morphological analysis using TEM and by Western blotting using the EVs-specific markers CD63 and Flot-1 (Fig.38). The NTA analysis shows a poly-dispersed population of EVs in the size range of 30-500nm, with peaks at 128, 175, 295 and 415nm and the concentration of EVs was determined based on the NTA quantification of particles per ml and estimated as 1.29e10 +/- 1.22e9 particles/ml in EVs per 1ml Cod mucus. Western blotting analysis shows a positive band for EV-specific marker CD63 at the

expected band size of 26kDa and Flot-1 at the expected size of 47kDa. Transmission electron microscopy (TEM) analysis in Fig. 30 shows representative morphological images of poly-dispersed EV population, all images scale bar at 200nm, confirming the classic morphology of EVs.

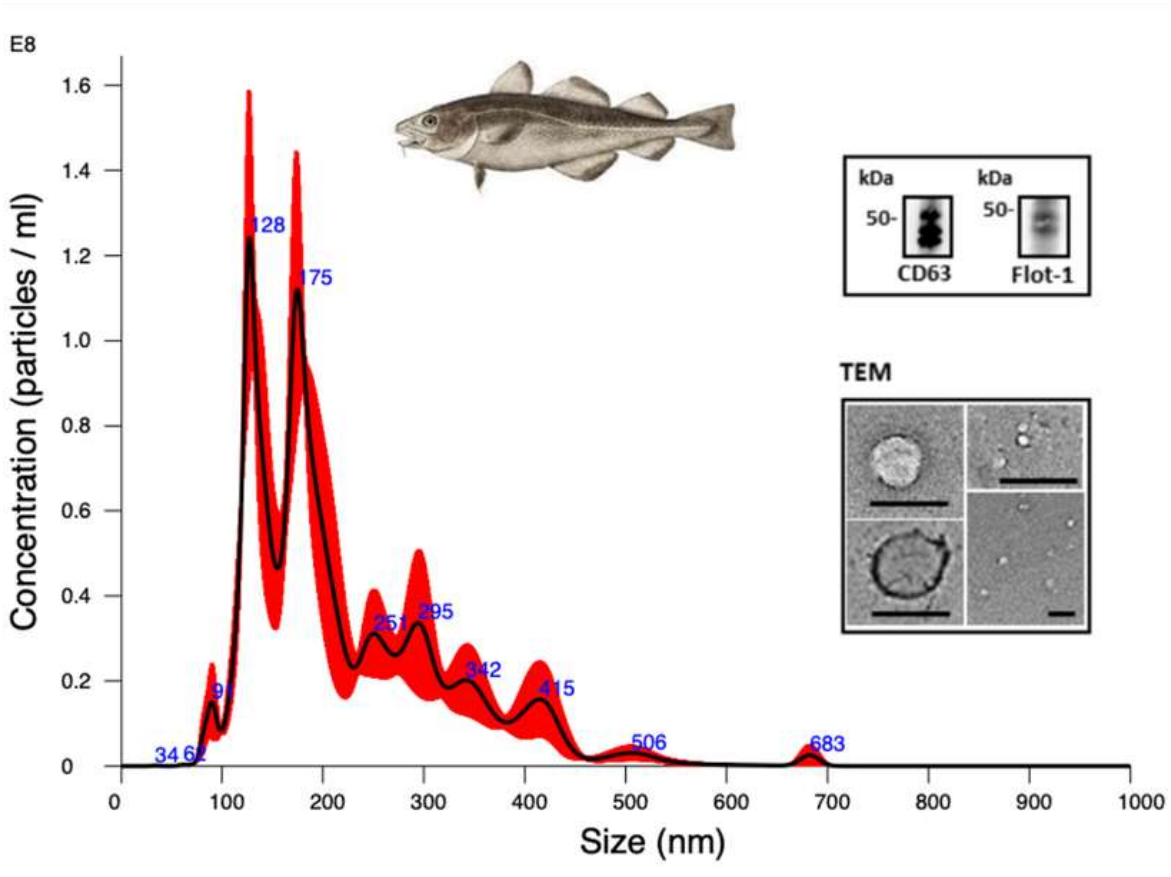

Figure 38. Cod mucus EVs characterisation. Characterisation of EVs isolated from cod mucus by NTA (Nanoparticle tracking analysis) for size distribution a representative NTA histogram is shown, this black line representing the mean and the red line (broad lone) represents the standard error for the mean (SEM), based on four 60s replicate video recordings of the same sample), by TEM (Transmission electron microscopy) for EVs morphology and by Western blotting for EV-specific markers CD63, Flot-1 and Alix (all antibodies diluted 1/1000).

5.3.2. LC-MS/MS Analysis of Whole Proteome of Cod Serum and Mucus EVs

In the present investigation, an examination of the entire proteome was conducted on EVs derived from Atlantic cod serum and mucus. Previous research has already

detailed the citrullinome of serum and mucus cod EVs (Magnadóttir *et al*., 2018, 2019, 2020). Tandem mass spectrometry (LC-MS/MS) was employed to analyse the complete proteome of serum and mucus EVs. The whole serum EVs data were submitted to the in-house Mascot (Cambridge Centre for Proteomics) using the *Gadus_morhua*_20190405 database (1283 sequences: 308668 residues), with settings at a significant threshold of $p < 0.05$ and a cut-off at Ion score 33. The identified protein hits for cod serum EVs are presented in Table 15, including protein ID, species name, matches, and total score. Eight protein hits were identified: Fast skeletal muscle alpha-actin, Beta-actin, Serotransferrin, 60s ribosomal protein L22, Galectin, Elongation factor 1 alpha, Ribosomal protein L15, and Profilin.

Table 15. Whole cod serum EVs protein content identified by tandem mass spectrometry (LC-MS/MS) analysis in *Gadus morhua* (Atlantic Cod). Highlighted protein hits are hits identified as common to the cod serum EVs proteome and cod mucus EV proteome.

Protein ID ***Protein name***	***Species name*** **Common name**	**Matches** **(Sequences)**	**Total score** **(p<0.05)‡**
Q78AY8_GADMO *Fast skeletal muscle alpha-actin*	*Gadus morhua* Atlantic Cod	5 (5)	214
Q2PDJ0_GADMO *Beta-actin*	*Gadus morhua* Atlantic Cod	4 (4)	138
Q92079|TRFE_GADMO *Serotransferrin*	*Gadus morhua* Atlantic Cod	17 (2)	106
P52865|RL22_GADMO *60S ribosomal protein L22*	*Gadus morhua* Atlantic Cod	1 (1)	65
G8ENP0_GADMO *Galectin*	*Gadus morhua* Atlantic Cod	1 (1)	40

A8CZC9_GADMO *Elongation factor 1 alpha*	*Gadus morhua* Atlantic Cod	3 (1)	40
A0A067XLH1_GADMO *Profilin*	*Gadus morhua* Atlantic Cod	3 (1)	35
Q8JHA8_GADMO *Ribosomal protein L15*	*Gadus morhua* Atlantic Cod	1 (1)	21

† Ion score is −10*Log(P), where P is the probability that the observed match is a random event. Individual ion scores <33 indicate identity or extensive similarity ($p < 0.05$). Protein scores are derived from ion scores as a non-probabilistic basis for ranking protein hits.

Whole Atlantic cod mucus-derived EVs proteome files were submitted to in-house Mascot (Cambridge Centre for Proteomics) using the following database: *Gadus_morhua*_20190405 (1283 sequences; 308668 residues), with settings at significant threshold $p < 0.05$ and cut- off at Ions score 15. Identified protein hits for Atlantic cod mucus-derived EVs proteome are reported below (Table 16) with protein ID, species name, matches and total score. Fifty-seven protein hits were identified, and eight of the identified protein were in common with the protein hits identified in Atlantic cod serum-derived EVs proteome.

Table 16. Atlantic cod mucus-derived EVs proteome, identified by tandem mass spectrometry (LC-MS/MS) analysis in *Gadus morhua*. Highlighted protein hits are hits commonly found in Atlantic cod serum-derived EVs proteome and Atlantic cod mucus-derived EV proteome.

Protein ID ***Protein name***	***Species name*** **Common name**	**Matches** **(Sequences)**	**Total score** **(p<0.05)[‡]**
Q92079|TRFE_GADMO *Serotransferrin*	*Gadus morhua* Atlantic Cod	32 (28)	1747
V9I305|V9I305_GADMO *Transglutaminase 2*	*Gadus morhua* Atlantic Cod	26 (18)	1086
G8DZS1_GADMO *Heat shock cognate 70 kDa protein (Fragment)*	*Gadus morhua* Atlantic Cod	29 (14)	1081
Q9PUG4_GADMO *Tubulin beta chain*	*Gadus morhua* Atlantic Cod	30 (16)	996
A8CZC9_GADMO *Elongation factor 1-alpha*	*Gadus morhua* Atlantic Cod	25 (14)	805
V9I378_GADMO *Transglutaminase 1*	*Gadus morhua* Atlantic Cod	18 (13)	757
A0A067XL91_GADMO *Flotillin-1 (Fragment)*	*Gadus morhua* Atlantic Cod	11 (9)	616
K7SPU9_GADMO *MHC class I antigen (Fragment)*	*Gadus morhua* Atlantic Cod	13 (10)	599

A0A067XL41_GADMO *Calpain small subunit 1*	*Gadus morhua* Atlantic Cod	13 (11)	577
Q78AY8_GADMO *Fast skeletal muscle alpha-actin*	*Gadus morhua* Atlantic Cod	58 (9)	565
P56533|BADH_GADMC *Betaine aldehyde dehydrogen-ase*	*Gadus morhua* Atlantic Cod	11 (11)	540
K7S1G8_GADMO *MHC class I antigen (Fragment)*	*Gadus morhua* Atlantic Cod	12 (9)	532
Q2PDJ0_GADMO *Beta-actin (Fragment)*	*Gadus morhua* Atlantic Cod	58 (8)	511
Q6WEU6_GADMO *S2 ribosomal protein (Frag-ment)*	*Gadus morhua* Atlantic Cod	9 (8)	467
Q8JHA8_GADMO *Ribosomal protein L15 (Fragment)*	*Gadus morhua* Atlantic Cod	11 (7)	419
G8DZS2_GADMO *Nucleoside diphosphate kinase (Fragment)*	*Gadus morhua* Atlantic Cod	10 (6)	388
G0XNX4_GADMO *Peptidyl-prolyl cis-trans isomer-ase*	*Gadus morhua* Atlantic Cod	7 (6)	331
P83456|PPB_GADMO *Alkaline phosphatase*	*Gadus morhua* Atlantic Cod	8 (8)	307

Q5XQS6_GADMO *Preproapolipoprotein A-I (Fragment)*	*Gadus morhua* Atlantic Cod	5 (4)	305
A0A067XLH1_GADMO *Profilin*	*Gadus morhua* Atlantic Cod	7 (4)	249
A0A0G2QMS5_GADMO *Histone H3 (Fragment)*	*Gadus morhua* Atlantic Cod	31 (3)	205
D5LIQ8_GADMO *Putative ribosomal protein L8 (Fragment)*	*Gadus morhua* Atlantic Cod	6 (4)	201
G0XNX5_GADMO *Cystatin B*	*Gadus morhua* Atlantic Cod	9 (5)	201
A8CZB9_GADMO *20-beta hydroxysteroid dehydrogenase*	*Gadus morhua* Atlantic Cod	4 (4)	197
P81600|ADHH_GADMO *Alcohol dehydrogenase class-3 chain H*	*Gadus morhua* Atlantic Cod	3 (3)	184
P52865|RL22_GADMO *60S ribosomal protein L22 (Fragment)*	*Gadus morhua* Atlantic Cod	4 (2)	182
G0XNX6_GADMO *Mannan-binding lectin*	*Gadus morhua* Atlantic Cod	4 (4)	169
A0A343ANK4_GADMO *Cytochrome c oxidase subunit 2*	*Gadus morhua* Atlantic Cod	4 (3)	142

D5LIQ2_GADMO *Pantophysin*	*Gadus morhua* Atlantic Cod	2 (2)	138
G8ENP0_GADMO *Galectin (Fragment)*	*Gadus morhua* Atlantic Cod	13 (2)	136
E3U9P6_GADMO *Bloodthirsty*	*Gadus morhua* Atlantic Cod	3 (3)	117
Q8AWX8_GADMO *Glyceraldehyde-3-phosphate dehydrogenase*	*Gadus morhua* Atlantic Cod	3 (2)	115
G0XNX7_GADMO *Peptidylprolyl isomerase*	*Gadus morhua* Atlantic Cod	2 (2)	108
D5LIQ1_GADMO *Putative ribosomal protein L17b (Fragment)*	*Gadus morhua* Atlantic Cod	3 (2)	106
A7XA14_GADMO *Nascent polypeptide-associated complex alpha polypeptide NACA (Fragment)*	*Gadus morhua* Atlantic Cod	1 (1)	74
Q9YGI3_GADMO *Beta-2-microglobulin*	*Gadus morhua* Atlantic Cod	2 (1|)	66
K9LCP7_GADMO *Caspase 3 (Fragment)*	*Gadus morhua* Atlantic Cod	1 (1)	55
D7R9W9_GADMO *Fas (Fragment)*	*Gadus morhua* Atlantic Cod	1 (1)	44

D7R9Z6_GADMO *Mitogen-activated protein kinase 1 (Fragment)*	*Gadus morhua* Atlantic Cod	2 (1)	42
D7R9Y5_GADMO *Toll-like receptor 9 (Fragment)*	*Gadus morhua* Atlantic Cod	1 (1)	41
Q6DTY9_GADMO *Glucose transporter 3*	*Gadus morhua* Atlantic Cod	1 (1)	34
A7XA12_GADMO *Aminopeptidase puromycin-sensitive protein (Fragment)*	*Gadus morhua* Atlantic Cod	1 (1)	27
A4ZGE0_GADMO *Non-specific cytotoxic cell receptor protein 1*	*Gadus morhua* Atlantic Cod	1 (1)	24
B8XJS4_GADMO *Hemoglobin alpha 1 chain*	*Gadus morhua* Atlantic Cod	1 (1)	24
Q9PV18_GADMO *RAG1 protein (Fragment)*	*Gadus morhua* Atlantic Cod	1 (1)	24
D6MXZ1_GADMO *Acyl-Coenzyme A dehydrogenase (Fragment)*	*Gadus morhua* Atlantic Cod	1 (1)	24
Q8JIV4_GADMO *Fast skeletal myosin heavy chain (Fragment)*	*Gadus morhua* Atlantic Cod	1 (1)	23
G8DZS4_GADMO	*Gadus morhua* Atlantic Cod	1 (1)	23

Hypoxanthine phosphoribosyl-transferase (Fragment)			
A0A0D3RBU4_GADMO *Interferon regulatory factor protein 7*	*Gadus morhua* Atlantic Cod	1 (1)	23
A7XA16_GADMO *Titin isoform b (Fragment)*	*Gadus morhua* Atlantic Cod	1 (1)	23
F8SXV2_GADMO *Osteonectin (Fragment)*	*Gadus morhua* Atlantic Cod	(1)	23
A7XA17_GADMO *Titin isoform c (Fragment)*	*Gadus morhua* Atlantic Cod	1 (1)	22
Q1M164_GADMO *Interleukin-8*	*Gadus morhua* Atlantic Cod	1 (1)	22
F8TW94_GADMO *Activating transcription factor 3*	*Gadus morhua* Atlantic Cod	1 (1)	22
A0A0C6EYL8_GADMO *Amine oxidase*	*Gadus morhua* Atlantic Cod	1 (1)	22
D7R9Z7_GADMO *Mitogen-activated protein kinase (Fragment)*	*Gadus morhua* Atlantic Cod	1 (1)	21
A7UFK3_GADMO *Hexokinase 1a*	*Gadus morhua* Atlantic Cod	1 (1)	21

† Ion score is −10*Log(P), where P is the probability that the observed match is a random event. Individual ion scores <15 indicate identity or extensive similarity ($p < 0.05$). Protein scores are derived from ion scores as a non-probabilistic basis for ranking protein hits.

The above tables (Table 15 and 16) highlight protein hits identified to be common to Atlantic cod serum-derived EVs and Atlantic cod mucus-derived EVs' whole proteome. These hits are highlighted in yellow. They include fast skeletal muscle alpha-actin, beta-actin, serotransferrin, 60s ribosomal protein L22, Galectin, Elongation factor 1 alpha, Profilin, and Ribosomal protein L15.

5.3.3 Atlantic Cod Serum and Mucus Derived- EVs Application to In-vitro Wound Healing Model.

5.3.3.1 3T3.L1 Mouse Fibroblast in-vitro Wound Healing Model

In the first instance, due to feasibility and for optimisation of protocols and cell culture, mouse fibroblasts were used to assess the potential of cod serum EVs on wound healing. Scratch assays were performed on mouse fibroblasts (3T3-L1 cell line) cells, cultured in a 12-well plate until 80-90% confluency was reached; a linear scratch was performed using a sterile 200µl plastic pipette tip and cellular debris washed with phosphate-buffered saline (PBS). Fresh 1ml of DMEM was added to a set of three wells (control group) and derived-EVs preparation from 1ml cod serum was diluted in 1ml DMEM and added to a set of three wells (treatment group); each treatment well contained about $1.55x10^{10}$ +/- $9.17x10^{8}$ particles/ml of cod serum EVs, control wells contained medium only. Images were taken using EVOS FL Auto Imaging Systems (Thermo Fisher Scientific) at 0, 6h and 24h with a 4x objective. Images were then imported into PowerPoint, where scratches were manually defined with the drawing selection (Fig.39) and exported into ImageJ for gap area measurements, using the hand-free selection by tracing the line previously drawn in PowerPoint for accuracy.

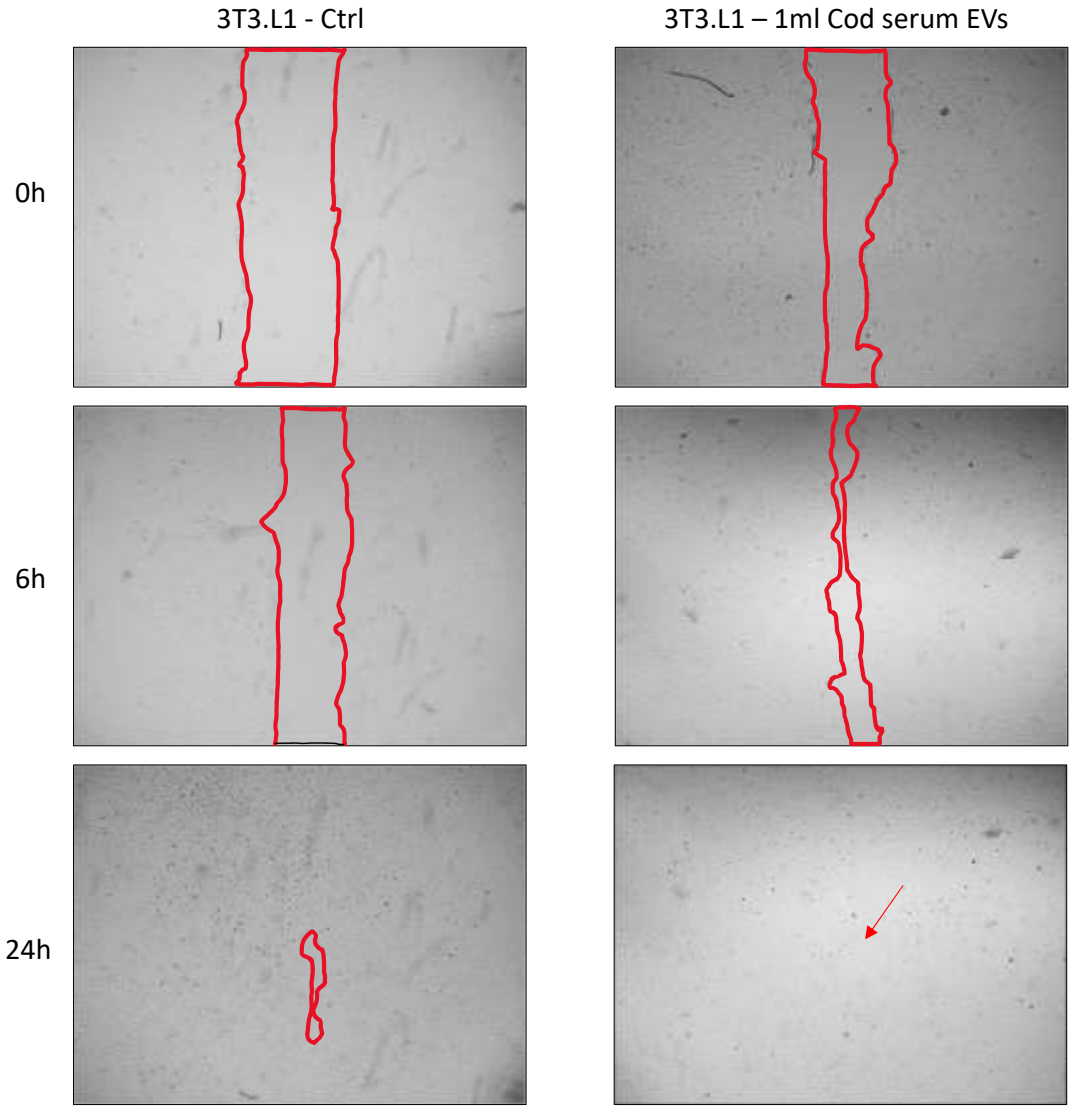

Figure 39. 3T3.L1 scratch assay. Representative images of mouse fibroblasts (3T3-L1 cell line) scratch assay analysis of control group and treated group with cod serum EVs derived from 1ml serum and cell migration assessed at 6h and 24h. Wound scratch assay images were taken with EVOS FL Auto Imaging Systems (Thermo Fisher Scientific) with x4 objective, at time points of 0h, 6h and 24h performed in a 12-well plate using 3T3-L1 monolayer as an *in vitro* wound model. The experiment replicates n=3 per group (See Appendix 1, 1.1 3T3.L1 cell line).

The investigation into the time points for cell migration of 3T3.L1 cells (mouse fibroblasts) subjected to treatment with Atlantic cod serum-derived extracellular vesicles (EVs) involved assessments at 6h and 24h, employing Ordinary one-way ANOVA tests. Generally, the behaviour of 3T3.L1 mouse fibroblasts demonstrated a descending trend in wound scratch, albeit without statistical significance (p=0.9921; mean difference=240.0), following treatment with Atlantic cod serum-derived EVs after 6h (n=3; mean=2738). This was compared to the control group at 6h (n=3; mean=2978). Likewise, at the 24-hour mark, there was no notable difference (p=0.9963; mean difference=185.7) between the negative control group at 24h (n=3; mean=185.7) and the cod serum-EVs treatment group at 24h (n=3; mean=0.000). Furthermore, the mean difference between the negative control group and the treatment group at 0h was calculated (mean difference=-238.7). However, the observed disparity between the groups did not reach statistical significance (p=0.9922) (Fig.40-A). Exploring changes between the control group at 0h and the control and treatment groups at 0h, 6h, and 24h revealed noteworthy statistical differences. Significant changes were observed between the control group at 0h and both the control (**p=0.0021) and treatment (**p=0.0015) groups at 24h. Meanwhile, the alterations between the control group at 0h and both the control (p=0.3924) and treatment (p=0.2681) groups at 6h, although indicative of a decreasing trend in wound closure when 3T3.L1 cells were treated with 1ml of cod serum-derived EVs, did not attain statistical significance (Fig.40-B).

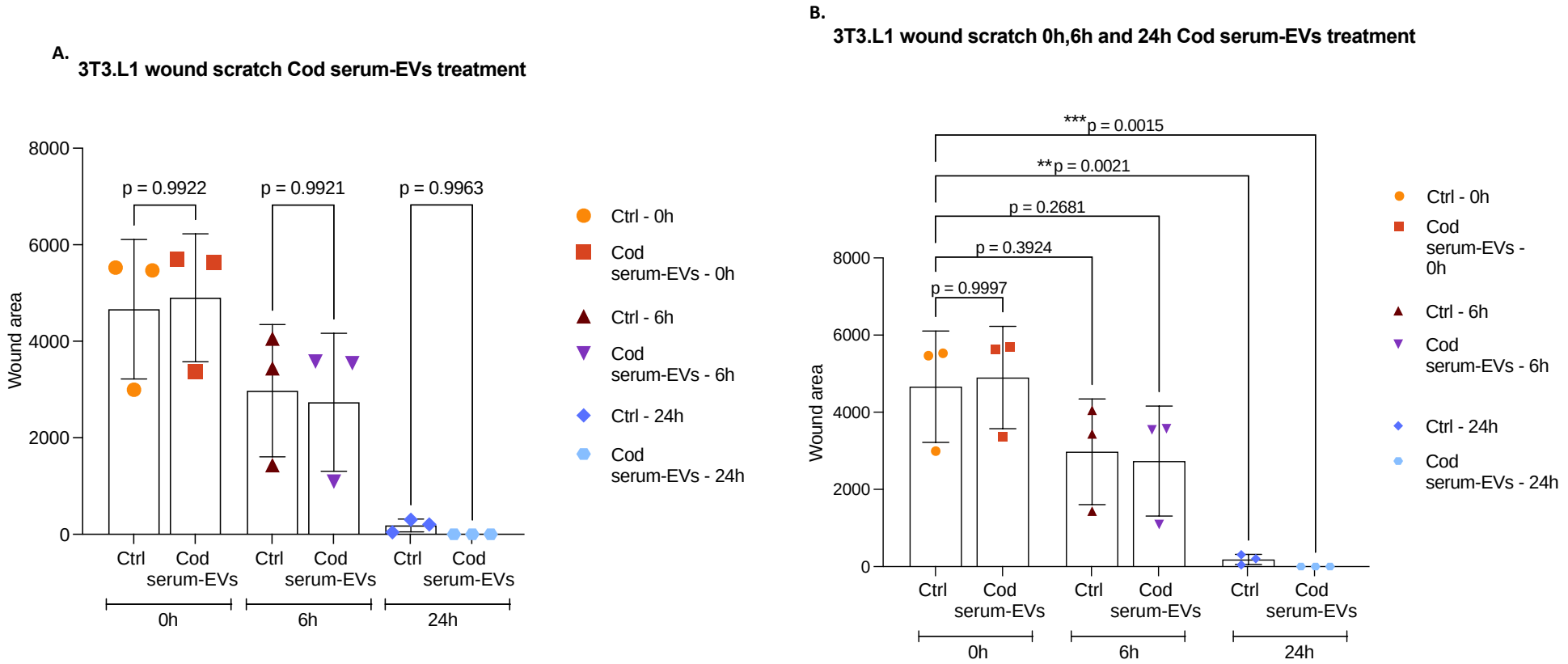

Figure 40. Assessment of cod serum derived-EVs *in-vitro* efficiency in promoting wound healing closure in 3T3.L1 mouse fibroblasts, at 6h and 24h. Comparison of means between the negative control group and cod serum derived-EVs treatment group at 0h, 6h and 24h (A). Comparison of mean negative control group at 0h and mean cod serum derived-EVs control and treatment groups at 6h and 24h (B). Data are represented as mean ± standard deviation (SD) from three independent experiments. Statistical significance was determined using Ordinary one-way ANOVA, where *p < 0.05, **p < 0.01, ***p < 0.001.

When comparing the mean of the negative control group (mean=4663) with the mean of the treatment group at 6h (mean=2738), no statistically significant difference was observed (p=0.6790, mean difference=1925). However, there was a noticeable trend suggesting a reduction in wound scratches. Similarly, comparing the mean of the positive control group (Cod serum-EVs) at 0h (mean=4902) with the mean of the treatment group (Cod serum-EVs) at 6h (mean=2738) showed a reduction in wound scratch; however, the difference was not statistically significant (p=0.2551). The comparison between the negative control group at 6h and the treatment group at 6h, also, did not have a significant difference (p=0.9985) (Fig.41-A). Significant differences were found in two instances: between the mean of the control group at 0h (mean=4663) and the mean of the treatment group (cod serum-EVs) at 24h (mean=0.000) (mean difference=4663; **p=0.0012), indicating complete wound closure of 3T3.L1 cells *in vitro*; and between the mean of the treatment group at 0h (mean=4902) and the treatment group at 24h (mean=0.000) (mean difference=4902; **p=0.0009), suggesting the efficacy of Atlantic cod serum-derived EVs in an *in vitro* wound scratch model over 24h. However, no significant difference was found between the control group at 24h and the treatment group at 24h (p=0.9944) (Fig.41-B).

Conversely, when comparing the negative control group with the treatment group at 6h and 24h, the treatment group at 6h with the treatment group at 24h, and the control groups at 6h with the control group at 24h (Fig.41-C), all showed statistically significant differences (ctrl 6h/Cod serum-EVs 24h *p=0.0247; cod serum-EVs 6h/cod serum-EVs 24h *p=0.0379; ctrl 6h/ctrl 24h p=0.0343), suggesting the efficiency of Atlantic cod serum-derived EVs in promoting wound regeneration over the 18h period.

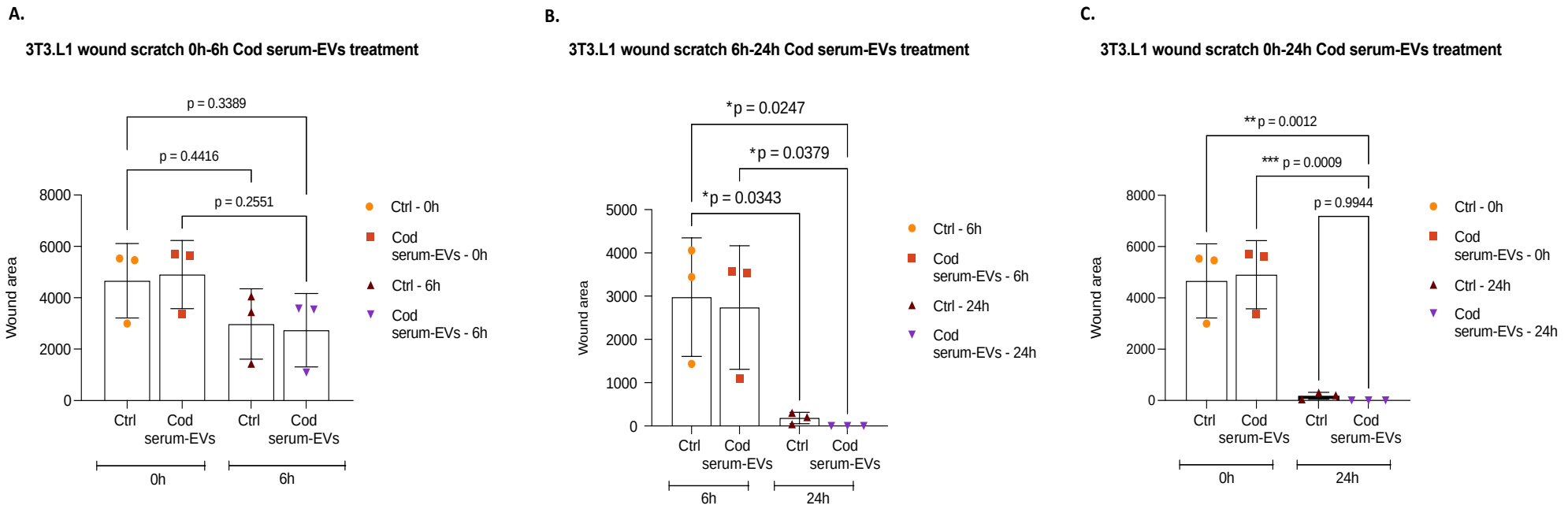

Figure 41. Assessment of changes in *in-vitro* wound area upon treatment with 1ml of cod serum derived-EVs on 3T3.L1 mouse fibroblasts. Mean comparison between the control group and treatment group, between treatment groups and between control groups at 0h and 6h (A), 0h and 24h (B), and 6h and 24h (C). Data are represented as mean ± standard deviation (SD) from three independent experiments. Statistical significance was determined using the Ordinary one-way ANOVA test, where *p < 0.05, **p < 0.01, ***p < 0.001.

Due to potential relevance and translatability to humans, the experiments were next moved to two human cell lines for modelling wound healing, using human keratinocytes and human fibroblasts, as shown in Sections 5.3.3.2 and 5.3.3.3 below. Further detail on optimising the mouse fibroblast cultures and various troubleshooting is shown in Appendix 1, section 1.1.

5.3.3.2 Human Immortalized Keratinocytes (HaCat) in-vitro Wound Healing Model

HaCat (Human immortalised keratinocytes) cell lines were seeded and cultured in 12-well plates and treated with cod-derived EVs from 1ml and 2ml of serum for 24. After the generation of a scratch to the cell monolayers, cells of the treatment group were treated with 1ml (x3 wells) (See Appendix 1, section 1.2) of cod EVs preparation (total cod EVs in 1ml $1.55x10^{10}$ +/- $9.17x10^{8}$ particles/ml) mixed with 1ml DMEM, and 2ml of cod EVs preparation ($3,1x10^{10}$) were added to another set of three wells. Control groups were treated with 1ml of fresh medium. Pictures were taken at 0h and 24h using EVOS FL Auto Imaging Systems (Thermo Fisher Scientific). Representative images for HaCat scratch assays are shown in figure 42 below.

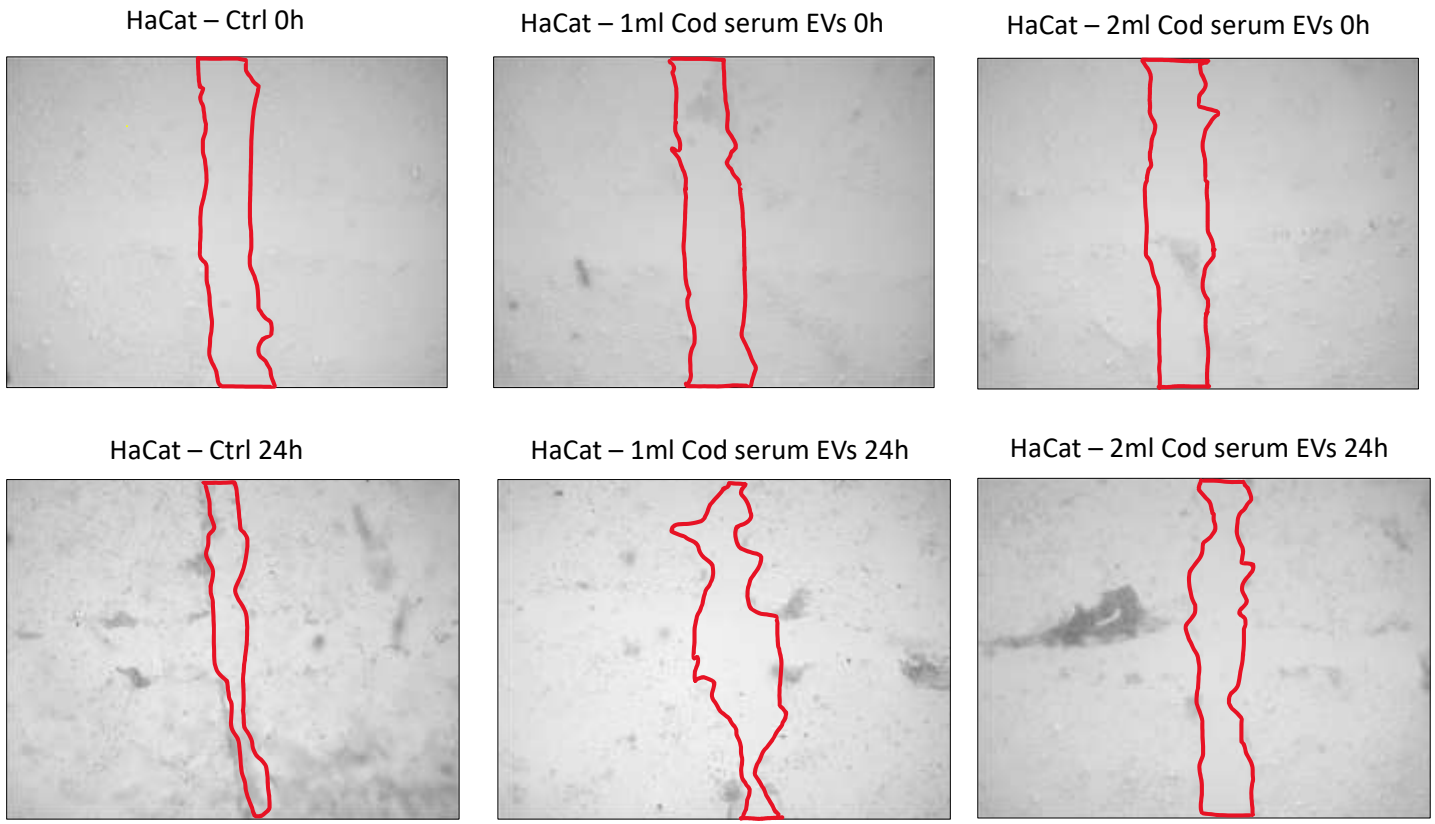

Figure 42. Representative images for HaCat cells scratch assay analysis. Wound scratch assay images were taken with EVOS FL Auto Imaging Systems (Thermo Fisher Scientific) with an x4 objective at time points of 0h and 24h. The assay was performed on a 12-well plate using a HaCat monolayer as an in-vitro wound model and treated with different concentrations (1ml/2ml) of cod serum derived EVs (1ml of cod serum EVs = 1.5x109 particles/ml). The experiment replicates n = 3 per group (See Appendix 1, section 1.2).

Assessment of *in-vitro* wound scratch healing of human keratinocytes, treated with different EVs yield (1ml and 2ml) from the same cod serum EVs preparation, revealed an overall trend for reduction after 24h. This reduction, however, was not statistically significant (p=0.3973) when comparing the control group at 0h and the group treated with 1ml of cod serum-derived EVs) at 24h, neither when comparing the control group at 0h and the control group at 24h (p=0.5482)(Fig.43-A). Conversely, the reduction observed was statistically significant when comparing the control group at 0h and the treatment group, which received 2ml of cod serum-derived EVs at 24h (**p=0.0200). This was also the case for the control group at 24h, compared with the control group at 0h (*p=0.0349)(Fig.43-B).

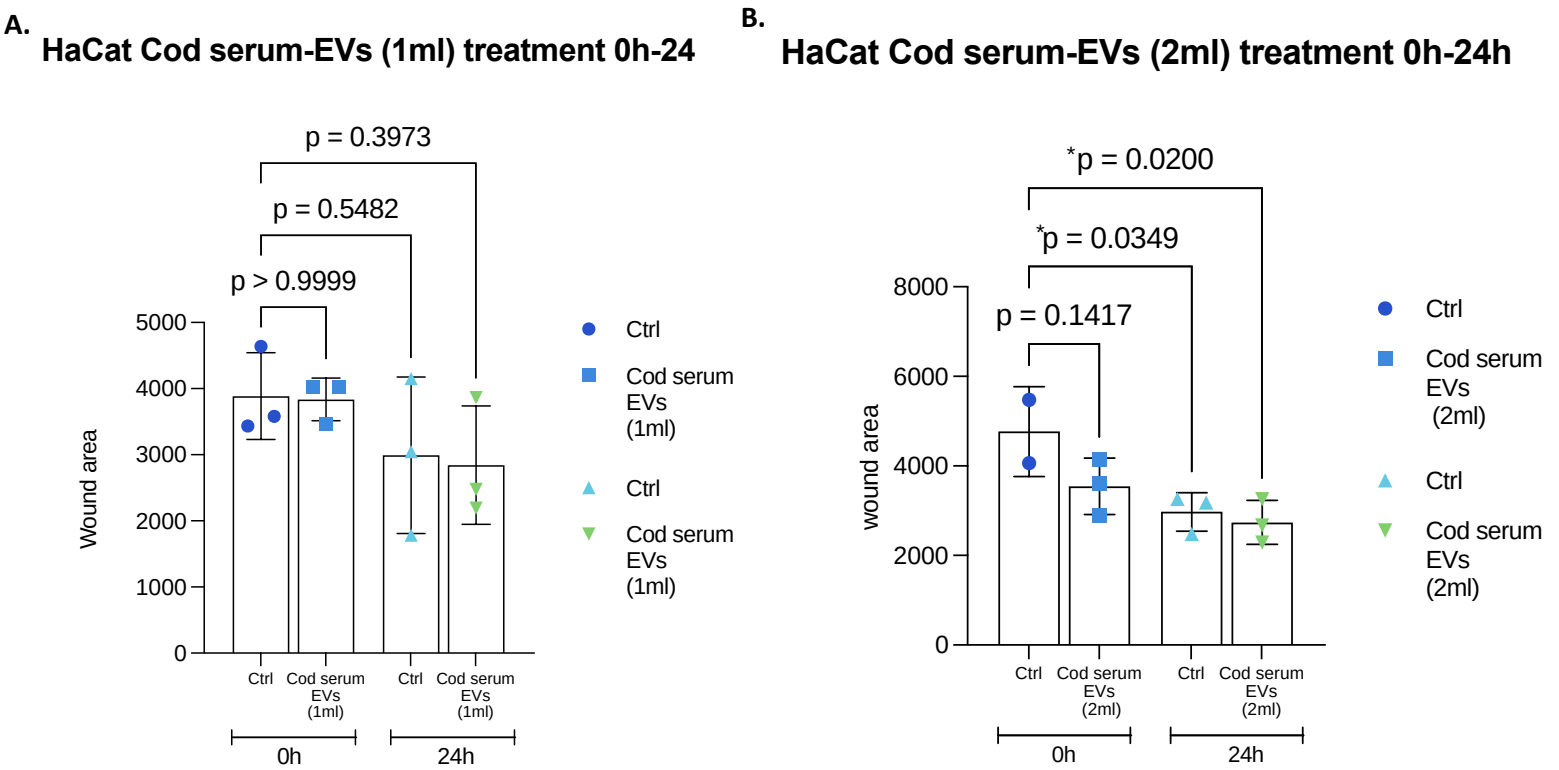

Figure 43. Assessment of cod serum derived EVs in-vitro efficiency in promoting wound healing closure in HaCat cells at 0h and 24h. (A) Mean comparison between the control group and treated HaCat cells with 1ml of cod serum-derived EVs at 0h and 24h. (B) Mean comparison between the control group and treated HaCat cells with 2ml of cod serum EVs at 0h and 24h. Data are represented as mean ± standard deviation (SD) from three independent experiments. Statistical significance was determined using Ordinary one-way ANOVA, where *p < 0.05, **p < 0.01, ***p < 0.001.

5.3.3.3 Human Dermal Fibroblasts, adult (HDFa) in vitro Wound Healing Model Human dermal fibroblasts and adult (HDFa) cells were chosen as an in vitro model to assess the regenerative potential of Cod serum-derived EVs. Cells were seeded in a 12-well plate at 2x102 seeding density and allowed to settle at the bottom of the wells before proceeding with the wound scratch assay. Cell monolayers were scratched with a sterile 200µl plastic pipette tip, and cellular debris was washed with phosphate-buffered saline (PBS). Fresh 1ml of DMEM was added to a set of three wells (control group) and derived-EVs preparation from 1ml cod serum was diluted in 1ml DMEM and added to a set of three wells (treatment group); each treatment well contained about 1.55x1010 +/- 9.17x108 particles/ml of cod serum EVs, control wells contained medium only. Images were taken using EVOS FL Auto Imaging Systems (Thermo Fisher Scientific) at time points of 0h and 24h with a 4x objective and imported into PowerPoint, where scratches were manually defined with the drawing selection (Fig.44), and thereafter exported into ImageJ for gap area measurements, using the hand-free selection, by tracing the line previously drawn in PowerPoint, for accuracy.

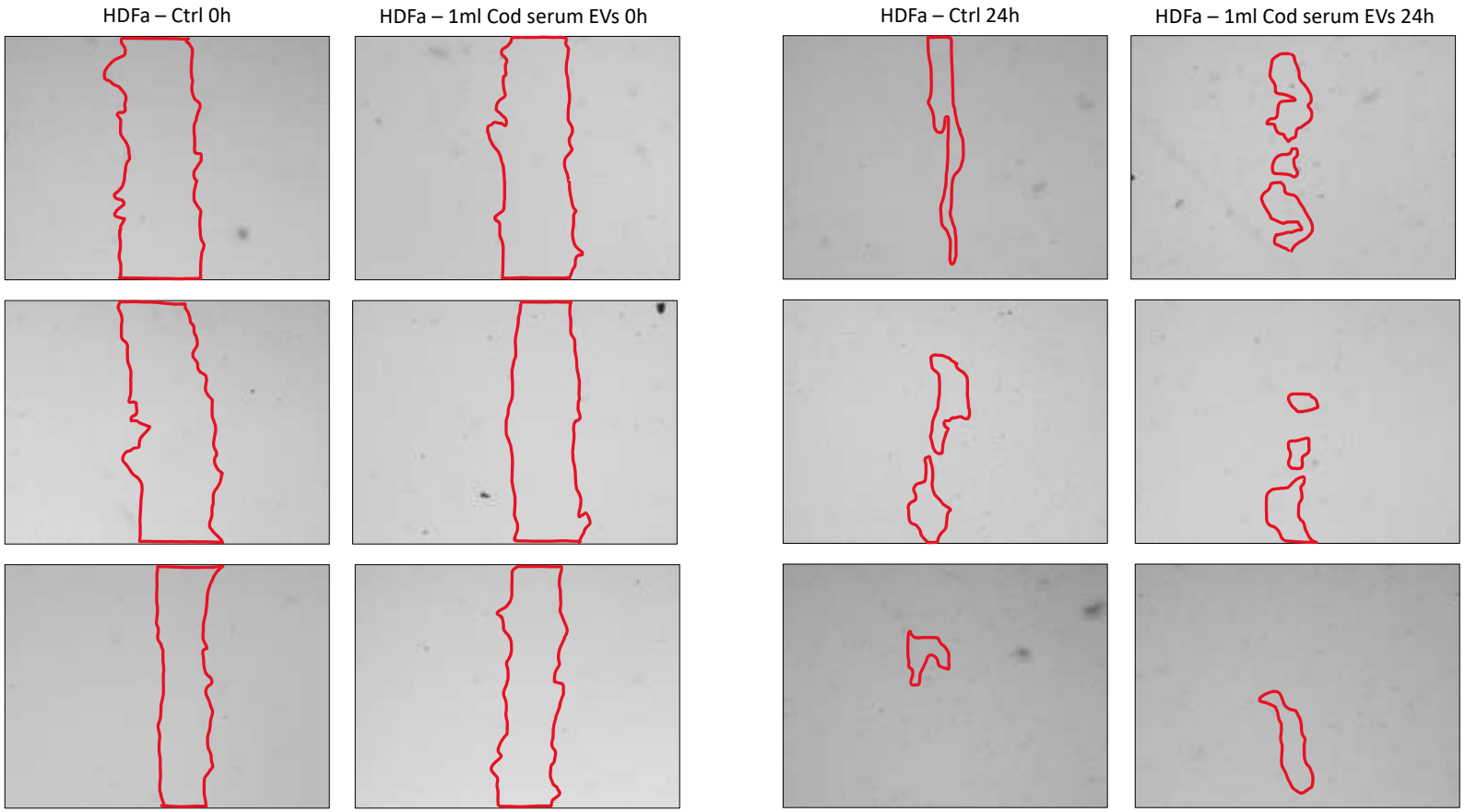

Figure 44. Representative images for HDFa cells scratch assay. Wound scratch assay images were taken with EVOS FL Auto Imaging Systems (Thermo Fisher Scientific) with an x4 objective at the time points of 0h and 24h, performed on 12-well plates using HDFa monolayer as an *in-vitro* wound healing model and treated with 1 ml of cod serum derived EVs (1 ml of cod serum EVs = 1.5x109 particles/ml). The experiment replicates n = 3 per group.

In vitro wound healing assessment on HDFa cells, treated with 1ml ($1.55x10^{10}$ cells/ml) Cod serum EVs, revealed a statistically significant closure of the wound when comparing the mean of the control group at 0h and the treatment group at 24h (p=0.0003) and between treatment groups at 24h (p=0.0006) (Fig.45). These findings suggest variations in the concentration or treatment protocols within the Cod serum EVs groups may have influenced the wound healing outcomes, indicating potential avenues for optimisation and further investigation. Moreover, statistical analysis revealed a significant difference in wound closure between control groups over the 24-hour period (p=0.0002), implying that other factors, beyond the treatment itself, may have played a role in influencing the observed wound healing outcomes in both control groups.

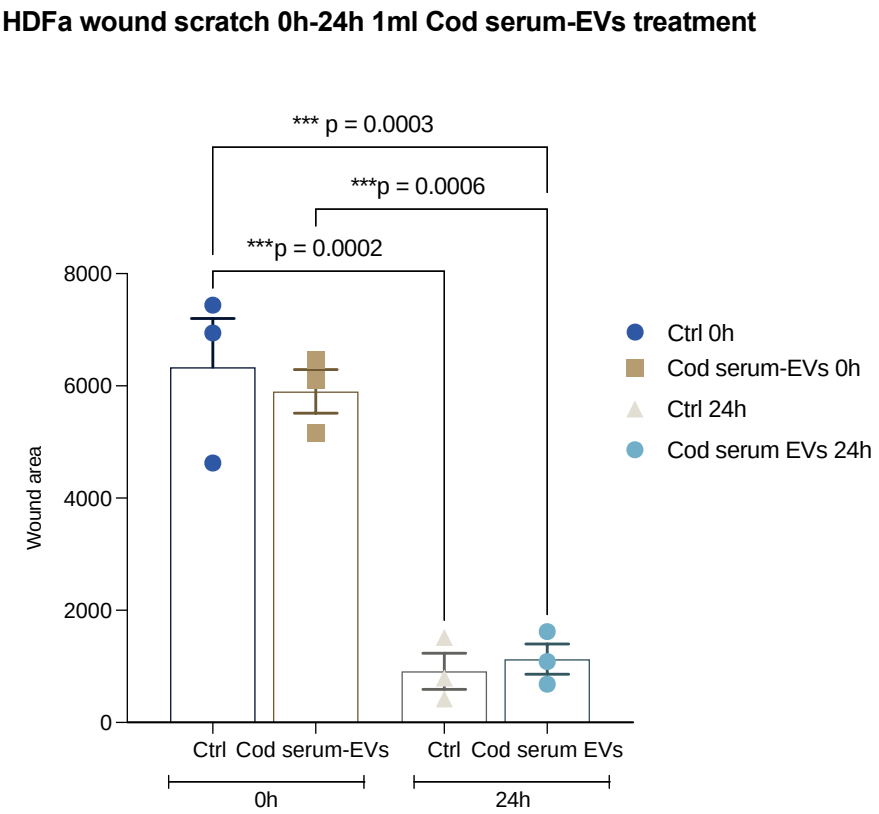

Figure 45. Assessment of cod serum derived EVs in-vitro efficiency in promoting wound healing closure in HDFa cells at 0h and 24h. Data are represented as mean ± standard deviation (SD) from three independent experiments. Statistical significance was determined using Ordinary one-way ANOVA, where *p < 0.05, **p < 0.01, ***p < 0.001.

5.3.4. HDFa immunostaining with Anti-Vimentin and Anti-FGF2 antibodies with cod serum and cod mucus derived-EVs treatment

Various growth factors impact the wound healing process, and modifications in their expression or receptor expression are noticeable during this phase. Within the fibroblast growth factors (FGF) family, FGF-1, FGF-2, and KFG are identified as crucial regulators of wound healing (Grazul-Bilska et al., 2003). FGF-2 plays a key role in stimulating collagen synthesis, epithelialisation, fibronectin and proteoglycan synthesis. Animal models have demonstrated the ability to induce cell migration, neovascularisation, and granulation tissue formation (Grazul-Bilska et al., 2003). FGF-2 also holds significant functions in organ systems' development, remodelling, and various disease states. Among its well-known activities is the regulation of the growth and function of vascular cells (Nugent and Iozzo, 2000). FGFs contribute to the proliferation and/or migration of essential cell types involved in the wound healing process, both *in vitro* and *in vivo*, such as fibroblasts and keratinocytes. Furthermore, the potential therapeutic use of FGF-2 as an anti-scarring agent in wound healing has been explored (Kashpur et al., 2013). Vimentin, belonging to the extensive family of Intermediate Filaments (IFs), has been identified as a highly adaptable cytoskeletal protein crucially engaged in various essential aspects of wound healing. Its significant role in epithelial-mesenchymal transition (EMT) during wound healing is well established (Coelho-Rato *et al*.,2023). Furthermore, vimentin actively contributes to diverse cellular processes, including growth, proliferation, migration, cell survival, and stress resilience. As a result, vimentin plays a participatory role in all phases of the wound healing process. (Coelho-Rato *et al*.,2023).

In this particular investigation, the impact of FGF-2 and Vimentin on human dermal fibroblast (HDFa) was evaluated using an *in vitro* wound scratch model. The aim was

to assess changes in their expression following treatment with serum- and mucus-derived EVs from Atlantic cod fish. HDFa cells were treated with 250µl cod serum and mucus-derived EVs, as described in section 5.2.6, and then stained with anti-FGF2 (Fig.46) and anti-Vimentin antibodies (Fig.47) to assess changes in protein expression in response to cod serum derived EVs treatment. This experiment lays the foundation for future experiments (not included in the current study due to shortage of cod serum and mucus available) in which both antibodies will be tested on HDFa cells, treated with cod-derived mucus and serum EVs at different time points to assess, expression of proteins of interests during wound closure. Preliminary findings of this part of the study are shown in Figure 46. ICC images were taken with EVOS FL Auto Imaging Systems (Thermo Fisher Scientific) with a x4 objective. Image settings, such as contrast, brightness and sharpness, were previously set on a control image and kept the same for consistency. Images were exported firstly into PowerPoint for picture formatting and then into ImageJ software (FIJI). Antibodies fluorescence was quantified by measuring the mean grey value of the picture, and measurements were imported to GraphPad for statistical analysis. The expression of FGF-2 protein revealed a slight increase, although not significant (p=0.3140), in fluorescent signal on HDFa cells treated with cod serum-EVs, compared to the control group, also stained for FGF-2. Similarly, HDFa cells stained for Anti-Vimentin showed a slight increase in protein expression, although no significant (p=01464), in cells treated with cod mucus derived-EVs, compared to the control group (Fig.47-B).

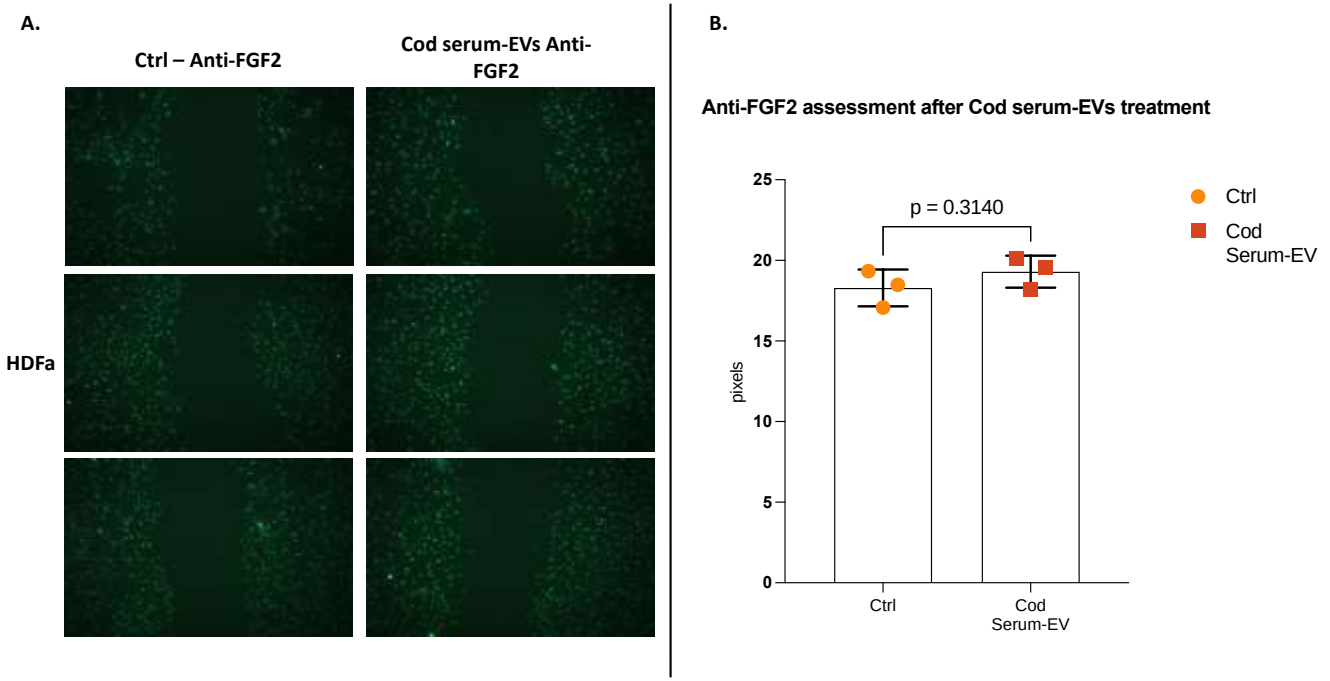

Figure 46. ICC Assessment of FGF-2 expression in HDFa treated with Cod serum-derived EVs. (A) Representative immunofluorescence images showing HDFa cells treated with 250µl ($6.2x10^7$ particles) cod serum EVs, probed for FGF-2 primary antibody(1/500) coupled with Goat Anti-Rabbit IgG H&L secondary antibody, labelled with Alexa Fluor 488 green dye (1/1000). (B) Histograms represent changes in fluorescence intensity of HDFa control and treated cells with cod EV derived from serum, stained for anti-FGF2. Data are represented as mean ± standard deviation (SD) from three independent experiments.

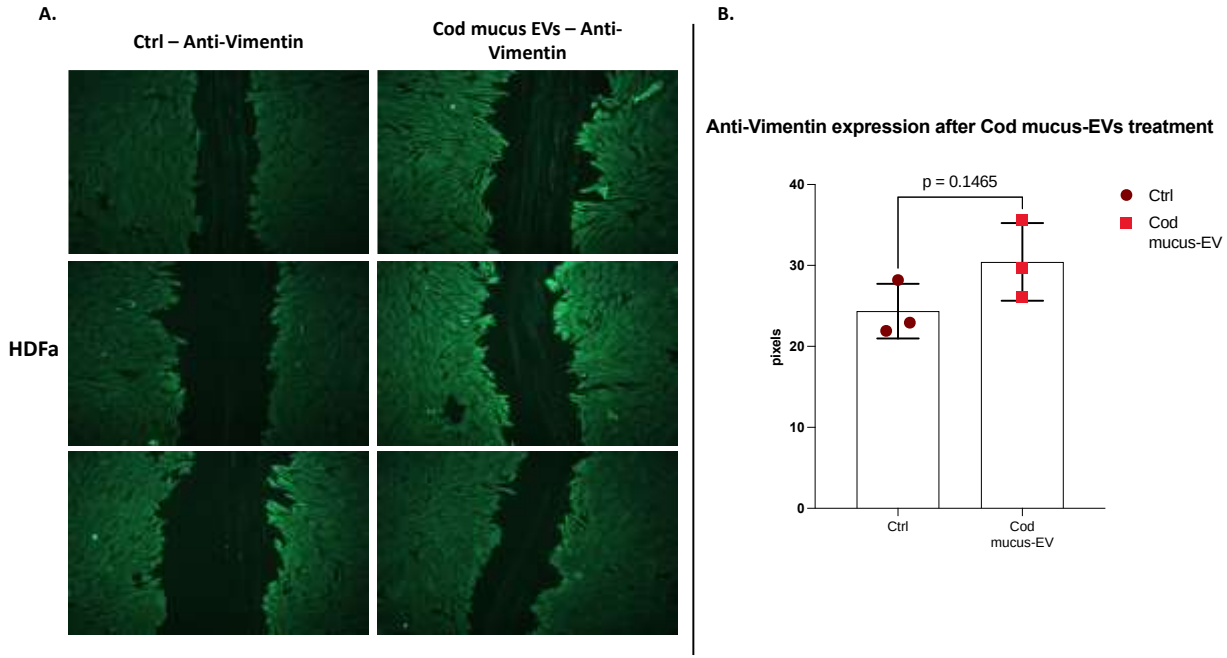

Figure 47. ICC assessment of Vimentin expression in HDFa treated with Cod mucus-derived EVs. (A) Representative immunofluorescence images showing HDFa cells treated with 250µl (3,88x10^9 particles/µl) cod serum EVs, probed for Vimentin antibody (1/500), coupled with Goat Anti-Rabbit IgG H&L secondary antibody, labelled with Alexa Fluor 488 green dye (1/1000). (B) Histograms represent changes in fluorescence intensity of HDFa control and treated cells with cod EV derived from mucus, stained for anti-vimentin. Data are represented as mean ± standard deviation (SD) from three independent experiments. Statistical significance was determined using the Unpaired t-test, where *p < 0.05, **p < 0.01, ***p < 0.001.

Further investigations involved the assessment of FGF-2 protein expression on HDFa cells, following incubation with 250µl of Atlantic cod serum derived-EVs ($3{,}88x10^9$ particles/µl) (Fig.48) and 250µl of cod mucus derived-EVs ($3{,}23x10^9$ particles/µl)(Fig-41). First, FGF-2 expression was assessed on HDFa cells treated with 250µl of cod serum derived-EVs at 8h and 24h, coupled with a secondary antibody labelled with Alexa Fluor 647 red dye. ICC images were taken at time points of 8h and 24h with EVOS FL Auto Imaging Systems (Thermo Fisher Scientific) with a x4 objective, and image settings, such as contrast, brightness and sharpness, were previously set on a control image and kept the same for consistency (Fig.48-A). Images were exported firstly into PowerPoint for picture formatting and then into ImageJ software (FIJI). Antibodies fluorescence was quantified by measuring the mean grey value of the picture, and measurements were imported to GraphPad for statistical analysis. Statistical analysis revealed an increased fluorescent signal of FGF-2 after 8h (p=0.2334) compared with the control group at 8h and 24h (p=0.5241), although not statistically significant. Moreover, a difference in expression was observed between the treatment group at 8h and 24h. An increase was observed in the fluorescence signal on HDFa cells probed for FGF-2 and treated with cod serum derived-EVs after 24h when compared with the treatment group at 8h (p=0.8600) (Fig.48-B); however, this change was not statistically significant.

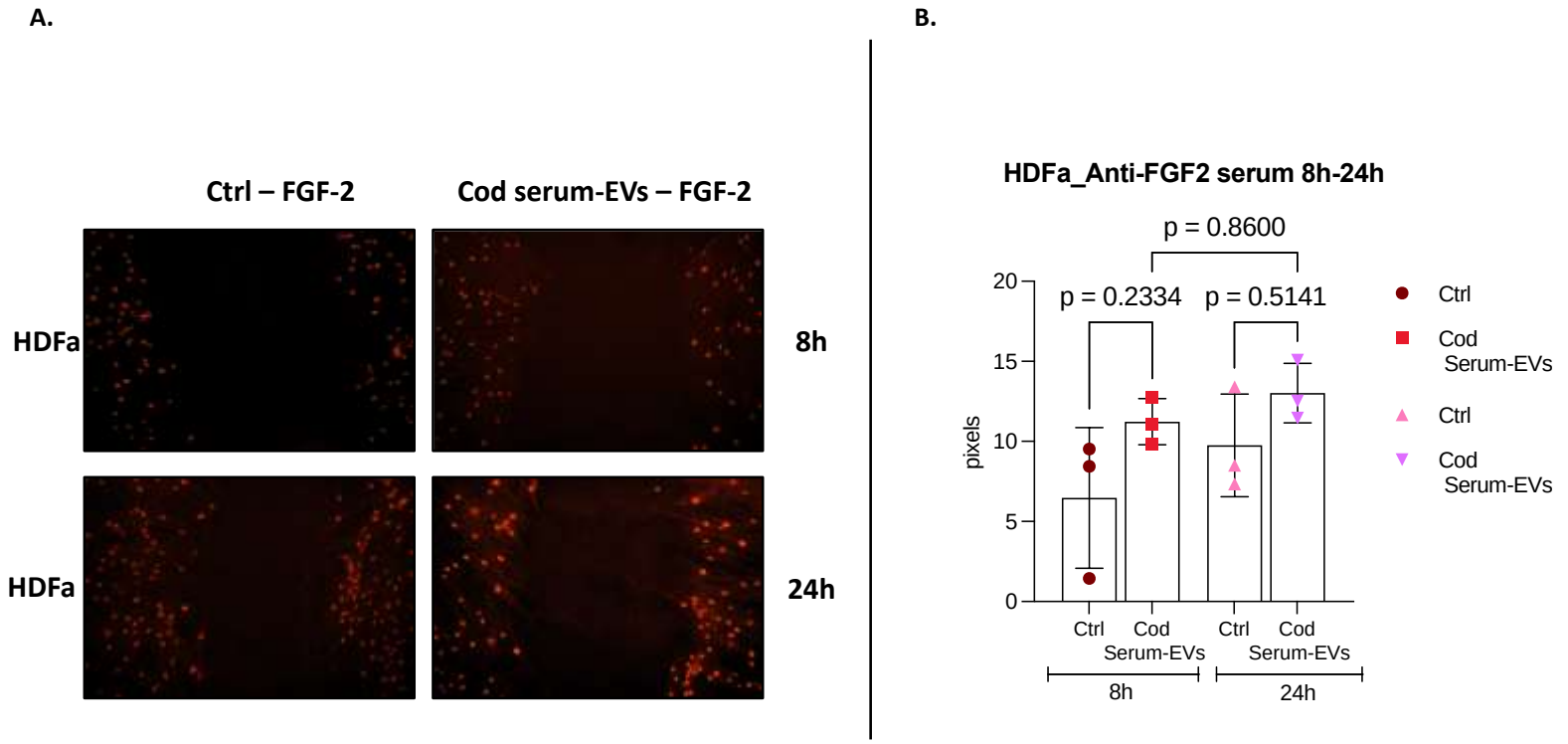

Figure 48. ICC assessment of FGF-2 expression in HDFa cells, treated with cod serum-derived EVs at 8h and 24. (A) Representative immunofluorescence images showing HDFa cells treated with 250µl (3,88x10^9 particles/µl) cod serum EVs, probed for FGF-2 antibody (1/500) at 8h and 24h, coupled with Goat Anti-Rabbit IgG H&L secondary antibody, labelled with Alexa Fluor 647 gred dye (1/1000). (B) Histograms representing changes in fluorescence intensity of HDFa control and cod serum derived-EVs, stained for anti-FGF2 antibody. Data are represented as mean ± standard deviation (SD) from three independent experiments. Statistical significance was determined using Unpaired t-test, where *p < 0.05, **p < 0.01, ***p < 0.001.

FGF-2 expression was also assessed on HDFa cells treated with 250µl of cod mucus derived-EVs ($3{,}23 \times 10^9$ particles/µl) at 8h and 24h (Fig.49-A). In this instance, the fluorescence signal of FGF-2 of cells treated with cod mucus-EVs did not change for 8h when compared to the control group (p=0.9998); the signal slightly increased over the period of 16h (p=0.9877) when compared with the treatment group at 8h, while a decrease in signal is observed when compared with the control group at 24h (p=0.4406) (Fig.49-B).

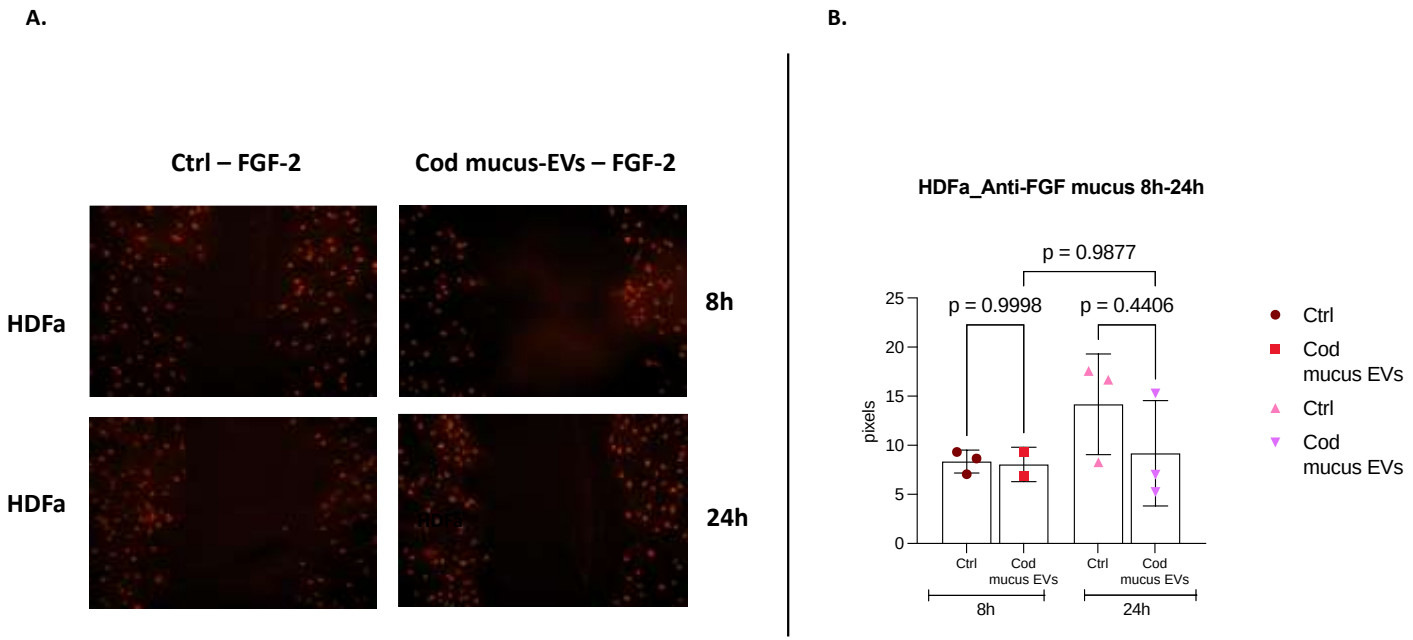

Figure 49. ICC assessment of FGF-2 expression in HDFa cells, treated with cod mucus-derived EVs. (A) Representative immunofluorescence images showing HDFa cells treated with 250µl (3,23x10^9 particles/µl) cod mucus derived-EVs, probed for FGF-2 antibody (1/500) at 8h and 24h, coupled with Goat Anti-Rabbit IgG H&L secondary antibody, labelled with Alexa Fluor 647 gred dye (1/1000). at 8h and 24h. (B) Histograms representing changes in fluorescence intensity of HDFa control and cod mucus derived-EVs at 8h and 24h stained for anti-FGF2 antibody. Data are represented as mean ± standard deviation (SD) from three independent experiments. Statistical significance was determined using Unpaired t-test, where *p < 0.05, **p < 0.01, ***p < 0.001.

These experiments will require further in-depth investigation in future studies to validate and gain a deeper understanding of these observations. This will shed light on the potential impact of cod serum and mucus-derived EVs on protein expression during wound closure. Addressing the limitations of the present study, such as the constrained availability of cod serum and mucus samples, will be essential to enhance the robustness and completeness of further experiments.

5.4 – Discussion

Wound healing and tissue regeneration constitute fundamental biological processes critical for maintaining tissue homeostasis and restoring structural integrity following injury or trauma. The pursuit of efficacious wound healing therapies has prompted the urge to explore novel therapeutic techniques that exploit the regenerative potential of biological agents. Amongst these, extracellular vesicles (EVs), released by all cells in the extracellular environment and delimited by a lipid bilayer (Welsh *et al*.,2024), have emerged as biological agents and mediators of intracellular communication (Chung *et al*.,2020). Through their selective cargo delivery of protein, lipids, and nucleic acids, EVs modulate various physiological processes such as angiogenesis, inflammation, cell proliferation and differentiation, thereby exerting profound effects on tissue repair mechanisms (Silva *et al.,*2017, Koga *et al.,*2022) EVs derived from multiple human cell sources, such as stem cells, and in particular mesenchymal stem cells (MSC), platelets, dendritic cells, macrophages, epithelial cells, and tumour cells, have been extensively studied regarding their function and therapeutic properties in the field of tissue regenerative Antich-Rosselló *et al.,*2022; Silva *et al.,*2017; Wang *et al*.,2020; Oh *et* al.,2020; Glady, Vandebroek and Yasui,2021). However, human cell lines require extensive optimisation of several parameters; to cultivate human cells successfully, various factors must be considered and improved, including the techniques used for isolating and storing cells, the formulation of the culture medium, and methods for expanding cells to

achieve the desired quantity and density. These, together with the process of cell senescence and yield limitations, represent a complication of the use of human EVs in clinical trials, as their volume availability is scarce, the costs are higher, and matters of safety and ethical compliance are extremely fundamental (Paganini *et al*.,2019). While specific applications may necessitate particular human cell lines, these restrictions have prompted the investigation of other potential sources for EVs. Studies have investigated the function and therapeutic role of EVs derived from different biological sources in the context of tissue regeneration, such as milk (Herwijnen *et al*.,2016; Zonneveld *et* al.,2021); EVs derived from bees royal jelly (Àlvarez *et al*.,2023); plants (Kim *et al*.,2021) and fruits, e.g., grapefruit (Savci *et al*.,2021), lemon (Urzí *et al*.,2023). Limited research has been conducted in this context, including on the therapeutical potential of EVs derived from marine organisms. Despite the therapeutic potential of EVs-derived products from different biological sources, no studies have been conducted on the therapeutical potential of EVs derived from the serum and mucus of Atlantic cod (*Gadus morhua*). The genome sequence of Atlantic cod has revealed a unique immune system, which makes this species distinctive from other teleosts (Star *et al.,*2011). Cod-derived products, such as Atlantic cod skin collagen (Furtado *et al*.,2022), cod liver oil (Kahzaeli *et al*.,2020) and skin xenografts from cod (Kirsner *et al*.,2020) have shown promising results in tissue regeneration; however, up to date, no studies have explored the regenerative potential of EVs derived from Atlantic cod serum and mucus in cellular wound healing models. On the other hand, EVs derived from cod serum and mucus were recently characterised, and their deiminated cargo was analysed, providing insights into their immune defences and tissue regeneration, but functional studies have not been carried out (Magnadóttir *et al*.,2019; Magnadóttir *et al*.,2020). Therefore, this study aimed, for the first time, to explore the cod serum- and mucus-derived EV proteomes to identify proteins contributing to the active

therapeutical function in wound healing and investigate the therapeutic potential of EVs derived from a comparative animal model with unusual immunological properties in an *in vitro* wound healing model. Atlantic cod serum and mucus EVs were isolated using previous standardised protocols in our lab (Kosgodage *et al.,* 2018; Lange *et al.,*2019; Criscitiello *et al.,* 2019; Criscitiello *et* al.,2020 a,b,c); Pamenter *et al.,* 2019; Phillips *et al.,* 2020; Bowden *et al.,* 2020(a), and according to the Minimal Information for Studies of Extracellular Vesicles 2023 (MISEV2023) guidelines (Welsh *et al.,*2024) involving sequential centrifugation and ultracentrifugation. EVs isolated from Atlantic cod serum and mucus were assessed by transmission electron microscopy (TEM), validating their size and morphology in both biofluids, further confirmed by Western Blot, which showed positive bands for the specific EVs markers CD63 and Flotillin-1. Cod serum and mucus-derived EVs' size distribution was determined using nanoparticle tracking analysis (NTA), which showed an EV poly-dispersed population in the 70 to 500nm size range in both Atlantic cod mucus and serum samples. Similar size distribution was observed in previous Atlantic cod serum and mucus-derived EVs studies conducted in our lab (Magnadóttire *et al.,*2019 and 2020) and further observed in studies investigating other marine species, as in the case of *Pinctada martensii* (Akoya pearl oyster) mucus (Wu *et al*.,2022) and olive flounder plasma (Jayathilaka et al., 2023). However, compared to the current study, the above investigations into the regenerative potential of marine species-derived EVs showed an EV yield greater (6.3×10^{10} particles/ml and 1.11×10^{12} particles/ml, respectively) than the EV concentration of Atlantic cod serum (1.55×10^{10} particles/ml) and mucus (1.29×10^{10} particles/ml) observed in this study. Although this might suggest a less regenerative efficacy of cod serum and mucus-derived EVs, it is important to highlight the biological differences between the species investigated in these studies and, most importantly, the different isolation approaches used in each investigation.

Proteomic analysis of Atlantic cod serum- and mucus-derived EVs by LC-MS/MS revealed eight protein hits commonly found in cod serum and mucus EVs. The common protein hits identified were fast skeletal muscle alpha-actin, beta-actin, serotransferrin, 60S ribosomal protein L22, ribosomal protein L15, galectin, elongation factor 1, alpha and profilin. These are discussed below, highlighting their contribution to the regenerative potential of cod serum and mucus-derived EVs.

Fast skeletal muscle alpha-actin is a protein found in the skeletal muscle tissues of vertebrates, including fish like Atlantic cod. It plays a crucial role in the structure and function of muscle cells. Alpha-actins are a family of actin proteins that contribute to the contractile apparatus of muscle cells, allowing for muscle contraction and movement. The "fast" designation indicates that this isoform is associated with fast-twitch muscle fibres, which are responsible for quick and powerful muscle contractions, such as those needed for rapid movements (Wang *et al*.,2022). In a previous study from our lab, this protein was identified as deiminated in Atlantic cod mucosa (Magnadóttir *et al.*,2018) and cod mucus-derived EVs, as well as in Atlantic cod serum-derived EVs (Magnadóttir *et al*.,2020).

Beta Actin participate in cytoskeletal rearrangement and has been linked to mucosal responses in Atlantic cod following infection (Rajan *et* al.,2013). In a previous study, beta-actin was found to be deiminated in Atlantic cod mucosa (Magnadóttir *et al*.,2018) and cod mucus-derive EVs (Magnadóttir *et al.,*2019a); moreover, deimination of this protein target has been linked to EVs release and biogenesis (Kholia *et al*., 2015). This study identified it in Atlantic cod serum- and mucus-derived EV proteomes.

Serotransferrin target protein has been previously identified in its deiminated form in Atlantic cod mucosa (Magnadóttir et al.,2018), while in this study, it is found to be present in both cod serum and mucus EVs. It acts as an antimicrobial agent and is at

the frontier in the innate immune mechanisms in fish (Stafford and Belosevic, 2003; Mohd-Padil et al.,2013). Transferrin is an essential element for the growth of microorganisms and is an acute-phase protein involved during the inflammatory response process of removing iron from deteriorated tissue (Bayne and Gerwick, 2011).

60S ribosomal protein L22 is a protein component of the ribosome's large subunit (60S) and plays a role in the assembly and function of the ribosome during translation. Deiminated 60S ribosomal protein L22 forms were previously found in Atlantic cod mucosa (Magnadóttir *et al*.,2018) and cod serum-derived EVs (Magnadóttir *et al*.,2020).

Galectin was found to be deiminated in whole Atlantic cod mucus (Magnadóttir *et al*.,2018), cod mucus-derived EVs, and it has different functions in embryogenesis and innate immunity. Other forms of galectins are present in teleost fish, two of which have been described in cod mucus (Rajan *et al*.,2013); they are involved in apoptosis and many pathological processes, including autoimmune, acute, and chronic inflammatory diseases (Sciacchitano *et al*.,2018). It regulates wound healing through inflammation, angiogenesis, re-epithelialization and fibrosis (McLeod *et al*.,2018).

Elongation factor 1 alpha has been previously identified in its deiminated form in Atlantic cod serum EVs (Magnadóttir *et al*.,2020), in Atlantic cod total mucosa (Magnadóttir *et al*.,2018), and cod mucus EVs (Magnadóttir *et al.,*2019). Elongation factor 1 alpha regulates cell growth, apoptosis, and the immune response. It has also been linked to the degranulation of neutrophils (Talapatra et al.,2002), and it mainly acts in cytoskeleton organisation and nuclear export of proteins (Khacho *et al*.,2008).

Profilin is a family of small multi-ligand proteins structurally conserved among eukaryotes. Profilin is pivotal as a key regulator of actin polymerisation, demonstrating

critical importance in cellular functioning. The actin cytoskeleton relies significantly on profilin, which is engaged in nearly all cellular processes, such as motility, endocytosis, metabolism, signal transduction, and gene transcription. By interacting with various actin-binding proteins that feature proline repeat domains, profilins facilitate membrane protrusion and contribute to cell motility (Davey and Moens,2020). Profilin protein was previously identified by our group in its deiminated form in both cod mucus (Magnadóttir *et al*.,2018) and serum (Magnadóttir *et al.*,2020).

Ribosomal protein L15 is a component of the 60S ribosome subunit, responsible for synthesising proteins in the cell. It has been linked to the mucosal response of cod during infection (Rajan et al.,2013), and in sea urchins, it is increased under immune challenge and injury. In this study, ribosomal protein L15 was found to be present in both whole serum- and mucus-derived EVs proteome and previously identified by our group in its deiminated form in both serum EVs (Magnadóttir *et al*.,2020) and total cod mucus (Magnadóttir *et al*.,2018) citrulline.

In addition, fifty other protein hits were identified in cod mucus-derived EV proteome, revealing differences in EV cargoes between cod serum and mucus and how this could impact the EV regenerative potential.

In the current study, the regenerative efficacy of cod serum-derived EVs was assessed *in vitro* on three different cellular models (mouse fibroblasts (3T3.L1), immortalised human keratinocytes (HaCat), and human dermal fibroblasts, adult (HDFa)), confirming, overall, the cod serum EVs' regenerative potential. However, differences between the three models were observed in the results. Wound healing assay carried out on mouse fibroblasts (3T3-L1) showed a significant reduction of the wound gap after 6h treatment with 1ml ($1.55x10^{10}$ particles/ml) cod serum-derived EVs and complete wound closure at 24h. Similarly, HDFa cells treated with 1ml cod serum-EVs showed a

significant reduction of the wound gap after 24h treatment. This was not the case for the scratch assay performed on HaCat cells treated with 1 ml cod serum-EVs, which showed a reduction of the wound gap after 24h, albeit not significant. On the other hand, HaCat cells were also treated with 2 ml of cod serum-EVs, and in this instance, the wound was significantly reduced after 24h. Furthermore, HDFa cells treated with cod serum-EVs were stained to assess the expression of Vimentin and FGF-2 growth factor, crucial regulators of wound healing (Grazul-Bilska et al.,2003; Coelho-Rato et al.,2023) showing increased fluorescence on treated cells and therefore suggesting a role for EVs in enhancing wound healing processes by upregulating their protein activity (Ren *et al*.,2019).

It is important to note that this pilot study is laying the basis for a more extensive investigation on the role of Atlantic cod serum and mucus-derived EVs, which will need to address the regenerative activity of EVs in wound healing in more depth. Therefore, further investigations using different doses on each cellular model will need to be conducted, and their migration upon treatment with cod serum-EVs will be assessed at different time points. Moreover, assessing the cell viability, cellular uptake of EVs, and in-vitro toxicity of EVs could give further insights into the biological activity of Atlantic cod-derived EVs. Due to limited resource availability, the present pilot study is limited in analysing the proteomic content of the cod biofluid-derived EVs, assessing *in vitro* efficacy on different wound healing cellular models, and assessing the expression of factors involved in wound healing processes by immunostaining. In conclusion, this pilot study successfully isolates and characterises the EVs isolated from Atlantic cod serum and mucus, showing *in vitro* potential regenerative activity in wound healing processes, further confirmed by the upregulated expression of two important regulators, Vimentin and FGF-2, during inflammation and proliferation phases of wound

healing. Therefore, EVs isolated from Atlantic cod biofluids, such as mucus and serum, may present innovative therapeutic options for chronic and acute wound management.

General Conclusion – Summary of the studies

The different chapters of this PhD thesis collectively contribute to a comprehensive understanding of extracellular vesicles (EVs) and their cargoes across various animal species, shedding light on their roles in physiological processes such as immune response, metabolic regulation, and tissue regeneration. In the first aim of the study, the profiling of EV signatures and their deiminated protein cargoes across different species, including mammals, jawless fish, and Echinodermata, demonstrates the conservation of histone deimination and the broad implications of protein deimination in epigenetic regulation and innate immune responses. The second aim investigates circulatory EVs under stress conditions, focusing on changes in brain citrulline signatures. The study reveals potential pathways linking brain citrullinome changes to circulatory EV profile alterations, providing insights into the adaptive mechanisms of species like the naked mole-rat under hypoxic conditions. The third aim explores the regenerative potential of EVs derived from cod mucus and serum in cellular wound healing models. This investigation highlights the therapeutic potential of EVs from a comparative animal model with unique immunological properties, showcasing their efficacy in enhancing wound healing processes. Overall, this thesis underscores the importance of EV-mediated cellular communication in orchestrating diverse biological processes across phylogeny. The findings contribute to the growing body of knowledge on EV-based biomarkers, immune modulation, and regenerative medicine, offering promising avenues for future research and therapeutic development. Through comparative analyses and functional studies, this work enhances our understanding of EVs' roles in health

and disease, paving the way for innovative therapeutic interventions in various bio-medical contexts.

Bibliography

Abels, E. R., & Breakefield, X. (2016). Introduction to Extracellular Vesicles: Biogenesis, RNA Cargo Selection, Content, Release, and Uptake. *Cellular and Molecular Neurobiology*, 36,301–312.

Akbari, A., Jabbari, N., Sharifi, R., Ahmadi, M., Vahhabi, A., Seyedzadeh, S. J., Nawaz, M., Szafert, S., Mahmoodi, M., Jabbari, E., Asghari, R., & Rezaie, J. (2020). Free and hydrogel encapsulated exosome-based therapies in regenerative medicine. *Life Sciences*, *249*, 117447.

Albanese, A., Daly, L. A., Mennerich, D., Kietzmann, T., & Sée, V. (2021). The Role of Hypoxia-Inducible Factor Post-Translational Modifications in Regulating Its Localisation, Stability, and Activity. *International Journal of Molecular Sciences*, *22*(1), Article 1. https://doi.org/10.3390/ijms22010268

Alghamdi, M., Alasmari, D., Assiri, A., Mattar, E., Aljaddawi, A. A., Alattas, S. G., & Redwan, E. M. (2019). An Overview of the Intrinsic Role of Citrullination in Autoimmune Disorders. *Journal of Immunology Research*, *2019*, 7592851.

Alqatawni, A., Sharma, A.L., Attilus, B., Tyagi, M. and Daniel, R., 2020. Shedding light on the role of extracellular vesicles in HIV infection and wound healing. *Viruses,* 12(6), p.584.

Álvarez, S., Contreras-Kallens, P., Aguayo, S., Ramírez, O., Vallejos, C., Ruiz, J., Carrasco-Gallardo, E., Troncoso-Vera, S., Morales, B., & Schuh, C. M. A. P. (2023). Royal jelly extracellular vesicles promote wound healing by modulating underlying cellular responses. *Molecular Therapy - Nucleic Acids*, *31*, 541–552.

Alves, A. L., Marques, A. L. P., Martins, E., Silva, T. H., & Reis, R. L. (2017). Cosmetic Potential of Marine Fish Skin Collagen. *Cosmetics*, *4*(4).

Amir, Y., Insler, M., Giller, A., Gutman, D. and Atzmon, G., 2020. Senescence and longevity of sea urchins. *Genes*, *11*(5), p.573.

Amir, Y., Insler, M., Giller, A., Gutman, D., & Atzmon, G. (2020). Senescence and Longevity of Sea Urchins. *Genes*, *11*(5), 573.

An, Q., van Bel, A. J., & Hückelhoven, R. (2007). 'Do Plant Cells Secrete Exosomes Derived from Multivesicular Bodies?' *Plant Signaling & Behavior*, *2*(1), 4–7.

Andaloussi, S. E., Mäger, I., Breakefield, X., & Wood, M. (2013). Extracellular vesicles: biology and emerging

Antich-Rosselló, M., Forteza-Genestra, M. A., Monjo, M., & Ramis, J. M. (2021). Platelet-Derived Extracellular Vesicles for Regenerative Medicine. *International Journal of Molecular Sciences*, *22*(16), 8580.

Aryani, A. and Denecke, B. (2016) 'Exosomes as a Nanodelivery System: a Key to the Future of Neuromedicine?', *Molecular Neurobiology*, 53(2), pp. 818–834.

Baßler, J. and Hurt, E., 2019. Eukaryotic ribosome assembly. *Annual review of biochemistry*, *88*, pp.281-306.

Barrientos, S., Stojadinovic, O., Golinko, M. S., Brem, H., & Tomic-Canic, M. (2008). Growth factors and cytokines in wound healing. Wound Repair and Regeneration, 16(5), 585-601.

Bayne, C. J., & Gerwick, L. (2001). The acute phase response and innate immunity of fish. *Developmental and Comparative Immunology*, *25*(8–9), 725–743.

Beato, M. and Sharma, P., 2020. Peptidyl arginine deiminase 2 (PADI2)-mediated arginine citrullination modulates transcription in cancer— I*nternational journal of molecular sciences*, *21*(4), p.1351.

Beer, K. B., & Wehman, A. M. (2017). Mechanisms and functions of extracellular vesicle release *in vivo*—What we can learn from flies and worms. *Cell Adhesion & Migration*, *11*(2), 135–150.

Bielecka, E., Scavenius, C., Kantyka, T., Jusko, M., Mizgalska, D., Szmigielski, B., Potempa, B., Enghild, J.J., Prossnitz, E.R., Blom, A.M. and Potempa, J., 2014. Peptidyl arginine deiminase from Porphyromonas gingivalis abolishes anaphylatoxin C5a activity. *Journal of Biological Chemistry*, 289(47), pp.32481-32487.

Bister, N., Pistono, C., Huremagic, B., Jolkkonen, J., Giugno, R., & Malm, T. (2020). Hypoxia and extracellular vesicles: A review on methods, vesicular cargo and functions. *Journal of Extracellular Vesicles*, *10*(1), e12002.

Boehm, T., Hirano, M., Holland, S.J., Das, S., Schorpp, M. and Cooper, M.D., 2018. Evolution of alternative adaptive immune systems in vertebrates. *Annual review of immunology*, *36*, pp.19-42.

Bowden, T. J., Kraev, I., & Lange, S. 2020. – b. 'Post-translational protein deimination signatures and extracellular vesicles (EVs) in the Atlantic horseshoe crab (*Limulus polyphemus*)'. *Developmental & Comparative Immunology*, *110*, 103714.

Bowden, T.J., Kraev, I. and Lange, S., 2020 - a. Extracellular vesicles and post-translational protein deimination signatures in mollusca—the blue mussel (Mytilus edulis), soft shell clam (Mya arenaria), Eastern Oyster (Crassostrea virginica) and Atlantic Jacknife Clam (Ensis leei). *Biology*, *9*(12), p.416.

Bowden, T.J., Kraev, I. and Lange, S., 2020. – c. 'Extracellular vesicles and post-translational protein deimination signatures in haemolymph of the American lobster (Homarus americanus)'. *Fish & shellfish immunology*, *106*, pp.79-102.

Boyiadzis, M., Whiteside, T.L., 2017. 'The emerging roles of tumor-derived exosomes in hematological malignancies.' *Leukemia* 31, 1259–1268.

Briaud, P., & Carroll, R. K. (2020). Extracellular Vesicle Biogenesis and Functions in Gram-Positive Bacteria. *Infection and Immunity*, *88*(12), 10.1128/iai.00433-20.

Buffenstein, R.; Amoroso, V.; Andziak, B.; Avdieiev, S.; Azpurua, J.; Barker, A.J.; Bennett, N.C.; Brieno-Enriquez, M.A.; Bronner, G.N.; Coen, C.; et al. The naked truth: A comprehensive clarification and classification of current 'myths' in naked mole-rat biology. *Biol. Rev. Camb. Philos. Soc.* 2022, 97, 115–140.

Bunggulawa, E. J., Wang, W., Yin, T., Wang, N., Durkan, C., Wang, Y., & Wang, G. (2018). Recent advancements in the use of exosomes as drug delivery systems. *Journal of Nanobiotechnology*, *16*(1), 81.

Burgener, S.S. and Schroder, K., 2020. Neutrophil extracellular traps in host defense. *Cold Spring Harbor perspectives in biology*, *12*(7), p.a037028.

Carr, B. and Wright, M., 2008. Nanoparticle tracking analysis. *Innovations in Pharmaceutical Technology*, *26*, pp.38-40.

Carregari, V. C., Rosa-Fernandes, L., Baldasso, P., Bydlowski, S. P., Marangoni, S., Larsen, M. R., & Palmisano, G. (2018). Snake Venom Extracellular vesicles (SVEVs) reveal wide molecular and functional proteome diversity. *Scientific Reports*, *8*(1), 12067.

Casado-Díaz, A., Quesada-Gómez, J.M. and Dorado, G., 2020. Extracellular vesicles derived from mesenchymal stem cells (MSC) in regenerative medicine: applications in skin wound healing. *Frontiers in bioengineering and biotechnology*, 8.

Chaltel-Lima, L., Domínguez, F., Domínguez-Ramírez, L., & Cortes-Hernandez, P. (2023). The Role of the Estrogen-Related Receptor Alpha (ERRa) in Hypoxia and Its Implications for Cancer Metabolism. *International Journal of Molecular Sciences*, *24*(9), 7983.

Chang, L., Ni, J., Zhu, Y., Pang, B., Graham, P., Zhang, H., & Li, Y. (2019). 'Liquid biopsy in ovarian cancer: Recent advances in circulating extracellular vesicle detection for early diagnosis and monitoring progression.' *Theranostics*, *9*(14), 4130–4140.

Chaput, N., Schartz, N.E.C., Andre, F., Zitvogel, L., 2003. Exosomes for immunotherapy of cancer. *Adv Exp Med Biol* 532, 215–221.

Chargaff, E. and West, R., 1946. The biological significance of the thromboplastic protein of blood. *J Biol Chem*, 166(1), pp.189-197.

Chen, J., Laramore, C. and Shifman, M.I., 2016. Differential expression of HDACs and KATs in high and low regeneration capacity neurons during spinal cord regeneration. *Experimental Neurology*, *280*, pp.50-59.

Chen, L., Wu, F., Yuan, S. and Feng, B., 2016. Identification and characteristic of three members of the C1q/TNF-related proteins (CTRPs) superfamily in Eudontomyzon morii. *Fish & shellfish immunology*, *59*, pp.233-240.

Cheng, F., Shen, Y., Mohanasundaram, P., Lindström, M., Ivaska, J., Ny, T., & Eriksson, J. E. (2016). 'Vimentin coordinates fibroblast proliferation and keratinocyte

differentiation in wound healing via TGF-β–Slug signalling.' *Proceedings of the National Academy of Sciences*, *113*(30).

Cheng, F., Shen, Y., Mohanasundaram, P., Lindström, M., Ivaska, J., Ny, T., & Eriksson, J. E. (2016). Vimentin coordinates fibroblast proliferation and keratinocyte differentiation in wound healing via TGF-β–Slug signalling. *Proceedings of the National Academy of Sciences*, *113*(30).

Cheng, H., Sebaa, R., Malholtra, N., Lacoste, B., Hankouri, Z. E., Kirby, A., Bennett, N. C., Jaarsveld, B. van, Hart, D. W., Tattersall, G. J., Harper, M.-E., & Pamenter, M. E. (2021). 'Naked mole-rat brown fat thermogenesis is diminished during hypoxia through a rapid decrease in UCP1.' *Nature Communications*, *12*.

Chiaramonte, M. and Russo, R., 2015. The echinoderm innate humoral immune response. *Italian Journal of Zoology*, *82*(3), pp.300-308.

Cho, J.H., Sung, B.H. and Kim, S.C., 2009. Buforins: histone H2A-derived antimicrobial peptides from toad stomach. *Biochimica et Biophysica Acta (BBA)-Biomembranes*, *1788*(8), pp.1564-1569.

Chung, I.-M., Rajakumar, G., Venkidasamy, B., Subramanian, U., Thiruvengadam, M., (2020) 'Exosomes: Current use and future applications', *Clinica Chimica Acta*, 500, pp. 226–232.

Ciferri, M.C., Quarto, R. and Tasso, R. (2021) 'Extracellular Vesicles as Biomarkers and Therapeutic Tools: From Pre-Clinical to Clinical Applications', *Biology*, 10(5), p. 359.

Clancy, J.W., Schmidtmann, M. and D'Souza-Schorey, C., The Ins and Outs of Microvesicles. *FASEB BioAdvances*.

Coates, C. J., Kraev, I., Rowley, A. F., & Lange, S. (n.d.). Extracellular vesicle signatures and protein citrullination are modified in shore crabs (Carcinus maenas) infected with Hematodinium sp. *Virulence*, *14*(1), 2180932.

Colino, J., Snapper, C.M., 2007. 'Dendritic cell-derived exosomes express a Streptococcus pneumoniae capsular polysaccharide type 14 cross-reactive antigen that

induces protective immunoglobulin responses against pneumococcal infection in mice.' *Infect Immun* 75, 220–230.

Couch, Y., Buzàs, E.I., DivVizio, D., Gho, Y.S., Harrison, P., Hill, A.F., Löt-vall, J., Raposo, G., Stahl, P. D., Théry, C., Witwer, K. W., & Carter, D. R. F. (2021). A brief history of nearly EV-erything – The rise and rise of extracellular vesicles. *Journal of Extracellular Vesicles*, 10, e12144.

Crawford, N., 1971. The presence of contractile proteins in platelet microparticles isolated from human and animal platelet-free plasma. *British journal of haematology,* 21(1), pp.53-69.

Criscitiello, M.F., Kraev, I. and Lange, S., 2020 - b. Post-translational protein deimination signatures in serum and serum-extracellular vesicles of Bos taurus reveal immune, anti-pathogenic, anti-viral, metabolic and cancer-related pathways for deimination. *International journal of molecular sciences*, *21*(8), p.2861.

Criscitiello, M.F., Kraev, I. and Lange, S., 2020 – a. Deiminated proteins in extracellular vesicles and serum of llama (Lama glama)—Novel insights into camelid immunity. *Molecular immunology*, *117*, pp.37-53.

Criscitiello, M.F., Kraev, I., Petersen, L.H. and Lange, S., 2020 – c. Deimination protein profiles in Alligator mississippiensis reveal plasma and extracellular vesicle-specific signatures relating to immunity, metabolic function, and gene regulation. *Frontiers in Immunology*, *11*, p.651.

Criscitiello, Michael F., Igor Kraev, and Sigrun Lange. "Deiminated proteins in extracellular vesicles and plasma of nurse shark (Ginglymostoma cirratum)-novel insights into shark immunity." *Fish & shellfish immunology* 92 (2019): 249-255.

Cronin, M.A., MacNeil, M.D. and Patton, J.C., 2006. Mitochondrial DNA and microsatellite DNA variation in domestic reindeer (Rangifer tarandus tarandus) and relationships with wild caribou (Rangifer tarandus granti, Rangifer tarandus groenlandicus, and Rangifer tarandus caribou). *Journal of Heredity*, *97*(5), pp.525-530.

Cummings, T.F., Gori, K., Sanchez-Pulido, L., Gavriilidis, G., Moi, D., Wilson, A.R., Murchison, E., Dessimoz, C., Ponting, C.P. and Christophorou, M.A., 2022. Citrullination

was introduced into animals by horizontal gene transfer from cyanobacteria. *Molecular biology and evolution*, *39*(2), p.msab317.

D'Alessio S, Cheng H, Eaton L, Kraev I, Pamenter ME, Lange S. Acute Hypoxia Alters Extracellular Vesicles Signatures and the Brain Citrullinome of Naked Mole-Rats (*Heterocephalus glaber*).2022. *International Journal of Molecular Sciences* 2022:23(9):4683

D'Alessio, S., Buckley, K.M., Kraev, I., Hayes, P. and Lange, S., 2021. Extracellular Vesicle Signatures and Post-Translational Protein Deimination in Purple Sea Urchin (Strongylocentrotus purpuratus) Coelomic Fluid—Novel Insights into Echinodermata Biology. *Biology*, *10*(9), p.866. (b)

D'alessio, S., Thorgeirsdóttir, S., Kraev, I., Skírnisson, K. and Lange, S., 2021. Post-translational protein deimination signatures in plasma and plasma evs of reindeer (Rangifer tarandus). *Biology*, *10*(3), p.222. (a)

Damgaard, D., Senolt, L., Nielsen, M.F., Pruijn, G.J. and Nielsen, C.H., 2014. Demonstration of extracellular peptidylarginine deiminase (PAD) activity in synovial fluid of patients with rheumatoid arthritis using a novel assay for citrullination of fibrinogen. *Arthritis research & therapy*, *16*(6), pp.1-7.

Darrah, E., Rosen, A., Giles, J.T. and Andrade, F., 2012. Peptidylarginine deiminase 2, 3 and 4 have distinct specificities against cellular substrates: novel insights into autoantigen selection in rheumatoid arthritis. *Annals of the rheumatic diseases*, *71*(1), pp.92-98.

Davey, R. J., & Moens, P. D. (2020). Profilin: Many facets of a small protein. *Biophysical Reviews*, *12*(4), 827–849.

De Jong, O.G., Van Balkom, B.W., Schiffelers, R.M., Bouten, C.V. and Verhaar, M.C., 2014. Extracellular vesicles: potential roles in regenerative medicine. *Frontiers in immunology*, 5, p.608.

De Zoysa, M., Nikapitiya, C., Whang, I., Lee, J.S. and Lee, J., 2009. Abhisin: a potential antimicrobial peptide derived from histone H2A of disk abalone (Haliotis discus discus). *Fish & shellfish immunology*, *27*(5), pp.639-646.

Deatherage, B.L. and Cookson, B.T., 2012. Membrane vesicle release in bacteria, eukaryotes, and archaea: a conserved yet underappreciated aspect of microbial life. *Infection and immunity*, 80(6), pp.1948-1957.

Diller, R. B., & Tabor, A. J. (2022). The Role of the Extracellular Matrix (ECM) in Wound Healing: A Review. *Biomimetics*, *7*(3).

Dodds, A.W. and Matsushita, M., 2007. The phylogeny of the complement system and the origins of the classical pathway. *Immunobiology*, *212*(4-5), pp.233-243.

Dorrington, T., Villamil, L. and Gómez-chiarri, M., 2011. Upregulation in response to infection and antibacterial activity of oyster histone H4. *Fish & shellfish immunology*, *30*(1), pp.94-101.

Dort J, Sirois A, Leblanc N, Côté CH, Jacques H. Beneficial effects of cod protein on skeletal muscle repair following injury. *Appl Physiol Nutr Metab*. 2012;37(3):489-498. doi:10.1139/h2012-021

Doyle, L. M., & Wang, M. Z. (2019). Overview of Extracellular Vesicles, Their Origin, Composition, Purpose, and Methods for Exosome Isolation and Analysis. *Cells*, 8.

El-Sayed, A.S., Shindia, A.A., AbouZaid, A.A., Yassin, A.M., Ali, G.S. and Sitohy, M.Z., 2019. Biochemical characterization of peptidylarginine deiminase-like orthologs from thermotolerant Emericella dentata and Aspergillus nidulans. *Enzyme and microbial technology*, *124*, pp.41-53.

Ellis, S., Lin, E. J., & Tartar, D. (2018). Immunology of Wound Healing. *Current Dermatology Reports*, *7*(4), 350–358.
Enoch, S., & Leaper, D. J. (2005). *Basic science of wound healing*.

Eming, S. A., Krieg, T., & Davidson, J. M. (2007). Inflammation in wound repair: molecular and cellular mechanisms. Journal of Investigative Dermatology, 127(3), 514-525.

Esposito, G., Vitale, A.M., Leijten, F.P.J., Strik, A.M., Koonen-Reemst, A.M.C.B., Yurttas, P., Robben, T.J.A.A., Coonrod, S. and Gossen, J.A., 2007. Peptidylarginine deiminase (PAD) 6 is essential for oocyte cytoskeletal sheet formation and female fertility. *Molecular and cellular endocrinology*, *273*(1-2), pp.25-31.

Fernandes, J.M., Kemp, G.D., Molle, M.G. and Smith, V.J., 2002. Anti-microbial properties of histone H2A from skin secretions of rainbow trout, Oncorhynchus mykiss. *Biochemical Journal*, *368*(2), pp.611-620.

Ferreira, A.D.F. and Gomes, D.A., 2019. Stem cell extracellular vesicles in skin repair. *Bioengineering*, 6(1), p.4.

Fiakos, G., Kuang, Z., & Lo, E. (2020). Improved skin regeneration with acellular fish skin grafts. *Engineered Regeneration*, *1*, 95–101.

Fuhrmann, J. and Thompson, P.R., 2016. Protein arginine methylation and citrullination in epigenetic regulation. *ACS chemical biology*, *11*(3), pp.654-668.

Furtado, M., Chen, L., Chen, Z., Chen, A., & Cui, W. (2022). Development of fish collagen in tissue regeneration and drug delivery. *Engineered Regeneration*, *3*(3), 217–231.

Gavinho B, Sabatke B, Feijoli V, Rossi IV, da Silva JM, Evans-Osses I, Palmisano G, Lange S, Ramirez MI (2020). Peptidylarginine Deiminase inhibition abolishes the production of large extracellular vesicles from Giardia intestinalis, affecting host-pathogen interactions by hindering adhesion to host cells. *Front. Cell. Infect. Microbiol.* doi: 10.3389/fcimb.2020.00417 (in press).

Gallucci, R. M., Simeonova, P. P., Matheson, J. M., Kommineni, C., Guriel, J. L., Sugawara, T., & Luster, M. I. (2000). Impaired cutaneous wound healing in interleukin-6–deficient and immunosuppressed mice. The FASEB Journal, 14(15), 2525-2531.

Gerst, J.E., 2018. Pimp my ribosome: ribosomal protein paralogs specify translational control. *Trends in Genetics*, *34*(11), pp.832-845.

Grada, A., Mervis, J. and Falanga, V., 2018. Research techniques made simple: animal models of wound healing. *Journal of Investigative Dermatology*, 138(10), pp.2095-2105.

Green, G.R., Collas, P., Burrell, A. and Poccia, D.L., 1995, August. Histone phosphorylation during sea urchin development. In *seminars in CELL BIOLOGY* (Vol. 6, No. 4, pp. 219-227). Academic Press.

Gudmundsdóttir A, Hilmarsson H, Stefansson B. Potential use of Atlantic cod trypsin in biomedicine. *Biomed Res Int*. 2013;2013:749078.

Guerrin, M., Ishigami, A., Méchin, M.C., Nachat, R., Valmary, S., Sebbag, M., Simon, M., Senshu, T. and Serre, G., 2003. cDNA cloning, gene organization and expression analysis of human peptidylarginine deiminase type I. *Biochemical Journal*, *370*(1), pp.167-174.

Guo, Q., Bedford, M.T. and Fast, W., 2011. Discovery of peptidylarginine deiminase-4 substrates by protein array: antagonistic citrullination and methylation of human ribosomal protein S2. *Molecular BioSystems*, *7*(7), pp.2286-2295.

Gurunathan, S., Kang, M.-H., Qasim, M., Khan, K., & Kim, J.-H. (2021). Biogenesis, Membrane Trafficking, Functions, and Next Generation Nanotherapeutics Medicine of Extracellular Vesicles. *International Journal of Nanomedicine*, *Volume 16*, 3357–3383.

Gurung, S., Perocheau, D., Touramanidou, L. and Baruteau, J., 2021. The exosome journey: From biogenesis to uptake and intracellular signalling. *Cell Communication and Signaling*, *19*(1), pp.1-19.

György, B., Szabó, T.G., Pásztói, M., Pál, Z., Misják, P., Aradi, B., László, V., Pállinger, E., Pap, E., Kittel, A. and Nagy, G., 2011. Membrane vesicles, current state-of-the-art: emerging role of extracellular vesicles. *Cellular and molecular life sciences*, 68(16), pp.2667-2688.

Ha, D., Yang, N. and Nadithe, V. (2016) 'Exosomes as therapeutic drug carriers and delivery vehicles across biological membranes: current perspectives and future challenges', *Acta Pharmaceutica Sinica. B*, 6(4), pp. 287–296.

Harding, C., Heuser, J., & Stahl, P. (1983). 'Receptor-mediated endocytosis of transferrin and recycling of the transferrin receptor in rat reticulocytes.' *The Journal of cell biology*, *97*(2), 329–339.

Henderson, B. and Martin, A.C., 2014. Protein moonlighting: a new factor in biology and medicine. *Biochemical society transactions*, *42*(6), pp.1671-1678.

Henderson, B., & Martin, A. C. R. (2014). Protein moonlighting: A new factor in biology and medicine. *Biochemical Society Transactions*, *42*(6), 1671–1678.

Hessvik, N. P., & Llorente, A. (2017). Current knowledge on exosome biogenesis and release. *Cellular and Molecular Life Sciences*, *75*, 193–208. https://doi.org/10.1007/s00018-017-2595-9.

Hibino, T., Loza-Coll, M., Messier, C., Majeske, A.J., Cohen, A.H., Terwilliger, D.P., Buckley, K.M., Brockton, V., Nair, S.V., Berney, K. and Fugmann, S.D., 2006. The immune gene repertoire encoded in the purple sea urchin genome. *Developmental biology*, *300*(1), pp.349-365.

Inal, J. M., Hristova, M., & Lange, S. (2022). A Pilot Study on Peptidylarginine Deiminases and Protein Deimination in Animal Cancers across Vertebrate Species. *International Journal of Molecular Sciences*, *23*(15), Article 15.

Jadli, A.S., Ballasy, N., Edalat, P. and Patel, V.B., 2020. Inside (sight) of tiny communicator: exosome biogenesis, secretion, and uptake. *Molecular and cellular biochemistry*, 467(1), pp.77-94.

Jasinskiene, N., Jasinskas, A. and Langmore, J.P., 1995. Embryonic regulation of histone ubiquitination the sea urchin. *Developmental genetics*, *16*(3), pp.278-290.

Jayathilaka, E. H. T. T., Edirisinghe, S. L., Lee, J., Nikapitiya, C., & Mahanama De Zoysa. (2022). Isolation and characterization of plasma-derived exosomes from olive flounder (Paralichthys olivaceus) and their wound healing and regeneration activities. *Fish & Shellfish Immunology*, *128*, 196–205.

Jayathilaka, E. H. T. T., Edirisinghe, S. L., Oh, C., Nikapitiya, C., & De Zoysa, M. (2023). Exosomes from bacteria (Streptococcus parauberis) challenged olive flounder (Paralichthys olivaceus): Isolation, molecular characterization, wound healing, and regeneration activities. *Fish & Shellfish Immunology*, *137*, 108777.

Jeffery, C. J. (2016). Protein species and moonlighting proteins: Very small changes in a protein's covalent structure can change its biochemical function. *Journal of Proteomics*, *134*, 19–24.

Jeffery, C.J., 2018. Protein moonlighting: what is it, and why is it important?. *Philosophical Transactions of the Royal Society B: Biological Sciences*, *373*(1738), p.20160523.

Jin, Y., Ma, L., Zhang, W., Yang, W., Feng, Q., & Wang, H. (2022). Extracellular signals regulate the biogenesis of extracellular vesicles. *Biological Research*, *55*, 35.

Johnstone, R.M., Bianchini, A. and Teng, K., 1989. Reticulocyte maturation and exosome release: transferrin receptor containing exosomes shows multiple plasma membrane functions. *Blood*, 74(5), pp.1844-1851.

Johnstone, R.M., Mathew, A., Mason, A.B. and Teng, K., 1991. Exosome formation during maturation of mammalian and avian reticulocytes: evidence that exosome release is a major route for externalization of obsolete membrane proteins. *Journal of cellular physiology,* 147(1), pp.27-36.

Kadota, T., Yoshioka, Y., Fujita, Y., Kuwano, K., & Ochiya, T. (2017). 'Extracellular vesicles in lung cancer—From bench to bedside', *Seminars in Cell & Developmental Biology*, 67, pp. 39–47.

Kell, D. B., & Pretorius, E. (2022). The potential role of ischaemia–reperfusion injury in chronic, relapsing diseases such as rheumatoid arthritis, Long COVID, and ME/CFS: Evidence, mechanisms, and therapeutic implications. *Biochemical Journal*, *479*(16), 1653–1708.

Keshtkar, S., Azarpira, N. and Ghahremani, M.H., 2018. Mesenchymal stem cell-derived extracellular vesicles: novel frontiers in regenerative medicine. *Stem cell research & therapy*, 9(1), pp.1-9.

Khacho, M., Mekhail, K., Pilon-Larose, K., Pause, A., Côté, J. and Lee, S., 2008. eEF1A is a novel component of the mammalian nuclear protein export machinery. *Molecular Biology of the Cell*, *19*(12), pp.5296-5308.

Khazaeli, P., Alaei, M., Khaksarihadad, M. and Ranjbar, M., 2020. Preparation of PLA/chitosan nanoscaffolds containing cod liver oil and experimental diabetic wound healing in male rats study. *Journal of Nanobiotechnology*, *18*(1), pp.1-9.

Kholia, S., Jorfi, S., Thompson, P.R., Causey, C.P., Nicholas, A.P., Inal, J.M. and Lange, S., 2015. A novel role for peptidylarginine deiminases in microvesicle release reveals therapeutic potential of PAD inhibition in sensitizing prostate cancer cells to chemotherapy. *Journal of extracellular vesicles*, *4*(1), p.26192.

Kietzmann M, Braun M. Effekte der Zinkoxid/Lebertran-Salbe Zincojecol auf das Wundheilungsgeschehen im Tiermodell [Effects of the zinc oxide and cod liver oil containing ointment Zincojecol in an animal model of wound healing]. *Dtsch Tierarztl Wochenschr*. 2006;113(9):331-334.

Kim, M. K., Choi, Y. C., Cho, S. H., Choi, J. S., & Cho, Y. W. (2021). The Antioxidant Effect of Small Extracellular Vesicles Derived from Aloe vera Peels for Wound Healing. *Tissue Engineering and Regenerative Medicine*, *18*(4), 561–571.

Kirby, A.M.; Fairman, G.D.; Pamenter, M.E. Atypical behavioural, metabolic and thermoregulatory responses to hypoxia in the naked mole rat (Heterocephalus glaber). *J. Zool.* 2018, 305, 106–115.

Kirsner RS, Margolis DJ, Baldursson BT, et al. Fish skin grafts compared to human amnion/chorion membrane allografts: A double-blind, prospective, randomized clinical trial of acute wound healing. *Wound Repair Regen*. 2020;28(1):75-80.

Kirsner, R.S., Margolis, D.J., Baldursson, B.T., Petursdottir, K., Davidsson, O.B., Weir, D. and Lantis, J.C., 2020. Fish skin grafts compared to human amnion/chorion membrane allografts: A double-blind, prospective, randomized clinical trial of acute wound healing. *Wound Repair and Regeneration*, 28(1), pp.75-80.

Koike, Y., Yozaki, M., Utani, A., & Murota, H. (2020). Fibroblast growth factor 2 accelerates the epithelial–mesenchymal transition in keratinocytes during wound healing process. *Scientific Reports*, *10*(1), 18545.

Kosgodage, U. S., Uysal-Onganer, P., MacLatchy, A., Kraev, I., Chatterton, N. P., Nicholas, A. P., Inal, J. M., & Lange, S. 2018. Peptidylarginine Deiminases Post-Translationally Deiminate Prohibitin and Modulate Extracellular Vesicle Release and MicroRNAs in Glioblastoma Multiforme. *International Journal of Molecular Sciences*, *20*(1).

Kosgodage, U.S., Matewele, P., Mastroianni, G., Kraev, I., Brotherton, D., Awamaria, B., Nicholas, A.P., Lange, S. and Inal, J.M., 2019. Peptidylarginine deiminase inhibitors reduce bacterial membrane vesicle release and sensitize bacteria to antibiotic treatment. *Frontiers in cellular and infection microbiology*, *9*, p.227.

Kotronoulas, A., de Lomana, A.L.G., Karvelsson, S.T., Heijink, M., Stone II, R., Giera, M. and Rolfsson, O., 2021. Lipid mediator profiles of burn wound healing: Acellular cod fish skin grafts promote the formation of EPA and DHA derived lipid mediators following seven days of treatment. *Prostaglandins, Leukotrienes and Essential Fatty Acids*, *175*, p.102358.

Kotronoulas, A., Jónasdóttir, H.S., Sigurðardóttir, R.S., Halldórsson, S., Haraldsson, G.G. and Rolfsson, Ó., 2020. Wound healing grafts: Omega-3 fatty acid lipid content differentiates the lipid profiles of acellular Atlantic cod skin from traditional dermal substitutes. *Journal of Tissue Engineering and Regenerative Medicine*, *14*(3), pp.441-451.

Kozlowski, H.N., Lai, E.T., Havugimana, P.C., White, C., Emili, A., Sakac, D., Binnington, B., Neschadim, A., McCarthy, S.D. and Branch, D.R., 2016. Extracellular histones identified in crocodile blood inhibit in-vitro HIV-1 infection. *Aids*, *30*(13), pp.2043-2052.

Kristmundsson, Á., Erlingsdóttir, Á. and Lange, S., 2021. Peptidylarginine Deiminase (PAD) and Post-Translational Protein Deimination—Novel Insights into Alveolata Metabolism, Epigenetic Regulation and Host–Pathogen Interactions. *Biology*, *10*(3), p.177.

Kristmundsson, Á., Erlingsdóttir, Á., & Lange, S. (2021). Peptidylarginine Deiminase (PAD) and Post-Translational Protein Deimination—Novel Insights into Alveolata Metabolism, Epigenetic Regulation and Host–Pathogen Interactions. *Biology*, *10*(3), Article 3.

Kuraku, S. and Kuratani, S., 2006. Time scale for cyclostome evolution inferred with a phylogenetic diagnosis of hagfish and lamprey cDNA sequences. *Zoological science*, *23*(12), pp.1053-1064.

Lamichhane, T.N., Sokic, S., Schardt, J.S., Raiker, R.S., Lin, J.W. and Jay, S.M., 2015. Emerging roles for extracellular vesicles in tissue engineering and regenerative medicine. Tissue Engineering Part B: Reviews, 21(1), pp.45-54.

Lange, S., 2021. Peptidylarginine deiminases and extracellular vesicles: Prospective drug targets and biomarkers in central nervous system diseases and repair. *Neural Regeneration Research*, *16*(5), p.934.

Lange, S., Bambir, S., Dodds, A.W. and Magnadóttir, B., 2004. The ontogeny of complement component C3 in Atlantic cod (Gadus morhua L.)—an immunohistochemical study. *Fish & Shellfish Immunology*, *16*(3), pp.359-367.

Lange, S., Dodds, A.W., Gudmundsdóttir, S., Bambir, S.H. and Magnadóttir, B., 2005. The ontogenic transcription of complement component C3 and Apolipoprotein AI tRNA in Atlantic cod (Gadus morhua L.)—a role in development and homeostasis?. *Developmental & Comparative Immunology*, *29*(12), pp.1065-1077.

Lange, S., Gallagher, M., Kholia, S., Kosgodage, U.S., Hristova, M., Hardy, J. and Inal, J.M., 2017. Peptidylarginine deiminases—roles in cancer and neurodegeneration and possible avenues for therapeutic intervention via modulation of exosome and microvesicle (EMV) release?. *International journal of molecular sciences*, *18*(6), p.1196.

Lange, S., Gögel, S., Leung, K.Y., Vernay, B., Nicholas, A.P., Causey, C.P., Thompson, P.R., Greene, N.D. and Ferretti, P., 2011. Protein deiminases: new players in the developmentally regulated loss of neural regenerative ability. *Developmental biology*, *355*(2), pp.205-214.

Lee, E.Y., Choi, D.Y., Kim, D.K., Kim, J.W., Park, J.O., Kim, S., Kim, S.H., Desiderio, D.M., Kim, Y.K., Kim, K.P. and Gho, Y.S., 2009. Gram-positive bacteria produce membrane vesicles: proteomics-based characterization of Staphylococcus aureus-derived membrane vesicles. *Proteomics*, 9(24), pp.5425-5436.

Lee, H.-J. (2019). Microbe-Host Communication by Small RNAs in Extracellular Vesicles: Vehicles for Transkingdom RNA Transportation. *International Journal of Molecular Sciences*, *20*(6), Article 6.

Li, C., Song, L., Zhao, J., Zhu, L., Zou, H., Zhang, H., Wang, H. and Cai, Z., 2007. Preliminary study on a potential antibacterial peptide derived from histone H2A in hemocytes of scallop Chlamys farreri. *Fish & Shellfish Immunology*, *22*(6), pp.663-672.

Lin, Z., Chen, L., Chen, X., Zhong, Y., Yang, Y., Xia, W., Liu, C., Zhu, W., Wang, H., Yan, B. and Yang, Y., 2019. Biological adaptations in the Arctic cervid, the reindeer (Rangifer tarandus). *Science*, *364*(6446), p.6312.

Liu, X., Arfman, T., Wichapong, K., Reutelingsperger, C.P., Voorberg, J. and Nicolaes, G.A., 2021. PAD4 takes charge during neutrophil activation: Impact of PAD4 mediated NET formation on immune-mediated disease. *Journal of Thrombosis and Haemostasis*, *19*(7), pp.1607-1617.

Liu, Y., Defourny, K. A. Y., Smid, E. J., & Abee, T. (2018). Gram-Positive Bacterial Extracellular Vesicles and Their Impact on Health and Disease. *Frontiers in Microbiology*, *9*.

Ma, J., Wang, Y., Chen, L., Yang, B., Jiang, Y., Wang, L., Chen, Z., Ma, G., Fang, L., & Wang, Z. (2023). Dauer larva-derived extracellular vesicles extend the life of Caenorhabditis elegans. *Biogerontology*, *24*(4), 581–592.

Ma, Z., Wang, Y. and Li, H., 2020. Applications of extracellular vesicles in tissue regeneration. *Biomicrofluidics,* 14(1), p.011501.

Magnadóttir, B., Audunsdottir, S. S., Bragason, B. Th., Gisladottir, B., Jonsson, Z. O., & Gudmundsdottir, S. (2011). The acute phase response of Atlantic cod (Gadus morhua): Humoral and cellular response. *Fish & Shellfish Immunology*, *30*(4), 1124–1130.

Magnadóttir, B., Bragason, B.T., Bricknell, I.R., Bowden, T., Nicholas, A.P., Hristova, M., Guðmundsdóttir, S., Dodds, A.W. and Lange, S., 2019. Peptidylarginine deiminase and deiminated proteins are detected throughout early halibut ontogeny-complement components C3 and C4 are post-translationally deiminated in halibut (Hippoglossus hippoglossus L.). *Developmental & Comparative Immunology*, *92*, pp.1-19.

Magnadóttir, B., Hayes, P., Hristova, M., Bragason, B.T., Nicholas, A.P., Dodds, A.W., Guðmundsdóttir, S. and Lange, S., 2018. Post-translational protein deimination in

cod (Gadus morhua L.) ontogeny novel roles in tissue remodelling and mucosal immune defences?. *Developmental & comparative immunology*, *87*, pp.157-170.

Magnadóttir, B., Kraev, I., Guðmundsdóttir, S., Dodds, A. W., & Lange, S. (2019) – a. Extracellular vesicles from cod (Gadus morhua L.) mucus contain innate immune factors and deiminated protein cargo. *Developmental & Comparative Immunology*, *99*, 103397.

Magnadóttir, B., Uysal-Onganer, P., Kraev, I., Dodds, A. W., Guðmundsdóttir, S., & Lange, S. (2020). Extracellular vesicles, deiminated protein cargo and microRNAs are novel serum biomarkers for environmental rearing temperature in Atlantic cod (Gadus morhua L.). *Aquaculture Reports*, *16*, 100245.

Magnadóttir, B., Uysal-Onganer, P., Kraev, I., Svansson, V., Hayes, P., & Lange, S. (2020). Deiminated proteins and extracellular vesicles—Novel serum biomarkers in whales and orca. *Comparative Biochemistry and Physiology Part D: Genomics and Proteomics*, *34*, 100676.

Magnadóttir, B., Uysal-Onganer, P., Kraev, I., Svansson, V., Skírnisson, K., & Lange, S. (2020). Deiminated proteins and extracellular vesicles as novel biomarkers in pinnipeds: Grey seal (*Halichoerus gryptus*) and harbour seal (*Phoca vitulina*). *Biochimie*, *171–172*, 79–90.

Manchon, E., Hirt, N., Bouaziz, J.-D., Jabrane-Ferrat, N., & Al-Daccak, R. (2021). Stem Cells-Derived Extracellular Vesicles: Potential Therapeutics for Wound Healing in Chronic Inflammatory Skin Diseases. *International Journal of Molecular Sciences*, *22*(6).

Manuwar, A., Dreyer, B., Böhmert, A., Ullah, A., Mughal, Z., Akrem, A., Ali, S. A., Schlüter, H., & Betzel, C. (2020). Proteomic Investigations of Two Pakistani Naja Snake Venoms Species Unravel the Venom Complexity, Posttranslational Modifications, and Presence of Extracellular Vesicles. *Toxins*, *12*(11).

Marzluff, W.F., Sakallah, S. and Kelkar, H., 2006. The sea urchin histone gene complement. *Developmental biology*, *300*(1), pp.308-320.

Matsushita, M., 2018. The complement system of agnathans. *Frontiers in immunology*, *9*, p.1405.

Matsushita, M., Matsushita, A., Endo, Y., Nakata, M., Kojima, N., Mizuochi, T. and Fujita, T., 2004. Origin of the classical complement pathway: Lamprey orthologue of mammalian C1q acts as a lectin. *Proceedings of the National Academy of Sciences*, *101*(27), pp.10127-10131.

McLeod, K., Walker, J. T., & Hamilton, D. W. (2018). Galectin-3 regulation of wound healing and fibrotic processes: Insights for chronic skin wound therapeutics. *Journal of Cell Communication and Signaling*, *12*(1), 281–287.

Mercer, A., Jaunmuktane, Z., Hristova, M., & Lange, S. (2022). Differential, Stage Dependent Detection of Peptidylarginine Deiminases and Protein Deimination in Lewy Body Diseases—Findings from a Pilot Study. *International Journal of Molecular Sciences*, *23*(21), Article 21.

Mohd-Padil, H., Mohd-Adnan, A., & Gabaldón, T. (2013). Phylogenetic Analyses Uncover a Novel Clade of Transferrin in Nonmammalian Vertebrates. *Molecular Biology and Evolution*, *30*(4), 894–905.

Mondal, S. and Thompson, P.R., 2019. Protein arginine deiminases (PADs): biochemistry and chemical biology of protein citrullination. *Accounts of chemical research*, *52*(3), pp.818-832.

Moon, Y., 2011. Mucosal injuries due to ribosome-inactivating stress and the compensatory responses of the intestinal epithelial barrier. *Toxins*, *3*(10), pp.1263-1277.

Moon, Y., 2014. Ribosomal alteration-derived signals for cytokine induction in mucosal and systemic inflammation: noncanonical pathways by ribosomal inactivation. *Mediators of Inflammation*, *2014*.

Moore, S.J., Kunkle, R., Greenlee, M.H.W., Nicholson, E., Richt, J., Hamir, A., Waters, W.R. and Greenlee, J., 2016. Horizontal transmission of chronic wasting disease in reindeer. *Emerging infectious diseases*, *22*(12), p.2142.

Moros, M., Fergola, E., Marchesano, V., Mutarelli, M., Tommasini, G., Miedziak, B., Palumbo, G., Ambrosone, A., Tino, A., & Tortiglione, C. (2021). The Aquatic Invertebrate Hydra vulgaris Releases Molecular Messages Through Extracellular Vesicles. *Frontiers in Cell and Developmental Biology*, *9*.

Morrow T. Healing Becomes a Fishy Business. *Manag Care*. 2016;25(12):38-39.

Munhoz Da Rocha, I. F., Amatuzzi, R. F., Lucena, A. C. R., Faoro, H., & Alves, L. R. (2020). Cross-Kingdom Extracellular Vesicles EV-RNA Communication as a Mechanism for Host–Pathogen Interaction. *Frontiers in Cellular and Infection Microbiology*, *10*, 593160.

Nachat, R., Méchin, M.-C., Takahara, H., Chavanas, S., Charveron, M., Serre, G., & Simon, M. (2005). Peptidylarginine Deiminase Isoforms 1–3 Are Expressed in the Epidermis and Involved in the Deimination of K1 and Filaggrin. *Journal of Investigative Dermatology*, *124*(2), 384–393.

Narauskaitė, D., Vydmantaitė, G., Rusteikaitė, J., Sampath, R., Rudaitytė, A., Stašytė, G., Aparicio Calvente, M. I., & Jekabsone, A. (2021). Extracellular Vesicles in Skin Wound Healing. *Pharmaceuticals*, *14*(8), Article 8.

Nicholas, A.P. and Whitaker, J.N., 2002. Preparation of a monoclonal antibody to citrullinated epitopes: its characterization and some applications to immunohistochemistry in human brain. *Glia*, *37*(4), pp.328-336.

Nunez, E.A., Wallis, J. and Gershon, M.D., 1974. 'Secretory processes in follicular cells of the bat thyroid. III. The occurrence of extracellular vesicles and colloid droplets during arousal from hibernation.' *American Journal of Anatomy*, 141(2), pp.179-201.

Ogawa, Y., Kanai-Azuma, M., Akimoto, Y., Kawakami, H., & Yanoshita, R. (2008). Exosome-like vesicles in *Gloydius blomhoffii blomhoffii* venom. *Toxicon*, *51*(6), 984–993.

Ostrowska-Podhorodecka, Z., Ding, I., Norouzi, M., & McCulloch, C. A. (2022). Impact of Vimentin on Regulation of Cell Signaling and Matrix Remodeling. *Frontiers in Cell and Developmental Biology*, *10*.

Palmer, M.V., Martins, M., Falkenberg, S., Buckley, A., Caserta, L.C., Mitchell, P.K., Cassmann, E.D., Rollins, A., Zylich, N.C., Renshaw, R.W. and Guarino, C., 2021. Susceptibility of white-tailed deer (Odocoileus virginianus) to SARS-CoV-2. *Journal of virology*, *95*(11), pp.00083-21.

Palmer, M.V., Stoffregen, W.C., Rogers, D.G., Hamir, A.N., Richt, J.A., Pedersen, D.D. and Waters, W.R., 2004. West Nile virus infection in reindeer (Rangifer tarandus). *Journal of veterinary diagnostic investigation*, *16*(3), pp.219-222.

Pamenter, M.E., Uysal-Onganer, P., Huynh, K.W., Kraev, I. and Lange, S., 2019. Post-translational deimination of immunological and metabolic protein markers in plasma and extracellular vesicles of naked mole-Rat (Heterocephalus glaber). *International journal of molecular sciences*, *20*(21), p.5378.

Park, T.J.; Reznick, J.; Peterson, B.L.; Blass, G.; Omerbasic, D.; Bennett, N.C.; Kuich, P.H.J.L.; Zasada, C.; Browe, B.M.; Hamann, W.; et al. Fructose-driven glycolysis supports anoxia resistance in the naked mole-rat. *Science* 2017, 356, 305–308.

Peng, J., Wang, W., Hua, S., Liu, L., 2018. 'Roles of Extracellular Vesicles in Metastatic Breast Cancer', *Breast Cancer: Basic and Clinical Research*, 12, p. 1178223418767666.

Peršurić, Ž., & Pavelić, S. K. (2021). Bioactives from Bee Products and Accompanying Extracellular Vesicles as Novel Bioactive Components for Wound Healing. *Molecules*, *26*(12).

Penn, J. W., Grobbelaar, A. O., & Rolfe, K. J. (2012). The role of the TGF-β family in wound healing, burns and scarring: a review. International Journal of Burns and Trauma, 2(1), 18-28.

Phillips, R.A., Kraev, I. and Lange, S., 2020. Protein deimination and extracellular vesicle profiles in Antarctic seabirds. *Biology*, *9*(1), p.15.

Pollard, C.A., Burns, D.S., Ho, B. and Johnston, A.M., 2018. Meningoencephalitis in a Royal Marine after skinning reindeer in Norway. *BMJ Military Health*, *164*(2), pp.117-119.

Rajan, B., Lokesh, J., Kiron, V., & Brinchmann, M. F. (2013). Differentially expressed proteins in the skin mucus of Atlantic cod (Gadus morhua) upon natural infection with Vibrio anguillarum. *BMC Veterinary Research*, *9*(1), 103.

Rani, S. and Ritter, T., 2016. The exosome-A naturally secreted nanoparticle and its application to wound healing. Advanced materials, 28(27), pp.5542-5552.

Rani, S., Ryan, A. E., Griffin, M. D., & Ritter, T. (2015). Mesenchymal Stem Cell-derived Extracellular Vesicles: Toward Cell-free Therapeutic Applications. *Molecular Therapy*, *23*(5), 812–823.

Raposo, G., & Stoorvogel, W. (2013). Extracellular vesicles: Exosomes, microvesicles, and friends. *The Journal of Cell Biology*, *200*, 373–383.

Raposo, G., Nijman, H.W., Stoorvogel, W., Liejendekker, R., Harding, C.V., Melief, C.J. and Geuze, H.J., 1996. B lymphocytes secrete antigen-presenting vesicles. *The Journal of experimental medicine*, 183(3), pp.1161-1172.

Rast, J.P., D'Alessio, S., Kraev, I. and Lange, S., 2021. Post-translational protein deimination signatures in sea lamprey (Petromyzon marinus) plasma and plasma-extracellular vesicles. *Developmental & Comparative Immunology*, *125*, p.104225.

Rebl, A., Köllner, B., Anders, E., Wimmers, K., & Goldammer, T. (2010). Peptidylarginine deiminase gene is differentially expressed in freshwater and brackish water rainbow trout. *Molecular Biology Reports*, *37*(5), 2333–2339.

Rohrbach, A.S., Slade, D.J., Thompson, P.R. and Mowen, K.A., 2012. Activation of PAD4 in NET formation. *Frontiers in immunology*, *3*, p.360.

Romanenko, L.A., Uchino, M., Frolova, G.M. and Mikhailov, V.V., 2007. Marixanthomonas ophiurae gen. nov., sp. nov., a marine bacterium of the family Flavobacteriaceae isolated from a deep-sea brittle star. *International journal of systematic and evolutionary microbiology*, *57*(3), pp.457-462.

Sancandi, M., Uysal-Onganer, P., Kraev, I., Mercer, A. and Lange, S., 2020. Protein deimination signatures in plasma and plasma-evs and protein deimination in the brain vasculature in a rat model of pre-motor parkinson's disease. *International journal of molecular sciences*, *21*(8), p.2743.

Sánchez Romano, J., Grund, L., Obiegala, A., Nymo, I.H., Ancin-Murguzur, F.J., Li, H., Król, N., Pfeffer, M. and Tryland, M., 2019. A multi-pathogen screening of captive reindeer (Rangifer tarandus) in Germany based on serological and molecular assays. *Frontiers in veterinary science*, *6*, p.461.

Saperas, N., Chiva, M., Ribes, E., Kasinsky, H.E., Rosenberg, E., Youson, J.H. and Ausio, J., 1994. Chromosomal proteins of the sperm of a cephalochordate (Branchiostoma floridae) and an agnathan (Petromyzon marinus): compositional variability of the nuclear sperm proteins of deuterostomes. *The Biological Bulletin*, *186*(1), pp.101-114.

Saraiva, F. M. S., Cosentino-Gomes, D., Inacio, J. D. F., Almeida-Amaral, E. E., Louzada-Neto, O., Rossini, A., Nogueira, N. P., Meyer-Fernandes, J. R., & Paes, M. C. (2022). Hypoxia Effects on Trypanosoma cruzi Epimastigotes Proliferation, Differentiation, and Energy Metabolism. *Pathogens*, *11*(8), 897.

Savcı, Y., Kırbaş, O. K., Bozkurt, B. T., Abdik, E. A., Taşlı, P. N., Şahin, F., & Abdik, H. (2021). Grapefruit-derived extracellular vesicles as a promising cell-free therapeutic tool for wound healing. *Food & Function*, *12*(11), 5144–5156.
Schmidt, O., & Teis, D. (2012). The ESCRT machinery. *Current Biology: CB*, *22*(4), R116-120.

Sciacchitano, S., Lavra, L., Morgante, A., Ulivieri, A., Magi, F., De Francesco, G. P., Bellotti, C., Salehi, L. B., & Ricci, A. (2018). Galectin-3: One Molecule for an Alphabet of Diseases, from A to Z. *International Journal of Molecular Sciences*, *19*(2), 379.

Seo, J.K., Stephenson, J. and Noga, E.J., 2011. Multiple antibacterial histone H2B proteins are expressed in tissues of American oyster. *Comparative Biochemistry and Physiology Part B: Biochemistry and Molecular Biology*, *158*(3), pp.223-229.

Sjöqvist, S. (2019). *Oral Mucosa Keratinocytes and Their Exosomes for Epithelial Tissue Regeneration* [Ph.D., Karolinska Institutet (Sweden)].

Skokos, D., Botros, H.G., Demeure, C., Morin, J., Peronet, R., Birkenmeier, G., Boudaly, S., Mécheri, S., 2003. 'Mast cell-derived exosomes induce phenotypic and functional maturation of dendritic cells and elicit specific immune responses *in vivo*.' *J Immunol* 170, 3037–3045.

Smith, A.B. and Kroh, A., 2013. Phylogeny of sea urchins. In *Developments in Aquaculture and Fisheries Science* (Vol. 38, pp. 1-14). Elsevier.

Smith, V.J. and Dyrynda, E.A., 2015. Antimicrobial proteins: from old proteins, new tricks. *Molecular immunology*, *68*(2), pp.383-398.

Sodergren, E., Weinstock, G.M., Davidson, E.H., Cameron, R.A., Gibbs, R.A., Angerer, R.C., Angerer, L.M., Arnone, M.I., Burgess, D.R., Burke, R.D. and Coffman, J.A., 2006. The genome of the sea urchin Strongylocentrotus purpuratus. *Science*, *314*(5801), pp.941-952.

Sruthy, K.S., Nair, A., Antony, S.P., Puthumana, J., Singh, I.B. and Philip, R., 2019. A histone H2A derived antimicrobial peptide, Fi-Histin from the Indian White shrimp, Fenneropenaeus indicus: Molecular and functional characterization. *Fish & Shellfish Immunology*, *92*, pp.667-679.

Stafford, J. L., & Belosevic, M. (2003). Transferrin and the innate immune response of fish: Identification of a novel mechanism of macrophage activation. *Developmental and Comparative Immunology*, *27*(6–7), 539–554.

Star, B., Nederbragt, A.J., Jentoft, S., Grimholt, U., Malmstrøm, M., Gregers, T.F., Rounge, T.B., Paulsen, J., Solbakken, M.H., Sharma, A. and Wetten, O.F., 2011. The genome sequence of Atlantic cod reveals a unique immune system. *Nature*, *477*(7363), pp.207-210.

Street, J.M., Barran, P.E., Macky, C.L., Balmforth, C., Walsh, T.S., Chalmers, R.T., Webb, D.J., Dear, J.W. (2012). 'Identification and proteomic profiling of exosomes in human cerebrospinal fluid.' *Journal of Translational Medicine*, 10 (1), 5.

Strodtbeck, F. (2001). Physiology of wound healing. *Newborn and Infant Nursing Reviews*, *1*(1), 43–52.

Stuffers, S., Sem Wegner, C., Stenmark, H. and Brech, A., 2009. Multivesicular endosome biogenesis in the absence of ESCRTs. *Traffic*, *10*(7), pp.925-937.

Sun, C.N. (1966). 'Lattice structures and osmiophilic bodies in the developing respiratory tissue of rats.' *Journal of Ultrastructure Research*, 15 (3), 380–388.

Sundaram, A.Y., Kiron, V., Dopazo, J. and Fernandes, J.M., 2012. Diversification of the expanded teleost-specific toll-like receptor family in Atlantic cod, Gadus morhua. *BMC evolutionary biology*, *12*(1), pp.1-17.

Takagi, T., Yoshioka, Y., Zayasu, Y., Satoh, N., & Shinzato, C. (2020). Transcriptome Analyses of Immune System Behaviors in Primary Polyp of Coral Acropora

digitifera Exposed to the Bacterial Pathogen Vibrio coralliilyticus under Thermal Loading. *Marine Biotechnology*, *22*(6), 748–759.

Talapatra, S., Wagner, J.D.O. and Thompson, C.B., 2002. Elongation factor-1 alpha is a selective regulator of growth factor withdrawal and ER stress-induced apoptosis. *Cell Death & Differentiation*, *9*(8), pp.856-861.

Talbott, H. E., Mascharak, S., Griffin, M., Wan, D. C., & Longaker, M. T. (2022). Wound healing, fibroblast heterogeneity, and fibrosis. *Cell Stem Cell*, *29*(8), 1161–1180.

Taylor, R.S., Horn, R.L., Zhang, X., Golding, G.B., Manseau, M. and Wilson, P.J., 2019. The caribou (Rangifer tarandus) genome. *Genes*, *10*(7), p.540.

Terkelsen LH, Eskild-Jensen A, Kjeldsen H, Barker JH, Hjortdal VE. Topical application of cod liver oil ointment accelerates wound healing: an experimental study in wounds in the ears of hairless mice. *Scand J Plast Reconstr Surg Hand Surg*. 2000;34(1):15-20. doi:10.1080/02844310050160123

Théry, C., Boussac, M., Véron, P., Ricciardi-Castagnoli, P., Raposo, G., Garin, J. and Amigorena, S., 2001. Proteomic analysis of dendritic cell-derived exosomes: a secreted subcellular compartment distinct from apoptotic vesicles. *The Journal of Immunology,* 166(12), pp.7309-7318.

Théry, C., Witwer, K.W., Aikawa, E., Alcaraz, M.J., Anderson, J.D., Andriantsitohaina, R., Antoniou, A., Arab, T., Archer, F., Atkin-Smith, G.K. and Ayre, D.C., 2018. Minimal information for studies of extracellular vesicles 2018 (MISEV2018): a position statement of the International Society for Extracellular Vesicles and update of the MISEV2014 guidelines*. Journal of extracellular vesicles*, 7(1), p.1535750.

Thiam, H.R., Wong, S.L., Wagner, D.D. and Waterman, C.M., 2020. Cellular mechanisms of NETosis. *Annual review of cell and developmental biology*, *36*, pp.191-218.

Thompson, A. G., Gray, E., Heman-Ackah, S. M., Mäger, I., Talbot, K., Andaloussi, S. E., Wood, M. J., & Turner, M. R. (2016). 'Extracellular vesicles in neurodegenerative disease—Pathogenesis to biomarkers.' *Nature Reviews. Neurology*, *12*(6), 346–357.

Thompson, A.G. *et al.* (2016) 'Extracellular vesicles in neurodegenerative disease - pathogenesis to biomarkers', *Nature Reviews. Neurology*, 12(6), pp. 346–357.

Tian, J., Casella, G., Zhang, Y., Rostami, A., & Li, X. (2020). 'Potential roles of extracellular vesicles in the pathophysiology, diagnosis, and treatment of autoimmune diseases.' *International Journal of Biological Sciences*, *16*(4), 620–632.

Trajkovic, K., Hsu, C., Chiantia, S., Rajendran, L., Wenzel, D., Wieland, F., Schwille, P., Brügger, B. and Simons, M., 2008. Ceramide triggers budding of exosome vesicles into multivesicular endosomes. *Science*, *319*(5867), pp.1244-1247.

Trams, E. G., Lauter, C. J., Norman Salem, Jr., & Heine, U. (1981). Exfoliation of membrane ecto-enzymes in the form of micro-vesicles. *Biochimica et Biophysica Acta (BBA) - Biomembranes*, *645*(1), 63–70.

Tryland, M., Beckmen, K.B., Burek-Huntington, K.A., Breines, E.M. and Klein, J., 2018. Orf virus infection in Alaskan mountain goats, Dall's sheep, muskoxen, caribou and Sitka black-tailed deer. *Acta veterinaria scandinavica*, *60*(1), pp.1-11.

Turchinovich, A., Drapkina, O. and Tonevitsky, A., 2019. Transcriptome of extracellular vesicles: state-of-the-art. *Frontiers in immunology*, *10*, p.202.

U, K. P., Subramanian, V., Nicholas, A. P., Thompson, P. R., & Ferretti, P. (2014). Modulation of calcium-induced cell death in human neural stem cells by the novel peptidylarginine deiminase–AIF pathway. *Biochimica et Biophysica Acta (BBA) - Molecular Cell Research*, *1843*(6), 1162–1171.

Uhlén, M., Fagerberg, L., Hallström, B. M., Lindskog, C., Oksvold, P., Mardinoglu, A., Sivertsson, Å., Kampf, C., Sjöstedt, E., Asplund, A., Olsson, I., Edlund, K., Lundberg, E., Navani, S., Szigyarto, C. A.-K., Odeberg, J., Djureinovic, D., Takanen, J. O., Hober, S., Pontén, F. (2015). Tissue-based map of the human proteome. *Science*, *347*(6220), 1260419.

Urzì, O., Cafora, M., Ganji, N. R., Tinnirello, V., Gasparro, R., Raccosta, S., Manno, M., Corsale, A. M., Conigliaro, A., Pistocchi, A., Raimondo, S., & Alessandro, R. (2023). Lemon-derived nanovesicles achieve antioxidant and anti-inflammatory effects activating the AhR/Nrf2 signaling pathway. *iScience*, *26*(7), 107041.

Uysal-Onganer, P., D'Alessio, S., Mortoglou, M., Kraev, I. and Lange, S., 2021. Peptidylarginine deiminase inhibitor application, using Cl-Amidine, PAD2, PAD3 and PAD4 isozyme-specific inhibitors in pancreatic cancer cells, reveals roles for PAD2 and PAD3 in cancer invasion and modulation of extracellular vesicle signatures. *International journal of molecular sciences*, *22*(3), p.1396.

Uysal-Onganer, P., MacLatchy, A., Mahmoud, R., Kraev, I., Thompson, P.R., Inal, J.M. and Lange, S., 2020. Peptidylarginine deiminase isozyme-specific PAD2, PAD3 and PAD4 inhibitors differentially modulate extracellular vesicle signatures and cell invasion in two glioblastoma multiforme cell lines. *International journal of molecular sciences*, *21*(4), p.1495.

Vagner, T., Chin, A., Mariscal, J., Bannykh, S., Engman, D.M. and Di Vizio, D., 2019. Protein composition reflects extracellular vesicle heterogeneity. *Proteomics*, *19*(8), p.1800167.

Valadi, H., Ekström, K., Bossios, A., Sjöstrand, M., Lee, J.J. and Lötvall, J.O., 2007. Exosome-mediated transfer of mRNAs and microRNAs is a novel mechanism of genetic exchange between cells. *Nature cell biology*, 9(6), pp.654-659.

Van der Pol, E., Böing, A.N., Harrison, P., Sturk, A. and Nieuwland, R., 2012. Classification, functions, and clinical relevance of extracellular vesicles. *Pharmacological reviews*, 64(3), pp.676-705.

Van Niel, G., Charrin, S., Simoes, S., Romao, M., Rochin, L., Saftig, P., Marks, M.S., Rubinstein, E. and Raposo, G., 2011. The tetraspanin CD63 regulates ESCRT-independent and-dependent endosomal sorting during melanogenesis. *Developmental cell*, *21*(4), pp.708-721.

Van Niel, G., d'Angelo, G. and Raposo, G., 2018. Shedding light on the cell biology of extracellular vesicles. *Nature reviews Molecular cell biology*, *19*(4), p.213.

Van Niel, G., Mallegol, J., Bevilacqua, C., Candalh, C., Brugière, S., Tomaskovic-Crook, E., Heath, J. K., Cerf-Bensussan, N., & Heyman, M. (2003). 'Intestinal epithelial exosomes carry MHC class II/peptides able to inform the immune system in mice.' *Gut*, *52*(12), 1690–1697.

Venturella, M.; Criscuoli, M.; Carraro, F.; Naldini, A.; Zocco, D. Interplay between Hypoxia and Extracellular Vesicles in Cancer and Inflammation. *Biology* 2021, 10, 606

Vera, M., Pani, B., Griffiths, L.A., Muchardt, C., Abbott, C.M., Singer, R.H. and Nudler, E., 2014. The translation elongation factor eEF1A1 couples transcription to translation during heat shock response. *Elife*, *3*, p.e03164.

Vieira, S., Franco, A.R., Fernandes, E.M., Amorim, S., Ferreira, H., Pires, R.A., Reis, R.L., Martins, A. and Neves, N.M., 2018. Fish sarcoplasmic proteins as a high value marine material for wound dressing applications. *Colloids and Surfaces B: Biointerfaces*, *167*, pp.310-317.

Villagra-Blanco, R., Silva, L.M., Conejeros, I., Taubert, A. and Hermosilla, C., 2019. Pinniped-and cetacean-derived ETosis contributes to combating emerging apicomplexan parasites (Toxoplasma gondii, Neospora caninum) circulating in marine environments. *Biology*, *8*(1), p.12.

Vossenaar, E.R., Zendman, A.J., van Venrooij, W.J. and Pruijn, G.J., 2003. PAD, a growing family of citrullinating enzymes: genes, features and involvement in disease. *Bioessays*, *25*(11), pp.1106-1118.

Wang, H., Li, B., Yang, L., Jiang, C., Zhang, T., Liu, S., & Zhuang, Z. (2022). Expression profiles and transcript properties of fast-twitch and slow-twitch muscles in a deep-sea highly migratory fish, Pseudocaranx dentex. *PeerJ*, *10*, e12720.

Wang, L.L., Song, Y.P., Mi, J.H. and Ding, M.L., 2021. Peptidyl arginine deiminase 4 and its potential role in Alzheimer's disease. *Medical Hypotheses*, *146*, p.110466.

Wang, S. and Wang, Y., 2013. Peptidylarginine deiminases in citrullination, gene regulation, health and pathogenesis. *Biochimica et Biophysica Acta (BBA)-Gene Regulatory Mechanisms*, *1829*(10), pp.1126-1135.

Wang, Y.-X., Cheng, L., Zhao, H., Li, Z., Chen, J., Cen, Y., & Zhang, Z. (2022). The Therapeutic Role of ADSC-EVs in Skin Regeneration. *Frontiers in Medicine*, *9*, null.

Wang, Y., Li, M., Stadler, S., Correll, S., Li, P., Wang, D., Hayama, R., Leonelli, L., Han, H., Grigoryev, S. A., Allis, C. D., & Coonrod, S. A. (2009). Histone hypercitrullination

mediates chromatin decondensation and neutrophil extracellular trap formation. *Journal of Cell Biology*, *184*(2), 205–213.

Wang, Y., Zhao, M., Liu, S., Guo, J., Lu, Y., Cheng, J., & Liu, J. (2020). Macrophage-derived extracellular vesicles: Diverse mediators of pathology and therapeutics in multiple diseases. *Cell Death & Disease*, *11*(10), 1–18.

Wei, H., Chen, Q., Lin, L., Sha, C., Li, T., Liu, Y., Yin, X., Xu, Y., Chen, L., Gao, W., Li, Y., & Zhu, X. (2021). Regulation of exosome production and cargo sorting. *International Journal of Biological Sciences*, *17*(1), 163–177.

Wei, Q., Liu, X., Su, J.-L., Wang, Y., Chu, Z., Ma, K., Huang, Q., Li, H., Fu, X.-B., & Zhang, C. (2023). Small extracellular vesicles from mesenchymal stem cells: A potential Weapon for chronic non-healing wound treatment. *Frontiers in Bioengineering and Biotechnology*, *10*.

Wei, Q., Wang, Y., Ma, K., Li, Q., Li, B., Hu, W., Fu, X., & Zhang, C. (2022). Extracellular Vesicles from Human Umbilical Cord Mesenchymal Stem Cells Facilitate Diabetic Wound Healing Through MiR-17-5p-mediated Enhancement of Angiogenesis. *Stem Cell Reviews and Reports*, *18*(3), 1025–1040.

Weldenegodguad, M., Pokharel, K., Ming, Y., Honkatukia, M., Peippo, J., Reilas, T., Røed, K.H. and Kantanen, J., 2020. Genome sequence and comparative analysis of reindeer (Rangifer tarandus) in northern Eurasia. *Scientific reports*, *10*(1), pp.1-14.

Welnar, T., Bailey, T. and Smrkolj, V., 2009. The wound healing process: an overview of the cellular and molecular mechanisms. *Journal of International Medical Research*, 37(5), pp.1528-1542.

Welsh, J. A., Goberdhan, D. C. I., O'Driscoll, L., Buzas, E. I., Blenkiron, C., Bussolati, B., Cai, H., Di Vizio, D., Driedonks, T. A. P., Erdbrügger, U., Falcon-Perez, J. M., Fu, Q.-L., Hill, A. F., Lenassi, M., Lim, S. K., Mahoney, M. G., Mohanty, S., Möller, A., Nieuwland, R., … Witwer, K. W. (2024). Minimal information for studies of extracellular vesicles (MISEV2023): From basic to advanced approaches. *Journal of Extracellular Vesicles*, *13*(2), e12404.

Williams, E.S. and Young, S., 1980. Chronic wasting disease of captive mule deer: a spongiform encephalopathy. *Journal of wildlife diseases*, *16*(1), pp.89-98.

Witalison, E., R Thompson, P. and J Hofseth, L., 2015. Protein arginine deiminases and associated citrullination: physiological functions and diseases associated with dysregulation. *Current drug targets*, *16*(7), pp.700-710.

Wolf, P., 1967. The nature and significance of platelet products in human plasma. British journal of haematology, 13(3), pp.269-288.

Wu, Z., Ma, L., Lin, P., Dai, Z., Lu, Z., Yan, L., Zhou, C., Qian, Z.-J., Hong, P., & Li, C. (2022). Extracellular vesicles derived from *Pinctada martensii* mucus regulate skin inflammation via the NF-κB/NLRP3/MAPK pathway. *Biochemical and Biophysical Research Communications*, *634*, 10–19.

Xu, T., Wang, Y., Li, J., Shu, C., Han, J., & Chu, Q. (2016). Comparative genomic evidence for duplication of TLR1 subfamily and miiuy croaker TLR1 perceives LPS stimulation via MyD88 and TIRAP. *Fish & Shellfish Immunology*, *56*, 336–348.

Xun, C., Wang, L., Yang, H., Xiao, Z., Deng, M., Xu, R., Zhou, X., Chen, P., & Liu, Z. (2021). Origin and Characterization of Extracellular Vesicles Present in the Spider Venom of Ornithoctonus hainana. *Toxins*, *13*(8).
Yaghoubi, S.; Najminejad, H.; Dabaghian, M.; Karimi, M.H.; Abdollahpour-Alitappeh, M.; Rad, F.; Mahi-Birjand, M.; Mohammadi, S.; Mohseni, F.; Sobhani Lari, M.; et al. How Hypoxia Regulate Exosomes in Ischemic Diseases and Cancer Microenvironment? *IUBMB Life* 2020, 72, 1286–1305.

Yáñez-Mó, M., Siljander, P.R.M., Andreu, Z., Bedina Zavec, A., Borràs, F.E., Buzas, E.I., Buzas, K., Casal, E., Cappello, F., Carvalho, J. and Colás, E., 2015. Biological properties of extracellular vesicles and their physiological functions. *Journal of extracellular vesicles*, 4(1), p.27066.

Yang, X.U., Si-Wei, Z.H.U. and Qing-Wei, L.I., 2016. Lamprey: a model for vertebrate evolutionary research. *Zoological research*, *37*(5), p.263.

York, J.R. and McCauley, D.W., 2020. Functional genetic analysis in a jawless vertebrate, the sea lamprey: insights into the developmental evolution of early vertebrates. *Journal of Experimental Biology*, *223*(Suppl_1), p. jeb206433.

Yu, B., Zhang, X., & Li, X. (2014). Exosomes derived from mesenchymal stem cells. *International Journal of Molecular Sciences*, *15*(3), 4142–4157.

Yu, K. and Proost, P., 2022. Insights into peptidylarginine deiminase expression and citrullination pathways. *Trends in Cell Biology*.

Yuan, Q., Zhang, Y., & Chen, Q. (2020). Mesenchymal Stem Cell (MSC)-Derived Extracellular Vesicles: Potential Therapeutics as MSC Trophic Mediators in Regenerative Medicine. *The Anatomical Record*, *303*(6), 1735–1742.

Yun, Y.-R., Won, J. E., Jeon, E., Lee, S., Kang, W., Jo, H., Jang, J.-H., Shin, U. S., & Kim, H.-W. (2010). Fibroblast Growth Factors: Biology, Function, and Application for Tissue Regeneration. *Journal of Tissue Engineering*, *2010*, 218142.

Zhang, B., Tian, X., Hao, J., Xu, G. and Zhang, W., 2020. 'Mesenchymal stem cell-derived extracellular vesicles in tissue regeneration.' *Cell transplantation*, 29, p.0963689720908500.

Zhang, H., Peng, L., Wang, Y., Zhao, W., Lau, W. B., Wang, Y., Li, Y., Du, Y., Li, L., Huang, Y., Nie, S., Qin, Y., Ma, X., & Wei, Y. (2022). Extracellular vesicle-derived miR-144 as a novel mechanism for chronic intermittent hypoxia-induced endothelial dysfunction. *Theranostics*, *12*(9), 4237–4249.

Zhang, J., Dai, J., Zhao, E., Lin, Y., Zeng, L., Chen, J., Zheng, H., Wang, Y., Li, X., Ying, K. and Xie, Y., 2004. cDNA cloning, gene organization and expression analysis of human peptidylarginine deiminase type VI. *Acta Biochimica Polonica*, *51*(4), pp.1051-1058.

Zhang, L., Wei, W., Ai, X., Kilic, E., Hermann, D. M., Venkataramani, V., Bähr, M., & Doeppner, T. R. (2021). Extracellular vesicles from hypoxia-preconditioned microglia promote angiogenesis and repress apoptosis in stroke mice via the TGF-β/Smad2/3 pathway. *Cell Death & Disease*, *12*(11), 1–14.

Zhou, W., Woodson, M., Neupane, B., Bai, F., Sherman, M. B., Choi, K. H., Neelakanta, G., & Sultana, H. (2018). Exosomes serve as novel modes of tick-borne flavivirus transmission from arthropod to human cells and facilitates dissemination of viral RNA and proteins to the vertebrate neuronal cells. *PLOS Pathogens*, *14*(1), e1006764.

Zhou, X., Brown, B. A., Siegel, A. P., El Masry, M. S., Zeng, X., Song, W., Das, A., Khandelwal, P., Clark, A., Singh, K., Guda, P. R., Gorain, M., Timsina, L., Xuan, Y., Jacobson, S. C., Novotny, M. V., Roy, S., Agarwal, M., Lee, R. J., … Ghatak, S. (2020). Exosome-Mediated Crosstalk between Keratinocytes and Macrophages in Cutaneous Wound Healing. *ACS Nano*, *14*(10), 12732–12748.

Zitvogel, L., Regnault, A., Lozier, A., Wolfers, J., Flament, C., Tenza, D., Ricciardi-Castagnoli, P., Raposo, G. and Amigorena, S., 1998. 'Eradication of established murine tumors using a novel cell-free vaccine: dendritic cell derived exosomes.' *Nature medicine*, 4(5), pp.594-600.

Appendices

Appendix 1 – Cell cultures

1.1 3T3.L1 Mouse Fibroblast cell culture: Setup, Troubleshooting and Optimisation

3T3.L1 cell line (mouse fibroblasts) was used, in the first instance, as an *in vitro* model, to assess the regenerative potential of EVs derived from Atlantic cod serum. Different preparations of cod serum-derived EVs have been assessed in this model, at different time points. The experiment set up for wound scratch assay involved seeding 3T3.L1 cells at a concentration of $2x10^2$ cells/well in a 12-well plate and allowing cells to adhere at the bottom of the wells. The cell monolayer was scratched with a 200µl yellow tip, and cellular debris was washed with fresh PBS. Each control received 1ml of fresh DMEM (n=3), while 1ml, 500µl and 200µl of EVs preparation derived from cod serum, were added to a well and topped up with fresh DMEM. Images of the 6 well-plate were acquired with the EVOS microscope, before being incubated for 24h at 37ºC. The plate was subsequently imaged after the 24-hour incubation to assess wound closure. The pictures obtained at time points of 0h and 24h, were exported to PowerPoint, where the area of the scratch was manually delineated with a red line (Fig. 50).

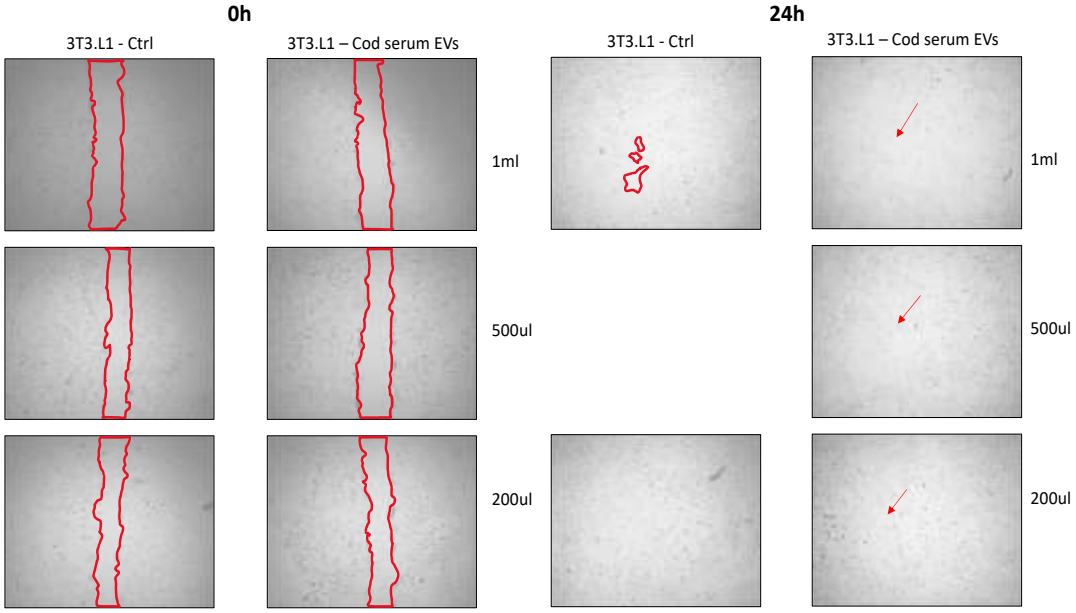

Figure 50. 3T3.L1 *In vitro* scratch assay set up in a 12-well plate. 3T3.L1 cells were seeded at concentration of $2x10^2$ cells/well treated with 200µl, 500µ and 1ml cod serum-derived EVs, and incubated at 37ºC for 24h.

Observations of the previous set-up wound scratch assay experiment, in which was noted that the linear scratch of the control group reached closure at the same time as the treatment group, therefore concluding that the different preparations of cod serum-derived EVs, were not appropriate to assess the potential of cod-serum EVs in the regeneration of mouse fibroblasts (3T3.L1) *in-vitro* wound model. Further assay optimisation was carried out on a 12-well plate. 3T3.L1 cells were seeded at the optimal concentration of $2x10^2$ cells/well and allowed to adhere at the bottom of the wells. Once cells had settled, a linear scratch was performed on the cellular monolayer, with a 200µl yellow tip, and cellular debris, was removed by washing the cells with fresh PBS until clear. Afterwards, cells (n=3 wells) were treated with 2ml of cod serum-derived EVs preparation and topped up with fresh DMED to reach a volume of 1ml/well, while the control group (n=3 wells) received 1ml of DMED, to have equal volumes in each well. Images of scratches were acquired before the cells were incubated at 37ºC,

for 24h. Further images of the 6 well plates were acquired after the period of incubation to capture the mouse fibroblasts and wound closure of the control group and the treatment group. The images were then exported into PowerPoint, where the area of the wound of each image was manually traced with a red line (Fig.51) before proceeding with any further observations or analysis.

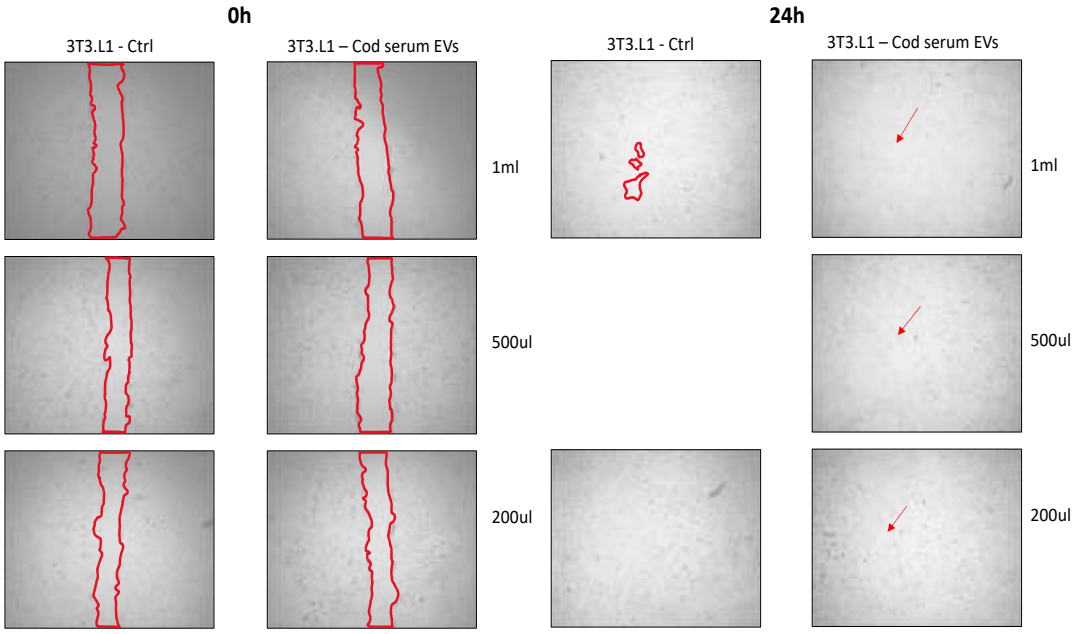

Figure 51. 3T3.L1 *In vitro* scratch assay set up in a 12-well plate. 3T3.L1 cells were seeded at a concentration of $2x10^2$ cells/well treated with 2ml of cod serum-derived EVs, and incubated at 37ºC for 24h.

Observations made on the previous set-up wound scratch assay experiment, in which was noted that the linear scratch of the control group reached closure at the same time as the treatment group, resulted in a reconsideration of the setup. From the above observations, it was concluded that the different preparations of cod serum-derived EVs were not appropriate to assess the potential of cod-serum EVs in the regeneration of mouse fibroblasts (3T3.L1) *in-vitro* wound model, and, therefore, a further optimisation of the experiment was required. The new optimisation of the experiment set-up

included the assessment of 1ml cod serum-derived EVs preparation and regenerative potential in mouse fibroblasts (3T1.L1 cells) at time points of 6h and 24h. Mouse fibroblasts were seeded into a 12-well plate at $2x10^2$ cells/well concentration. The cells were allowed to settle and adhere at the bottom of the well, before proceeding with scratching the 3T3.L1 monolayer with a 200µl yellow tip and rinsed with fresh PBS until the scratch was clearly visible. The cells were then treated with 1ml of cod serum EVs preparation topped up with fresh DMEM while the control group received 1ml of DMEM only.

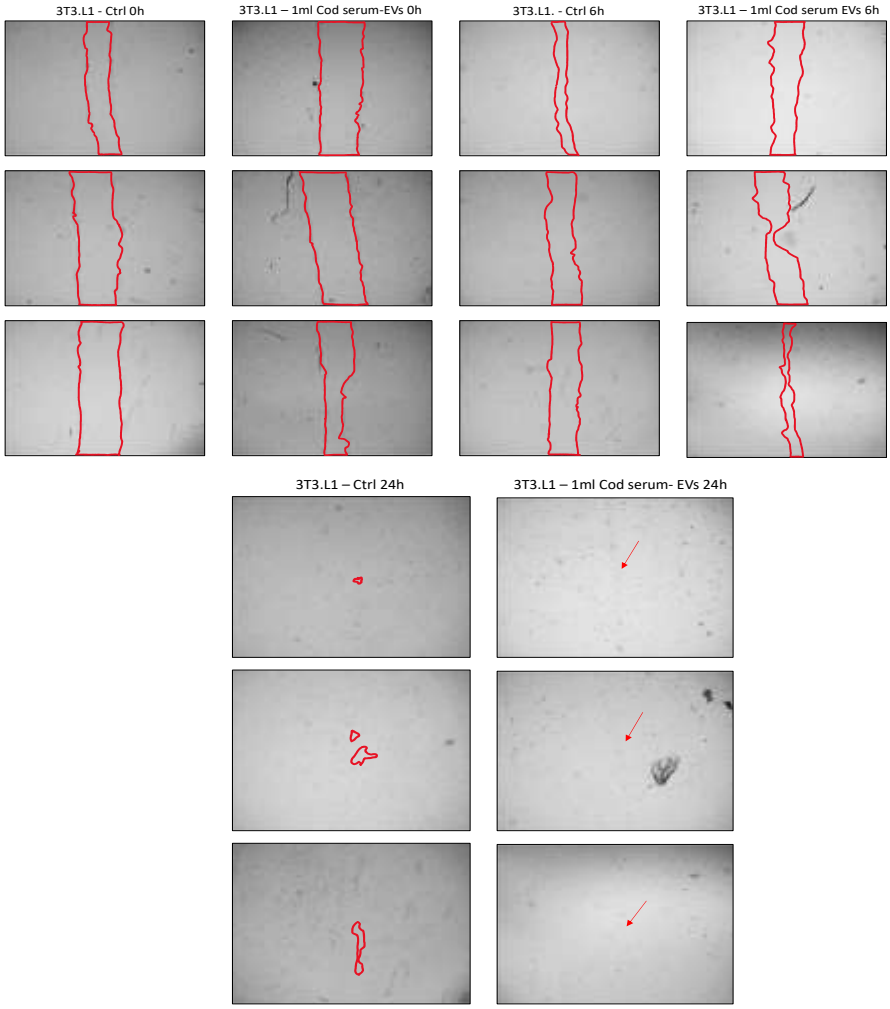

Figure 52. 3T3.L1 *In vitro* scratch assay set up in 12-well plate. 3T3.L1 cells were seeded at a concentration of $2x10^2$ cells/well treated with 1ml of cod serum-derived EVs, and incubated at 37ºC for 6h and 24h.

The above wound scratch healing assay set-up was considered optimal to assess cod serum-derived EVs in a different, and, more translatable into human, *in vitro* wound healing model.

1.2 HaCat Cell Culture: Setup, Troubleshooting and Optimisation

Immortalised human keratinocytes (HaCat) were used in this pilot study to assess cod serum-derived EVs functionality in promoting wound healing *in vitro* human cellular model. HaCat cells were seeded on a 12-well plate at 2 x 10^{10} cell/well and treated with 1ml (1.55x10^{10} particles/ml) and 2ml of cod serum-derived EVs. Cell migration was assessed over 24h period.

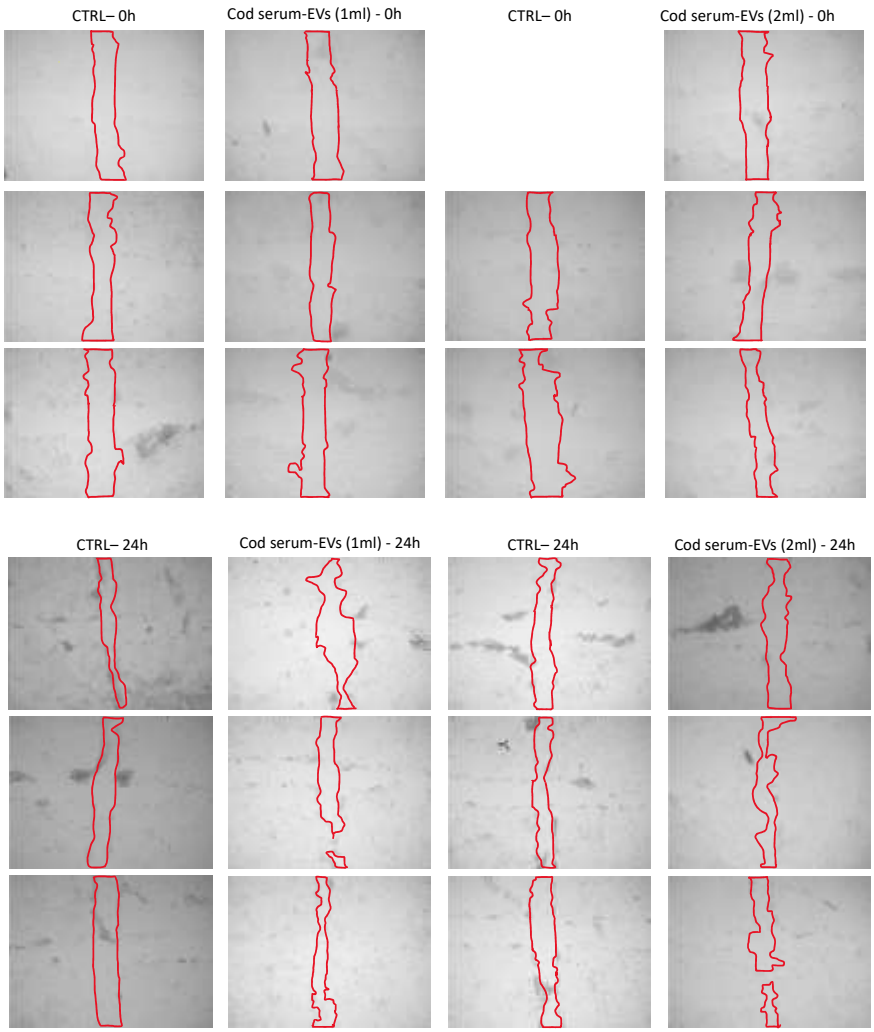

Figure 53. HaCat *in vitro* scratch assay set up in 12 well-plate.

1.3 HDFa cell culture: Setup, troubleshooting and optimisation

Human Dermal Fibroblasts, adult (HDFa) cells were used in this pilot study to assess cod serum-derived EVs functionality in promoting wound healing *in vitro* human cellular model. HDFa cells were seeded on a 12-well plate at 2 x 10^{10} cell/well and treated with different concentration of cod serum-derived EVs, for optimisation. Cell migration was assessed over 24h period (Fig. 54).

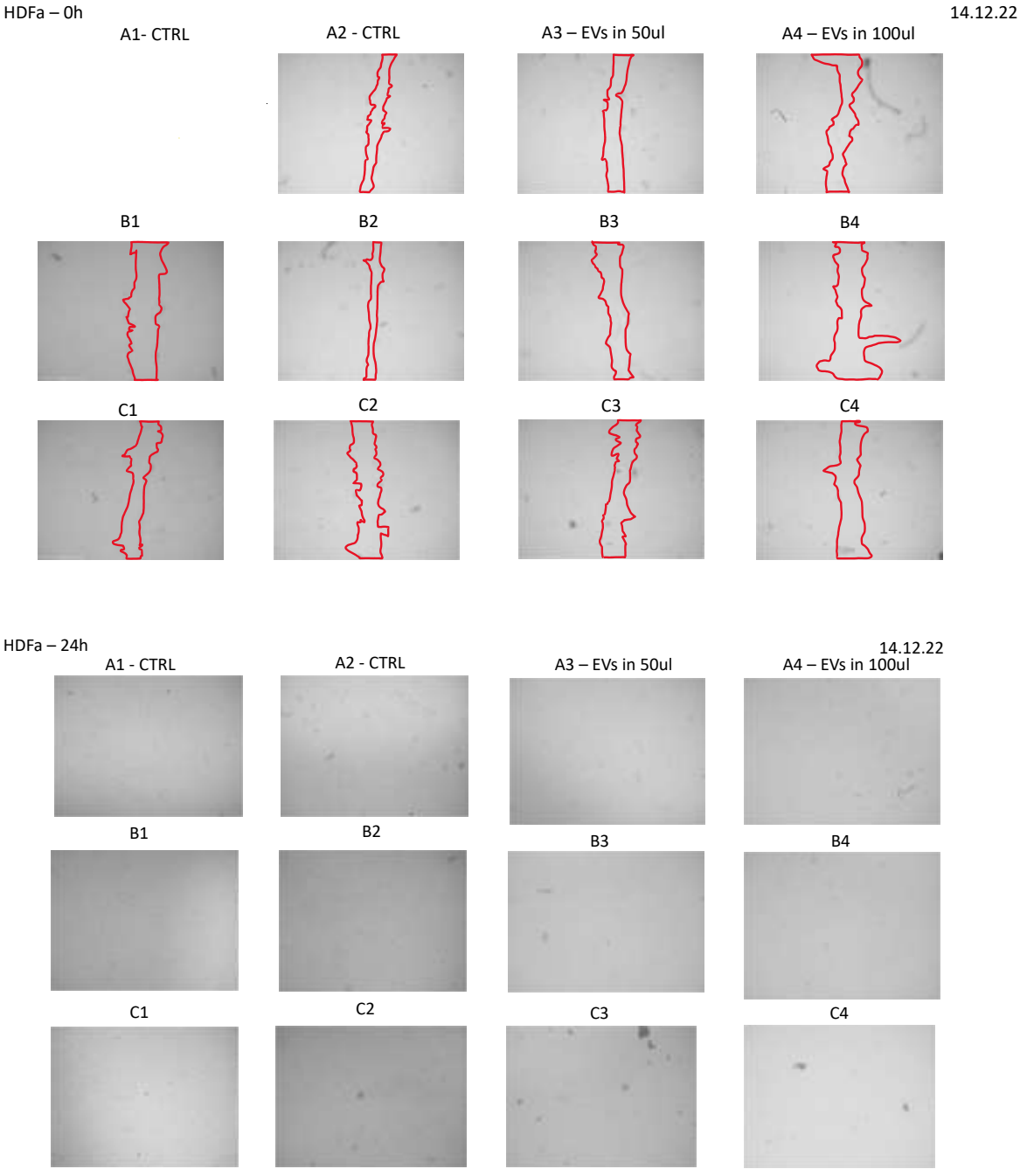

Figure 54. HDFa *in vitro* scratch assay set-up and optimisation in 12 well-plate.

Appendix 2 - ICC

2.1 HDFa ICC with FGF2 and Vimentin – no treatment

Immunocytochemistry protocol was assessed on HDFa cells (Fig. 55) before treatment with cod serum and mucus-derived EVs to assess staining of proteins of interest, such as Vimentin and FGF2. Cells were cultured following the method previously described in Chapter 2, Section 2.8 – HDFa cell culture and a linear scratch was performed in the cell monolayer before proceeding with the ICC protocol described in Chapter 2, Section 2.8.2

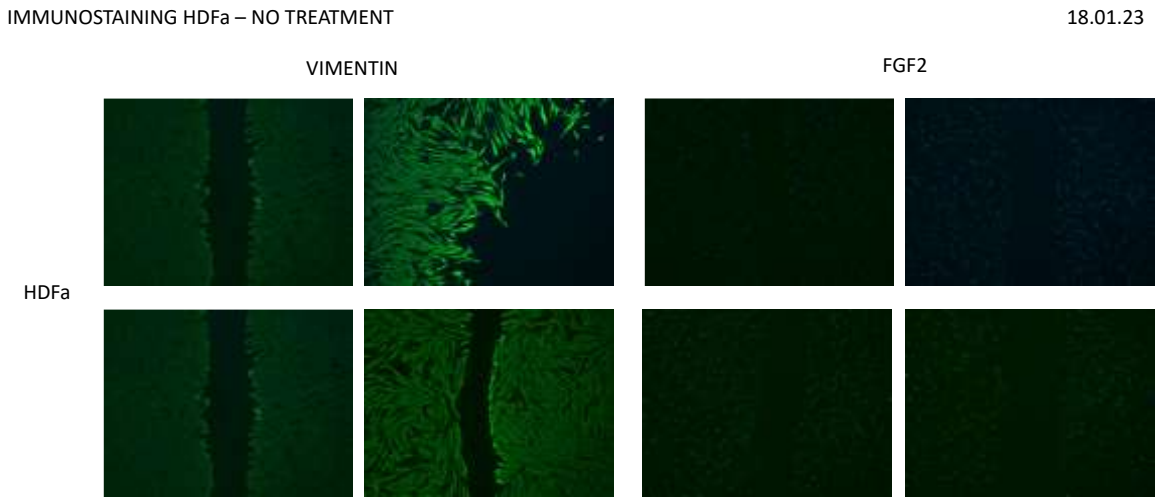

Figure 55. HDFa ICC set-up and assessment before cod-serum and mucus-derived EVs treatment.

2.2 HDFa ICC Assessment of Anti-FGF2 changes at 8h and 24h upon Cod-derived serum and mucus EVs treatment

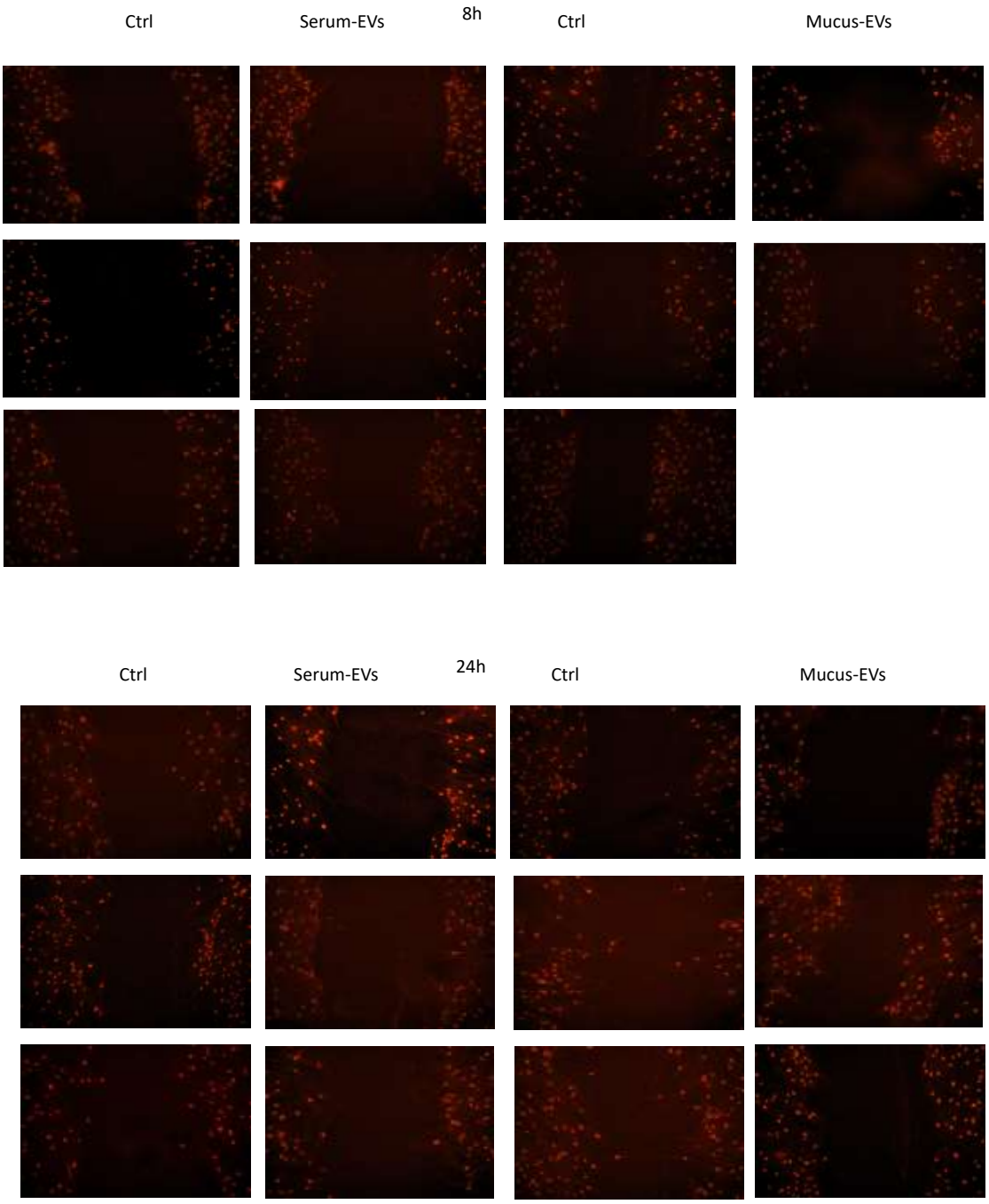

Figure 56. HDFa ICC set-up in 12-well plate. Assessement of Anti-FGF2 expression at 8h and 24h upon treatment with 1ml of cod serum and mucus-derived EVs.